THE BEHAVIOR OF ASH IN PULVERIZED COAL

UNDER SIMULATED COMBUSTION CONDITIONS

by

ASHOK S. PADIA

B.E. (Hons.), Birla Institute of Technology and Science
Pilani, India (1970)

S. M., Massachusetts Institute of Technology
(1971)

Ch.E., Massachusetts Institute of Technology
(1973)

Submitted in partial fulfillment of
the requirements for the degree

Doctor of Science

at the

Massachusetts Institute of Technology

January 1976

Signature of Author:

Signature Redacted

Department of Chemical Engineering
January 1976

Certified by:

Signature Redacted

Adel F. Sarofim, Thesis Supervisor

Signature Redacted

Jack B. Howard, Thesis Supervisor

Signature Redacted

Approved by:

Glenn C. Williams, Thesis Supervisor
Chairman, Departmental Committee on
Graduate Students

THE BEHAVIOR OF ASH IN PULVERIZED COAL
UNDER SIMULATED COMBUSTION CONDITIONS

by

ASHOK S. PADIA

Submitted to the Department of Chemical Engineering on January 14, 1976 in partial fulfillment of the requirements for the degree of Doctor of Science.

ABSTRACT

A systematic study of the physical and chemical behavior of mineral matter during rapid combustion of pulverized coal particles was performed by first completely characterizing the distribution of mineral matter in the coal with respect to its composition and particle size distribution, and then oxidizing the coal particles in a preheated drop-tube furnace. Two types of coals, a Montana lignite and a Pittsburgh seam bituminous, pulverized and size graded into two fractions 38-45μm and 75-90μm, were used in the study.

In order to obtain the distribution of mineral matter in the original coal, mineral matter was separated from coal samples in its essentially unaltered state by low temperature ashing. Major minerals present in the coals were identified by x-ray diffraction patterns. Examination of the mineral matter under a scanning electron microscope with simultaneous energy dispersive x-ray analysis to obtain elemental composition made it possible to characterize the composition and particle size distribution of the mineral matter in coal. The major minerals in coal consisted of kaolinite [$Al_2Si_2O_5(OH)_4$] ranging from 1 to 5μm platelets (2.5μm mass median size), carbonates and sulfates mainly of calcium of about 2μm mass median size and pyrites [FeS_2] about 1μm mass median size. The overall mass median size of low temperature ash was determined to be about 2μm.

The high temperature behavior of mineral matter from both coals was studied in a drop tube furnace operated at temperatures up to 1830°K with an oxidizing atmosphere. The particle residence time was about 1 second and the heating rates were of the order of 10^5°C/second. The weight loss of mineral matter and the particle size distribution of ash were measured as a function of temperature, coal type and coal size.

Loss of about 30 percent by weight of the mineral matter at temperatures up to the ASTM ashing temperature (750°C) can be attributed to the thermal decomposition of kaolinite and carbonates and the oxidation of pyrites. Additional loss of about 25 percent by weight of ASTM ash for lignite and about 6 percent for bituminous was observed when the ash was heated to 1830°K. This additional loss was contributed mainly by $CaSO_4$ decomposition and some (about 3 percent) silica vaporization. These results of thermal decomposition of kaolinite, carbonates and sulfates and oxidation of pyrites are supported by successive diffraction patterns obtained for each sample. Significant effects of combustion conditions (oxidizing or inert) are observed on the weight loss of ash.

During heating the individual mineral particles fuse at about 1000-1200°K and agglomerate as the carbon burnout progresses. Surface tension forces are high enough to retain the fused ash particle on the burning char surface. If all the mineral matter particles in one coal particle agglomerate without separation from char surface during combustion, this would result in the formation of 1 ash/coal particle. The experimental observations suggest that about 3 ash particles/coal particle for lignite and 5 ash particles per coal particle for bituminous coal are produced. Combustion temperature from 1250 to 1830°K did not have any noticeable effect on the resulting particle size distribution. The mean particle size of ash produced was proportional to the mean particle size of parent coal particles. Physical observations of burning behavior of lignite and bituminous coals provide evidence of fragmentation of char particles and formation of hollow spheres (cenospheres) of char in the case of bituminous coals. The formation of more than 1 ash particle per coal particle is consistent with the observed physical behavior of the char during oxidation.

Ash also formed cenospheres due to evolution of gas by thermal decomposition. The formation of cenospheres resulted in a distribution of specific gravities of ash ranging from less than 1 to 3.5. The formation of cenospheres is governed by the viscous relaxation of the fused ash and the kinetics of gas evolution. The temperature range in which cenospheres were formed could be explained by use of a simple theoretical model.

Some experiments performed with silica and carbon in inert atmosphere up to 2250°K temperature showed that SiC formed at high temperatures. Silica also seemed to volatilize in the form of more volatile SiO which disproportionates into SiO_2 and Si. Condensation products about 0.5μm in size, probably due to disproportionation of SiO, were observed on the cooler portions of the furnace.

The implications of the above findings to ash vaporization and heat transfer pertinent to MHD combustors are also outlined. Recommendations have been made for further work.

Thesis Supervisors and Titles:

Professor Adel F. Sarofim, Professor of Chemical Engineering

Professor Jack B. Howard, Professor of Chemical Engineering

Professor Glenn C. Williams, Professor of Chemical Engineering

Department of Chemical Engineering
Massachusetts Institute of Technology
Cambridge, Massachusetts   02139

January 1976

Professor Irving Kaplan
Secretary of the Faculty
Massachusetts Institute of Technology
Cambridge, Massachusetts 02139

Dear Professor Kaplan:

In accordance with the regulations of the faculty, I herewith submit a thesis entitled "The Behavior of Ash in Pulverized Coal under Simulated Combustion Conditions", in partial fulfillment of the requirements for the degree of Doctor of Science in Chemical Engineering at the Massachusetts Institute of Technology.

Respectfully submitted,
Signature Redacted

Ashok S. Padia

ACKNOWLEDGEMENTS

I wish to express my deepest gratitude to my thesis supervisors, Professor A.F.Sarofim, Professor J.B.Howard and Professor G.C.Williams. Their invaluable contributions and continued encouragement are most appreciated. Thanks are also due to Professor J.F.Elliott and Professor H.C.Hottel for their valuable comments and suggestions during committee meetings.

The Office of Coal Research made funds available for this research. Their support is gratefully acknowledged.

Professor J. P. Longwell first introduced me to low temperature ashing technique, for which I am extremely grateful. Thanks are due to Professor C. Hamrin of the University of Kentucky for providing me with low temperature ash samples of our coals and due to LFE Corporation, Waltham, Massachusetts, for letting me use their low temperature asher. I am grateful also to Professor R.E. Ogilvie, Dr. Kaplesh Kumar and Joe Adario of the Department of Metallurgy for their assistance on x-ray diffraction studies. Leonard Suddenfield and Dr. Allen Parks are acknowledged for their assistance in scanning electron microscopy and electron microprobing, respectively. Thermosystem Incorporation demonstrated their laser doppler anemometer which made it possible to measure particle velocities. Their courtesy is sincerely appreciated.

Dedicated to my family

TABLE OF CONTENTS

LIST OF FIGURES

LIST OF TABLES

Chapter 1

SUMMARY

1.1 Introduction

1.1.1 Background and Motivation

Coals invariably contain mineral matter varying widely in amount and composition between different deposits. Although some of this mineral matter can be separated from the coals by crushing and flotation, a significant amount, of the order of 10 percent by weight of an average U. S. coal is finely distributed throughout the carbonaceous coal matrix. The finely distributed matter is present as inclusions, having characteristic dimensions of 1 to 4 μm, in the coal and must be removed either in the process of coal conversion to alternative fuels or, in the case of combustion, from the exhaust products.

This study is concerned with the physical and chemical behavior of the mineral matter in pulverized coal during combustion. More specifically, the determination of the effects of combustion conditions on the particle size distribution, the thermal decomposition, the vaporization, and the reaction with each other and the supporting carbonaceous matrix of the ashed mineral constituents. The information to be gained from this study is of potential value for purposes of evaluating the (i) contribution by ash to emissivity of coal combustion products (ii) ease of separation of ash from combustion products (iii) vapor-

ization and subsequent condensation as submicron particles of the ash constituents, and (iv) erosion and corrosion by slag deposits formed by the ash.

1.1.2 Previous Studies

Although the mineral matter in coal and its behavior on heating has been the subject of extensive studies, the information gathered bears only indirectly on the objectives of this investigation. The mineral matter in selected coals has been studied by, amongst others, Selvig and Gibson (1956), Brown and Swaine (1964), Kemezys and Taylor (1964), Gluskoter (1967), O'Gorman and Walker (1971) and Littlejohn (1966). The results of these studies are difficult to generalize because of the variability of the mineral matter in coal and are not directly applicable to the present investigation for which interest is restricted to the portion of the mineral constituent that is carried to a combustor with pulverized coal (i.e., excluding mineral matter removed during pulverized coal feed preparation). The behavior on heating of the mineral matter in coal has been studied by, amongst others, O'Gorman and Walker (1971), Mitchell and Gluskoter (1975), Rost and Ney (1956), Sinaiski et. al. (1964). Most of these studies have been carried out by heating ash in crucibles to various prescribed temperatures. Although providing val-

uable insight on the chemical behavior of the mineral mat-
ter at high temperatures, these studies do not simulate
the rapid heating encountered in pulverized coal combustion,
do not allow for the reactions that may occur in coal
between the mineral matter and the carbonaceous matrix,
and provide no information on the changes in particle
size distribution of the mineral matter that occurs
during coal combustion.

1.1.3 Method of Approach

The novel aspect of the present study is in the
examination of the details of both physical and chemical
transformations of mineral matter under simulated combus-
tion conditions. To provide a starting point the miner-
al matter in the coals studied was characterized both
physically and chemically. The physical and chemical
transformations of the mineral matter were then determined
by collecting the ash produced by the combustion of coal
in a laboratory furnace operated over a wide range
of temperatures, covering the range of interest in prac-
tical combustors. In order to identify the reactions
between the mineral matter and the carbonaceous matrix,
complementary studies were performed heating coal and
ashed coal over the same temperature range in both
oxidizing and reducing conditions. The equipment and
procedures used are described below:

1.2 Apparatus and Procedure

1.2.1 Mineral Matter Characterization

The distribution of the mineral matter in the coal was determined by the microscopic examination of sections of coal particles, and the determination of the composition of individual particles using an electron microprobe. The complete characterization of the mineral matter was obtained by use of low temperature ashing to remove the carbonaceous matrix, followed by the determination of the particle size distribution of the dominant mineral constituents of coal using a combination of crystal structure and energy dispersive x-ray analysis (EDXRA) for identification.

1.2.2 Drop-tube Furnace

In pulverized coal flames, coal particles are heated up to peak furnace temperatures (1500° K to 2700° K, depending on coal type and application) at rates of 10^5 to 10^6 °C/sec. The experimental furnace used to simulate these conditions is shown in Fig. 1.1. The furnace, an Astro Model 1000 A unit electrically heated with a graphite resistance heater, could be preheated to temperatures up to 2250° K with a graphite maffle tube or 1830° K with an alumina muffle tube. The inner diameter of the muffle tube is 4.5 cm. For the simulated combustion experiments.the furnace was purged continuously with air supplied at a rate of 1000 to 2000 cc/minute.

Coal Particles
and Carrier Gas

Main Gas

Honeycomb
Flow Straightener

Water Cooled
Particle Injector

Graphite
Heating
Element

Alumina
Muffle
Tube

6"
Hot
Zone

Alumina
Liner Tube
To Support
Honeycomb

Water
Cooled
Shell

Cooling
Section

Water Out

Particle Collecting
Porous Bronze Disc

Water In

Optical Grade Quartz
Plate

Vacuum
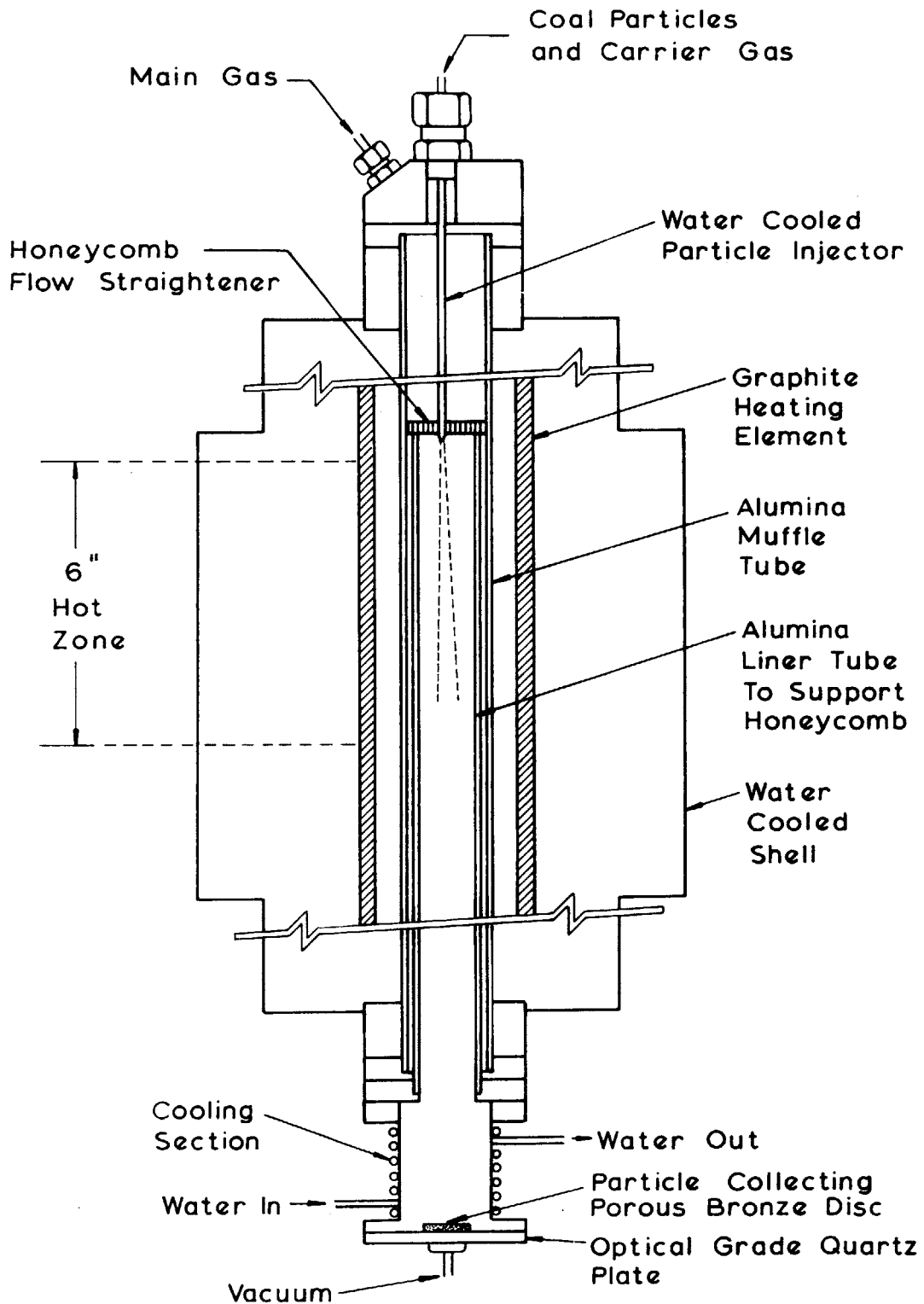
Figure 1.1 Schematic of the Free Fall Furnace

An alumina honeycomb was used to distribute the air across the cross-section of the furnace. Coal was injected at rates of about 0.1 gm/minute in a small air stream (about 2cc/min) by use of a partially fluidized, vibrating, vertical, water-cooled coal feeder. A narrow injector (2 mm I.D.) was used in order to obtain rapid-heating (10^5 to 10^6 °C/sec) of the coal/air stream by the surrounding hot air stream. The ash or partially burned coal particles were cooled by passage through a water-cooled section at the bottom of the furnace and then collected on a filter consisting of a sintered bronze disc placed between two fiberglass matts. The velocity of the particles was determined for selected conditions using a TSI laser-doppler anemometer. Axial and radial temperature profiles were determined by thermocouple traverses. The test-section, consisting of a 15 cm length of furnace below the coal injection point, was essentially isothermal. The residence-time of the particles in the hot zone of the furnace was about 1 second. The experimental conditions for the simulated combustor tests are summatized in Table 1.1.

1.2.3 Crucible Experiments

Samples of ash or coal were also introduced into the furnace in crucibles which were raised into the hot zone from the bottom of the furnace. Crucible experi-

TABLE 1.1

EXPERIMENTAL CONDITIONS

Coals - Lignite and Bituminous

Sizes - (38-45)μm and (75-90)μm

Mode of Experiments - Free-Fall

Stoichiometry - $\phi \simeq 0.5$

Main Gas Velocity - $V_{main} \simeq 4$ cm/sec at furnace temperature

Carrier Gas Velocity - $V_{carrier} \simeq 30$ cm/sec, at furnace temperature

Coal Flow Rate - $\dot{m}_{coal} \equiv 0.1$ gm/minute

Furnace Tempera- ture (K)	Particle* Tempera- ture (K)	Average Velocity of Particles (cm/sec)**		Residence Time (sec) in 15 cm Hot Zone	
		(38-45)μm	(75-90)μm	(38-45)μm	(75-90)μm
1000	1360				
1250	1465				
1500	1640	18.9	21.6	0.79	0.6
1830	1910	20.8***		0.72	

* Particle temperature by L&N Optical Pyrometer, possible error $\pm$ 30°C

** Average velocity by TSI Laser Doppler Anemometer with lignite particle in inert atmosphere

*** Determined at 1860°K Furnace Wall Temperature

ments, although providing heating rates much lower than expected for pulverized coal flames, were useful for evaluating mechanisms. Experiments were run with (1) ash from an ASTM ashing experiment heated in an oxidizing atmosphere (2) coal in an oxidizing atmosphere, (3) ash in an inert atmosphere, (4) coal in an inert atmosphere followed by ashing of the char at ASTM conditions (750° C), (5) mixtures of silica and graphite.

1.2.4 Analysis

Ash weight losses were obtained directly or, in the case in which samples contained unburned carbon, after ashing at ASTM conditions. X-ray diffraction was used to provide qualitative information on the minerals present and their transformation. Physical changes in the ash and coal were obtained using a Cambridge Stereo-scan electronmicroscope, combined with EDXRA when identification of the elemental composition of the particles was desired. Particle size distributions were measured using a Zeiss semi-automatic particle counter. Quantitative elemental analysis was obtained by atomic-absorption spectrometery.

1.2.5 Coals Studied

A highly swelling Pittsburgh seam bituminous coal and a slightly swelling Montana lignite were studied. The coals were size graded to yield nominal 38-45 μm and

and 75-90 µm fractions. The particle size distribution
of the coals were fitted by a Rosin-Rammler distribution
(Figure 1.2). The increase in the fitted coefficient
s above the value of 1.5 expected for a typical pulver-
ized coal provides a measure of the efficiency of the
size-fractionation. The size parameter, ultimate
analysis, proximate analysis, and oxide analyses for the
coals studied are summarized in Table 1.2

1.3 Results

1.3.1 Characterization of the Mineral Matter in Pulverized Coal

Microscipic examination of sections of pul-
verized coal (Fig. 1.3) indicate that the mineral mat-
ter is distributed as small separate inclusions in the
coal matrix. Electron microprobe analysis of some of the
inclusions (Table 1.3) indicate that the inclusions are
highly variable in chemical composition. A more quanti-
tative characterization is obtained by separating the
mineral matter in an essentially unaltered form by low
temperature (100-200° C) ashing (Gluskoter, 1965). The
particle size distribution of the mineral matter can then
be inferred using electronmicroscopy and the mineral
compositions from their crystal structure and by x-ray
diffraction (using CuKα, λ = 1.5404 A° radiation).

BIT (38-45) μm Raw Coal
Frequency Distribution
▲ — Data Points
—— Curve by Rosin - Rammler   Fit with S = 4
      X = 42 μm Obtained from Cumulative Plot
Rosin - Rammler Relation
Cumulative = R = 1 - exp $[-(X/X')^S]$
Frequency = $f(x) = \dfrac{dR}{dX} = bs(X)^{S-1}$ exp $[-bX^S]$;
      $b = (\dfrac{1}{X'})^{S'}$

BIT (38-45) μm Raw
Coal
Rosin Rammler Plot
X': 42.0 μm
S = 4
Cummulative
Distribution
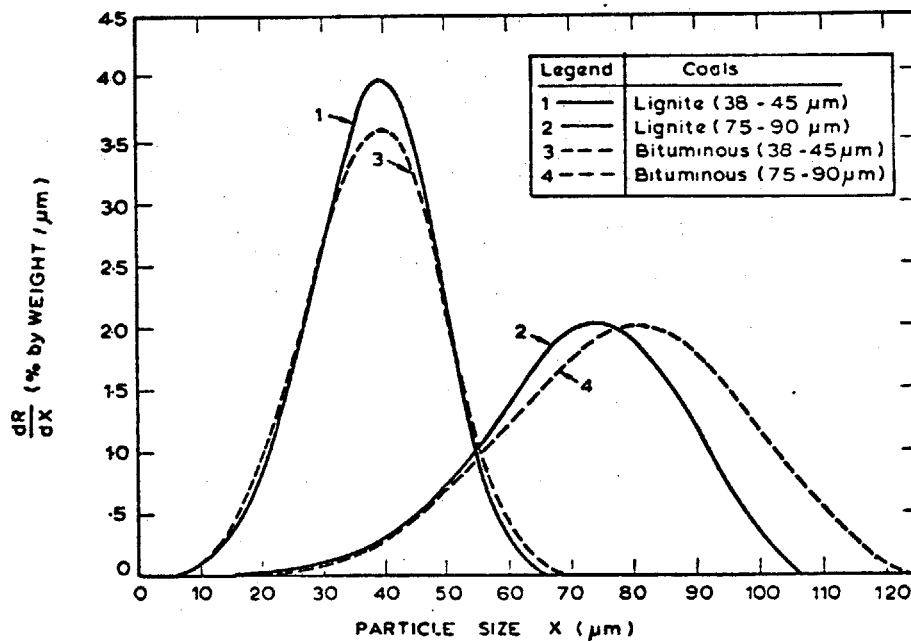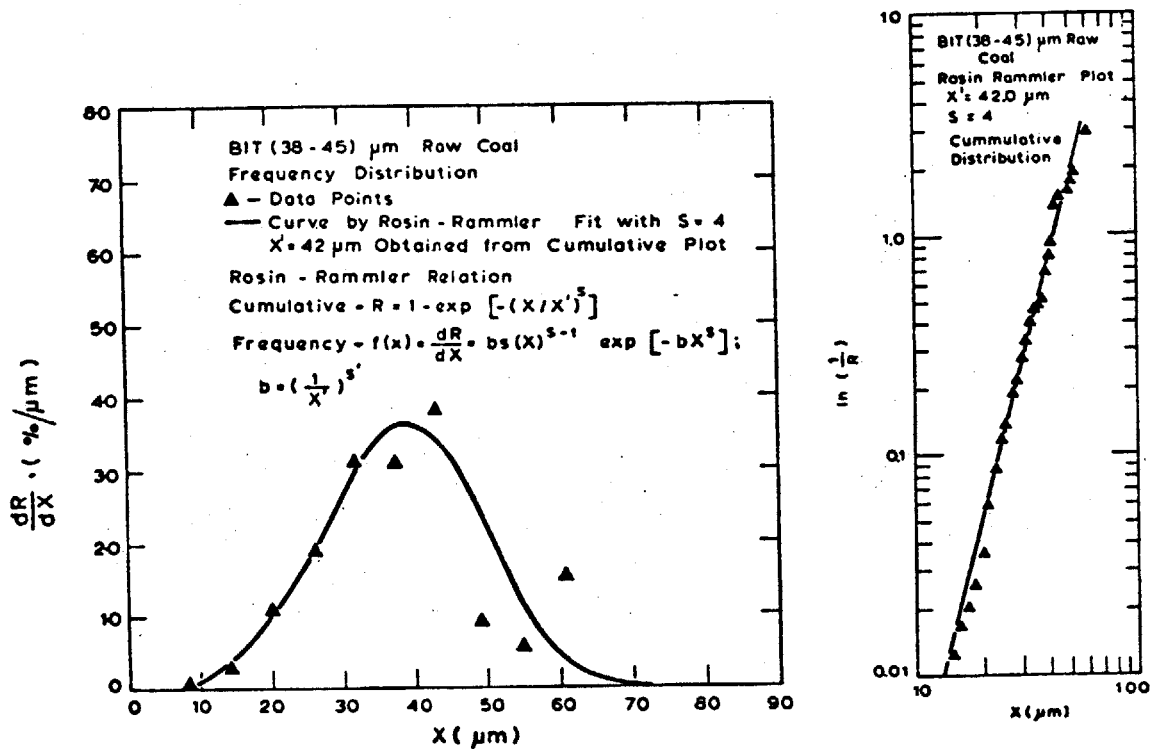
Figure 1.2 Partcle Size Distribution of Pulverized
Coals using Rosin Rammler Function

TABLE 1.2

PROPERTIES OF THE COALS USED

A. Size Distribution

[Rosin Rammler: $R=1-\exp[-(x/x')^S]$]

Coal ⟶	LIGNITE		BITUMINOUS	
Size ⟶	38-45μm	75-90μm	38-45μm	75-90μm
x' (μm)	41.6	77.4	42.0	85.2
S	4.3	5.2	4.0	4.6

B. Ultimate and Proximate Analysis

Moisture	13.63	13.37	2.22	2.24
Carbon	55.21	56.70	67.80	66.29
Hydrogen	4.93	5.17	5.00	4.94
Nitrogen	0.61	0.62	1.05	1.01
Chlorine	<0.01	<0.01	0.07	0.04
Sulfur - pyritic	0.15	0.16	2.51	2.58
sulfate	0.06	0.06	0.69	0.71
organic	0.61	0.63	1.63	1.66
Total	0.82	0.85	4.83	4.95
Ash	7.85	7.04	10.55	11.57
Oxygen (by diff.)	16.95	16.25	8.49	8.96
ASTM Volatile Matter	36.00	36.81	38.42	38.55

(All numbers are % of original coal)

C. Analysis of the Major Oxides

SiO_2	26.80	21.69	37.52	36.15
Al_2O_3	16.41	16.33	19.15	19.12
Fe_2O_3	3.41	4.07	29.34	28.87
CaO	28.44	31.95	4.65	5.36
MgO	9.02	9.68	0.73	0.73
SO_3	13.45	13.48	4.10	4.10

(All numbers are % by weight of dried ASTM ash)
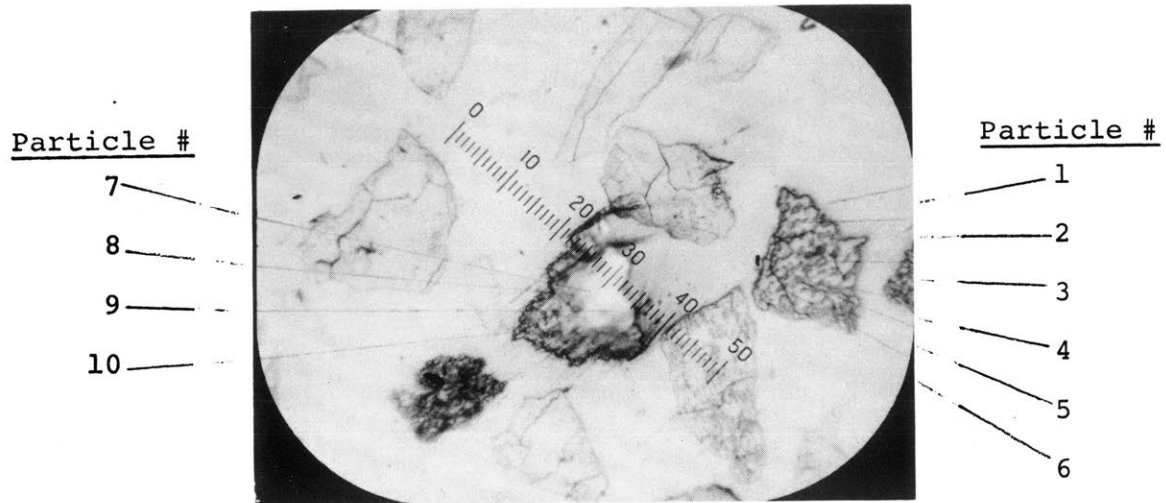
100 µm

Distribution of Ash in (75-90 µm) Bituminous Coal Particles. Center particle shows basically FeS_2 (white shiny); particle on the right hand side shows islands of kaolinite type structure.

Figure 1.3

TABLE 1.3 Analyses of Inclusions of Mineral

Matter on Coal Cross-Section in

Figure 1.3, as obtained by electron-

microprobing

a) "Silica-Aluminate" Particles

Particle Number	SiO_2	Al_2O_3	FeO	CaO	MgO	K_2O	Total	SiO_2/Al_2O_3
1	42.88	36.16	0.45	0.11	0.10	0.01	79.71	1.19
2	41.37	34.59	0.51	0.07	0.10	0.00	76.64	1.20
3	51.55	26.23	0.61	0.13	0.70	1.83	81.05	1.95
4	57.74	11.79	0.92	2.31	0.97	14.34	88.07	4.90
5	34.92	27.82	2.54	8.34	2.65	0.21	76.48	1.26
6	2.51	96.17	0.0	1.39	0.0	0.0	100.07	0.03

b) "Pyritic" Particles

								Fe Cal'd as FeS_2 (%)
7	0.07	0.00	55.57	0.05	0.04	0.00	55.73	92.88
8	0.27	0.18	57.75	0.24	0.11	0.11	58.66	96.52
9	0.33	0.29	56.07	0.24	0.14	0.13	57.20	93.71
10	0.97	3.31	54.20	0.29	0.23	0.20	59.20	90.59

All numbers are percent by weight of the inclusion under analysis.

The minerals identified in the lignite samples were mainly kaolinite [$Al_2Si_2O_5(OH)_4$], bassanite [$CaSO_4 \cdot \frac{1}{2}H_2O$], lawsonite [$CaAl_2SiO_4 \cdot 2H_2O$], quartz [$SiO_2$], dolomite [$CaMg(CO_3)_2$] and rutile [$TiO_2$]. The minerals identified in the bituminous coal were kaolinite, illite [$K_{1-1.5}Al_{5-5.6}Si_{6.5-7}O_{20}(OH)_4$], quartz, pyrite [$FeS_2$], coquimbite [$Fe_2(SO_4)_3 \cdot 9H_2O$], calcite [$CaCO_3$] and anhydrite [$CaSO_4$]. The three major components by weight in the mineral matter are kaolinite, a mixture of calcium carbonate and sulfate and pyrites, represen- tative electronmicrographs of which are shown in Figures 1.4, 1.5 and 1.6. Particle size distributions are shown in Figure 1.7. The overall particle size distribution can be obtained from these by assuming that the mineral matter in bituminous coal is approximately 50% kaolinite, 40% pyrite and 10% calcium sulfate and carbonate and that in lignite, it is 50% kaolinite, 10% pyrite and 40% calcium sulfate and carbonate. The mass median size of the mineral matter is found to be about 2 μm for both coals. The two size fractions of each coal gave essential- ly the same particle size distribution. This is consis- tent with the expectation that the distribution of mineral matter in pulverized coal will be independent of the coal particle size, as long as the coal particle size is much larger than that of the dispersed mineral matter i.e. much larger than 2 μm. Littlejohn (1966) has report- ed that the fraction of mineral matter in coal is higher

.A. Variety of Kaolin Type Mineral Particles Showing
Varying Composition of Si and Al

.B. EDXRA of Particles Encircled in Fig. A.

Typical Sample of LTA of Bituminous Coal

Figure 1.4

.A.1 A variety of Mineral Particles (5-7 μm) of
Widely Varying Composition

.A.2 The Circled Group of Particles in A at Higher
Magnification

Fig. B. B.   EDXRA of Fig. A.2 at Two
Locations

Sulfate and Carbonates in LTA of Bituminous (38-45 μm) Coal

Figure 1.5

A. 1. Variety of Mineral Particles Showing Varying
Composition.

A.2. The Circled Group in A.1 at Higher Magnification.
Crystals are pyritohedron, octahedron or combinations.

B. EDXRA of Fig. A.2.

Typical Pyrites in LTA of (75-90) μm Bituminous Coal

Figure 1.6

Rosin - Rammler Relation

$$\frac{dR}{dX} = 100\,bs\ X^{S-1}\exp(-bx^S)$$

$$b = (1/X')^S$$
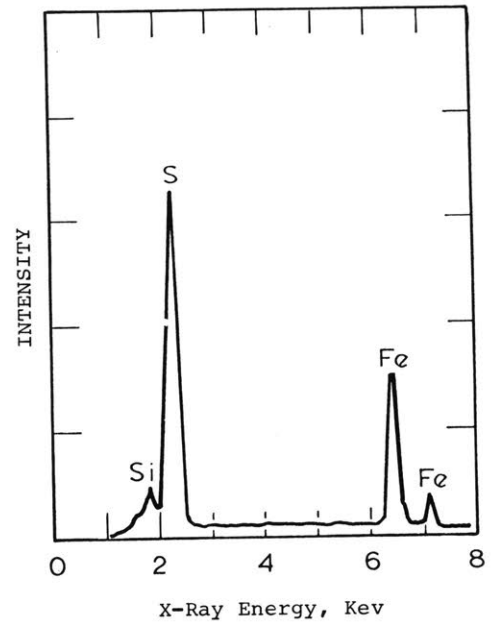
Species	Xmed (μm)	X' (μm)	s	b
1 Kaolinite	2.21	2.40	4.10	0.0276
2 Pyrites	1.224	1.31	4.64	0.2857
3 Sulfate Carbonate	1.98	2.18	4.00	0.0443

	Bituminous	Lignite
X' (μm)	1.90	2.20
Xmed (μm)	1.68	1.98
S	2.99	3.56

FREQUENCY DISTRIBUTION OF MINERAL MATTER IN COAL

Figure 1.7

at the low end of the particle size distribution, which
would be enriched by micron-sized ash. For the larger
size coal fractions of this study, there is not a con-
sistent trend in variation of mineral matter with coal
size (Table 1.2).

The mineral matter in coal undergoes both chemical
and physical changes as the coal is heated in either
inert or oxidizing atmospheres. The chemical transfor-
mations include thermal decomposition, the reaction of
the mineral matter with coal and the interaction of
different mineral constituents. The physical changes
include fusion, agglomeration and vaporization. Although
chemical and physical changes take place simultaneously,
they will be discussed separately with appropriate cross-
referencing.

1.3.2 Chemical Transformations

The reactions that the principal mineral
constituents undergo under oxidizing conditions and the
approximate reaction temperatures are summarized in
Table 1.4. Evidence that these reactions occur is pro-
vided by both the weight loss of the mineral matter in
coal and changes in x-ray diffraction patterns of the
mineral matter. A measure of the thermal decomposition
and oxidation reactions of the mineral matter in coal
oxidized at different furnace temperatures is provided

by the x-ray diffraction of the ash product. From the
disappearance and appearance of peaks in Figures 1.8
and 1.9, the following features may be noted: pyrites
(P) in oxidized to hematite (H) at relatively low temp-
eratures; $CaSO_4$ persists as anhydrite (A) up to a furnace
temperature of 1500° K; the decomposition of dolomite (D)
leads to the formation of magnesium oxide (MgO) and cal-
cium oxide (Li); the decomposition of calcite (C) leads
to the formation of calcium oxide (Li). The discussion,
so far, has assumed that the different mineral consti-
tuents act independently. An indication of agglomeration
of the ash is the appearance of the peaks of composite
minerals such as gehlenite (G) and anorthite (An) and the
increasing amorphous nature of the ash as evidenced by
the increase in the background radiation. In interpreting
the x-ray diffraction patterns it should be noted that
the measurements were made on samples that were cooled to
ambient temperatures and that the patterns reflect the
effects of both the reactions at high temperature and
phase changes occuring during cooling. A more quantita-
tive measure of the chemical reactions occuring is pro-
vided by the weight loss of the ash.

Under ASTM ashing conditions (oxidizing conditions
at 750° C) an asymptotic weight loss corresponding to
approximately 30 percent of the mineral matter is observed.
This weight loss is in good agreement with that calculated
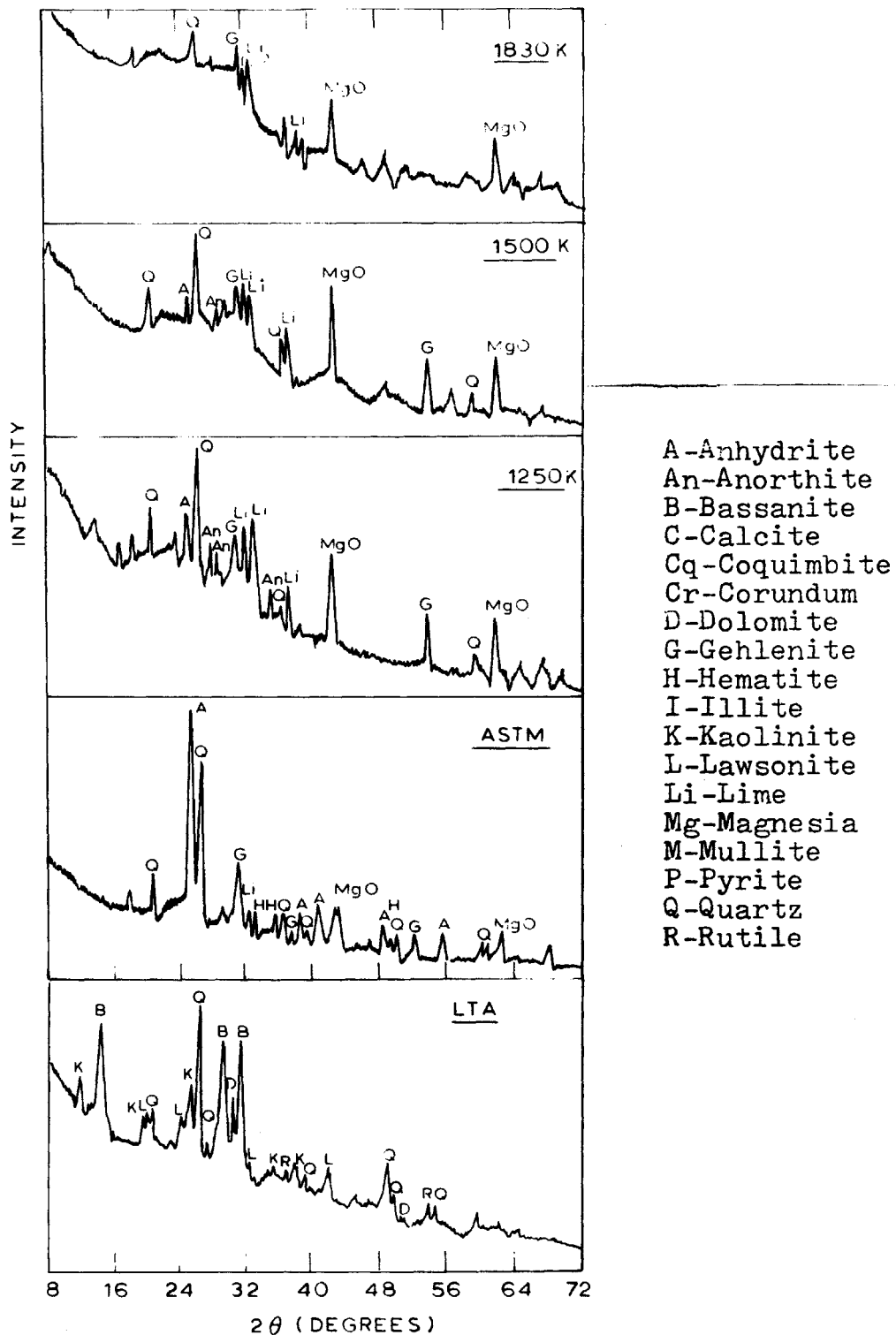
Figure 1.8

Diffraction Patterns Showing the Effect of
Temperature on Mineral Phases for Lignite
(38-45 μm)

A-Anhydrite
An-Anorthite
B-Bassanite
C-Calcite
Cq-Coquimbite
Cr-Corundum
D-Dolomite
G-Gehlenite
H-Hematite
I-Illite
K-Kaolinite
L-Lawsonite
Li-Lime
Mg-Magnesia
M-Mullite
P-Pyrite
Q-Quartz
R-Rutile
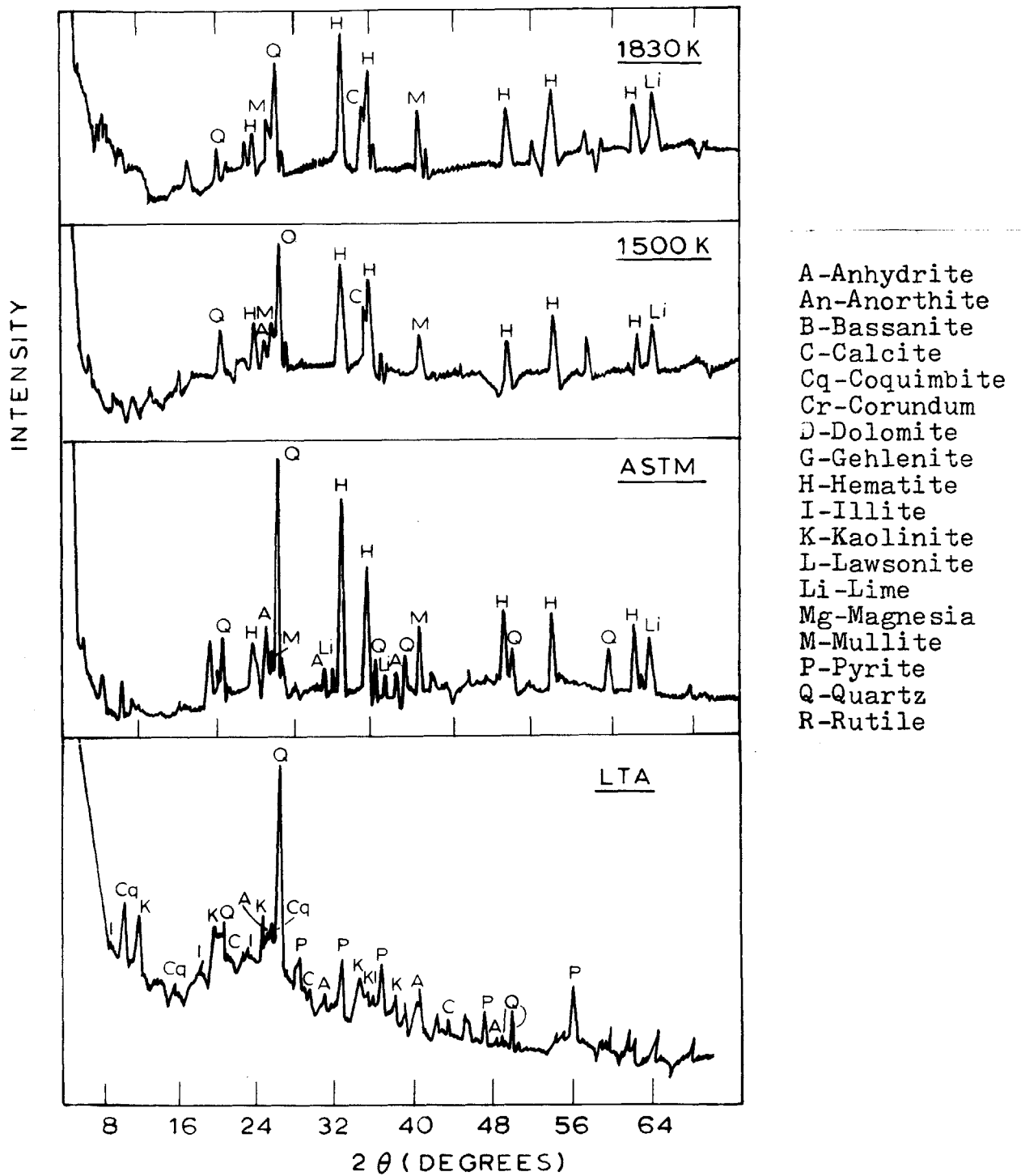
Figure 1.9

Diffraction Patterns Showing the Effect of
Temperature on Mineral Phases for Bituminous (38 - 45 μm) Coal

from the reactions in Table 1.4, after correction has been made for the fact that part of the sulfur (about 50 percent for thelignite and 4 percent for the bituminous coal) is retained by the ash principally in the form of calcium sulfate. The high percentage retention of sulfur in the lignite ash is consistent with the high calcium content of lignite and the thermodynamic stability of $CaSO_4$ at ASTM temperatures. A material balance on the ash constituents with allowance for sulfur retention yields the following relation between mineral matter and ash content.

$$M.M. = ASH + 0.625 \; S_{PYR \atop COAL} + 0.833 \left[S_{SULF \atop COAL} - S_{SULF \atop COAL} \frac{ASH}{100} \right]$$

$$+ \frac{ASH}{100} \left[0.162(SiO_2 + Al_2O_3)_{ASH} + 0.79 \; CaO_{ASH} \right.$$

$$\left. + 1.1 \; MgO_{ASH} \right] \qquad\qquad (1.1)$$

The coefficients in the equation are readily identified with the weight losses of the reactions in Table 1.4. Equation (1.1) yields values for the weight of mineral matter of 11.3% for 75-90 μm lignite, 12.9% for 38-45 μm lignite, 15.9% for 75-90 μm bituminous, and 14.3% for 38-45 μm bituminous coal in fair agreement with values of 11.5, 13.3, 18.1 and 15.6% measured by use of low-temperature ashing.

Completion of the decomposition reactions is expected

TABLE 1.4 Principal Reactions that Mineral Matter

Undergoes Under Oxidizing Conditions

	Mineral Matter Species	Reaction	Approx. Reaction Temp. (°C)	ASTM Ash Species	Weight Loss % of MM Specie	Weight Loss % of ASTM Ash Specie
1	Kaolinite $Al_2Si_2O_5(OH)_4$	$Al_2Si_2O_5(OH)_4 \rightarrow Al_2O_3 \cdot 2SiO_2 + 2H_2O$ $\downarrow$ $Al_2O_3 + 2SiO_2$ (14%) $Al_2O_3 + 2SiO_2$ (86%)	550-600	$Al_2O_3 + 2SiO_2$	14% of Kaolinite	16.2% of $(SiO_2 + Al_2O_3)$
2	Pyrite FeS_2	$2FeS_2 + 3.5 O_2 \rightarrow Fe_2O_3 + 2SO_2$ (sulfur=128) (oxygen=48)	500	Fe_2O_3	33% of FeS_2 or 62.5% of Pyritic Sulfur in Coal	50% of Fe_2O_3
3	Sulfates $CaSO_4$ $MgSO_4$ $Fe_2(SO_4)_3$	$CaSO_4 \rightarrow CaO + SO_3$ $MgSO_4 \rightarrow MgO + SO_3$ $Fe_2(SO_4)_3 \rightarrow Fe_2O_3 + 3SO_3$ $SO_4 = 96$ $SO_3 = 80$	1450 1000 600	CaO MgO Fe_2O_3	83.3% of Sulfate Sulfur in Coal	
4	Carbonates $CaCO_3$ $CaMg(CO_3)_2$	$CaCO_3 \rightarrow CaO + CO_2$ $CaMg(CO_3)_2 \rightarrow CaO + MgO + 2CO_2$	710-950 740-800	CaO MgO,CaO	44% of $CaCO_3$ 48% of dolomite	79% of CaO 110% of MgO

in the long-times associated with the ASTM ashing
experiments. The weight of ash obtained under the short
duration ($\sim$ 1 sec) simulated combustion conditions for
furnace temperatures ranging from ASTM values up to
1830° K was always less than that obtained in the ASTM
experiments suggesting that kinetics of mineral decompo-
sition are not controlling. The increments in measured
ash loss with increasing temperature can be explained
by the decomposition of $CaSO_4$ (the major source of
incremental loss for lignite ash), the vaporization of
silica and minor oxides. Weight losses due to these
sources were computed from the chemical analysis of the
ash and are found to be in good agreement with the mea-
sured value (Figure 1.10). Thermodynamic constraints
again determine the extent of $CaSO_4$ decomposition. Com-
putations of the extent of decomposition for free-fall
experiments (which could be approximated by a closed
system) are compared with the measured decomposition in
Figure 1.11. It should be noted that fair agreement
between calculated and measured values is obtained only
when allowance is made for the measured difference be-
tween the particle and furnace temperature. Losses of
silica of about 1-4% observed in the free fall experi-
ments are believed to be due to the formation of the
volatile SiO by SiO_2-C reactions such as
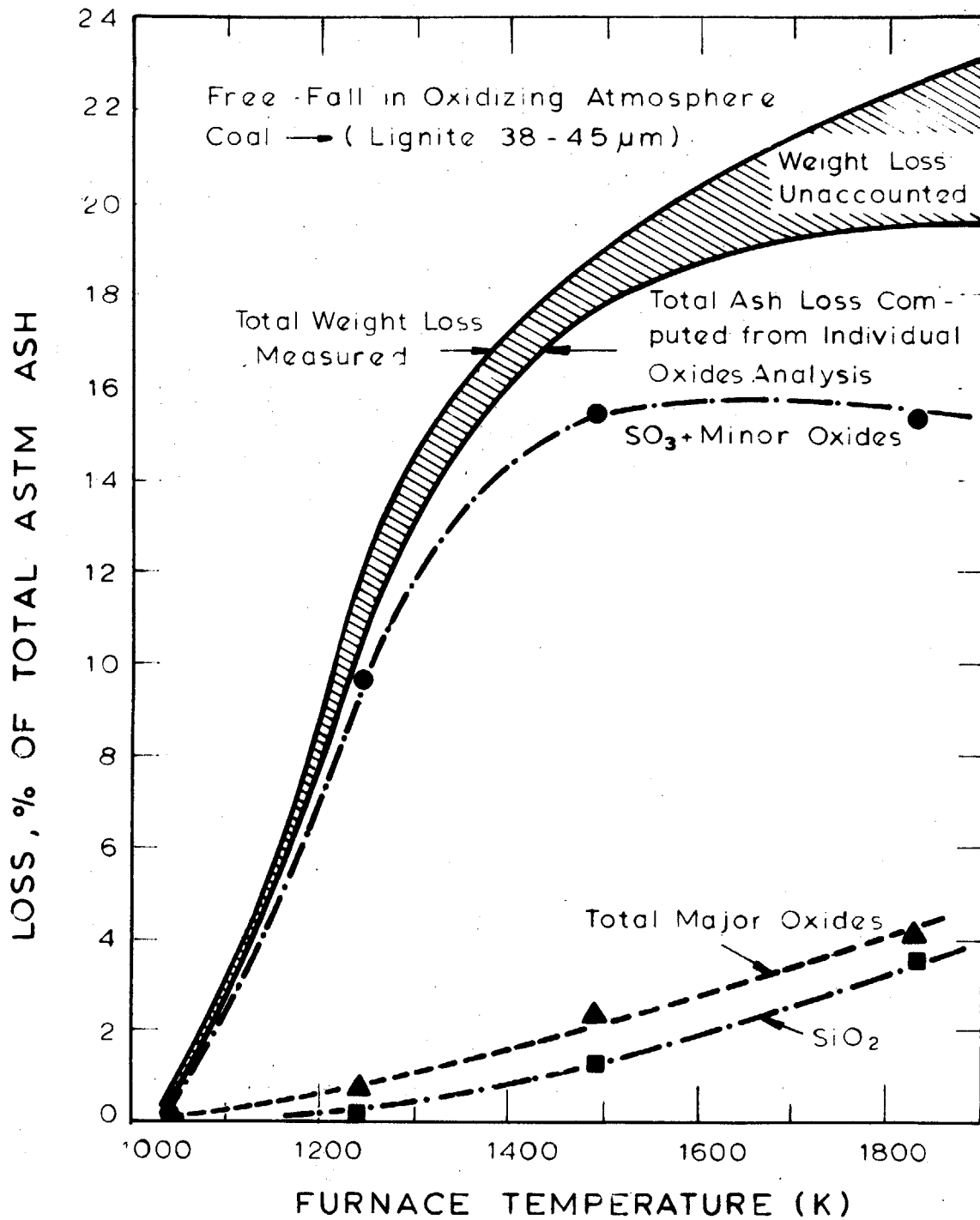
Figure 1.10 Weight Loss of ASTM Ash for Lignite
upto 1830 K
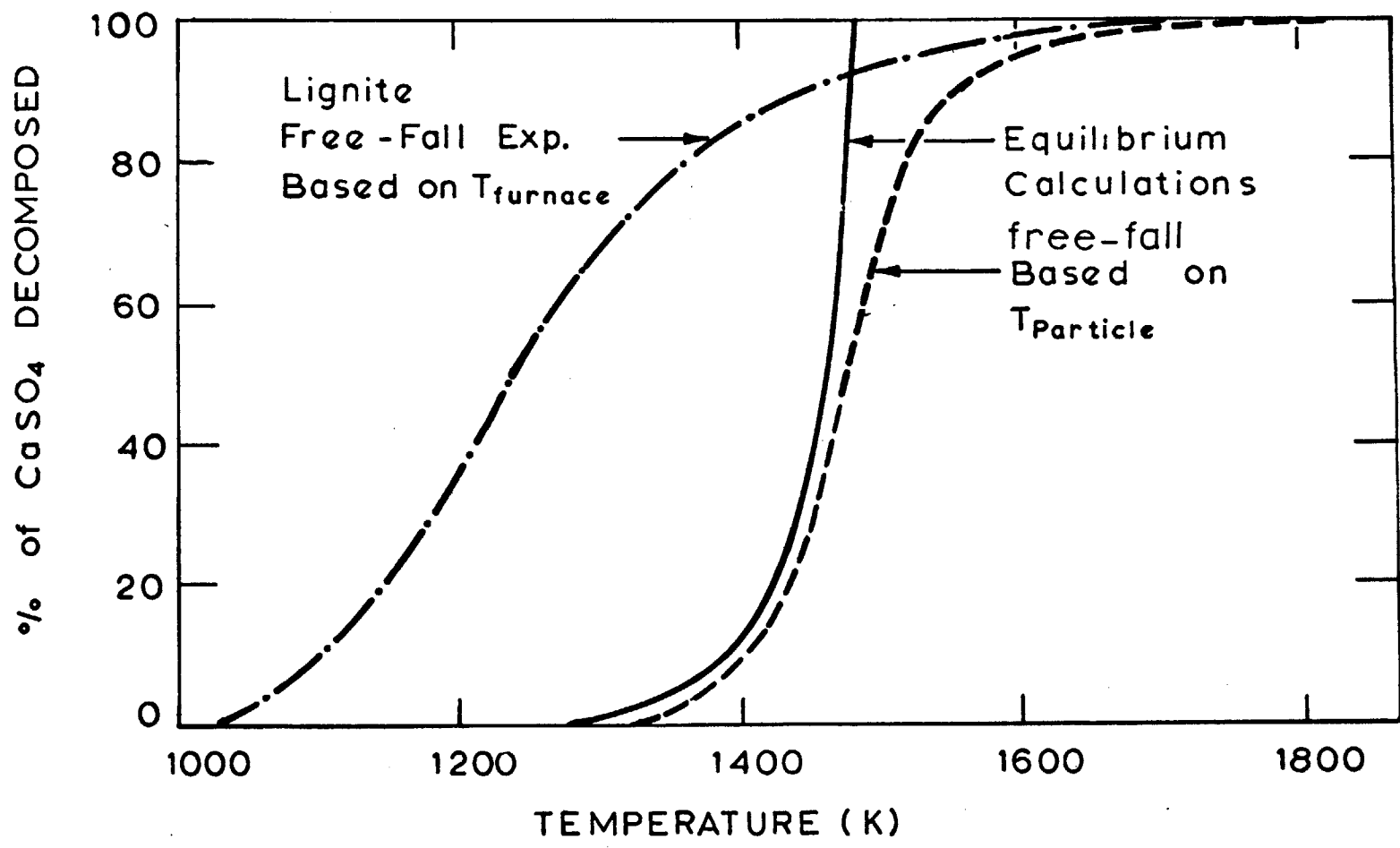
CaSO$_4$ Decomposition as a Function of Temperature for Lignite for Free Fall Experiments

Figure 1.11

$$SiO_2 \text{ (s)} + C \text{ (s)} \rightleftarrows SiO \text{ (g)} + SO \text{ (g)} \qquad (1.3)$$
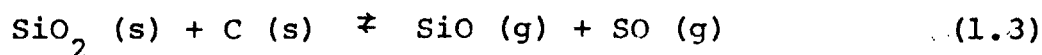
The vapor pressure of SiO_2 and the equilibrium concentration of SiO formed by the decomposition reaction (1.4)

$$SiO_2 \text{ (1)} \rightleftarrows SiO \text{ (g)} + \frac{1}{2} O_2 \text{ (g)} \qquad (1.4)$$
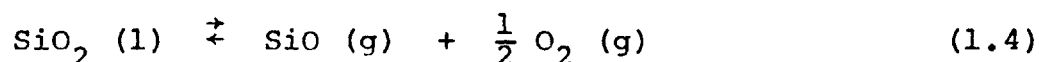
are too small ($< 10^{-5}$ mm Hg) to account for the observed weight loss of silica.

The reaction of SiO_2 with carbon to form SiO is expected to become increasingly significant as the temperature is increased above the 1830° K limit attainable when the present apparatus is operated under oxidizing conditions. In order to obtain insight on the reactions at higher temperature, mixtures of graphite and silica in a graphite crucible were heated in inert atmospheres up to 2250°K . The results of these experiments are summarized in Table 1.5. These show that 20 to 30% of the silica is converted to SiO at temperatures above 1967° K. At higher temperatures the residual silica is converted to silicon carbide. The reaction (1.5)

$$SiO_2 \text{ (1)} + 3C \text{ (s)} \rightleftarrows SiC \text{ (s)} + 2CO \text{ (g)} \qquad (1.5)$$
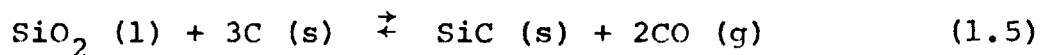
favors the formation of SiC at high temperatures and has been proposed as the kinetically favored reaction above

TABLE 1.5

RESULTS OF SILICA-GRAPHITE

HEATING EXPERIMENTS

Run No.	Temperature ($^{\circ}$K)	Time (min)	C/SiO_2 (Weight Ratio)	Absolute Loss of Silica Weight (%)	Fraction of Original Silica Converted to:	
					SiO	SiC
S1	2117	45	1.75	50.9	0.27	0.72
S2	2117	45	3.66	53.4	0.31	0.68
S3	2117	10	3.94	47.8	0.22	0.78
S4	2117	10	4.13	45.1	0.18	0.80
S5	2117	20	1.77	47.3	0.22	0.75
S6	2117	20	6.15	47.0	0.21	0.77
S11	2117	20	5.01	44.0	0.17	0.82
S12	2117	120	1.79	52.6	0.30	0.69
S13	2117	120	2.84	53.0	0.30	0.69
S14	2117	120	2.92	49.5	0.24	0.76
S15	2117	120	6.70	45.3	0.16	0.89
S16	2250	30	3.65	47.6	0.22	0.77
S17	2250	30	4.10	49.8	0.25	0.75
S18	1967	30	3.77	25.5	0.24	0.03
S19	1967	30	4.20	32.2	0.30	0.08

2000°K (Beecher and Rosenweig, 1961). It should be noted that the fractional conversion of SiO_2 to SiO and SiC reported here is biased by the experimental procedure; the crucibles were placed in position and the furnace heated to its final temperature over a period in about thirty minutes, a period long enough to permit partial vaporization of the silica to silicon monoxide during the transient heating period. Although these results are incomplete, they are of extreme significance since they indicate that the reactions of mineral and carbon can lead to augmentation of the vaporization of oxides with subsequent recondensation as submicron particles or on heat transfer surfaces. Experiments heating coal in inert atmosphere (Figures 1.12 and 1.13) also show higher weight losses than would be expected from the vapor pressures of the oxides suggesting a similar augmentation of losses by chemical reaction with carbon. It should be noted that such reactions are to be expected even in an oxidizing atmosphere since at high temperatures the reaction of coal is limited by diffusion of oxygen to the particle surface; within the coal particle reducing conditions will persist favoring the reduction of the oxides.

The oxidation history of a particle also influences the weight loss of the ash residue. The data on weight loss in Figures 1.12 and 1.13 were obtained by either
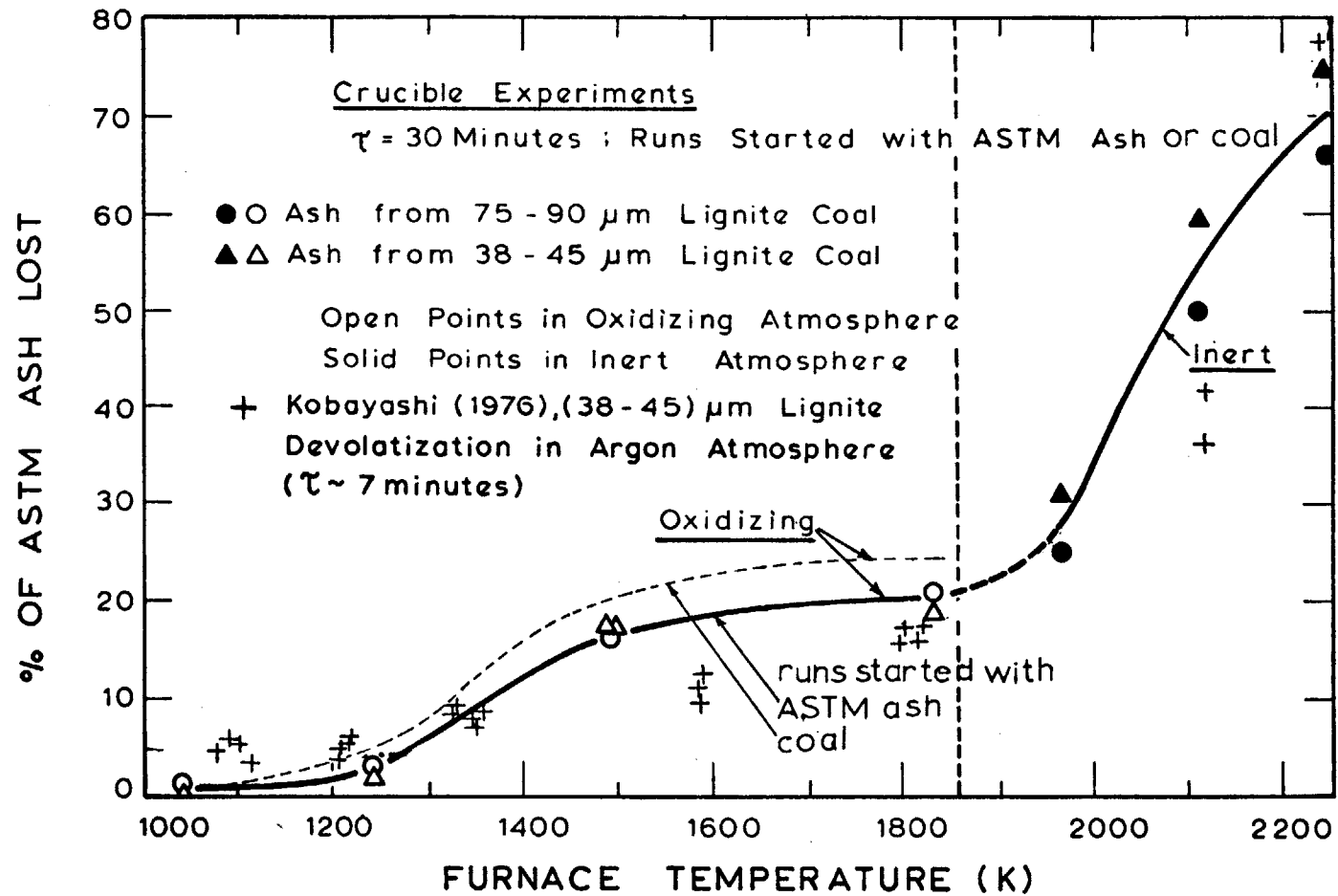
Effect of Temperature on Weight Loss of Lignite Ash up to 2250 K

Figure 1.12
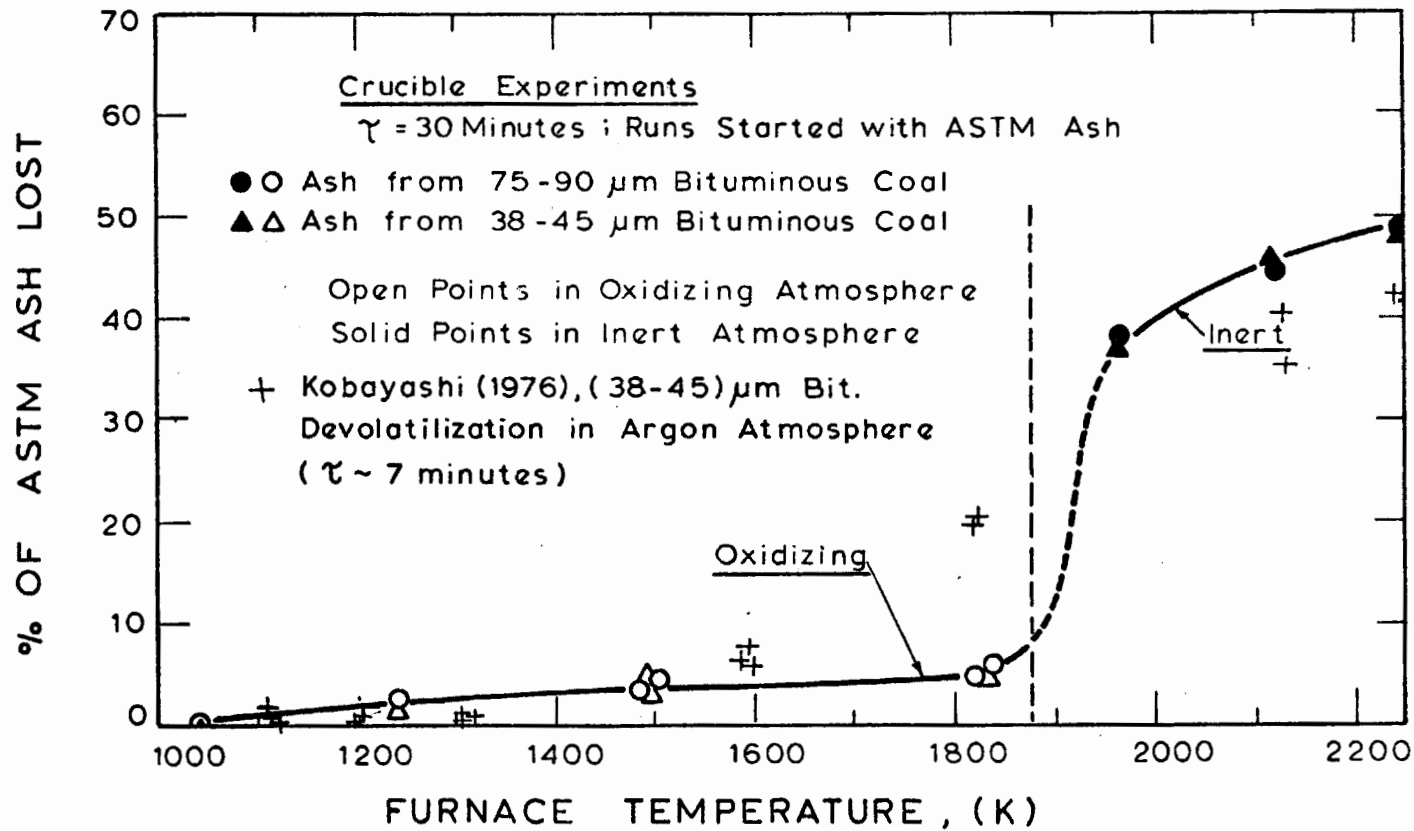
Effect of Temperature on Weight Loss of Bituminous Ash
Up to 2250 K

Figure 1.13

heating the coal in oxidizing atmosphere up to final
temperature or first heating the coal in an inert
atmosphere followed by ashing the residue at ASTM con-
ditions. The differences in weight losses for two sets
of conditions can be attributed to the decomposition of
pyrites and sublimation of sulfur under inert conditions
or the high temperature decomposition of $CaSO_4$ under
oxidizing conditions.

1.3.3 Physical Transformation

Inclusions of mineral matter in pulverized coal
may number several hundred to more than a thousand per par-
ticle for the coal types and sizes used in the present
study. This section examines the effect of combustion con-
ditions on the separation and agglomeration of the ash
particles formed by the mineral matter.

Tests on the devolatilization of pulverized coal par-
ticles in inert atmospheres indicate that negligible amounts
of the mineral matter is expelled with the volatile matter.
Although the bituminous coal particles swelled by factors
of four or more in linear dimensions during the devolatili-
zation process, the mineral matter was retained by the
carbonaceous matter forming the shell of the cenospheres
produced (Figure 1.14). The mineral matter is only exposed
when the carbonaceous matrix is oxidized away. At high
temperatures molten particles are formed which remain
attached to the receding carbonaceous surface (Fig. 1.15),

a   200 μm   b   c

Bituminous Coal (75-90) devolatilized in inert atmosphere, T = 1000 K
(Various types of cenospheres seen under reflected light)

Figure 1.14
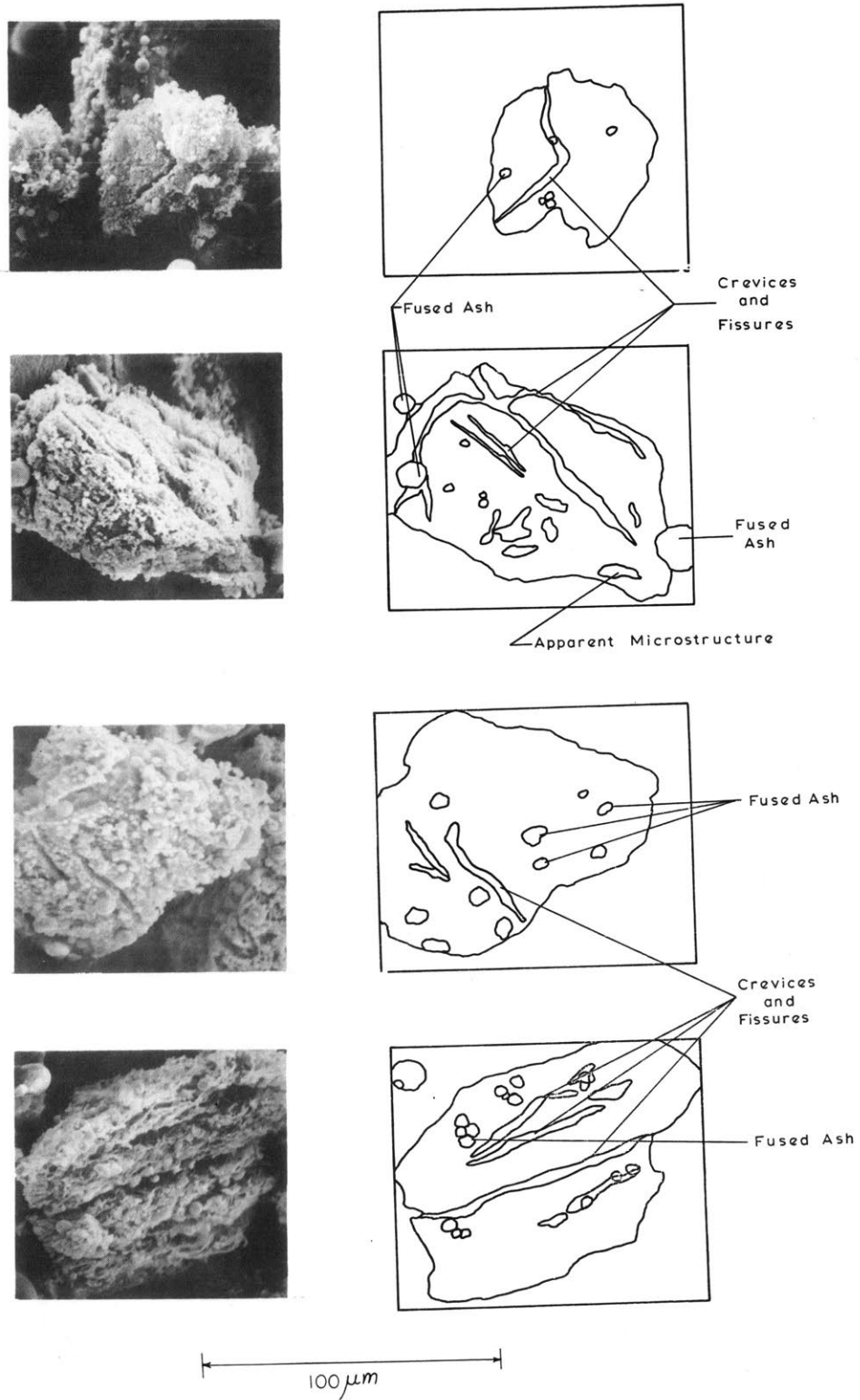
Fused Ash

Crevices and Fissures

Fused Ash

Apparent Microstructure

Fused Ash

Crevices and Fissures

Fused Ash

100 μm

Char Particles From LIGNITE (75-90) at 1830K Furnace Temperature Showing the Process of Fragmentation of Coal and Internal Agglomeration of Ash

Figure 1.15

probably by the ash surface tension. Even though molten ash does not appreciably wet carbon surface (Raask, 1966), only a slight wetting is needed to provide ash adherence since its surface tension is high (of the order of 320 dynes/cm (Raask, 1966)).*

As the carbon surface recedes the attached molten ash spheres are drawn together and agglomerate. If a coal particle retains its integrity up to the completion of combustion, a single ash particle will be produced per coal particle. If, however, the coal particle disintegrates during oxidation, the number of ash particles will be equal to that of the coal fragments produced.

The number of ash particles per coal particle produced under the simulated combustion conditions were obtained by density grading the ash particles and measuring the size distribution of the different density fractionation.

---

* The contact angle above which a particle of radius r, density ρ and surface tension σ is separated from a surface by gravitational forces is given by

$$\theta_c = \cos^{-1}(\frac{2r^2\rho g}{\sigma} - 1) \qquad (1.6)$$

For an ash particle 10μm in size, separation would require contact angle of 179.7°, an unreasonably high value.

The specific gravity distribution of the ash particles are shown in Figure 1.16. A significant fraction of the ash is considerably lighter than the original mineral matter (specific gravity $\simeq 3.5$). The low densities are a consequence of cenosphere formation, some of which are evident in the electron micrograph of the ash product (Figure 1.17). The data (Figure 1.16) show a marked peaking in the light density fraction of the ash at 1500°K. This can be rationalized by examination of the time constant for formation of cenospheres. The calculated times of formation of cenospheres of say 40μm starting with 12μm particles are of the order of 3×10^5 seconds at 1000°K, 4 seconds at 1200°K, 0.03 seconds at 1400°K and 0.002 seconds at 1600°K. This suggests that there is an optimum temperature of cenosphere formation between 1200°K and 1400°K below which the times of formation are too large and above which the gases evolved during decomposition would have ample time to escape from the molten ash.

The size distributions of particles after the fractions lighter than water has been removed are shown in Figures 1.18 and 1.19. These particles have a mean effective diameter that is insensitive to combustion temperature, but which is significantly smaller than the mean effective diameter that would result from the formation of a single ash particle per coal particle. It is estimated that about 3
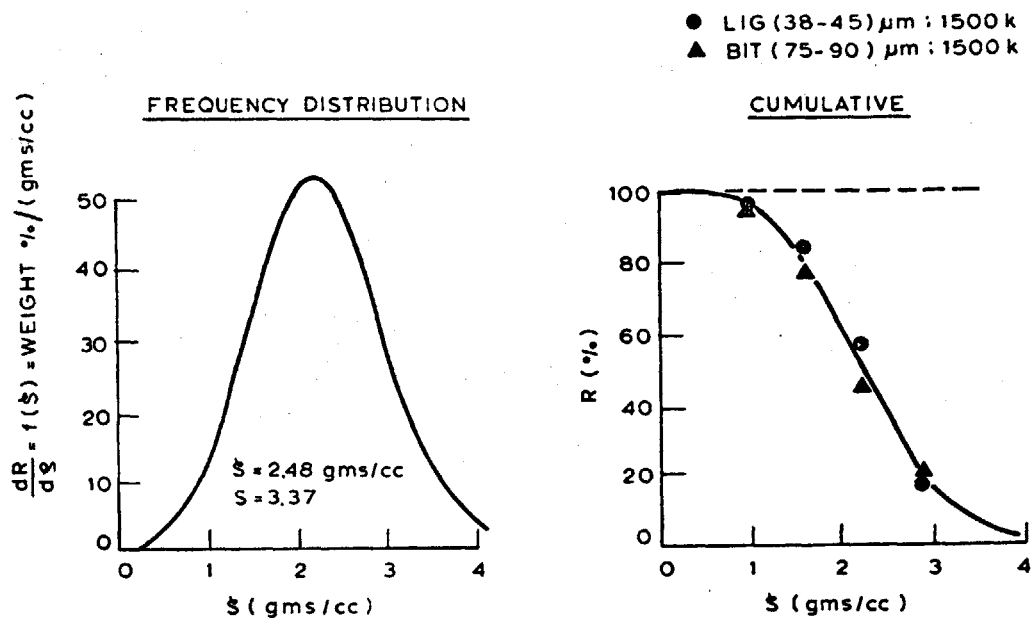
● LIG (38-45) µm : 1500 k
▲ BIT (75-90) µm : 1500 k

FREQUENCY DISTRIBUTION

CUMULATIVE

$\bar{S} = 2.48$ gms/cc
S = 3.37

1 Lig (38-45) and Bit (75-90) ; 1500 K
2 Bit (38-45) and Bit (75-90) ; 1830 K
3 Lig (38-45) and Lig (75-90) ; 1830 K
4 Lig (38-45) and Lig (75-90) : 1250 K

$$R = 100 \exp\left[-\left(\frac{\bar{S}}{\bar{S}}\right)^{S}\right]$$
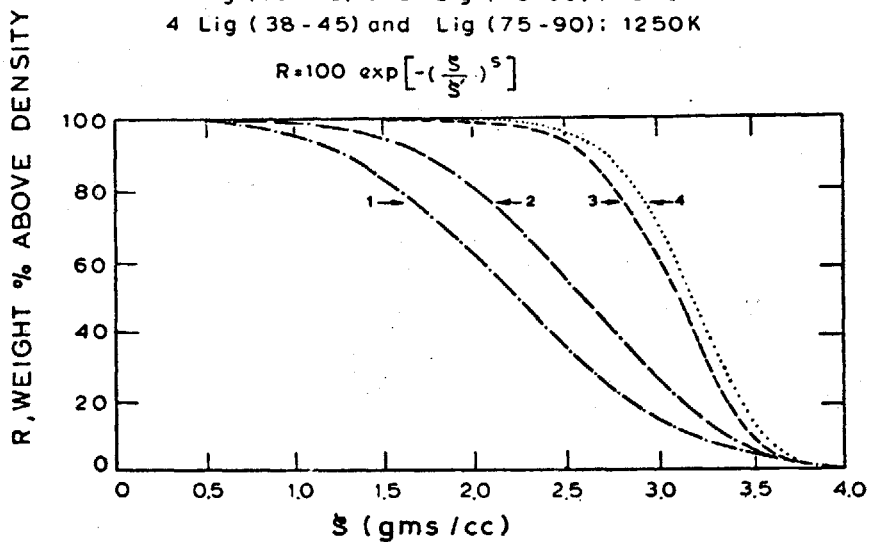
Density Variations of Ash Using Two Parameter Fits

Figure 1.16
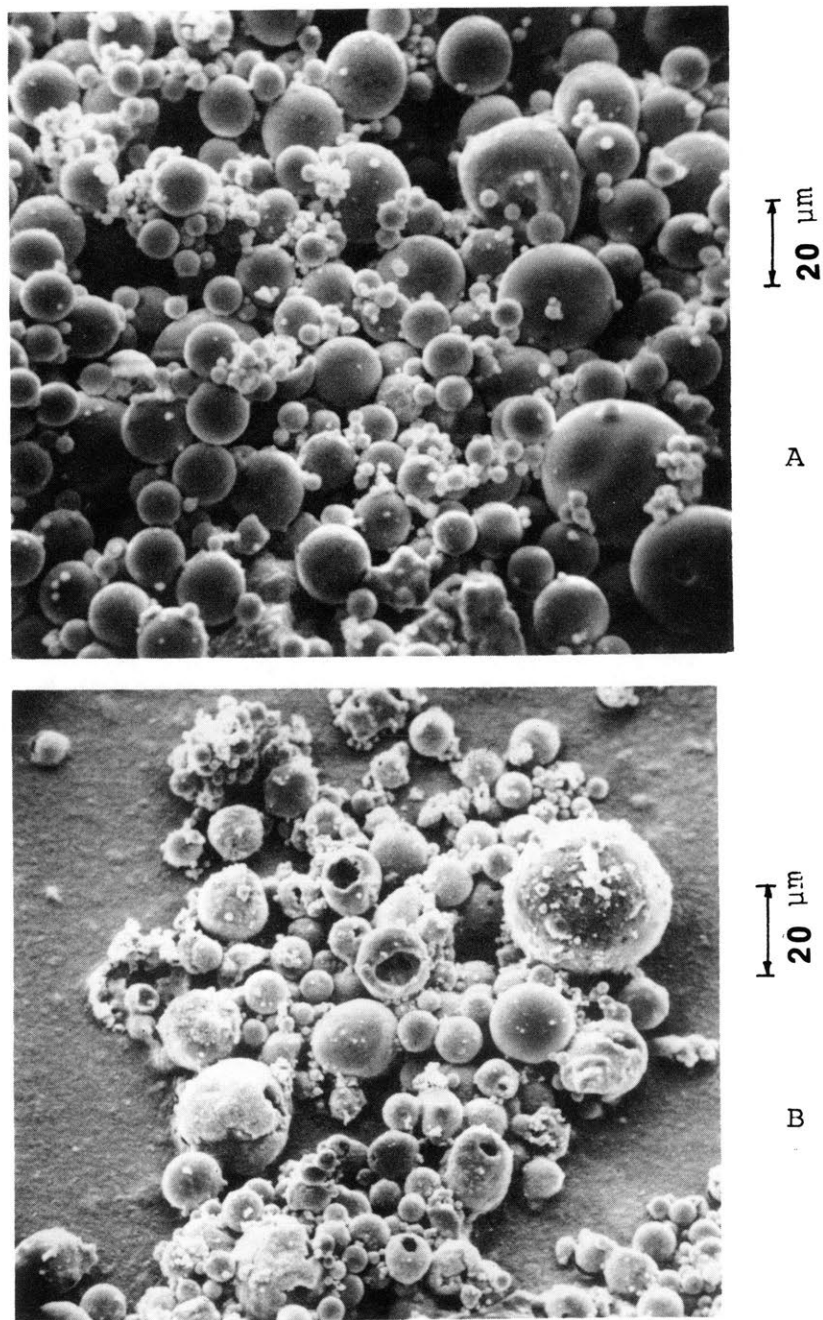
Ash produced at 1500°K Furnace Temperature showing
presence of cenospheres from

    A.   Lignite (75-90) μm

    B.   Bituminous (38-45) μm coal
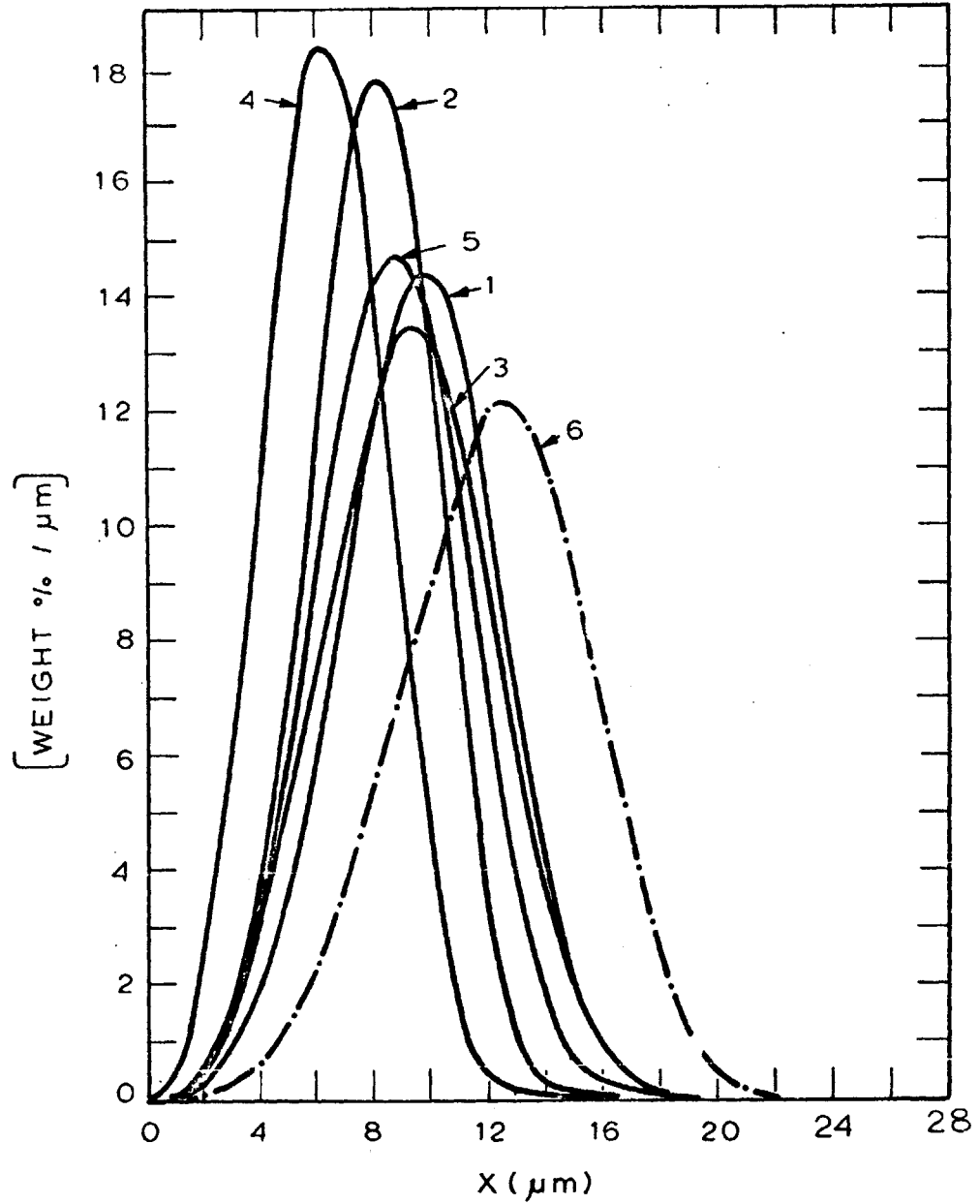
Figure 1.17

Particle Size Distribution of Dense Ash from (38 - 45) µm Lignite

	Temperature	Xm (µm)	X'(µm)	S
1	1250	9.79	10.62	4.0
2	1250	8.00	8.83	4.15
3	1500	9.26	10.26	3.57
4	1500	6.3	7.0	3.32
5	1830	9.2	10.1	3.68
6	1 Ash / Coal	11.99	13.37	4.30

Figure 1.18
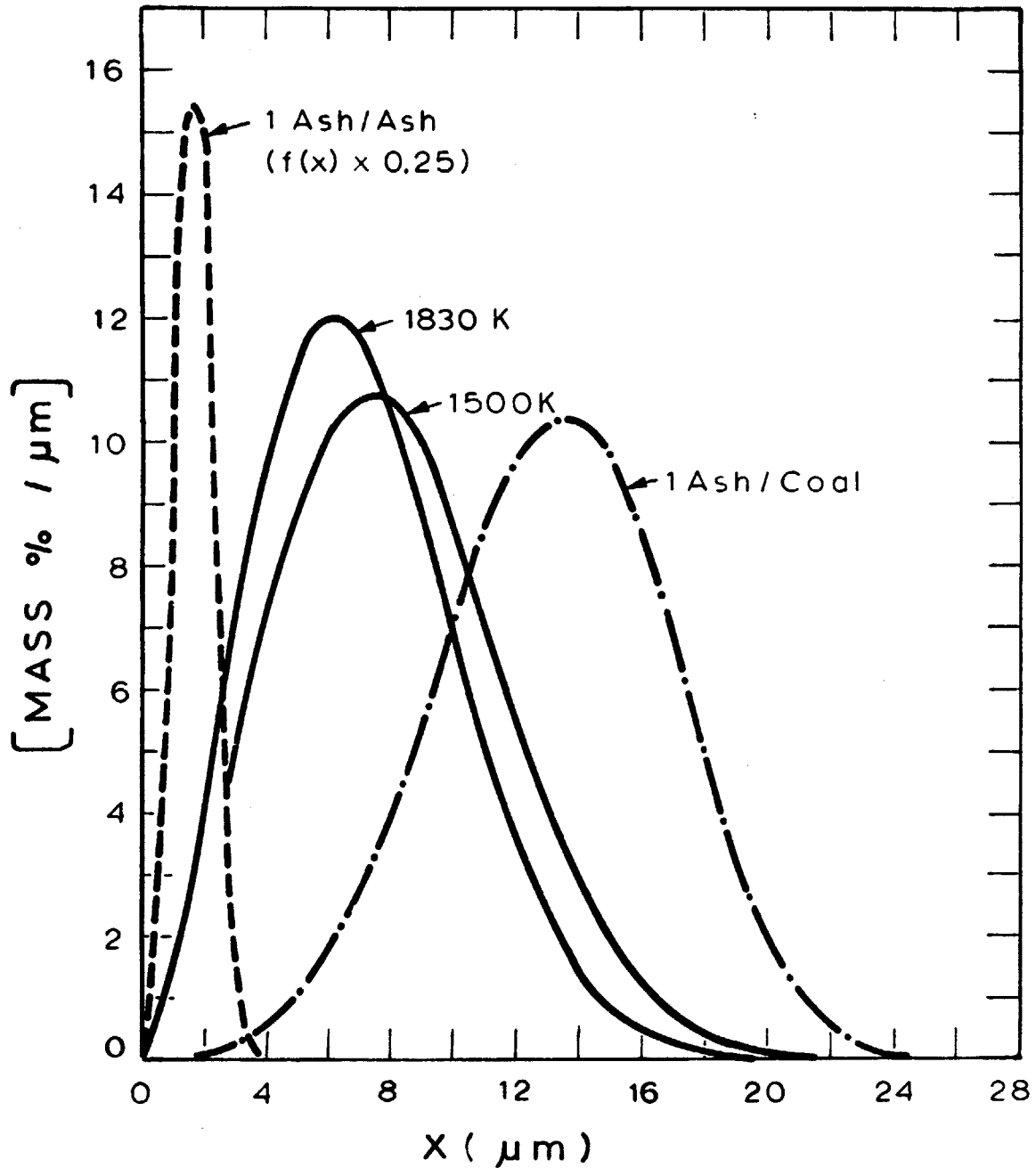
Dense Ash PSD from (38-45) um Bituminous Coal

Temperature (K)	X'(μm)	Xm(μm)	S
1500	9.17	7.9	2.42
1830	7.9	6.8	2.3
1Ash / Coal	14.58	13.50	4.0
1Ash / Ash	1.90	1.68	2.99

Figure 1.19

ash particles per coal particle are formed for the lignite and about 5 ash particles per coal particle are formed for bituminous coal. These numbers are consistent with the expectation that the cenospheres formed by bituminous coal will yield a larger number of fragments than the relatively non-swelling lignite. The extent of fragmentation is consistent with the visual observations of partially burned particles.

A simplified model of the consequences of receding front model suggests that the particles agglomerate mainly during the burnout of the last 25 percent of the coal particle (Figure 1.20).

1.4 Concluding Comments

The insight on the fate of the mineral matter finely distributed in coal particles has been derived from simulated combustion experiments.

The chemical decomposition of the mineral constituents is controlled more by thermodynamic than kinetic constraints. Allowance must be made, however, for the temperature differential between the particle and gas and for the relations between mineral matter and carbon.

Significant augmentation of the vaporization of mineral constituents such as silica may result from the formation of lower oxides by reduction with carbon.

Interaction between the mineral constituents occurs only during the final stages of burnout when the ash

SHRINKING SPHERE MODEL

Basis : Coal Size, 40 μm Mass
Median
Rosin Rammler Distribution
s = 4.5
Ash = 10 % by Weight of Coal
Ash in Original Coal 2.0
μm Mass Median
Rosin Rammler, s = 3.0

% Carbon Burnout		Ash Size (μm) Mass Median
1 ———	0	2.0
2 —·—·—	25	2.1
3 —————	50	2.6
4 —··—··—	75	3.8
5 —————	100	13.4

WEIGHT % / μm

ASH PARTICLE SIZE (μm)
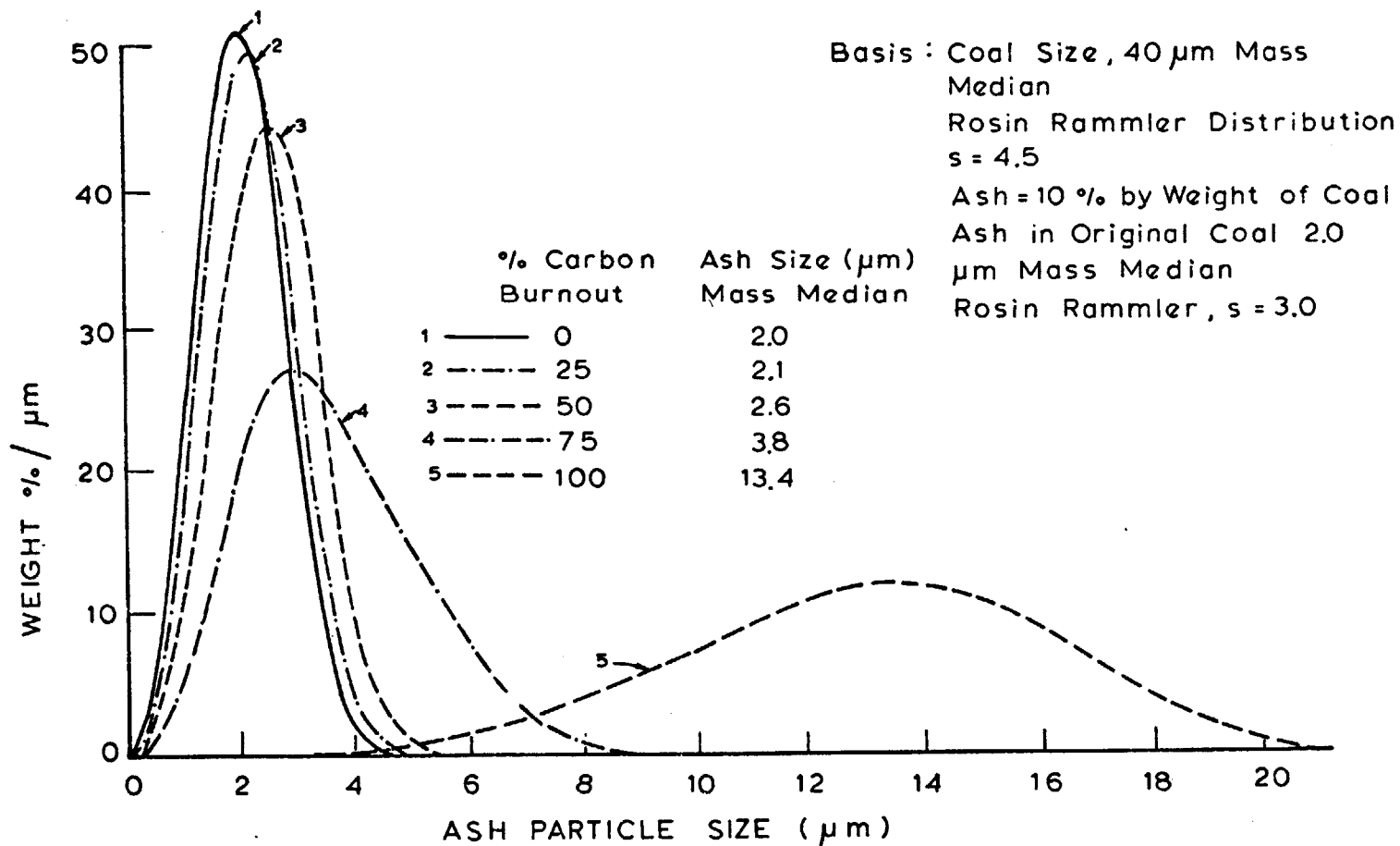
Effect of Carbon Burnout on PSD of Ash (Shrinking Sphere Model)

Figure 1.20

particles are drawn together on the receding reacting carbonaceous surface. Several ash particles, 3 to 5 for the conditions of the present study, are produced for every coal particle as a consequence of fragmentation during combustion.

The results have profound influence on the calculations of vaporization times of ash constituents (which are inversely proportional to the square of the particle diameter in addition to chemical composition), on the ash contribution to flame emissivity (absorption coefficient inversely proportional to particle diameter), on the ease of separation of the ash particles (dependent on both diameter and density) and on the formation of fine particulates by the augmented vaporization and recondensation of minerals, such as silica.

Chapter 2

INTRODUCTION

2.1 Background and General Objectives.

The increasing rate of energy consumption in the
United States, combined with the continuous depletion of
oil and gas reserves, has stimulated interest in in-
cressing the efficiency of energy utilization. Electrical
power production by magnetohydrodynamics (MHD), promising
about 60 percent overall efficiency compared to the maxi-
mum 40 percent efficiency possible in a conventional
steam turbine cycle, is one of the processes that show
promise. Coal being the abundant natural resource of
energy in the United States would be utilized as the fuel
in future power production by MHD.

All types of coal contain substances other than the
useful combustible matter, comprising mainly of hetero-
geneous mixtures of inorganic compounds, collectively
designated as "ash" or as "mineral matter." The ash
content typically of the order of 10 percent by weight
in United States coals, represent the mass of the
material which must be carried through the combustion
process and ultimately removed for disposal. The
presence of the inorganic constituents in coals is the
major obstacle to efforts to improve the thermal
efficiency of combustion processes. Not only do they
lower the calorific value of the fuel due to diluent

effect, but behave in a manner that leads to the formation of slags, or deposits on heat transfer surfaces (Brown 1970). Accumulation of ash or slags on steam generating and superheating surfaces retards heat transfer, obstruct the gas flow passages through tube banks causing the increase in draft losses and possibly leading to maldistribution of flow and temperature, reduction of capacity and forced shutdown. Severe abrasion of the heat-transfer surfaces by particles carried in the gas stream and the corrosion of pressure parts and supporting structures due to the corrosive compounds formed during or after combustion is often experienced.

The conventional combustors can be classified mainly into two catagories based on the method of burning coal, first where the fuel is stationary upon a grate and combustion air is passed through it, generally termed as fuel bed combustors, and second the suspension burning in which the coal after being pulverized is blown into the furnace by entraining with an air stream. Intermediate forms can be represented by spreader stoker and by the cyclone method of firing (Combustion Engineering, 1966). For continuous operation removal of ash is essential to all methods. In case of fuel bed combustors it is achieved by intermittent shaking or dumping of grate sections. In suspension firing, the ash particles are partly carried out of the furnace by gas stream and partly retained by settling or adherence to

boundary surfaces. Retained material is removed by periodic cleaning or, in case of combustors with sufficiently high temperatures, the retained ash is molten and is usually drained out through a tap hole. The gas borne, fly ash particles are handled by utilizing various techniques, including centrifugal separation in cyclone burners, settling in hoppers, by inertial electrostatic or water scrubbing separators, and interstage cyclone particulate collectors in gasifier combustor combinations. Regardless of the combustor and the ash separation equipment used, a more complete understanding of the nature and behavior of ash, particularly of the size and composition distribution, is needed in order to optimize the designs of combustors, gasifiers and ash removal equipment.

In the case of MHD combustors, operating at temperatures of the order of 2700°K, factors like vaporization and condensation of ash species on MHD channels are important. Opinions on the desirability of having slag carried over from the combustor to an MHD channel differ but current experimental evidence supports the view that coating of the channel walls with some slag carried over from the combustor may enhance electrode performance. Control of the slag rejection may be achieved by imparting swirl to the combustion air; by such means over 80 percent ash rejection has been achieved at MHD temperatures in pilot units in diameter 0.45 m [Heywood and Womack, (1969)]

and 0.65 m in diameter [Tager et al. (1971)]. The
remainder of the slag is either entrained as gasborne
droplets or vaporized, with the amount vaporized in-
creasing with increases in the residence time and tempera-
ture in the combustor.

Clearly, prediction of the amounts of ash rejected
and vaporized in a combustor requires detailed knowledge
of the ash particle size distribution and chemical compo-
sition during different stages of the combustion process
and the temperature history of the ash. Relatively little
information exists on ash particle-size distribution
during the conventional combustion of coal and less under
MHD conditions.

The general objective of this thesis is to provide
a better understanding of the nature and behavior of ash
regarding its composition and particle size distribution
in the original coal and during different stages of com-
bustion at high temperatures. This information is useful
in extending the progress in the use of coal for power
production by conventional and MHD processes.

2.2 Literature Review.

In order to list the objectives of the thesis, a
critical examination of the existing level of under-
standing in the pertinent field was performed. The
limited literature available about the ash behavior at
high temperatures was reviewed and the findings in the
literature are summarized in this section.

2.2.1. Ash Content in Original Coal

2.2.1.1 Ash Content in Bulk Coal.

Several researchers Selvig and Gibson 1956, Brown
and Swaine 1964, Kewezys and Taylor 1964, Gluskoter 1967,
O'Gorman and Walker 1971) have studied the ash content of
various coals with the conclusion that it is very dif-
ficult to generalize about the inorganic constituents of
bulk coal. Inorganic constituents vary considerably in
composition and distribution. In general ash content may
vary from a few percent to about 30 percent of the coal's
weight. The ash can be divided into three major cate-
gories:

(a) Inherent mineral matter is that portion of the
inorganic constituents derived from the original plant or
inorganic matter that has become inseparably combined
with the organic matter. The inherent mineral matter
rarely exceeds 2%.

(b) Adventitious mineral matter is that portion of
the inorganic matter that was introduced into the coal
during the biochemical processes related to coal for-
mation and during its subsequent geological history.

(c) Free dirt occurs as intra-seam bands containing
practically no carbonaceous material. The free dirt is
usually separated during treatment prior to combustion.
The major constituents of the ash, in general, are
silica, alumina, silicates, carbonates, sulfur bearing
minerals and other endless minerals in trace quantities.

a. <u>Silica and Alumina</u>: Silica and alumina represent about one half by weight the total inorganic matter present in the coal. Table 2.1 gives the chemical analysis of ash in some American coals expressed as oxides found by O'Gorman. Kaolinite (a hydrous layer lattice silicate $[Al_2Si_2O_5(OH_4)]$, quartz, and illite (a clay grade mica) are found in American coals. In Australian coals silica (S_iO_2) occurs in two forms, quartz and chalcedony (Kemezys and Taylor 1971). Quartz occurs typically in angular grains usually within layers rich in clay, 0.5 mm across and about 50 to 100µ size. Chalcedony occurs in veins adjacent to intrusions and in masses apparently invading and even replacing coal. Silicate clays are by far the most commonly occuring minerals in coals. Alumina (Al_2O_3) is usually incorporated within silicate structure. Clays are typically present in layers of a few microns to several centimeters in thickness interbedded with the coal.

b. Carbonates are observed both in American and Australian coals. Carbonates can be in the form of siderite $FeCO_3$, ankerite $Ca(Fe,Mg)(CO_3)_2$, or Calcite $CaCO_3$. Siderite, the most commonly observed carbonate, occurs as modules, either singly or in aggregates ranging from 1 to 2 mm. in size to about 5 mm across. Bigger aggregates of siderite measuring up to 6 feet across are also observed. Calcite and Ankerite occur in

Table 2.1 Chemical Analysis of Ash in Some American Coals (O'Gorman, 1971)

Sample No.	SiO_2	Al_2O_3	Fe_2O_3	TiO_2	CaO	MgO	Na_2O	K_2O	SO_3
PSOC-2	59.5	26.7	4.18	3.39	2.25	0.65	0.83	0.06	1.84
PSOC-3	68.5	20.8	2.55	3.58	1.35	0.40	0.63	0.04	1.69
PSOC-4	37.0	17.8	23.25	0.53	5.60	1.18	1.79	0.22	10.86
PSOC-82	53.0	33.3	4.05	3.35	1.95	1.00	0.13	0.38	1.99
PSOC-88	23.5	13.6	5.72	0.51	18.25	5.40	8.30	0.29	21.65
PSOC-100	9.8	12.9	6.82	0.99	33.38	7.85	1.56	0.18	21.74
PSOC-108	32.3	18.5	42.23	0.81	2.80	0.34	0.61	0.38	<0.01
PSOC-109	49.5	26.8	5.30	1.11	5.50	0.90	0.94	1.18	6.68
PSOC-110	46.6	27.8	17.75	1.07	1.65	0.61	0.42	1.13	0.55
PSOC-111	54.4	23.6	11.81	1.03	3.40	0.72	0.31	2.29	1.14
PSOC-120	55.1	23.9	2.18	1.68	7.25	0.40	0.32	0.40	6.77
PSOC-121	23.5	24.9	19.55	1.12	10.50	1.43	1.46	0.67	12.22

(all numbers are % by weight of total ash).

(Table 2.1 Continued)

Identification of Coals

PSOC Sample No.	Seam name	ASTM rank	Location in seam	Locality
2	Elkhorn No. 3	HVA bituminous	15-23 in. from bottom	Deane, Kentucky
3	Elkhorn No. 3	HVA bituminous	23-31 in. from bottom	Deane, Kentucky
4	Elkhorn No. 3	HVA bituminous	31-40 in. from bottom	Deane, Kentucky
82	Buck Mountain	anthracite	31-39 in. from top	Zerbe, Penna.
88	Zap	lignite	top 18 in.	Zap, North Dakota
100	Roland	subbituminous	unknown	Gillette, Wyoming
108	Pittsburgh	HVA bituminous	top 10 in.	Marianna, Penna.
109	Pittsburgh	HVA bituminous	10-35 in.	Marianna, Penna.
110	Pittsburgh	HVA bituminous	35-54 in.	Marianna, Penna.
111	Pittsburgh	HVA bituminous	54-72 in. (base)	Marianna, Penna.
120	Tioga	HVA bituminous	22-35 in. from bottom	Tioga, West Virginia
121	Tioga	HVA bituminous	0-22 in. from bottom	Tioga, West Virginia

small veins few hundred microns across.

c. Sulfur could be present in the coal in pyrite
or organic form. Pyrite sulfur concentrations are
generally low. In some coals the relative concentrations
could be comparable. In pyrites, sulfur is usually
present in the sulfide form, most common are iron sul-
fides, pyrite and marcasite (both FeS_2). Sphalerite
(ZnS), galena(Pbs) and chalcopyrite ($CuFeS_2$) have been
also observed. But iron sulfides occur in thin veins of
only 5-10μ. Organic sulfur usually occurs in the in-
herent mineral matter.

d. Numerous trace elements have been observed in
the coals studied by different investigators. Table 2.2
gives the list of elements and their composition in
different American coals as studied by O'Gorman. Kemezys
and Taylor (1964) studying Australian coals have reported
the trace element concentration in terms of fluorapatite
$(Ca_5(PO_4)_3(F,OH))$, zircon $(ZrSiO_4)$, iron oxides $(HFeO_2$,
$HFeO_2MH_2O)$ etc.

2.2.1.2 Ash Distribution in Pulverized Coal.

Ash distribution in the coal is a function of
particle size; therefore ash is distributed in different
proportion among the various sizes (ranging from about
10 to 200μ) in a pulverized coal). Obviously the total
ash content and the amount of each inorganic constituent
will be the same in the pulverized coal as it was in the
parent bulk coal, but the resulting ash distribution in

Table 2.2 Analysis of Trace Elements in Some American Coals (O'Gorman, 1971)

(parts per million on ash basis)

Element	PSOC-2	3	4	82	88	100	108	109	110	111	120	121
Ag	<1	<1	<1	<1	<1	50	<1	<1	<1	<1	<1	3
B	320	350	1600	68	820	1025	415	900	680	445	360	1325
Ba	1250	1160	4660	1340	13900	2600	630	630	450	450	805	450
Be	17	8	8	9	5	2	15	8	6	17	8	32
Co	25	58	65	68	16	31	100	31	56	42	85	170
Cr	315	275	105	285	23	33	200	160	180	155	135	140
Cu	645	550	595	530	58	2500	125	150	56	42	85	170
Ga	20	19	28	31	26	22	51	33	46	34	49	56
Ge	<20	<20	<20	<20	<20	100	20	<20	<20	<20	<20	<20
La	195	140	52	220	34	46	66	93	84	68	160	110
Mn	230	115	465	280	390	480	140	140	100	130	125	215
Ni	84	70	115	125	<20	41	170	103	118	107	195	610
Pb	80	54	80	86	48	50	112	53	68	75	74	560
Se	51	40	8	51	5	9	20	23	28	23	30	22
Sn	180	150	105	4250	8	62	97	80	22	74	660	50
Sr	2370	2030	7300	340	6400	8000	1520	1270	845	430	2280	9600
V	260	235	138	230	28	145	330	180	220	165	150	260
Y	180	165	52	120	45	21	86	64	58	49	97	135
Yb	15	15	12	12	4	<2	15	7	8	6	7	13
Zn	<50	<50	210	<50	50	96	190	84	220	80	<50	210
Zr	1250	1450	115	1200	205	130	220	230	220	215	360	230

the pulverized coal is not as obvious. Relatively very little effort has been devoted towards the understanding of ash distribution in pulverized coal. The discussion that follows is based mainly on the work of Littlejohn (1966). His results suggest that pulverized coal particles fall into 3 categories:

(a) 40 to 70 percent are organic particles containing 2 percent or less inherent mineral matter (i.e. that derived from the original vegetation).

(b) 20 to 40 percent are particles containing both organic and mineral matter.

(c) discrete mineral particles.

He noted that, the carbonaceous, mixed and discrete mineral particles are not uniformly distributed between the different size ranges. The mineral matter increases with decreasing particle size throughout the entire size range. The ash content of the smallest particle size fraction (below 10 microns) can be more than twice the average value for the bulk sample because as the particle size decreases, the proportion of clean coal decreases and the proportions of mixed particles and the discrete mineral fragments increase.

There is no information about the ash distribution within a mixed ash and carbonaceous particle in the literature. The characteristic ash distribution in pulverized coal is of great importance to the thesis as it represents

the starting point in the study of behavior of ash during combustion processes.

2.2.2 Behavior of Ash at High Temperatures.

Although minerals in coals have been studied in great detail by several investigators, very little information is available about the thermal behavior of coal ash. It is well recognized that at conventional combustor temperatures significant changes in mineral phases take place and at MHD temperatures, vaporization of ash becomes important. Ash fusion has been studied in great detail because of its relation to clinkering tendencies in combustors. The brief review of the literature under this section is divided into three sections: mineralogy, ash loss and fusion, and vaporization at high temperatures.

2.2.2.1 Mineralogy of Ash at High Temperatures.

The significant papers regarding the mineralogy of ash and its variation with temperature include, O'Gorman and Walker (1971), Mitchell and Gluskoter (1975) on American coals and Rost and Ney (1956), Sinaiskill et al (1964) on European coals. Most of the studies were performed by first obtaining mineral matter from coal in its essentially un-altered state by low temperature ashing (Gluskoter, 1965) and then subjecting the low temperature ash to high tempera-tures in a muffle furnace. Several methods are used to identify the mineral phases present in high temperature ash samples; the important ones are x-ray diffraction (Mitchell and Gluskoter, 1975), thermogravimetric and derivative thermogravimetric analysis (O'Gorman and Walker, 1971), and

infrared multicomponent analysis (Estep et al, 1967). The

finding by different investigators are described below

according to individual minerals present initially in the

coal.

Kaolinite:

The decomposition mechanism of kaolinite, the

major mineral accounting for silica and alumina in the coal

ash, has been studied very extensively. At 100-120°C

kaolinite losses its absorbed water and at 550-600°C losses

the water of hydroxyl, resulting in the formation of an

amorphous phase (metakaolinite). Metakaolinite remains un-

altered up to 950-1000°C, at which stage it converts either

to a spinel-like form of γ-alumina or to mullite

$(2SiO_2.3Al_2O_3)$. With further increase in temperature, the

γ-alumina is replaced by increasing amount of mullite and

at about 1200-1300°C, a tetragonal modification of silica

(cristobalite) appears and persists with the mullite up to

1500°C temperature. Above 1500°C mullite is the only

stable phase.

Quartz:

Quartz is a relatively stable phase. α-quartz trans-

forms to β-quartz at about 570°C and there is no change

thereafter up to 1000°C. It diminshes considerably at

about 1200°C and above 1300°C transforms into an amorphous

glass phase.

Illite:

Illite is one of the major clay mineral in coals. It

losses its hygroscopic moisture at about 50-150°C and its water of hydroxyl between 370 to 620°C. At about 850-900°C, complete destruction of lattice structure takes place. At higher temperatures (> 900°C) a spinel phase is formed which increases in particle size with increasing temperature and finally disappears at about 1300°C by dissolution into a glass phase. Mullite also forms from 1100°C and persists up to 1400°C.

Pyrite:

Pyrite is the main constituent in most coal minerals accounting for the total amount of iron present. The behavior of pyrite is largely governed by the combustor atmosphere utilized. In oxidizing atmosphere, pyrite oxidizes to form hematite at about 500°C which persists up to 1300 to 1400°C and then transforms into an amorphous phase. Hematite is frequently accompanied by small amount of anhydrite which is probably the result of the reaction between pyritic sulfur and calcite. In inert atmosphere, decomposition of pyrite takes place at about 325°C forming $FeS_{(1-x)}$ where x - 0.1-0.3, and further decomposition occurs at about 700°C resulting the formation of pyrrhotite (FeS) and sulfur.

Marcasite which is an alternate structure of iron sulfide occurs in minor quantities in coal. Marcasite behaves in almost the same manner as pyrite.

Calcite:

Calcite thermally decarbonizes at about 710 to 950°C

resulting in the formation of lime. Formation of new phases like anorthite [CaO·Al_2O_3·2SiO_2] and Gehlenite [2CaO.Al_2O_3.SiO_2] have been also observed at 900-1300°C, which could be due to the reaction between calcite and silica-aluminates derived from kaolinite and other clay minerals. Anorthite and Gehlenite phases are stable up to 1300°C.

Gypsum:

Gypsum is the main source of calcium in most coals. Gypsum undergoes a two stage dehydration: first a partial dehydration at 145°C resulting in the formation of bassanite, and the second at 174°C resulting in the formation of anhydrite [$CaSO_4$]. At 364°C, transformation from α $CaSO_4$ to β-$CaSO_4$ takes place. Anorthite and Gehlenite phases can also be formed starting from gypsum between 800-1300°C with reaction between anhydrite and silica and alumina from kaolinite and illite. Anhydrite decomposes to lime at about 1450°C.

Dolomite:

Dolomite is the major mineral in coal accounting for magnesium. Partial and complete decarbonation takes place at about 740-800°C and 815-910°C respectively resulting in the formation of calcium and magnesium oxides.

Coquimbite and Siderite:

Apart from pyritic type structure, β iron also exists in coal in the forms of sulfates and carbonates. Coquimbite, a hydrous iron sulfate dehydrates below 400°C and oxidizes

to hematite above 600°C. Siderite, a major iron carbonate, decomposes to form hematite.

Table 2.3 summarizes the thermal behavior of various minerals found in coal at high temperatures.

2.2.2.2 Fusion and Vaporization of Ash.

A. Fusion: Fusion characteristics of coal ash have been studied in great detail due to their contribution to the clinkering tendencies of different coals. Several methods have been developed to test and investigate the fusibility of coal ash. The ASTM method (1948) for determination of ash fusion characteristic is described by Lowry(1963). Fusion of coal ash is mainly described in terms of Initial Deformation Temperature (I.D.T.), Softening Temperatures (S.T.) and finally the Fluid Temperature (F.T.). The Softening Temperature (S.T.) at which melting of ash proceeds, is frequently reported as the index of fusibility.

It has been reported (Babcock and Wilcox Co., 1955) that coal ashes have higher values of fusion temperature in oxidizing atmosphere than in reducing atmosphere. The difference in two temperatures becomes greater when the iron content of coal ash increases. This is probably due to the difference in fluxing action of ferrous iron (FeO) from that of ferric iron (Fe_2O_3). The effect of iron content of the fusibility of ash is shown in Figure 2.1 (Babcock and Wilcox, 1955).

It is also well recognized that Ca, Mg, like Fe, K, Na,

Table 2.3 Effect of Temperature on Mineralogy of Ash
[O'Gorman and Walker 1971; Mitchell and Gluskoter, 1975]

1. Kaolinite $[Al_2Si_2O_5(OH)_4]$

Kaolinite $\xrightarrow[\substack{100-120°C \\ (end.)}]{}$ Kaolinite (dry) $\xrightarrow[\substack{550-600°C \\ (end.)}]{}$ Metakaolinite + $2H_2O$
$[Al_2Si_2O_7]$
(Amorphous)

(exo.) $\Big\downarrow$ 950-1000°C

Cristobalite $[SiO_2]$ + Mullite $\xleftarrow[1200-1300°C]{}$ Mullite $\xleftarrow[SiO_2]{T > 1000°C}$ γ-Alumina $[Al_2O_3]$
or
Mullite $[2SiO_2 \cdot 3Al_2O_3]$
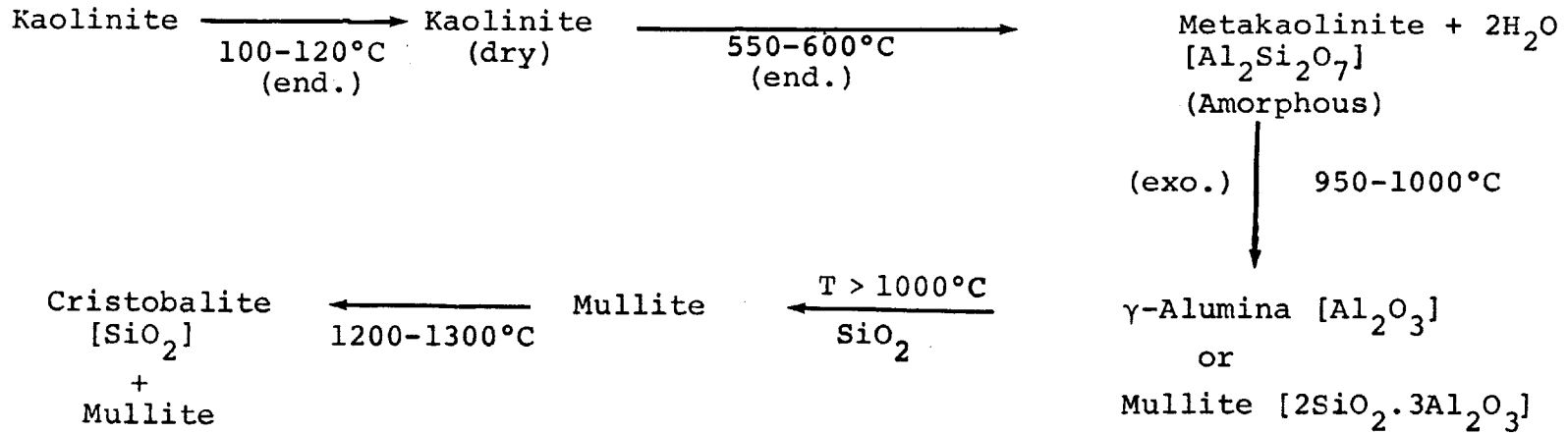
Above 1500°C only Mullite Stable Structure

2. Quartz $[SiO_2]$

Quartz $\xrightarrow[\substack{570°C \\ (end.)}]{}$ β Quartz $\xrightarrow[1000°C]{}$ β-Quartz (no change) $\xrightarrow[1200-1300°C]{\text{+ other compounds}}$ Amorphous Glass
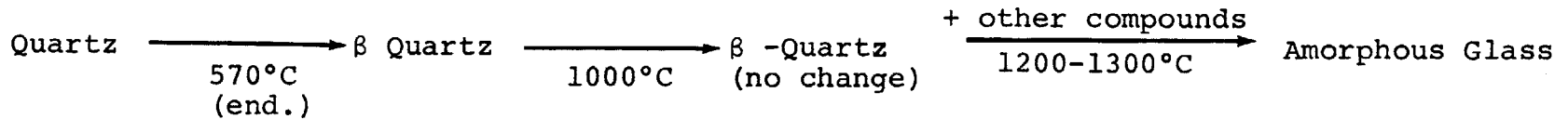
Table 2.3 (Continued)

3. <u>Illite</u> $\left[K_{1-1.5} \, Al_{5-5.5} \, Si_{6.5-7} \, O_{20} \, (OH)_4 \right]$

$$\text{Illite} \xrightarrow[\substack{50\text{-}150\,^\circ C \\ (end.)}]{} \substack{\text{Illite} \\ + \\ \text{hygroscopic} \\ \text{moisture}} \xrightarrow[\substack{320\text{-}620\,^\circ C \\ (end.)}]{} \substack{\text{Illite} \\ + \\ \text{hydroxyl} \\ \text{water}} \xrightarrow[\substack{850\text{-}900\,^\circ C \\ (end.)}]{} \substack{\text{destruction of} \\ \text{Illite} \\ \text{Structure}}$$

$$\substack{\text{Glass} \\ \text{Phase}} \xleftarrow{1400\,^\circ C} \text{Mullite} \xleftarrow{1100\,^\circ C}$$

$$\substack{\text{Glass} \\ \text{Phase}} \xleftarrow{1300\,^\circ C} \substack{\text{Spinel} \\ \text{Phase}} \xleftarrow[\substack{T > 900\,^\circ C \\ (exo.)}]{}$$

$$\left[\text{May be } \gamma\text{-Al}_2 O_3 \right]$$

4. <u>Pyrite</u> [FeS$_2$]

$$\text{Pyrite} \xrightarrow[500\,^\circ C, \, O_2]{} \substack{\text{Hematite} \\ \left[Fe_2 O_3 \right]} \xrightarrow[1300\text{-}1400\,^\circ C]{} \text{Amorphous Phase}$$

$$\text{Pyrite} \xrightarrow[500\,^\circ C, \, CaCO_3, \, O_2]{} \substack{\text{Anhydrite} \\ \left[CaSO_4 \right]} + \substack{\text{Hematite} \\ \left[Fe_2 O_3 \right]}$$

Table 2.3 (Continued)

Pyrite $\xrightarrow[\substack{325°C \\ (end.)}]{}$ FeS$_{(1-x)}$ $\xrightarrow[\substack{700°C \\ (end.)}]{}$ Pyrrhotite + Sulfur
[FeS]

$x = 0.1-0.3$
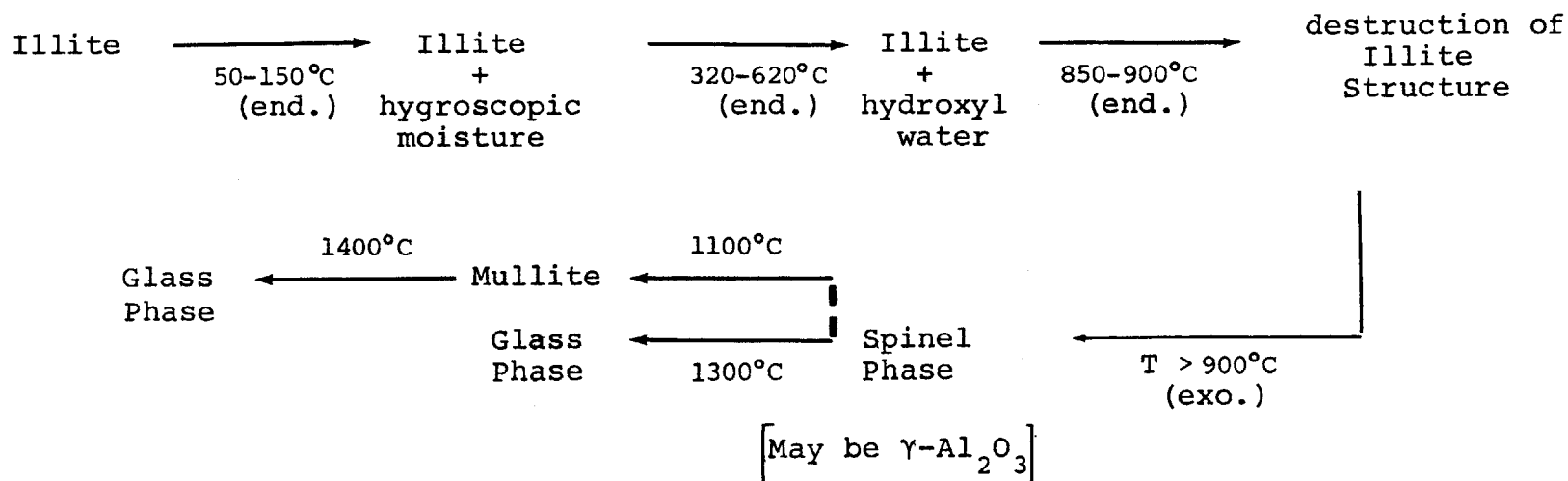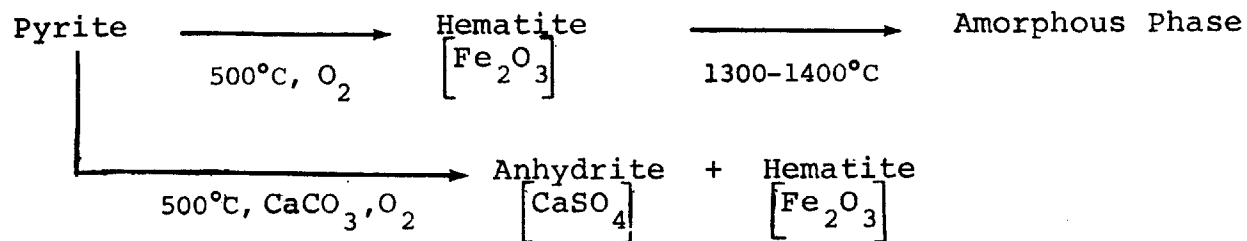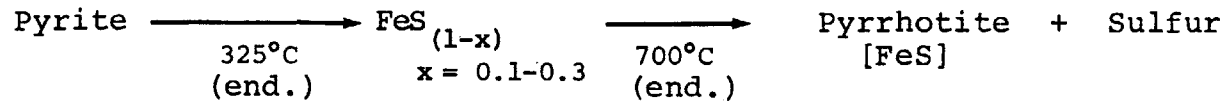
5. Marcasite [FeS$_2$]

   Behaviour similar to pyrite.

6. Calcite [CaCO$_3$]

   Calcite $\xrightarrow[\substack{710-950°C \\ (end.)}]{}$ Lime [CaO]

   Calcite $\xrightarrow[\substack{Al_2O_3 \text{ and } SiO_2 \\ \\ from \text{ Kaolinite and} \\ other \text{ clay minerals}}]{900-1300°C}$ $\left[\begin{array}{c} Anorthite \\ CaO.Al_2O_3.2SiO_2 \end{array}\right]$
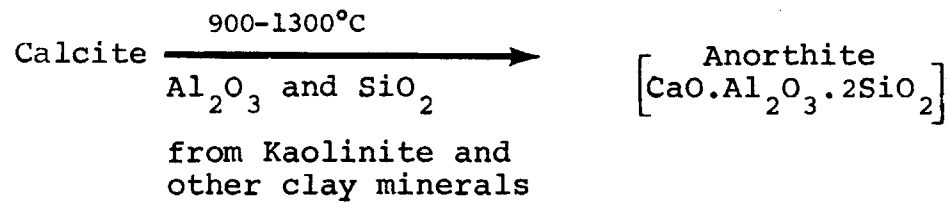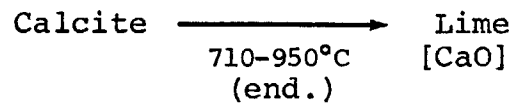
Table 2.3 (Continued)

7. Gypsum [$CaSO_4.2H_2O$]

Gypsum $\xrightarrow[\substack{145°C \\ (end.)}]{}$ Bassanite $\left[CaSO_4 \cdot \frac{1}{2} H_2O\right]$ $\xrightarrow[\substack{174°C \\ (end.)}]{}$ Anhydrite [$CaSO_4$] $\xrightarrow[\substack{364°C \\ (exo.)}]{}$ $\beta\ CaSO_4$

$\beta\ CaSO_4 \xrightarrow{1450°C} CaO$

Bassanite $\xrightarrow[\substack{\text{clay minerals}}]{800\text{-}1300°C}$ Anorthite $\left[CaO.Al_2O_3.2SiO_2\right]$

also

Gehlenite $\left[2CaO.Al_2O_3.SiO_2\right]$

8. Dolomite $\left[CaMg(CO_3)_2\right]$
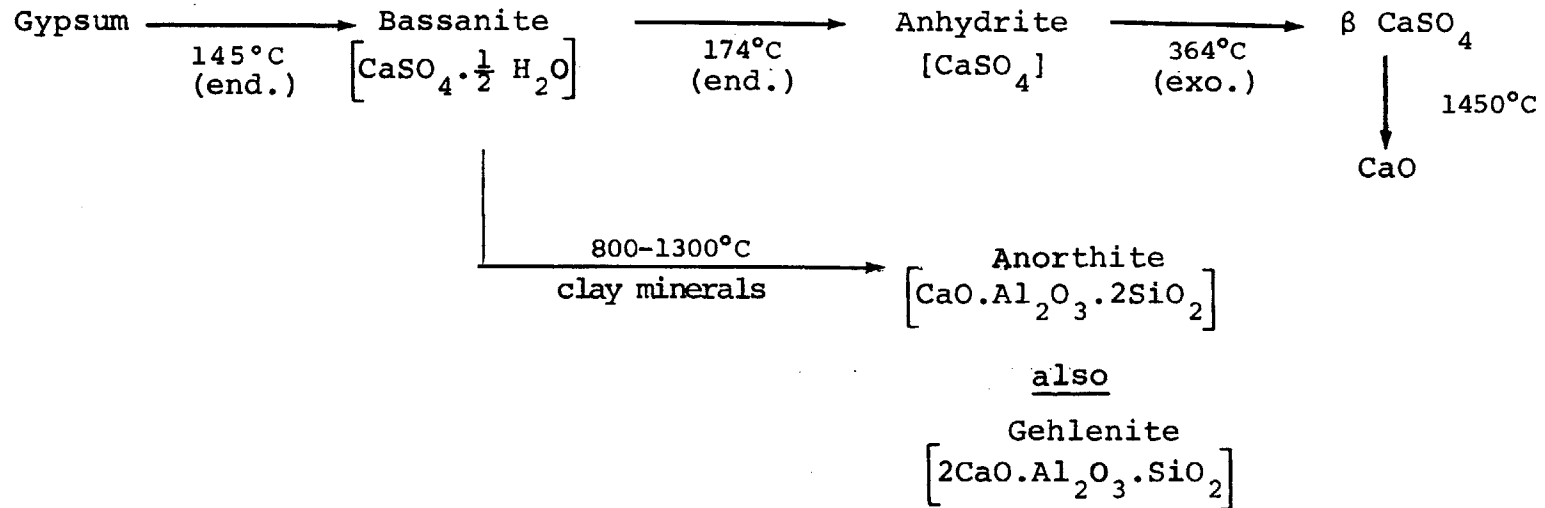
Dolomite $\xrightarrow[\substack{740\text{-}800°C \\ (end.)}]{}$ CaO,MgO,CO_2 $CaCO_3,MgCO_3$ $\xrightarrow[\substack{815\text{-}910°C \\ (end.)}]{}$ $CaO + MgO + CO_2$
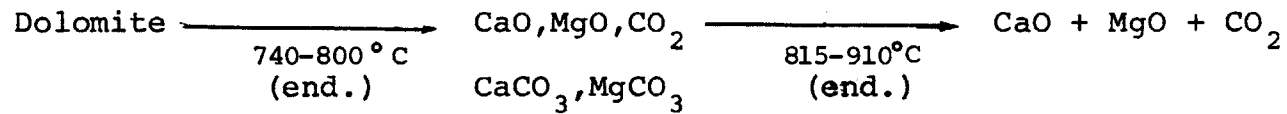
Table 2.3 (Continued)

9. Coquimbite $\left[Fe_2(SO_4)_3 \cdot 9H_2O \right]$

$$ \text{Coquimbite} \xrightarrow[\substack{< \ 400°C \\ \text{(end.)}}]{} Fe_2(SO_4)_3 \xrightarrow[> \ 600°C]{} \substack{\text{Hematite} \\ Fe_2O_3} $$

10. Siderite $[FeCO_3]$

$$ \text{Siderite} \xrightarrow[\substack{425°-610°C \\ \text{(end.)}}]{} Fe_2O_3 + CO_2 $$
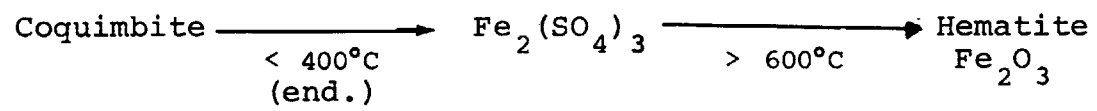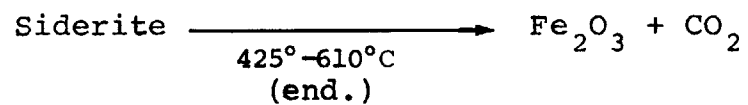
end.   -   endothermic reaction

exo.   -   exothermic reaction
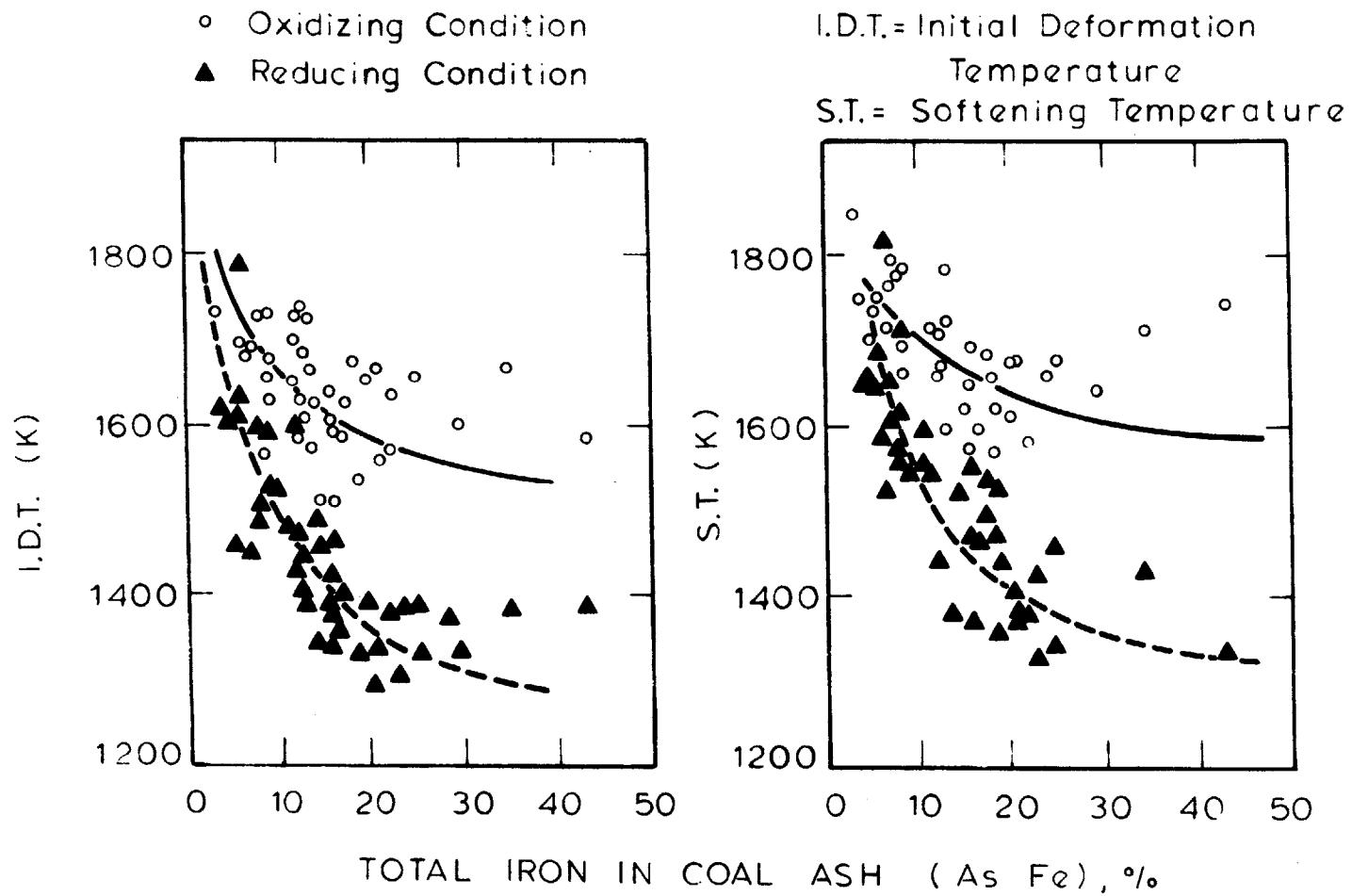
Fig. 2.1. Effect of Iron on Fusion Temperatures of Coal-
Ash (Babcock and Wilcox Co. , 1955)

act as fluxing agents. Although the oxides of major elements present in coal ash (Si, Al, Ca, Mg, Fe) would not fuse until about 1380°C (M. P. of FeO = 1380°C), see Appendix B for others. A combination of these oxides may fuse as low as 1000°C due to fluxing action of other elements. (Muan and Osborn, 1965).

The information regarding ash fusion is important in order to estimate the slagging properties and vaporization effects of ash in combustors at high temperature.

B. Vaporization: Although detailed information regarding the fusibility of different composition ashes are available, very little is known about the vaporization of coal ash at high temperatures, particularly those of interest to MHD combustors (2700°K).

Studies performed at BCURA by Kimber and Gray (1967), show a negligible amount of ash loss up to 1200°C and thereafter progressively increasing to 80% at 2650°C. The ash loss curve obtained by BCURA is reporduced in figure 2.2. The authors make no conjectures as to the possible mechanisms for the ash loss, although at the high temperatures studied, the main loss should be due to vaporization of molten ash. The weight loss could in part be accounted for by different chemical reactions and physical ejection during rapid devolatilization. The study did not include the vaporization of individual species.
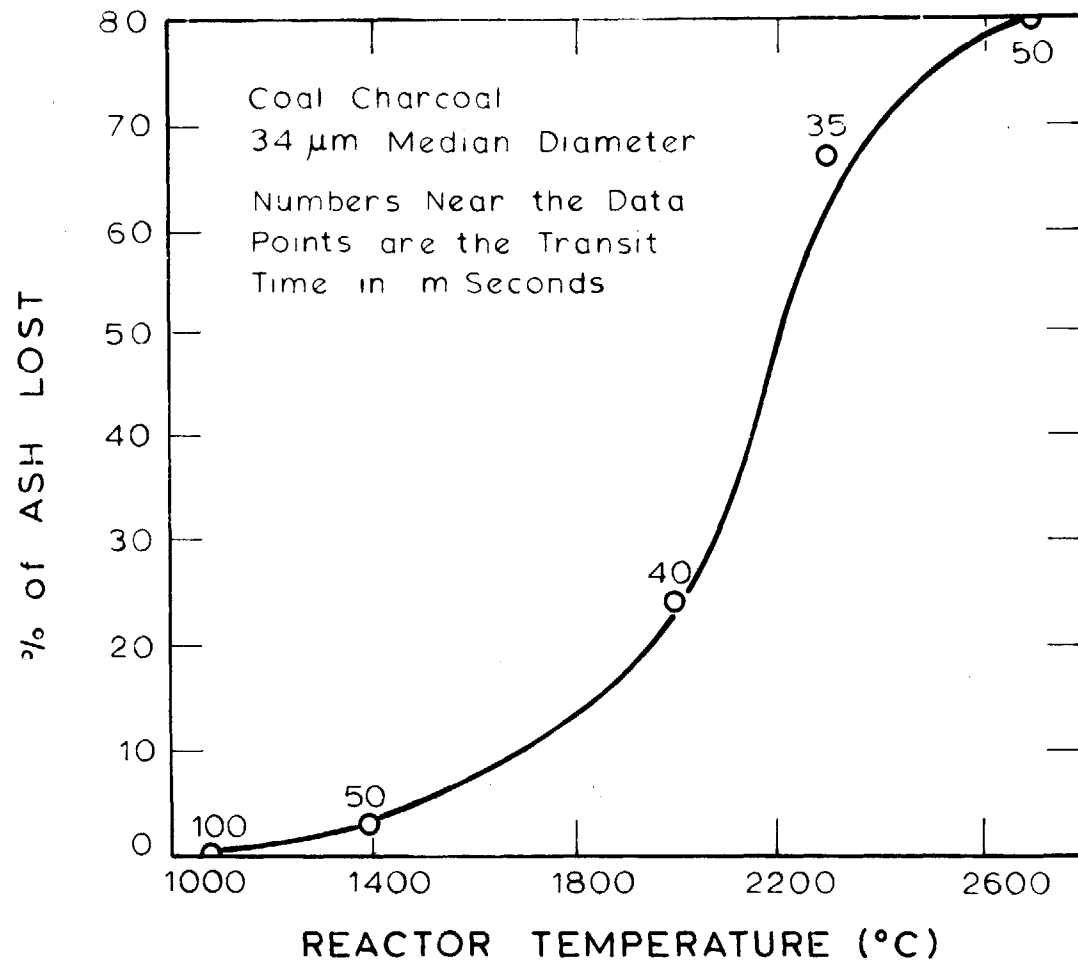
Fig. 2.2. Effect of Temperature on Ash Loss for Coal Charcoal [Kimber and Gray, 1967]

Vaporization of a number of inorganic oxides have been studied up to temperatures as high as 2800°K of interest here are those of Si, Al, Ca, Mg, Fe, etc., the major elements present in coal ash.

C. <u>Silicon Oxides</u>: The two known gaseous molecules of silicon oxide are monoxide and the dioxide. Raask <u>et al</u> (1965) studied the volatilization of silica (silicon dioxide) under gasification and combustion conditions. Their study shows that although the direct vaporization of silica is not significant up to 2100°C temperature, significant amount of silica volatilization takes place due to reduction of silica with carbon forming more volatile silicon monoxide. It is also postulated that at high temperatures less volatile silicon carbide (SiC) may form preventing the complete vaporization of SiO_2. Some of the important reactions possible are as below:

$$SiO_2 + C = SiO + CO \qquad (1)$$

$$SiO_2 + 2C = Si + 2CO \qquad (2)$$

$$SiO_2 + 3C = SiC + 2CO \qquad (3)$$
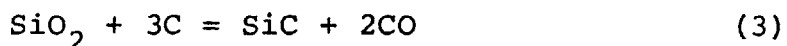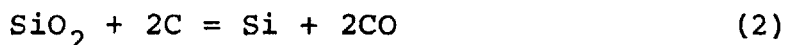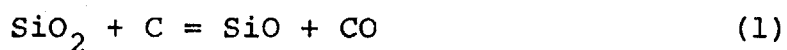
Figure 2.3 shows calculated equilibrium partial pressures of SiO (pco = 1 atm) with the competing reactions (1), (2) and (3).

The vaporization of other oxides become important at higher temperatures where vapor pressures of individual oxides become significant. An estimate of the vaporization
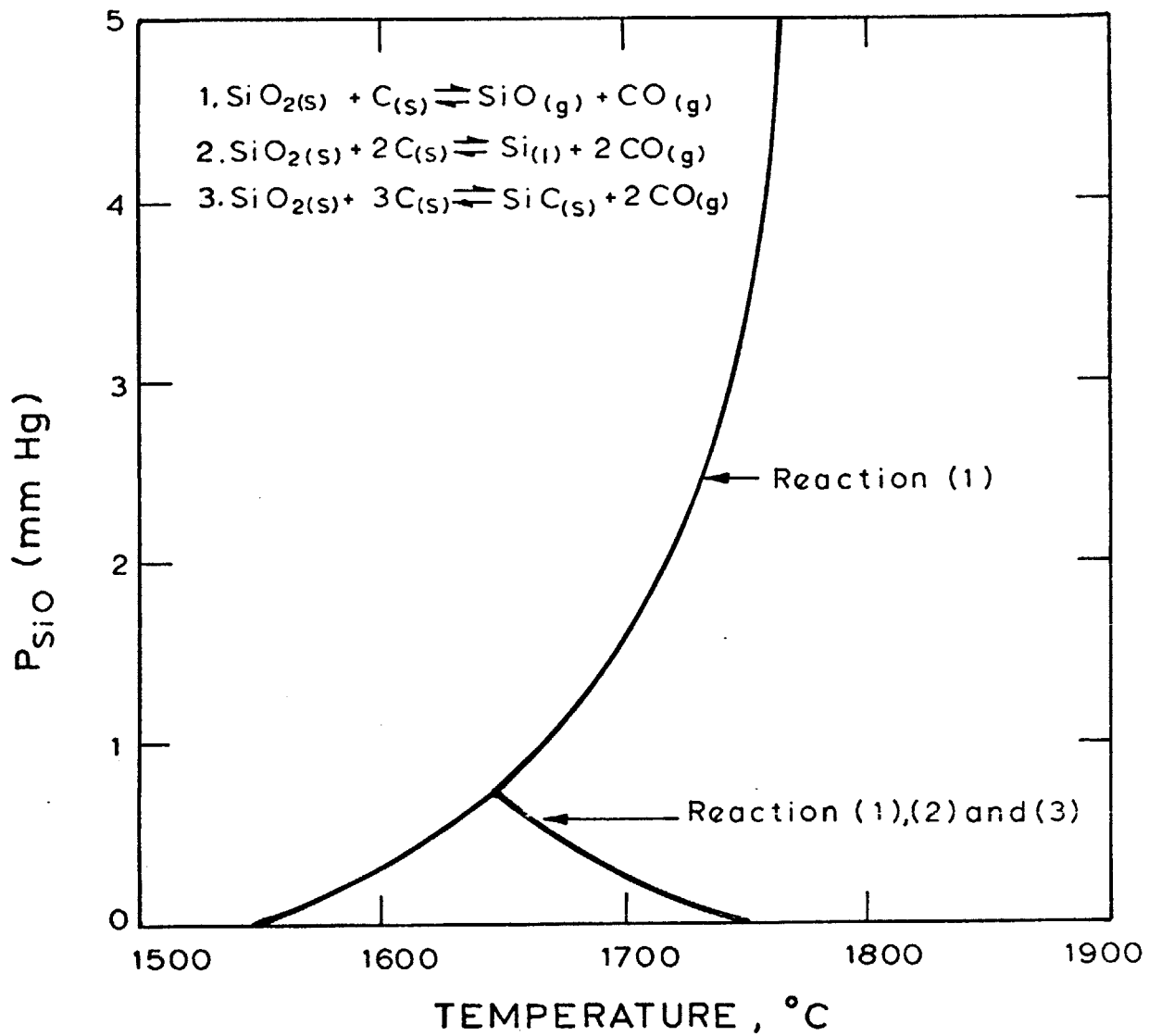
Fig 2·3 Partial Pressure of SiO in Equilibrium with a Partial Pressure of CO of 1 atm (Raask and Wilkins: 1965)

rate can be made from data on vapor pressures. Figure 2.4 shows the vapor pressure of many oxides and pure metals of interest to coal ash vaporization, as a function of temperature.

Although some information (Raask, 1965) is available regarding the behavior of silica under combustion and gasification condition, a systematic study of the vaporization and various other possible reactions of different mineral oxides at high temperature is not available.

2.2.2.3 Combustion Characteristics of Coal Ash.

During rapid combustion of coal particles, mineral matter not only decomposes, fuses and vaporizes but also goes through several interesting characteristic features. One of such feature is cenosphere formation. It has been observed before (Raask, 1968) that a small portion of the pulverized coal ash particles consists of thin walled hollow spheres called cenosphere. The amount of these cenosphere varies from 0.01 to 4.8 percent of the ash by weight but they could reach a substantial amount by volume up to 20% as the apparent density of cenosphere is about one fourth that of ash particle. These cenospheres are usually 20 to 200μ in diameter with non-porous shells about 2 to 10μ thick. Cenosphere are normally higher in silica content but lower in calcium oxide than the dense material. Upon heating, there is usually no change in size and shape up to 1250°C. Above 1250°C the size of the particle slowly decreases and about 1300°C it collapses to a dense blob.

$$\left(\frac{1}{T} \times 10^4\right) K^{-1}$$
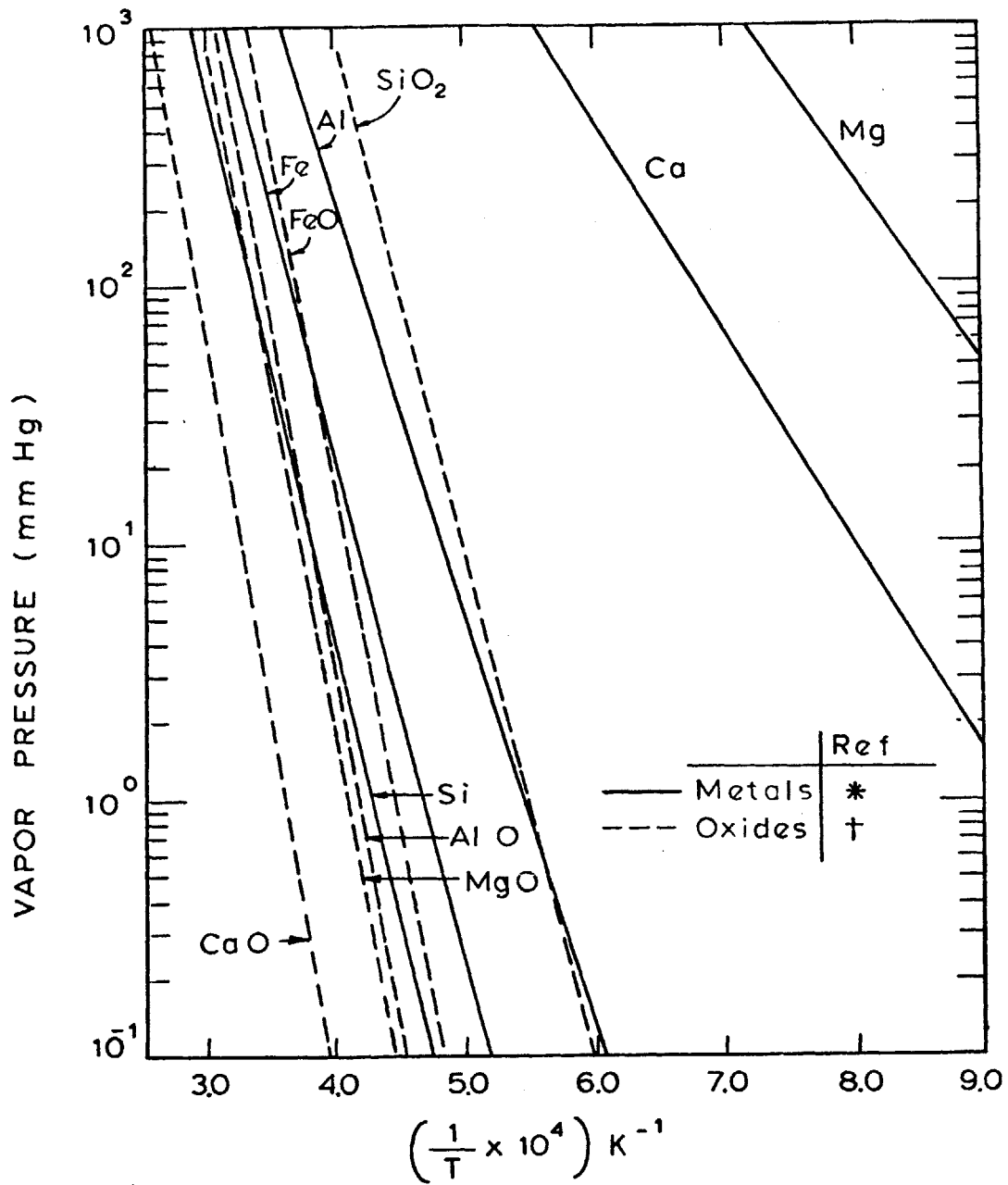
* Hultgren et al (1963) and Janaf Tables (1965)

† Ackermann and Thorn (1961)

Fig 2.4 Vapor Pressure of Major Metals and Oxides Present in Ash

Figure 2.5 shows the ash cenospheres formed by burning pulverized coal. The formation of cenospheres is influenced by the nature of mineral matter in the coal. The temperature of combustion is also a critical factor in determining the formation of cenospheres. Previous findings have concluded that the optimum temperature for the formation of ash cenospheres is about 1400°C. Above this temperature the thin shells of silicate glass would be liable to burst because of the low viscosity and faster rate of gas production. But there is insufficient evidence to prove this. It is important to determine in the regions in which cenosphere formation takes place as this information is necessary to predict the size distribution of ash particles during coal combustion.

2.2.3 Particle Size Distributions, (PSD).

An important aspect of this study is the determination of the effect of combustion chamber parameters on the particle size and composition distribution of ash. In order to optimally design any combustor, gasifier and ash separation equipment and to estimate ash vaporization rates, knowledge of composition and size distribution is essential.

2.2.3.1 Effect of Combustion Conditions on PSD.

It is well recognized that the basic factors affecting the PSD of fly ash are coal size, type of firing, equipment, gas velocities, turbulence, collection equipment, etc. The type of firing equipment is of utmost importance because gas velocity, terminal velocity of particles of fuel and ash,
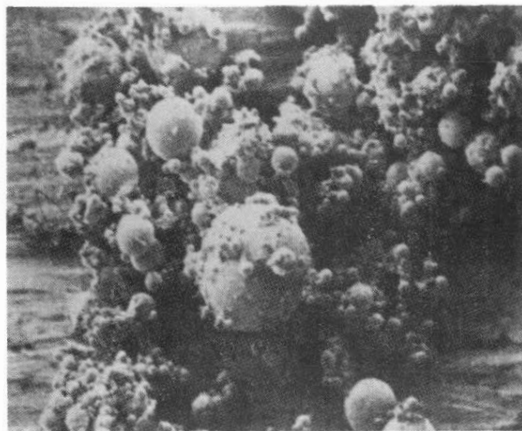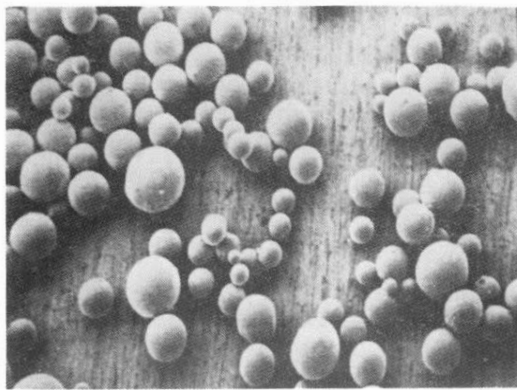
A. Dense Ash

B. Ash Cenospheres

Fig. 2.5   Dense Ash and Ash Cenospheres During Coal Combustion;
Combustion Temperature $\cong$ 1200°C [Raask, 1968 a]

and the conditions for combustion in the furnace space vary widely with different methods of burning coal. Consequently, the fly ash losses from boiler furnace are closely related to the firing equipment in use. Figure 2.6 shows a Rosin-Ramller plot for the size distribution of fly ash from different combustors (Kaiser, 1951) and Table 2.4 lists the effect of type of firing and combustion factors on the amount and mean particle size of emitted ash. Ash PSD results for bituminous coal firing in different combustors have been compiled by U.S. EPA (1972). Some results are repro-duced in Table 2.5. It is quite evident from these results that combustion conditions have a strong bearing on the particle size distribution of ash produced. This provides a motivation for the study of the effect of combustor design on PSD and composition of ash.

2.2.3.2 Effect of Original Coal Size on PSD of Ash.

It is also recognized that the original coal size have an impact on the particle size distribution for ash. The data of Littlejohn (1966) obtained on 14 different coals are indicative of this fact. Also it is shown that the ash particle size distribution is wider than the original coal size distribution. The results of five of the coals studied by Littlejohn are presented here. The Rosin-Rammler relation is used to describe the distribution
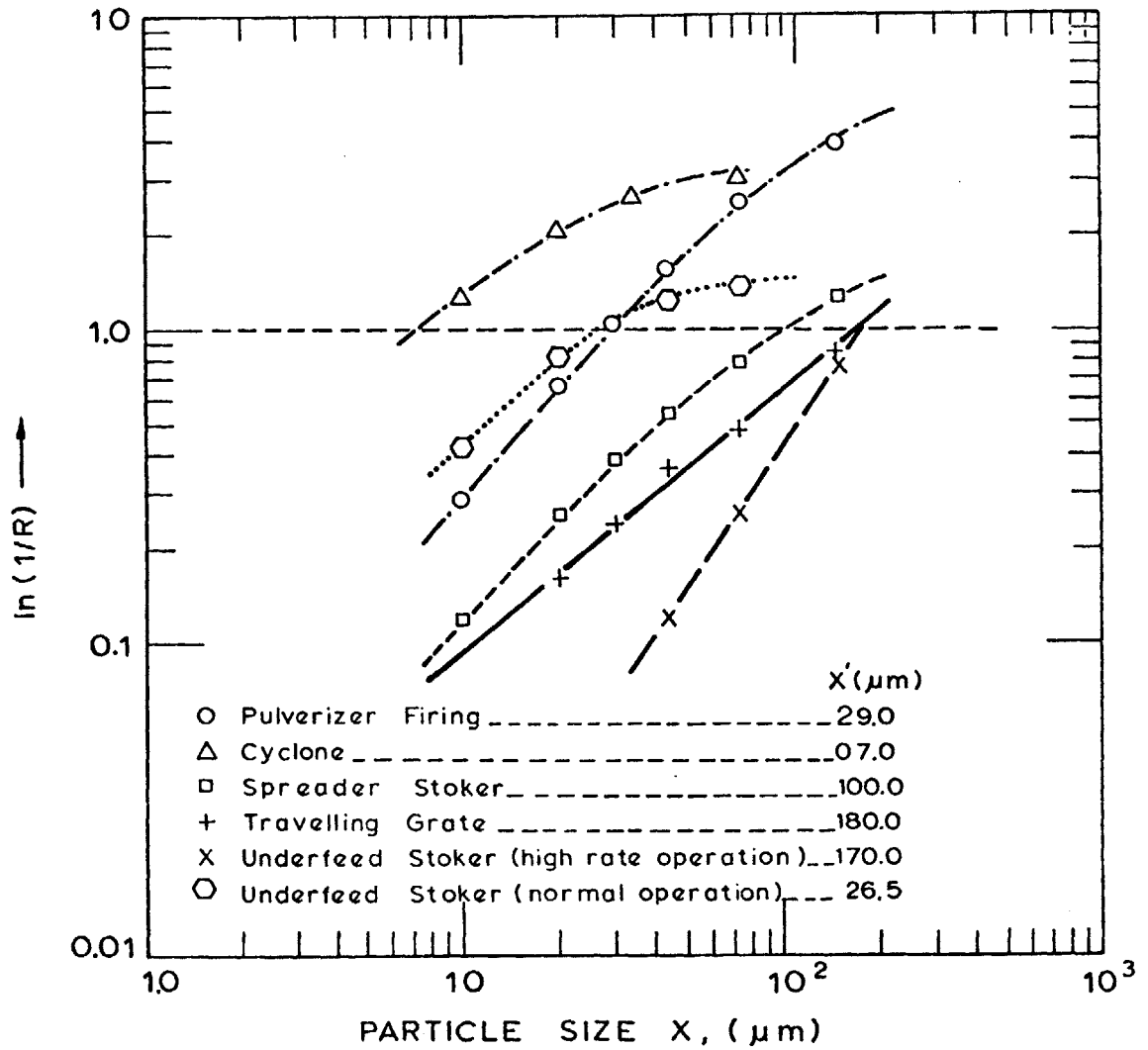
Figure 2.6 Rosin - Rammler Plot of the Size Distribution of Fly Ash from Different Combustors (Kaiser, 1951)

Table 2.4 Combustion Parameters and Mean Particle Size for
Different Combustors (Kaiser, 1951)

Type of Combustor	Coal Size	Mode of Combustion	Amount of Initial Ash in fly ash	Mean size of fly ash, μm *
Pulverizer Firing	70% below 200 mesh 93% below 100 mesh	Suspension burning	About 50%	29
Cyclone Burner	Minus 1/4 inch	Centrifugal force of a vortex of air and combustion gas	About 16%	7
Spreader Stoker	Wide variety up to 1 1/4"	Fuel bed	20-40%	100
Travelling Grate	Wide variety up to 1 1/4"	Fuel bed	About 15%	180
Underfeed	Small pieces (1/4" of coal & large pieces of coke	Fuel bed	5-30%	26.5 170+

* Mean size determined by Rosin Rammler fit

+ High rate operation. High velocity of gas through channels between the pieces enhancing agglomeration of ash.

Table 2.5 Size Distribution by Size of Particles From Selected
Source Without Control Equipment (EPA, 1972)

Type of Source	Particle by Size Range, %					Mean * Particle Size (µm)
	<5 µm	5-10 µm	10-20 µm	20-44 µm	>44 µm	
Pulverized	15	17	20	23	25	30
Cylcone	65	10	8	7	10	5.5
Stoker	4	6	11	18	61	~100

*Mean Particle Size is the size above which fraction oversize is $\frac{1}{e}$

function of both coal and ash. The Rosin-Rammler (1933) distribution function is given by eq. (1).

$$R = \exp[-b\,X^S] \tag{1}$$

where:

R = wt fraction of material of particle size
greater than X

b, S = parameters (determined empirically)

$\dfrac{1}{\sqrt[S]{b}}$ = measure of fineness of powder = size X for which the fraction oversize R is = $\dfrac{1}{e}$ = 0.368

S = measure of size dispersion. Low value indicating a wide size distribution.

Eqn (1) may be written as:

$$\text{Log}\,[\log 1/R] = s\,\log X + \text{constant} \tag{2}$$

so that a plot of log [log 1/R] against log X should give, for a size distribution obeying the Rosin-Rammler relation, a straight line of slope S.

The weight mean size $\overline{X}$ is defined as:

$$\overline{X} = \int_{x=0}^{\infty} x\,dR \tag{3}$$

which gives on substitution in (1)

$$X = \frac{1}{S\sqrt{b}}\ \Gamma\left(\frac{1}{S} + 1\right)$$

where:

Γ is the gamma function.

Figure 2.7 and 2.8 show the Rosin-Rammler distribution
fit for both coal and ash and Table 2.6 and 2.7 gives the
parameters computed from the fit in Figure 2.7 and 2.8.

Table 2.6   Parameters of Rosin-Rammler Fit for

Littlejohn's Coals (Fig. 2.7)

Coal #	S	b	$\overline{X}$ (μm)	X median
1	1.20	0.00581	69	54
2	1.21	0.00432	85	66
3	1.21	0.00801	51	40
4	1.21	0.00432	85	66
5	1.26	0.00318	90	71

Table 2.7   Parameters of Rosin-Rammler Fit for
Ash Produced from Littlejohn's Coals (Fig. 2.8)

Coal Ash #	S	b	$\overline{X}$ (μm)	X median
1	1.14	0.00873	61	46
2	1.13	0.00717	75	57
3	1.03	0.02297	39	27
4	1.1	0.00980	65	48
5	1.2	0.00611	66	51

2.2.3.3   Concentration v/s Particle Size Distribution of Ash.

As described earlier the important information needed for
the optimum design of combustors, gasifiers & ash separation
equipment and to estimate ash vaporization, is the knowledge
of both the concentration and the particle size distribution
of ash. Some studies, mainly relating to trace elements for
environmental significance have been performed previously.
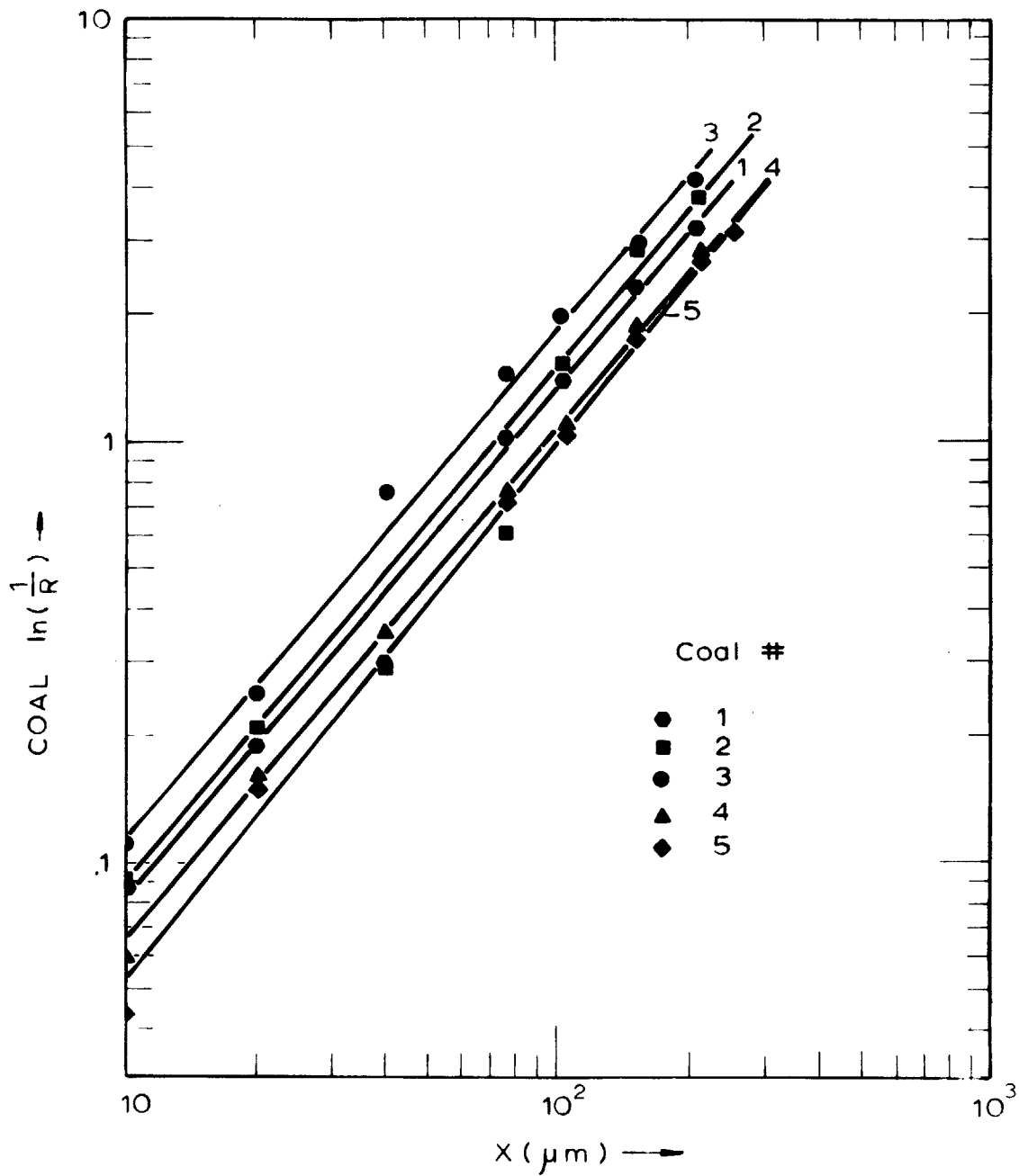
Littlejohn's Pulv. Coal Size Distribution

Figure 2.7
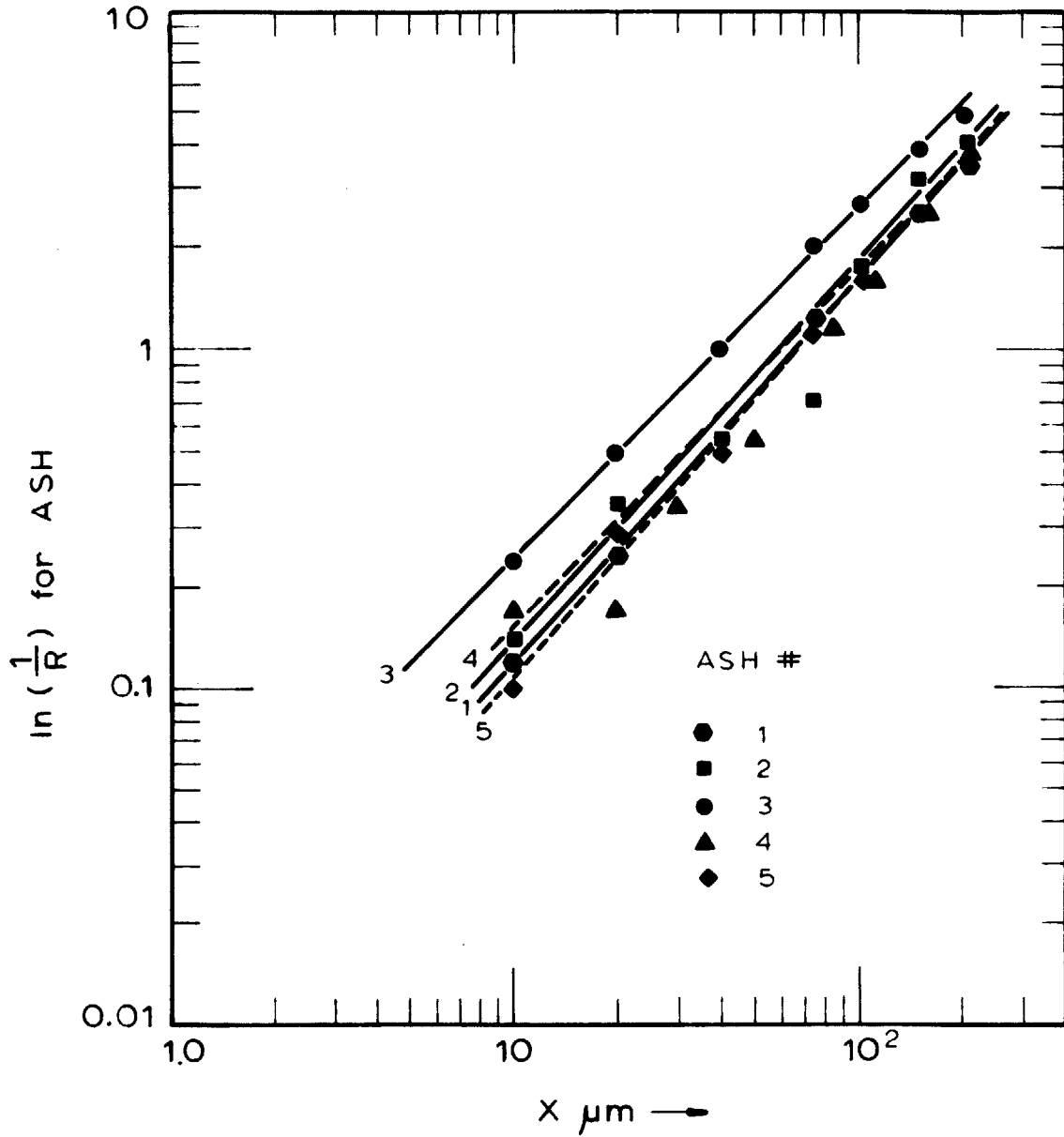
Littlejohn's P.F. Ash Size Distribution

Figure 2.8

Davison (1974) measured the concentration of 25 elements in fly ash emitted from coal-fired power plant as a function of particle size of ash. The main emphasis was on toxic elements like Pb, Se, Sd, Cd, Ni, V, Sn, Zn etc. Davison's results show that concentrations of Pb, Sb, Cd, Se, As, Zn, Ni, Cr and S increases markedly with decreasing particle size. Fe, Mn, V, Si, Mg, C, Be, Al show very limited concentration in the small sizes and Ca, Bi, Sn, Cu, Co, Ti, K show no concentration trends. The study did not include the various forms of the elements present in the different size fractions.

More precise information regarding PSD and composition is needed to study the behavior of ash at high temperatures.

2.3 Thesis Objectives

The principle objectives of this study were:

1. To characterize the distribution of mineral matter in coal with respect to its composition and particle size distribution.

2. To study the physical and chemical behavior of the mineral matter in coal under combustor simulated conditions to increase the understanding in the fields of:

   a. Thermal decomposition of the mineral species

   b. Particle size distribution of ash during combustion of coal

   c. Vaporization characteristics of the major mineral species at temperatures of up to 2250°K.

The study was designed to update and increase the knowledge regarding the behavior of mineral matter under rapid heating rates and at high temperatures (up to 2250°K) found in actual combustors. The equipment built has the potential for further explorations at higher temperatures (2700°K) pertinent to MHD combustors, with slight modifications.

The strategy of investigation can be summarized in the following steps.

1. A first order model of a coal fired combustor was generated and the missing gaps of information were identified (Sarofim, Howard, Padia and Kobayashi, 1975). To predict the behavior of ash at high

temperatures of the order of 2700 K, pertinent to MHD combustors, information regarding the particle size distribution and composition of ash is necessary because the vaporization of ash is inversely proportional to the square of the particle diameter and the vapor pressure is a function of the composition.

2. The literature on the occurance and behavior of ash during combustion of coal was reviewed to identify the existing state of knowledge in the field.

3. An experimental system was selected to simulate combustor conditions, and various analytical tools were examined to provide the information desired, once the samples were obtained from the reactor.

4. Mechanisms for the decomposition of mineral matter and ash loss by devolatilization are proposed to justify the experimental results.

Hopefully, the study would be able to provide some answers for the following questions:

1) What is the realistic nature of the distribution of mineral matter in coal? Is it present in a segregated form and what is the relationship between its composition and particle size?

2) During rapid combustion in actual combustors when coal is subjected to high heating rates, does the mineral matter agglomerate to form one particle or does it remain in its segregated form?

3) What percent of mineral matter originally present in the coal vaporizes and is gas borne with the combustion products? What is the composition and particle size distribution of the residual solid?

These questions are of practical interest for the design of any combustor, the estimation of the vaporization rates of different mineral species in case of an MHD combustor and for the design of ash separation equipment, e.g., electrostatic precipitator or cyclone separator, in case of conventional combustors.

EXPERIMENTAL APPARATUS AND PROCEDURE

3.1 Selection of Apparatus.

The temperature range up to 2500K, high heating rate of the order of $10^5 - 10^6$ °C/sec and combustion in dispersed phase are required in order to simulate actual combustor conditions. Although devolatilization at high temperatures about 2000K, may require only few milliseconds to complete (Kimber and Gray 1967), ash behavior studies, particularly relating to its particle size distribution, are only possible once char combustion is completed up to a certain extent. Char combustion at high temperatures, above 1800°C in diffusion limited and is the slower process compared to devolatilization, which may require up to a few seconds to complete even at high temperatures. Therefore, a combustion system capable of dispersing the pulverized coal particles at high temperatures of up to 2500K with heating rates of the order of $10^5 - 10^6$ °C/sec and providing residence times of few seconds is required to study the behavior of ash under combustor simulated conditions.

Various methods of coal heating have been tried in the literature which can be classified into stationary and moving systems. Among stationary methods like suspending a crucible containing coal in a preheated furnace, heating coal particles between

electrically heated screen (Anthony 1974; Juntgen and Van Heek 1968; Loison and Chauvin 1964) and heating stationary samples of coal by lasar pulse of microwave have been tried. Among the moving systems techniques like free fall reactor, entrained flow and fluidized beds have been tried.

Stationary techniques will not permit desired high heating rates and the short time studies due to the physical difficulties associated with factors like moving the sample in and out of the heated region quickly. Although laser irradiation techniques are capable of achieving very high heating rates but there are disadvantages like complexity in the experimental equipment and the absence of precise temperature measurement. Among the moving systems fluidized beds operations suffers from the problems of handling agglomerating and caking coals.

A free fall reactor could provide the desired residence time and heating rates [see Appendix A for calculations of heating rates and residence time in a free fall furnace]; and using ceramic tubes it is possible to use oxidizing environment required for char-burnout. Such a reactor was built by using a commercially available electrically heated high temperature furnace made by ASTRO Industries with 15 cm essentially constant temperature hot zone. A terminal velocity of about 7cm/sec for 100 μm size coal particle in air

atmosphere at 2000°C, provides about 2 seconds of residence time in the hot zone of 15 cm length, suitable for ash behavior studies.

3.2 Apparatus Description.

The experimental equipment consists essentially of three components:

a)   coal feeding system

b)   reactor furnace and

c)   char or ash collection system.

a)   Coal Feeding System.

Several methods of feeding pulverized coal have been tried in the literature. Feeders of the vibratory, screw, jet-dispersion and positive-displacement types have shown to be unsatisfactory due to unstable flowrates. However, some of the fluidized feeders have shown to be successful both on large scale and laboratory scale [Huff et al 1964, Hamor and Smith, 1971]. The requirements in the present experimental scheme was to have a pulverized coal feeder which can provide reasonably stable flow of coal particles with minimum amount of carrier gas to minimize any cooling effect caused by cold carrier gas.

The feeder used in the present study was a partially fluidized, vibrating, vertical coal feeder as shown in Figure 2.1. The feeder employs a mechanical vibrator and partial fluidization of coal particles to

Carrier Gas

Coal Feed
Port

Vacuum
or
Flush

Feed Rate
Control
Valve

Coal

Carrier Gas
Jet

Plexiglas
Body

Vibrator

Coal and Carrier Gas
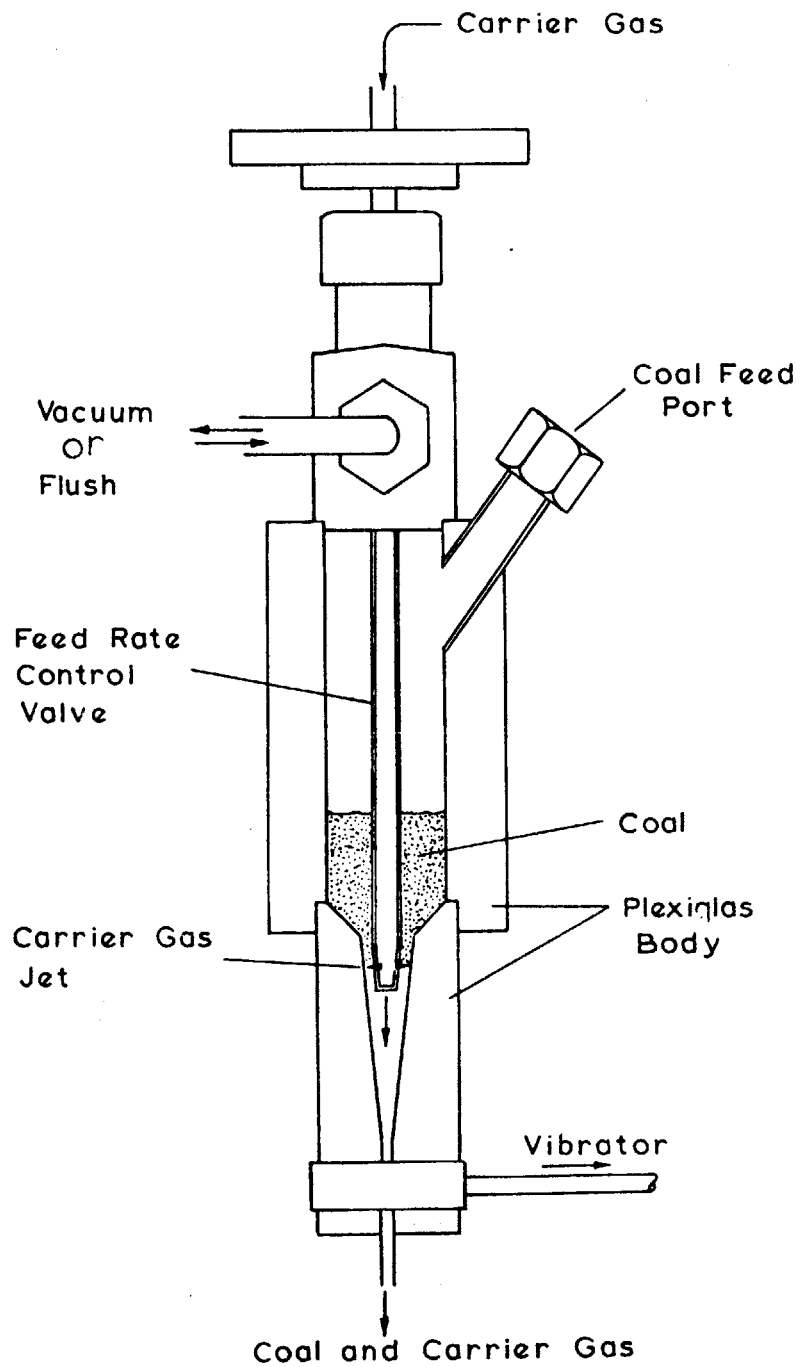
COAL FEEDER

Figure 3.1

get uniform feed rates. The coal particles are charged (about 2 gms in a batch) in the cylindrical body of the feeder and pass through the conical section into the water cooled section before going into furnace. The feed rate is controlled by the opening between conical section in the feeder and 1/8" stainless steel tube carrying carrier gas, the strength of vibration and the amount of carrier gas. Carrier gas is introduced in the feeder through four 5 mil holes drilled radially along the periphery of the 1/8" stainless steel tube. The exit of the feeder from the conical section is connected to a 1/8 inch stainless steel tube which is introduced into the furnace vertically. A water cooling jacket is provided on this 1/8" feeder tube. The vertical arrangement of the feeder allows extremely small carrier gas flow (as small as 2 cc/min where coal flow rate is about 0.1 gm/min) which helps in minimizing the cooling of furnace by carrier gas and heating the injected particles rapidly.

b)   Reactor Furnace

The main part of the system is an ASTRO model 1000A furnace. (Figure 2.2) A 3.5 inches I.D. 12 inches long graphite resistance heating element is placed at the center of the furnace. A 4 inches I.D. graphite radiation shield and packed graphite power provide necessary thermal insulation. The outer shell is watercooled and a sight hole and a boron graphite

Coal Particles
and Carrier Gas

Main Gas

Honeycomb
Flow Straightener

Water Cooled
Particle Injector

Graphite
Heating
Element

Alumina
Muffle
Tube

6"
Hot
Zone

Alumina
Liner Tube
To Support
Honeycomb

Water
Cooled
Shell

Cooling
Section

Water Out

Particle Collecting
Porous Bronze Disc

Water In

Optical Grade Quartz
Plate

Vacuum
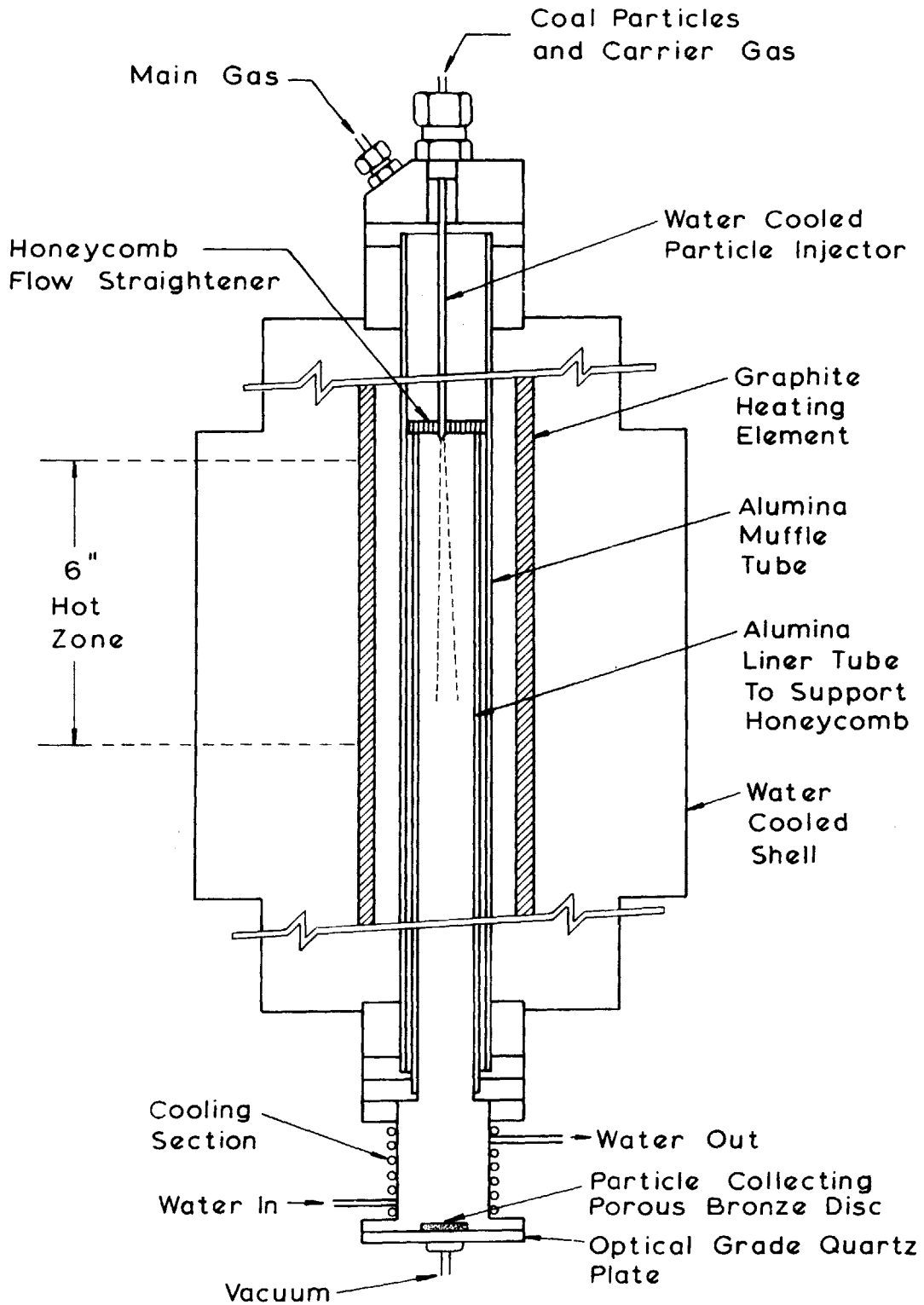
Figure 3.2 Equipment- Free Fall Furnace

thermocouple is located radially at the center. The furnace is capable of operating at 2700°K with graphite or zirconia muffle tube and at 2000°K with alumina muffle tube. The furnace is equipped with an automatic temperature controller and a programmer to heat up at desired heating rates. This feature is especially important for zirconia and alumina muffle tubes, since these ceramics are susceptible to thermal shock.

Detailed furnace description, procedure for the operation of furnace, temperature controller and programmer, can be found in the furnace operational manual.

The reactor furnace is equipped with an alumina tube assembly which allows the use of oxidizing atmosphere in the furnace. The alumina tube is 3 inch I.D. and 23" long. Another smaller alumina tube 2 inch I.D. and 15 inch long is used as a liner tube to support a 1 inch thick and 1/16" nominal pore size ceramic honeycomb which acts as a flow and temperature straightener for the incoming flow. The primary alumina tube is sealed with water cooled end fittings to the furnace and separates the inert atmosphere in graphite heating element from the oxidizing atmosphere inside ceramic tube needed for the combustion of coal particles.

A 9 inch long with 4 inch I.D. cooling section is connected to the bottom of the furnace in order to cool the samples before collecting them on the porous bronze collector.

The furnace can be heated to a desired temperature by selecting the appropriate setting on the temperature controller. The temperature profiles in the furnace at the four settings used with alumina muffle tube are shown in Figure 2.3.

c) Collection System.

The ash or char sample is collected by using a combination of three filters a porous bronze (1/8" thick, 2" diameter) and two fiberglass filters one on either side of the bronze filter. The bronze filter is capable of trapping particles about 5 μm and above while the fiberglass filters have capabilities of retaining particles of size 1 μm and below.

3.3 Procedure.

Two types of experiments were performed in oxidizing atmosphere in order to observe the behavior of ash during coal combustion; free fall and crucible. The experiments were performed at four different settings of the furnace giving peak temperatures of 1050, 1250, 1500 and 1830°K. Higher temperatures can be reached using a zirconia muffle tube.

In case of free fall experiments, 1.0 to 2.0 gm of coal particles were injected by a water cooled probe into the center of the hot muffle tube along with very small amount of carrier gas (4-5 cc/minute). Air flow rate was maintained such that the stoichiometry inside the furnace at all times was about 50 to 100% fuel
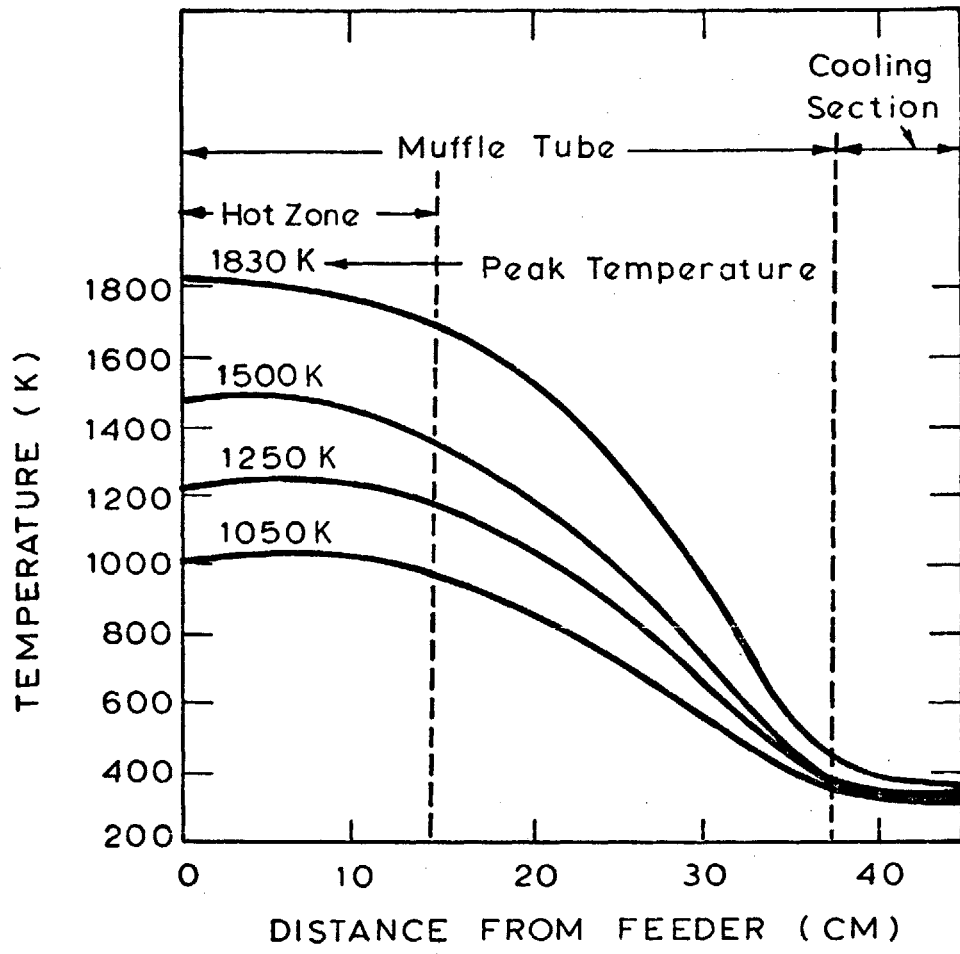
Axial Temperature Profile in Free-Fall Furnace

Figure 3.3

lean, in order to avoid local depletion of oxygen due to
sometimes uneven flow rate of coal particles. Samples
after combustion, partial or complete are collected on
the filter system described in Section 3.2.C, located
at the bottom of the furnace after a water cooled sec-
tion. The temperature in the furnace in the water
cooled section is below 500°K, so not to support any
additional burning of coal particles. The effective
burning time is about that which is experienced in the
hot zone of 15 cm length.

Temperature Measurements

Axial and radial temperature profiles were measured
at each furnace setting by thermocouple traverses.
Platinum/Rhodium or Iridium/Rhodium thermocouples were
used. Radial temperature profiles were found to be
almost flat. Axial temperature profiles at four furnace
settings are given in Figure 3.3.

Particle temperatures were measured by using a
Leeds & Northrup 8620-Series disappearing filament type
optical pyrometer. The pyrometer was first sighted on
the furnace wall and was calibrated by the known wall
temperatures from thermocouple traverses. The pyrometer
then was sighted on the burning particles viewing from
the bottom of the furnace through the optical grade
quartz plate. The optical pyrometer readings could be

taken within about a $\pm$ 30°C accuracy.

Particle Velocities

The velocity of the particles was determined for selected conditions using a laser-doppler anemometer made by Thermo-System Incorporation. The velocity of the particles for free fall case was found to be of the order of about 20 cm/sec providing a residence time of about 0.7 seconds. The details of the laser-doppler anemometer can be found elsewhere (Kobayashi, 1976). Experimental conditions for free-fall runs are summarized in Chapter 6.

Crucible Experiments

Samples of ash or coal were introduced into the furnace in crucibles which were raised into the hot zone from the bottom of the furnace. Crucible experiments, although providing heating rates much lower than expected for pulverized coal flames were useful for evaluating mechanisms. Experiments were run with:

(1) Ash from an ASTM ashing experiment heated in an oxidizing atmosphere

(2) Coal in an oxidizing atmosphere

(3) Ash in an inert atmosphere

(4) Coal in an inert atmosphere followed by ashing of the char at ASTM conditions (750°C)

(5) Mixtures of silica and graphite.

3.4 Analysis.

The most important part of the ash behavior study
is the analysis of the collected samples from the ex-
periments. It should be emphasized here that no one
method of analysis can provide all the information
needed to study this complicated problem. Several tools
are used and an effort is made to integrate and compli-
ment the results obtained by different methods.

The analysis include the original coal analysis
and the char and ash analysis for particle size distri-
bution, structure and composition. Gravimetric
analyses were performed in order to estimate ash weight
loss and char combustion. Various techniques were
used some of which are:

1. Low temperature Ashing - to obtain the amount
of mineral matter in the coal.

2. Electron microprobe analysis - to obtain the
distribution of ash in coal and char samples
on a microscopic scale.

3. Electron microscopy and EDXRA - to obtain
size and shape of samples and finally obtaining
the size distribution for coal and ash. Also
to identify the elements present in the
desired area by energy dispersive X-ray
analysis (EDXRA).

4. Atomic Absorption Spectrometry - to obtain the

metal elemental composition of mineral matter
in coal and char samples.

5. X-Ray Diffraction - to obtain mineral species
in the LTA or char and ash samples.

6. ASTM analysis for total ash.

following paragraphs describe the basic principles of these analysis techniques.

3.4.1 Low Temperature Ashing.

Low temperature ashing technique is used to separate mineral matter from coal without altering its structure and composition seriously. The ashing is performed under a controlled vacuum below a temperature of 200°C. Basic principle is the reaction of activated atomic oxygen with the organic material in the coal at low temperature.

Commercial-grade oxygen is passed through a high-energy electromagnetic field produced by a radio-frequency (r.f.) oscillator. An electrodeless ring discharge takes place in the gas, and activated oxygen is produced. The activated gas is a mixture of atomic and ionic species as well as electronically and vibrationally excited states. The activated oxygen, which is slightly warm, then passes over the sample and ashing proceeds without any other external source of heat. Because the sample temperature is low, volatility and diffusion losses are substantially lower than those

incurred in conventional high-temperature ashing. The
gaseous products of the oxidation, primarily carbon
dioxide and water vapour, are removed from the system
by a vacuum pump.

3.4.2 Electron Microprobe Analyzer.

An electron-probe analysis can provide a measure
of the local composition and structure of a heterogeneous
material like coal. The basic underlying principle is
that by irradiation of the sample with an electron beam
focused to about $1\mu m$ diameter at the surface of the
sample and the measurement of the characteristic X-rays
or the electrons emerging from the irradiated area
would allow one to get qualitative and quantitative
analysis of the chemical composition of the sample. The
wave length of the X-rays emitted follow the law

$$\lambda \propto \frac{1}{z^2}$$

where

λ = wavelength

z = Atomic number

and the intensity of the irradiation for a particular
wave length gives the concentration of the corresponding
element.

Electron probe analysis is a powerful tool in the
present study because of the very heterogeneous
structure of the coal. The behavior of ash cannot be

characterized with the average composition alone but would depend mainly on the distribution of the ash constituents with respect to both size and composition. It is also fortuitous that the degree of heterogeneity is on the micron size scale (which is apparent from photomicrographs of polished coal); this is about the practical limit for the effective X-ray source size.

Samples to be examined by electron microprobe are first mounted on a slide with epoxy as the binding material, and then polished carefully to expose the crystal structure. A thin layer of carbon is vacuum deposited to make the samples conducting. The slide prepared by this method is then probed from point to point. The metal oxides to be analyzed are chosen and the instrument is calibrated for those oxides by using standard samples of known oxide concentrations. The specimen to be analyzed is probed for each metallic oxide by counting photons of different energy levels. The number of photons are compared with the count rate of standard samples to provide concentration after correction for the interaction of the presence of other oxides. The concentration of the metals are reported in terms of percentage oxide concentrations.

Elements below 11 (sodium) and down to 5 (boron) require high vacuum and special detectors. The practical limit of detectability is approximately 100-500 ppm.

3.4.3 Scanning Electron Microscopy

Scanning Electron Microscope (SEM) is used to ex-
amine the microstructure of coal and ash. The SEM uses
secondary electrons emitted from the surface of a sample
to form seemingly three-dimensional images. The SEM has
a wide range of magnification (20 to 100,000X) and a
depth of field approximately 300 times that of the light
microscope. Resolution of better than 20 nm is possible
on available instruments as compared with resolution for
the visible light microscope of 200 nm. By using SEM
information on particle size, shape, texture and topo-
graphy of the surface is obtained. Contamination of the
particle surface is also readily apparent. Agglomeration
and purity can be observed directly, the SEM is also
equiped with an energy dispersive X-ray analyser (EDXRA)
which makes possible the semiquantitative analysis of
elemental composition.

In SEM a beam of high energy electrons is scanned
over a sample which is tilted at some angle, usually 45°.
The low energy secondary and back-scattered electrons
form the optical image of the sample.

3.4.4 Atomic Absorption Spectrometry-(AAS)

AAS is used to obtain overall elemental composition
of the ash samples. In principle, in atomic absorption
spectrometry, the absorption spectra of isolated atoms

are used to obtain information on the kind and number of

atoms present in a chemical sample. This information, in

turn, indicates the elemental composition of the sample.

The instrumentation used in atomic absorption spectrometry

provides a clear indication of the characteristics of

this powerful technique.

In an atomic absorption spectrometer, the flame is

illuminated with a primary source of radiation, a portion

of which is absorbed by ground-state atoms. Radiation

transmitted by the flame passes through a monochromator

and on to a photodetector-readout system which displays

the final signal in terms of either transmittance of

absorbance.

Slot burners which provide a long path length have

been developed for atomic absorption spectrometry.

Slot burners are of the premix type, but differ from

conventional premix burners in that the exit orifice is

a narrow slot between 5 and 10 centimeters in length

rather than an array of tiny holes. The premixed fuel

and oxidizer gases leave the bowl of the burner through

this slot, thereby defining the geometrial shape of the

resulting flame. The source of primary radiation is

directed down the long axis of the flame. The absorption

spectra for atomic species consist of extremely narrow

lines, usually on the order of 0.01 A wide. The source

of narrow-band radiation most commonly used in atomic

absorption spectrometry is the hollow-cathode lamp. In

the hollow-cathode lamp, a low power electrical discharge is sustained between an inert electrode (anode) and a second electrode (cathode) made from the element to be determined. Atoms from the cathode are therby excited, to produce a very pure line spectrum of the desired element in additon to the line spectrum of the inert fill-gas (argon or heon) present in the hollow-cathode lamp. The lamp being used in our analysis is a multielement lamp which emmits characteristic lines of Si, Al, Fe, Ca, Mg, the elements of interest to ash analysis.

3.4.5 X-Ray Diffraction

X-ray diffraction is one of the most powerful analytical tools for particle characterization and identification. Diffraction patterns can be obtained from either single crystals or a powdered mixture. X-ray diffraction is probably the only microanalytical technique that identifies any previously characterized compound as such. In other words, if the x-ray powder diffraction data for a given compound has been determined and tabulated, then subsequent samples of that compound can be identified by comparison of the measured data with the tabulation. The ASTM data file* holds powder diffraction data for well over 20,000 compounds and is being constantly expanded.

---

*Joint Committee on Powder Diffraction Standards, 16-1 Park Lane, Swarthmore, Pennsylvania 19081.

X-ray diffraction measures the interplanar spacing of atoms in a crystal. The Bragg equation, $\nu\lambda = 2d\sin\theta$ (where ν is an integer, λ the x-ray wavelength, d the interplanar spacing and θ the diffraction angle) is used to convert observed θ angles to corresponding d values.

Minerals in coal are present in crystalline form and change the form at high temperatures. At temperatures above 2000°K, generally a glassy non-crystalline phase resulted which did not give x-ray diffraction patterns interpretable by means of the Bragg equation. Original mineral matter also contained some amorphous, non-crystalline material which again did not give x-ray patterns.

Further details of x-ray diffraction methods and the type of equipment used in the study can be found in the classical text on x-ray diffraction by Cullity (1956).

3.4.6 ASTM Analysis for Total Ash

In order to obtain total ash content of coal or char samples, standard ASTM tests were used. The test involves heating of 1 gm of sample contained in a porcelain crucible in air atmosphere in a muffle furnace at 750°±20°C, up to constant weight. The furnace should be heated up gradually from room temperature to 500°C in

1 hour and from 500°C to 750±20°C in another 1 hour period. The constant weight of sample resulting after combustion at 750±20°C is defined as the ash content fraction of the original sample. Further details of the experimental equipment and procedure for ash determination are reported elsewhere (ASTM Standards, 1972).

All these techniques were used from time to time to characterize and identify the samples. The specific details of the techniques with the operational parameters are described along with the appropriate chapters in this thesis.

Chapter 4

COALS USED AND THEIR CHARACTERIZATION

4.1 Types, Origin and Morphology:

Two types of coals, supplied by the Institute of
Gas Technology, were used in this study. The coals were:

1. Bituminous Coal - a strongly caking coal from
    Consolidated Coal Company's Ireland Mine of
    the Pittsburgh No. 8 seam.

2. Lignite - Montana lignite from the Savage Mine
    owned by the Knife River Coal Mining Company.

The coals were pulverized using a ball mill and
sieved to separate different size fractions. Two size
fractions, nominal 38-45 μm representing proposed fuel
size for MHD and nominal 75-90 μm size were studied.

Figure 4.1 is a scanning Electron Micrograph of
pulverized lignite particles, size graded between 75
and 90 microns. Figure 4.1.b, which is a magnified
view of one lignite particle shows a number of small
shiny particles sticking on to the surface of the lignite.
Energy dispersive x-ray analysis shows that these small
particles are richer in mineral matter compared to the
parent black surface. As also can be seen, lignite
particles are angular in outline and do not show any
pore structure or fibrous striations.

SEM Photograph of PULVERIZED LIGNITE COAL PARTICLES
(75-90 μm size range)

(A)
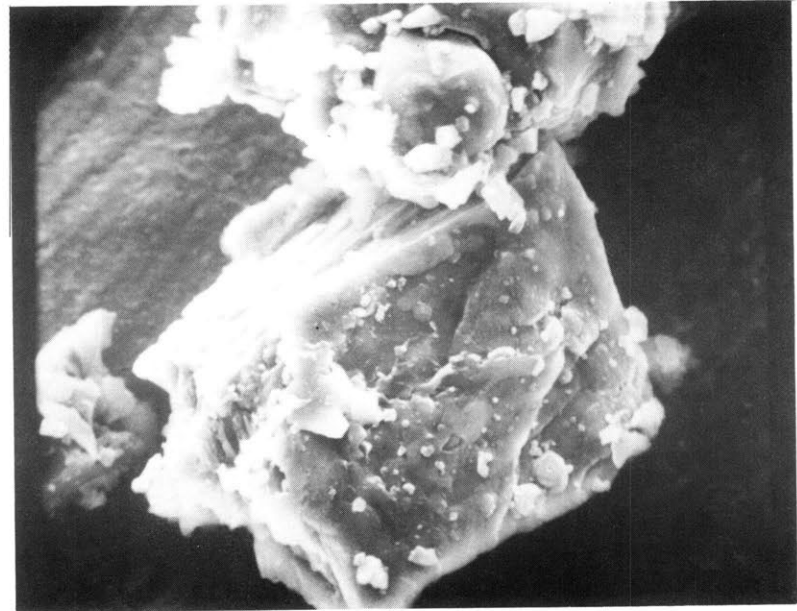
ONE PARTICLE AT HIGHER MAGNIFICATION

(B)

Figure 4.1

Figure 4.2 is a Scanning Electron Micrograph of a Bituminous coal particle in the size range 75-90 μm. Unlike lignite, bituminour particles do not show any sharp corners but pores and fissures are quite visible (Figure 4.2.b).

4.2 Particle Size Distribution:

Although coal particles were sieved with extreme precaution, a small amount of fines accompanied the sieved size fraction. The size distribution for coal particles was measured by first taking representative photographs of a large number of particles and then counting and measuring 200-500 particles in one photograph. The Rosin-Rammler relation was used to represent the size distribution of both the coal particles and the ash samples produced in this study. The relation is given by equations (4.1) and (4.2)

$$F(X) = B.S(X)^{S-1} \exp(-BX^S) \tag{4.1}$$

where

$F(X)$ = probability of finding particles of size X

B,S = characteristic parameters in the distribution function

$X' = (B)^{-1/S}$ = measure of the fineness of powder

= size X for which the fraction oversize is $1/e$

X_{median} = size X for which fraction oversize is 0.5.
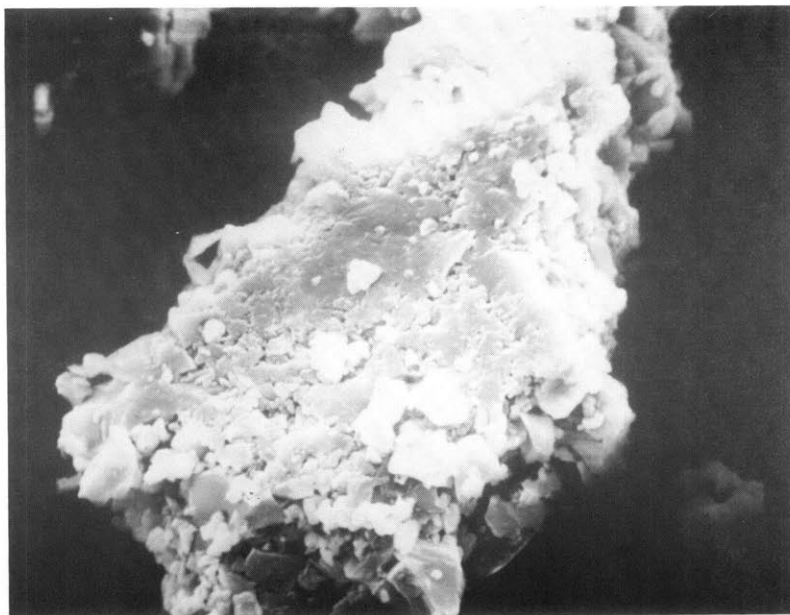
50 μm

Pulverized BITUMINOUS COAL PARTICLES
(75-90 μm size range)

(A)
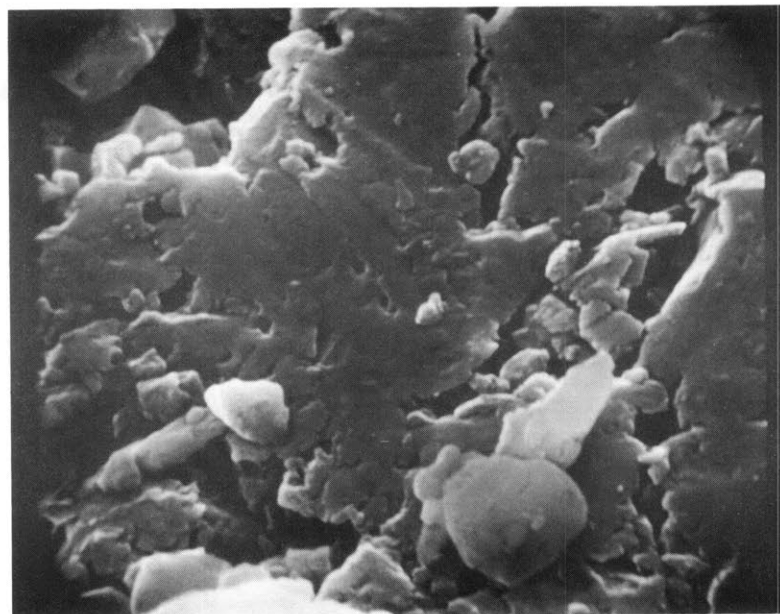
5 μm

Surface of one Particle at higher magnification

(B)

Figure 4.2

$$R = \exp\ [-BX^S] \qquad\qquad (4.2)$$

where

R = weight fraction of the particles above size X.

Figure 4.3 shows the probability distribution curve for all 4 coal samples and Table 4.1 gives the value of the parameters estimated by the Rosin-Rammler fit for the distribution.
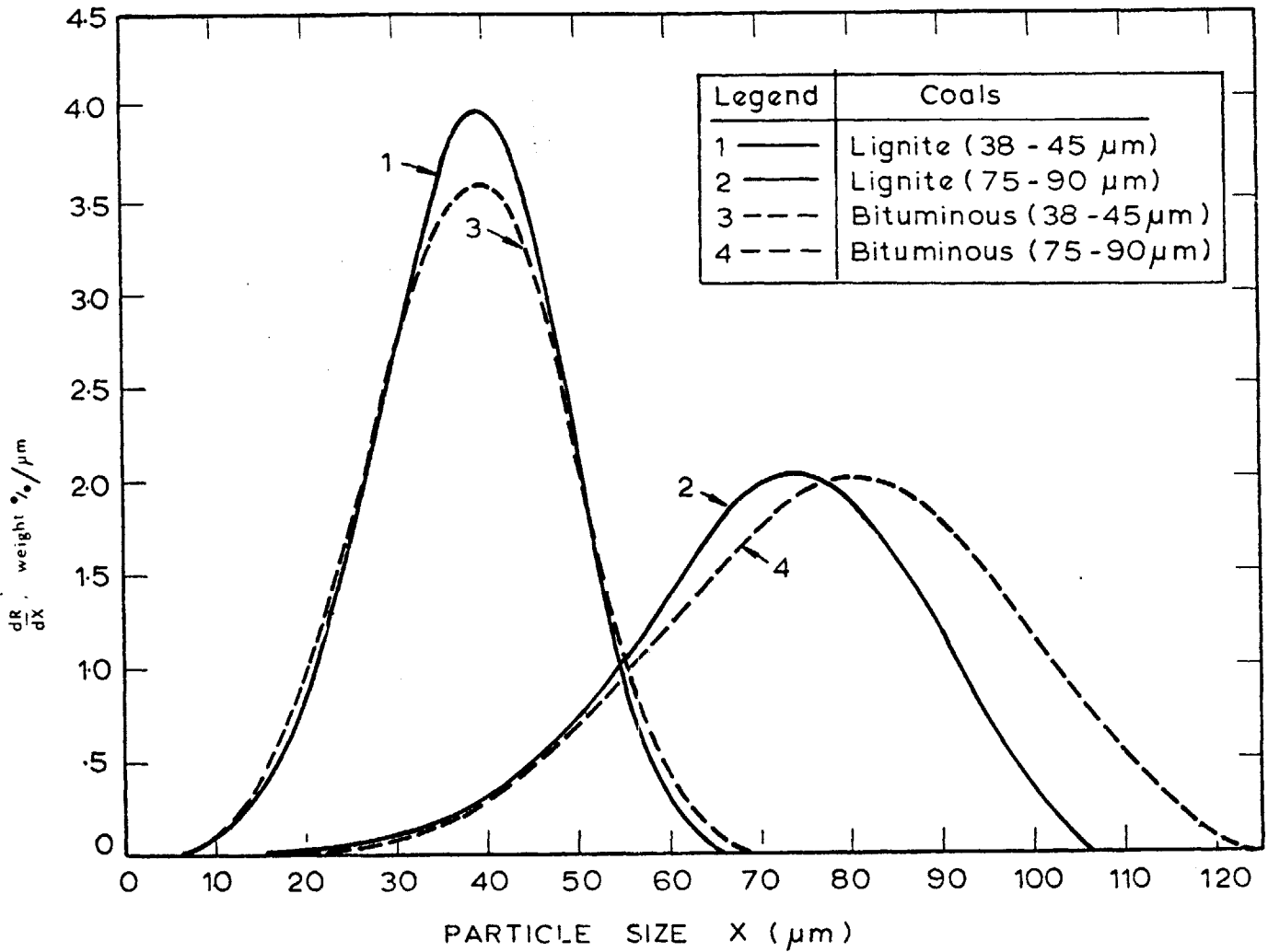
Probability Function for the Original Coal Particle Size Distribution using Rosen-Rammler Relation

Figure 4.3

Table 4.1 Rosin Rammler Coefficients for Coal Particle

Size Distribution of Figure 4.3

Coal Type	B	S	X_{median} (µm)	X' (µm)
1. LIGNITE (38-45 µm nominal)	1.091×10^{-7}	4.30	37.3	41.6
2. LIGNITE (75-90 µm nominal)	1.374×10^{-10}	5.22	71.0	77.4
3. BITUMINOUS (38-45 µm nominal)	3.21×10^{-7}	4.00	38.9	42.0
4. BITUMINOUS (75-90 µm nominal)	1.646×10^{-9}	4.55	82.0	85.2

4.3 Ultimate and Proximate Analysis.

Ultimate and proximate analysis of the coals used

are given in Tables 4.2 and 4.3.

Table 4.2 Ultimate Analysis of Coals Used

Coals →	LIGNITE		BITUMINOUS	
SIZE →	38-45 µm	75-90 µm	38-45 µm	75-90 µm
Moisture	13.63	13.37	2.22	2.24
Carbon	55.21	56.70	67.80	66.29
Hydrogen	4.93	5.17	5.00	4.94
Nitrogen	0.61	0.62	1.045	1.01
Chlorine	<0.01	<0.01	0.0695	0.035
Sulfur	0.82	0.85	4.83	4.95
Ash (wet basis)	7.85	7.04	10.545	11.57
Ash (dry basis)	9.09	8.12	10.785	11.83
Oxygen (by diff.)	16.95	16.25	8.49	8.96

Table 4.3 Proximate Analysis of the Coals Used

Coals →	LIGNITE		BITUMINOUS	
SIZE →	38-45 µm	75-90 µm	38-45 µm	75-90 µm
Moisture	12.23	13.26	1.98	1.90
Volatile Matter	36.00	36.81	38.42	38.55
Ash (dry)	9.60	8.38	10.96	12.40

Ultimate analysis was performed by Galbraith Laboratories, Inc., Knoxville, Tennessee and proximate analysis was performed in our laboratory facilities. The values reported in Table 4.3 are average of several runs; the moisture varied about 0.5 percent and ash varied about 0.2 percent from run to run. Comparison of the values of dry basis ASTM ash between Tables 4.2 and 4.3 shows small difference between the two values, part of which could be accounted for by the inhomoginity of the samples.

4.4 Ash Composition and Sulfur Forms.

Table 5 gives the oxides analysis of the ASTM ash produced from the coals and Table 6 gives the different forms of sulfur existing in the coals. (analysis of oxides performed by using Atomic Absorption Spectrometry; Analysis of minor oxides, sulfates and sulfur forms performed by Galbiaith Labs.)

Table 4.4 Oxides Analysis of ASTM Ash from Coals

[All numbers are percent by weight of dried ASTM Ash]

Coals →	LIGNITE		BITUMINOUS	
SIZE →	38-45 µm	75-90 µm	38-45 µm	75-90 µm
S_iO_2	26.80	21.69	37.52	36.15
Al_2O_3	16.41	16.33	19.15	19.12
Fe_2O_3	3.41	4.07	29.34	28.87
C_aO	28.44	31.95	4.65	5.36
M_gO	9.02	9.68	0.73	0.73
P_2O_5	1.02	1.03	0.32	0.32*
T_iO_2	0.50	0.46	0.58	0.58*
K_2O	0.35	0.37	1.38	1.38*
Na_2O	0.27	0.31	0.44	0.44*
SO_4^{--} and SO_3^{--} as SO_3	13.45	13.48	4.10	4.10*
Total Major oxides	84.08	83.72	91.39	90.23
Total Minor oxides	2.14	2.17	2.72	2.72
Total all [including sulfates]	99.67	99.37	98.21	97.05

*Not analyzed; assumed same as 38-45 µm size

Table 4.5 Different Sulfur Forms in Coals Used

Coals →	LIGNITE		BITUMINOUS	
SIZE →	38-45 µm	75-90 µm	38-45 µm	75-90 µm
Pyritic Sulfur	0.17 *	0.18	2.57 *	2.65
Sulfate Sulfur	0.07 *	0.07	0.71 *	0.73
Organic Sulfur	0.71 *	0.73	1.67 *	1.72
Total Sulfur	0.95	0.98	4.94	5.09

all numbers % of original coal (dry basis)

(*) samples not analyzed. Calculated by proportioning

assuming no size dependency of coal on sulfur

forms.

Chapter 5

DISTRIBUTION OF MINERAL MATTER IN PULVERIZED COAL

5.1 Introduction:

In spite of the extensive efforts devoted toward understanding of the occurrence and forms of mineral matter in coal by several investigators (Selvig and Gibson 1956, Kewezys and Taylor 1964, Brown and Swaine 1964, Gluskoter 1967, O'Gorman and Walker 1971, O'Gorman and Walker 1973), little is known regarding composition and particle size distribution of mineral matter in pulverized coals. The objective in this section is to characterize the composition and particle size distribution of mineral matter in the pulverized coals which are later used to study the high temperature behavior of ash.

Mineral matter are known to exist in coals in different forms and both crystalline as well as amorphous states. While Kaolinite, Illite, Pyrites, Carbonates and Sulfates take the major share of the mineral matter in coal, a number of accessory minerals could also be present in minor quantities. Table 5.1 gives a list of some of the major and minor minerals generally found in U. S. Coals.

In order to study the mineral matter in coal in their original form, it is desirable to separate the inorganic mineral matter from the organic structure of coal. Since mineral constituents of coal are intimately bound with the coal substance, it is not possible to completely separate the mineral matter by any physical method. High temperature (above 500°C) combustion of organic matter

Table 5.1 Minerals Associated With Coals

A. Major Minerals

SPECIES	MAIN ELEMENTS	CHEMICAL FORMULA
Kaolinite	Si, Aℓ	$Al_2Si_2O_5(OH)_4$
Illite	Si, Al, K	$K_{1-1.5}Al_{5-5.5}Si_{6.5-7}O_{20}(OH)_4$
Pyrites	Fe, S	FeS_2
Marcasite	Fe, S	FeS_2
Calcite	Ca	$CaCO_3$
Dolomite	Ca, Mg	$CaMg(CO_3)_2$
Gypsum	Ca, S	$CaSO_4 \cdot 2H_2O$
Bassanite	Ca, S	$CaSO_4 \cdot \frac{1}{2}H_2O$
Anhydrite	Ca, S	$CaSO_4$
Coquimbite	Fe, S	$Fe_2(SO_4)_3 \cdot 9H_2O$

B. Minor Minerals

SPECIES	MAIN ELEMENTS	CHEMICAL FORMULA
Muscovite	Si, Aℓ, K	$K_2Al_6Si_6O_{18}(OH)_8$
Quartz	Si	SiO_2
Siderite	Fe	$FeCO_3$
Hematite	Fe	Fe_2O_3
Magnetite	Fe	Fe_3O_4
Sphalerite	Zn, S	ZnS
Galena	Pb, S	PbS
Chalcopyrite	Cu, Fe, S	$CuFeS_2$
Fluorapitite	Ca, P, F	$Ca_3F(PO_4)_3$
Zircon	Zr, Si	$ZrSiO_4$
Iron Oxides	Fe	$HFeO_2, HFeO_2 \cdot nH_2O$

from coal would cause significant amount of thermal decomposition of the inorganic constituents making it impossible to study the composition and particle size distribution of original mineral matter in coal. The objective is achieved by using a low temperature ashing technique (described in detail under section 5.3) in which organic matter from coal is oxidized at temperatures of the order of 100°C, by using an atomic oxygen plasma, leaving behind the mineral matter of coal essentially in its unaltered state.

Low temperature ashing is a relatively new technique (first used for ashing coals by Gluskoter in 1965) and require expensive instrumentation, therefore, mineral matter in coals are traditionally characterized by ASTM ash analysis, which involves oxidation of the organic matter in coal at 750°C. Apparently, significant amount of thermal decomposition of mineral matter also takes place altering both the amount and composition of mineral matter in coal. In view of this it is desirable to relate ASTM ash to the original mineral matter or closest to it the low-temperature ash. Based on a theoretical systematic decomposition scheme, a relation is derived between the amount of low temperature and ASTM ash. This is a secondary objective of this chapter.

The characterization of particle size and composition of the mineral matter was performed by using a scanning electron microscope and an energy dispersive X-ray analysis system to obtain the semiquantitative estimates

of the elemental composition in the sighted area. Minerals were identified by comparing their crystal structure and the main elements with standard crystal structure of naturally occurring minerals. X-ray diffraction was performed on the low temperature ash samples to obtain a qualitative picture of the minerals present in the sample and to support the findings by the former method.

5.2 Coals Studied

In order to study the behavior of ash during different stages of combustion, two types of coals, supplied by the Institute of Gas Technology, were used. One is a strongly caking bituminous coal from Consolidation Coal Company's Ireland Mine of the Pittsburgh No. 8 seam, and the other coal is a Montana Lignite from the Savage Mine owned by the Knife River Coal Mining Company.

The particle size distribution, the ultimate and proximate analysis, ash composition and sulfur forms of these two coals for the two size fractions studied (38-45)μm and (75-90)μm, are described in details in Chapter 4.

5.3 <u>Experimental</u>:

5.3.1 <u>Low Temperature Ashing</u>.

Low temperature ash (LTA) was produced by oxygen plasma apparatus for all four coal samples by two different sources, first by the courtesy of LFE Corporation, Waltham, Mass., and second by the courtesy of Professor C. Hamrin at University of Kentucky, Lexington, Kentucky.

The device used by LFE Corporation is their model number LTA 505 Low Temperature Asher, a schematic of which is shown in Figure 5.1. Commercial-grade oxygen is admitted through a flowrator control (1). A high-energy electromagnetic field is produced by a radio frequency (r.f.) oscillator (2). An electrodeless ring discharge takes place in the gas, and activated oxygen is produced. The activated gas is a mixture of atomic and ionic species as well as electronically and vibrationally excited states. The activated oxygen reacts with the sample in the oxidation chamber (3), without any additional external source of energy. The sample is contained in a pyrex sample boat (4) which is positioned approximately two inches below the r.f. field. The sample temperature remains relatively low between 100-200°C. Therefore, losses due to vaporization, diffusion and thermal decomposition are substantially lower than those incurred in conventional high temperature (750°C) ASTM ashing procedure. The gaseous products of the oxidation, primarily carbon dioxide and water vapor, are exhausted
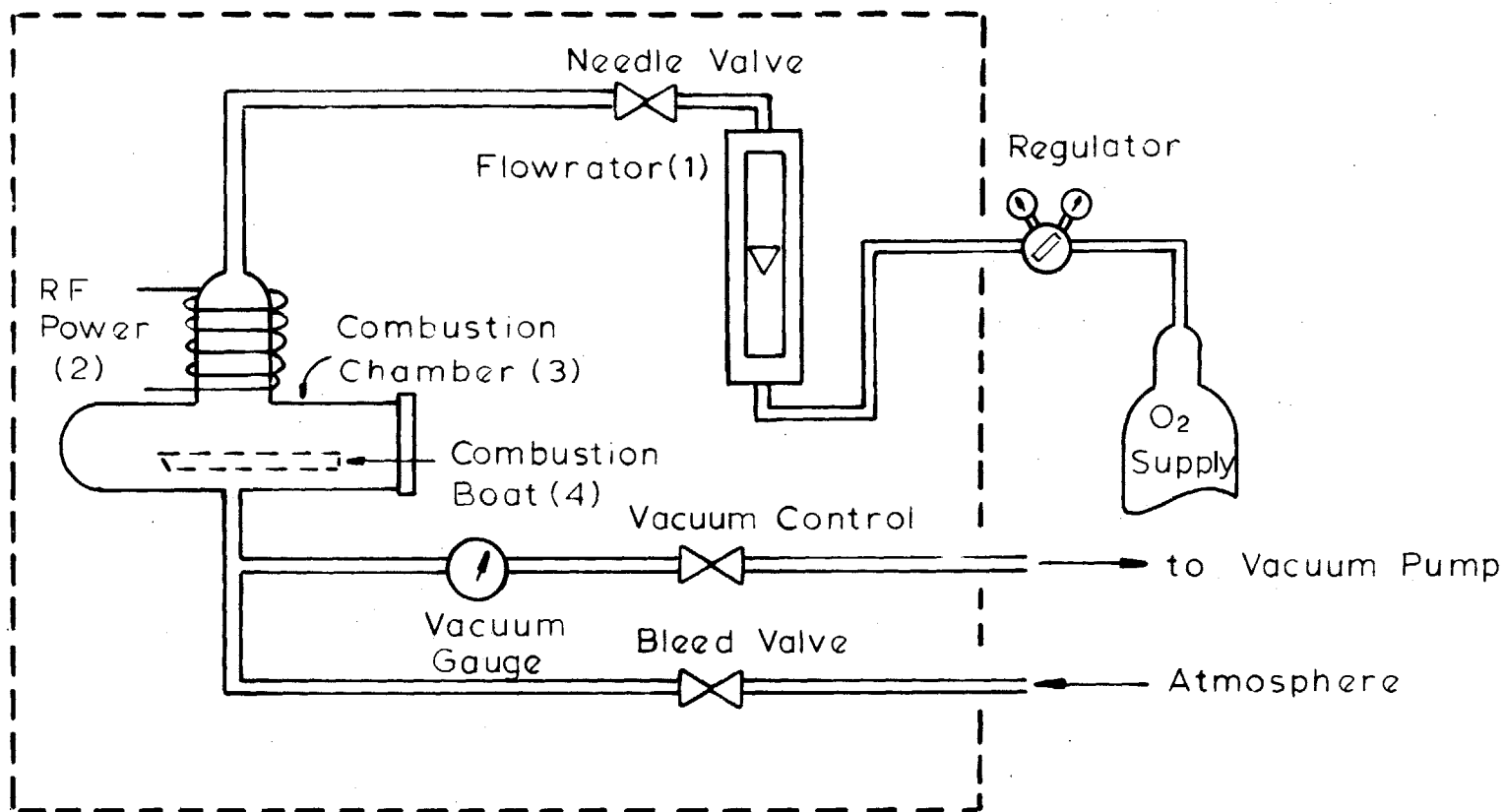
Schematic of LFE Low Temperature
Asher LTA 505

Figure 5.1

continuously by a mechanical vacuum pump, which is con-
trolled by values (5). The LTA 505 is designed to
process 5 samples at a time. Samples ranging from 0.25
to 0.75 gms were placed in the combustion boats. The
samples were automatically agitated every 4 minutes to
expose a newer surface for combustion.

The ashing time required for bituminous coals was
of the order of 24 hours. The lignite required con-
siderable longer time, ranging from 70 hours to 130 hours.
The samples are weighed periodically and ashed to
constant weight.

5.3.2 Analytical Methods.

After the production of low temperature ash by
oxygen plasma system, the characterization of mineral
matter was carried out mainly by two methods. A scanning
electron microscope (SEM) was used for particle shape
size and crystal structure identification and an energy
Dispersive X-ray Analysis System (EDXRA) to give com-
plementary semiquantitative information on the main
elements present in the particle. The samples prepared
for SEM were vacuum coated with copper instead of con-
ventional gold deposition. This was done to avoid any
interference of gold with sulfur since the peaks for
gold and sulfur occur very near to each other. Some
effort was devoted towards making very accurate
quantitative elemental analysis by microprobing a
polished section of coal. X-ray diffraction patterns

were obtained for the four low temperature ash samples

using a General Electric diffractometer. Each sample

was X-rayed by using monochromatic CuKα radiation

(λ = 1.54050 A°) from 2θ angle of 5° to 100° with a

scanning speed of 2° per minute and chart speed of 0.5

inch per minute. Minerals are identified by locating

the peaks of the diffracted beam intensity.

5.3.3 ASTM Analysis.

The Coal samples were ashed in a muffle furnace at

750°C according to standard ASTM procedure. The ash thus

produced for each of the coal sample can be compared with

the low temperature ash in order to develop a decompo-

sition scheme.

5.4 Results and Discussion:

5.4.1 Low Temperature Ash Characterization.

The primary purpose of low temperature ashing was

to separate mineral matter form coal in it essentially

unaltered state for further identification and charac-

terization of minerals with respect to composition and

particle size distribution. Small changes, for example

dehydration of some of the minerals, loss of small

amount of chlorine and sulfur could be expected, even

at this low temperature (100-200°C) of ashing

(Gluskoter 1965).

Major minerals present in the coal samples were

identified by performing X-ray diffraction on the low

temperature ashes in the same manner as described above.
Figures 5.2, 5.3, 5.4, and 5.5 show the X-ray diffrac-
tion patterns for the four low temperature ash samples,
with the major peaks labelled by the mineral names.
Table 5.2 gives the major minerals and expected 2θ in
degrees for the first eight intensities for CuKα radi-
ation.

The minerals commonly identified in bituminous coals
were kaolinite, illite, quartz, pyrite, coquimbite, cal-
cite and anhydrite. Anhydrite [CaSO$_4$] could be the re-
sult of dehydration of gypsum [CaSO$_4 \cdot 2$H$_2$O] during low
temperature ashing. There is almost no difference in the
diffraction patterns of the two different sizes (38-45μm)
and (75-90 μm).

The diffraction patterns of lignite LTA differed con-
siderably from those of bituminous coals. The major minerals
identified were bassanite [CaSO$_4 \cdot 1/2$ H$_2$O],kaolinite [Al$_2$
Si$_2$O$_5$(OH)$_4$], lawsonite [CaAl$_2$SiO$_4 \cdot 2$H$_2$O], quartz [SiO$_2$],
dolomite [CaMg(CO$_3$)$_2$] and rutile [TiO$_2$]. Bassanite again
could be the result of partial dehydration of the original
gypsum [CaSO$_4 \cdot 2$H$_2$O]. Bassanite could be the main source
of the high concentration of calcium in the lignite.
Another characteristic difference from bituminous coals
is the absence of clays and illite type structure. One
major calcium alumina silicate mineral lawsonite
[CaAl$_2$SiO$_4 \cdot 2$H$_2$O] could be identified. Small
differences were observed between the two size range

K - Kaolinite $\left[Al_2Si_2O_5(OH)_4\right]$

I - Illite

Q - Quartz $\left[SiO_2\right]$

P - Pyrites $\left[FeS_2\right]$

Cq - Coquimbite $\left[Fe_2(SO_4)_3 \cdot 9H_2O\right]$

C - Calcite $\left[CaCO_3\right]$

A - Anhydrite $\left[CaSO_4\right]$

2θ (DEGREES)
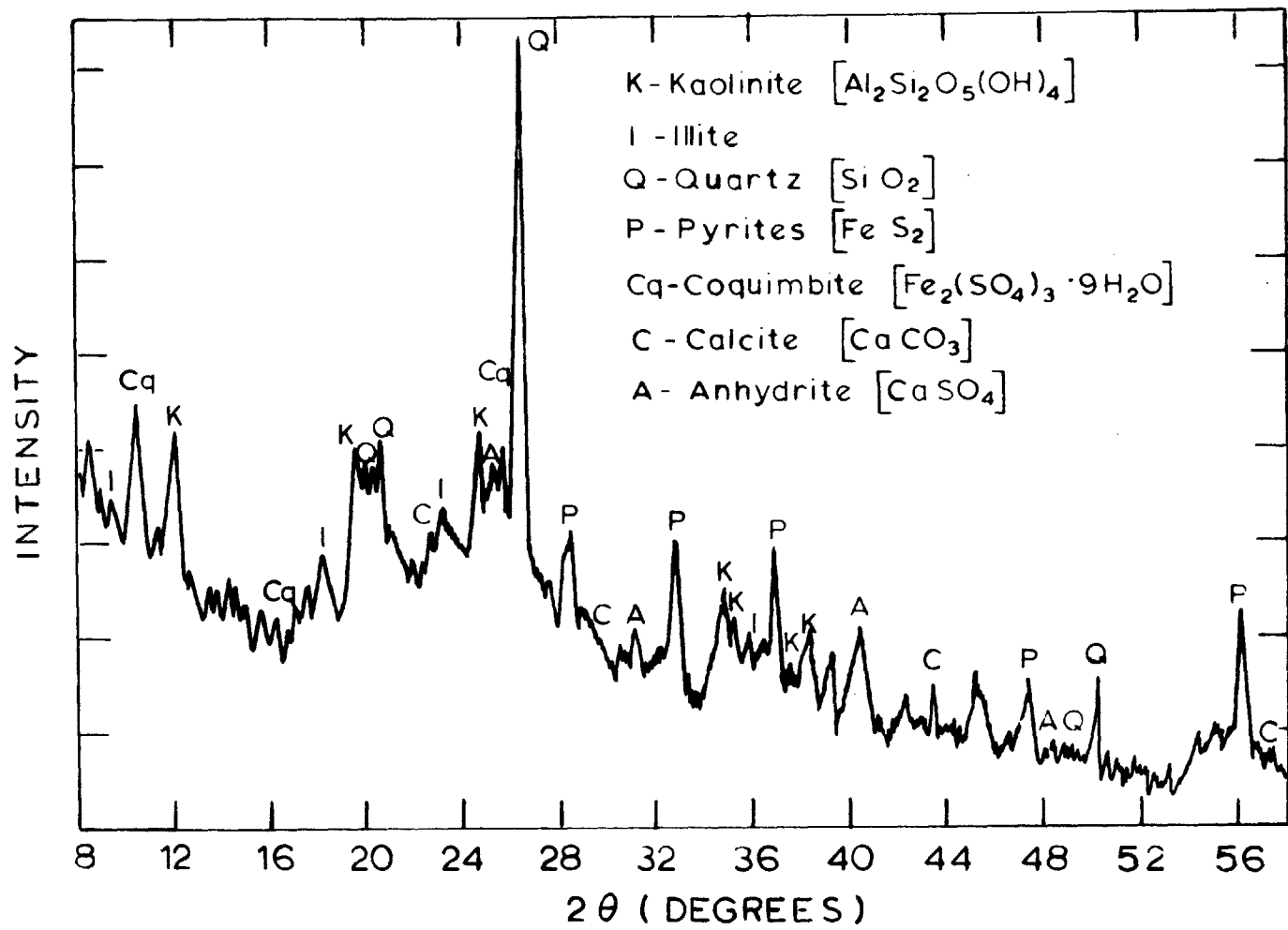
X-Ray Diffraction Pattern of Bituminous (38-45 μm) LTA

Figure 5.2

K - Kaolinite $[Al_2Si_2O_5(OH)_4]$

I - Illite

Q - Quartz $[SiO_2]$

P - Pyrite $[FeS_2]$

Cq - Coquimbite $[Fe_2(SO_4)_3 \cdot 9H_2O]$

C - Calcite $[CaCO_3]$

A - Anhydrite $[CaSO_4]$
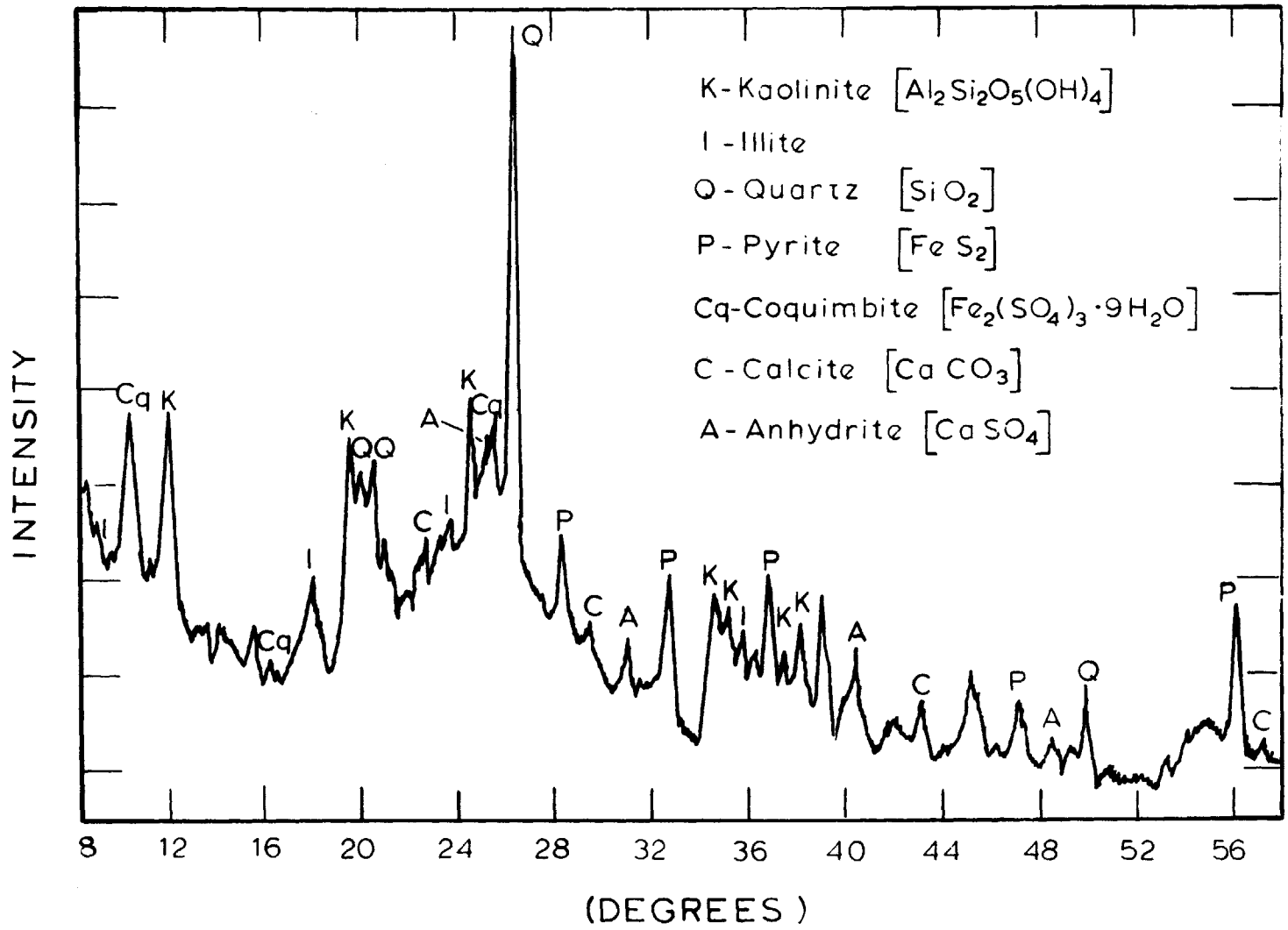
X-Ray Diffraction Pattern of Bituminous (75-90 μm) LTA

Figure 5.3

K - Kaolinite $[Al_2Si_2O_5(OH)_4]$
B - Bassanite $[CaSO_4 \cdot \frac{1}{2}H_2O]$
L - Lawsonite $[CaAlSiO_2 \cdot 2H_2O]$
Q - Quartz $[SiO_2]$
D - Dolomite $[CaMg(CO_3)_2]$
R - Rutile $[TiO_2]$
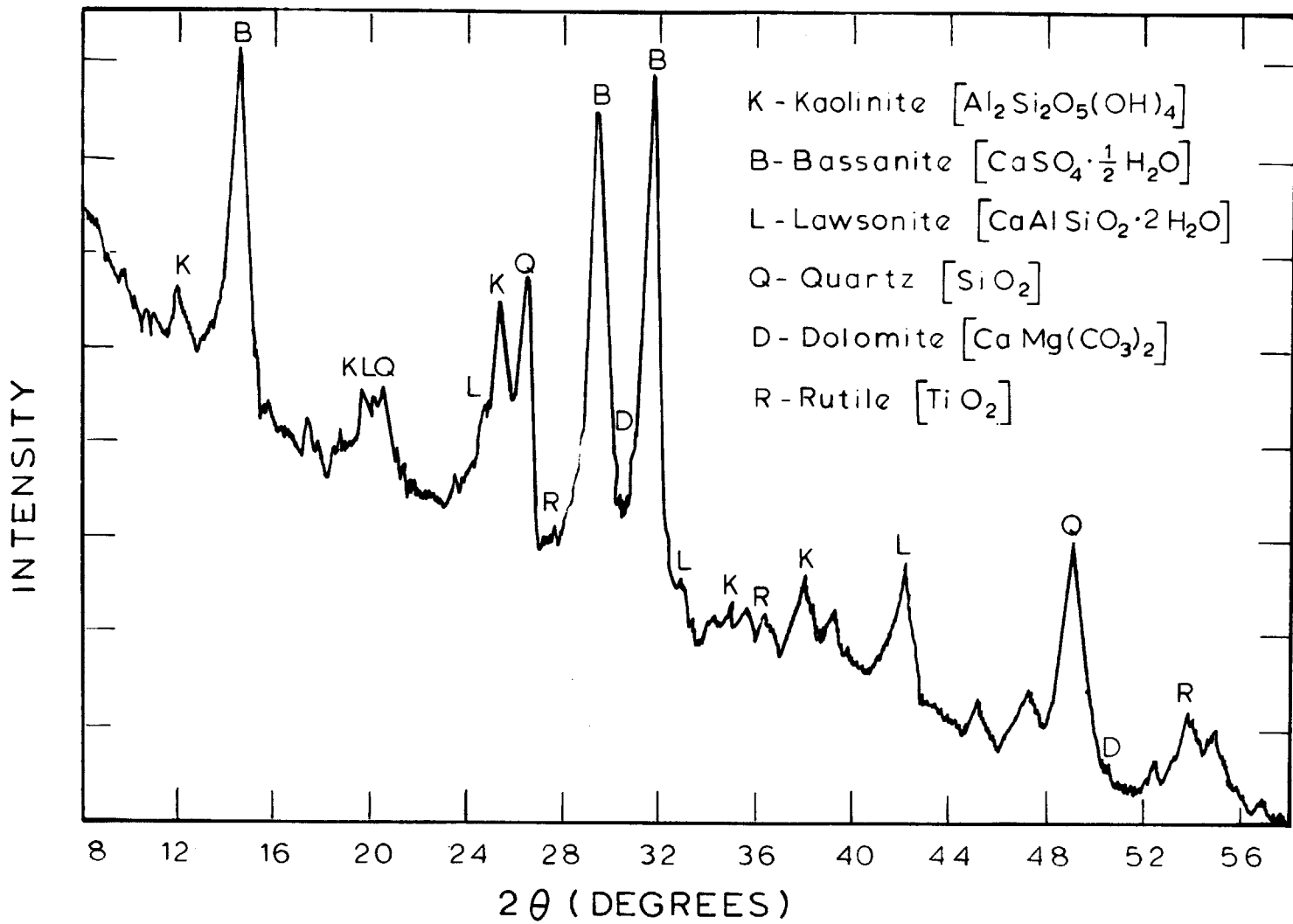
X-Ray Diffraction Pattern of Lignite (75-90 μm) LTA

Figure 5.4

K - Kaolinite $[Al_2 Si_2 O_5 (OH)_4]$

B - Bassanite $[CaSO_4 \cdot \frac{1}{2} H_2 O]$

L - Lawsonite $[CaAlSiO_4 \cdot 2 H_2 O]$

Q - Quartz $[SiO_2]$

D - Dolomite $[CaMg(CO_3)_2]$

R - Rutile $[TiO_2]$

INTENSITY
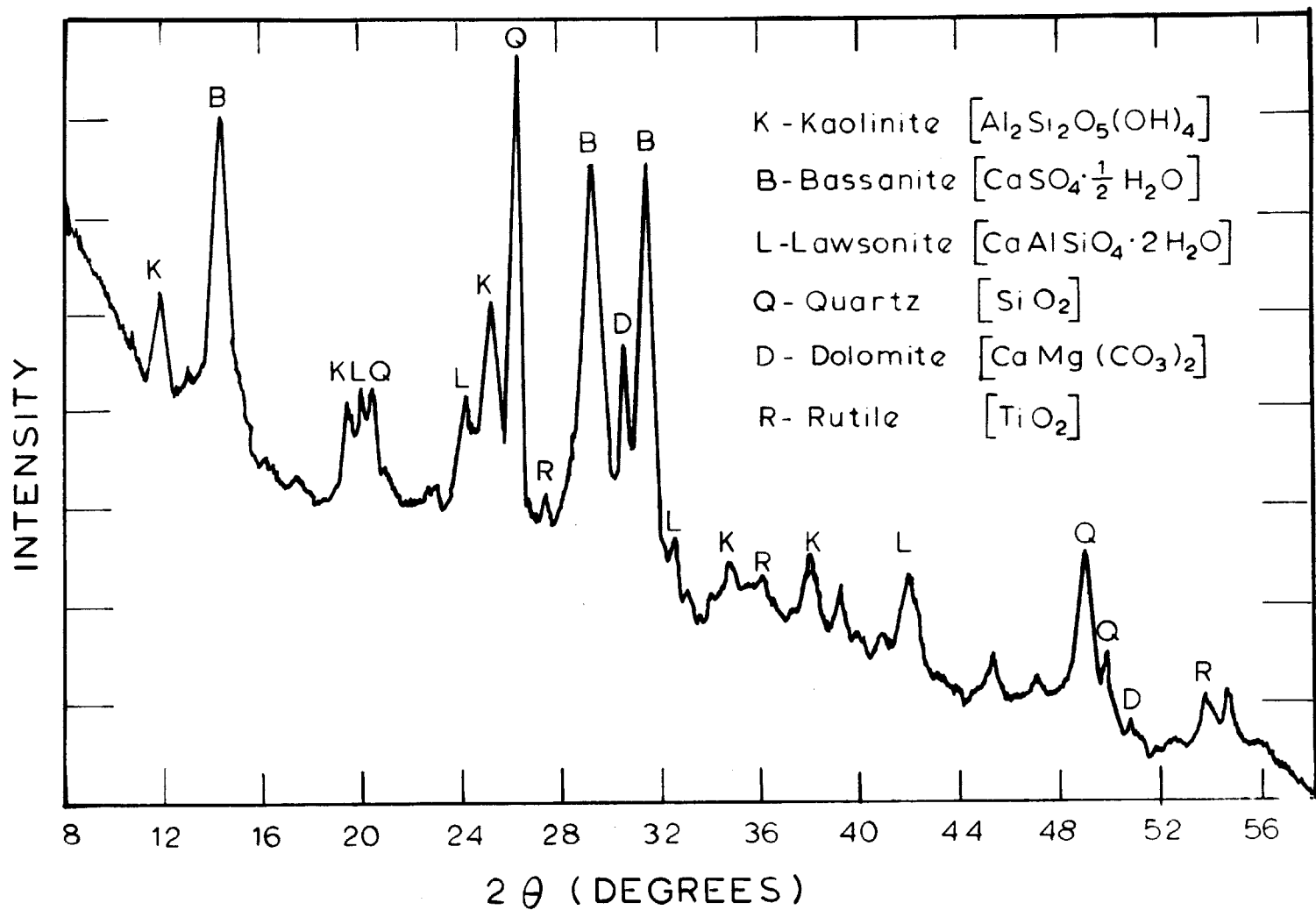
2θ (DEGREES)

X-Ray Diffraction Pattern of Lignite (38 - 45 μm) LTA

Figure 5.5

Table 5.2 Major Minerals and Their Peak Positions for CuKα Radiation [λ = 1.5405A°]

	MINERAL	FORMULA		2θ (degrees) for eight most intense peaks							
1	Kaolinite	$Al_2Si_2O_5(OH)_4$		24.9 (100)*	12.3 (100)	62.4 (100)	38.4 (90)	19.8 (80)	35.0 (80)	35.9 (80)	37.7 (80)
2	Illite	K,Na,Mg,Fe,Al, Si,O,H_2O		19.9 (100)	26.5 (100)	35.9 (100)	8.9 (80)	61.8 (80)	18.1 (60)	22.9 (60)	31.3 (60)
3	Calcite	$CaCO_3$		29.4 (100)	39.4 (18)	43.1 (18)	47.5 (17)	48.5 (17)	36.0 (14)	23.0 (12)	57.4 (8)
4	Aragonite	$CaCO_3$		26.2 (100)	45.9 (65)	27.2 (52)	33.2 (46)	37.9 (38)	36.2 (33)	48.3 (32)	38.4 (31)
5	Dolomite	$CaMg(CO_3)_2$		31.0 (100)	51.1 (30)	51.25 (30)	41.1 (30)	50.6 (20)	67.4 (15)	45.0 (15)	37.4 (10)
6	Bassanite	$CaSO_4 \cdot \frac{1}{2}H_2O$		29.8 (100)	14.7 (95)	31.9 (50)					
7	Gypsum	$CaSO_4 \cdot 2H_2O$		11.7 (100)	29.2 (57)	20.8 (51)	33.4 (28)	31.2 (27)	23.5 (21)	47.9 (16)	43.5 (10)
8	Anhydrite	$CaSO_4$		25.4 (100)	31.4 (33)	38.6 (22)	40.8 (20)	48.7 (15)	55.7 (14)	52.3 (11)	52.3 (10)
9	Pyrite	FeS_2		56.3 (100)	33.0 (84)	37.1 (66)	40.8 (52)	47.4 (40)	28.5 (36)	95.2 (27)	64.4 (24)
10	Marcasite	FeS_2		33.0 (100)	51.9 (63)	47.6 (30)	25.9 (40)	37.3 (25)	38.8 (25)	58.0 (20)	54.2 (15)

	MINERAL	FORMULA		2θ (degrees) for eight most intense peaks							
11	Coquimbite	$Fe_2(SO_4)_3 \cdot 9H_2O$		10.7 (100)	32.2 (76)	16.3 (64)	26.5 (62)	19.3 (44)	24.4 (42)	9.4 (40)	25.4 (34)
12	Lawsonite	$CaAl_2SiO_4 \cdot 2H_2O$		32.9 (100)	34.2 (70)	42.5 (70)	24.4 (60)	21.3 (50)	34.1 (50)	18.2 (40)	33.6 (40)
13	Quartz	SiO_2		26.0 (100)	49.2 (90)	58.8 (80)	65.7 (80)	67.1 (80)	40.6 (60)	44.1 (60)	73.2 (60)
14	α-Quartz	SiO_2		26.7 (100)	20.8 (35)	50.2 (17)	60.0 (15)	36.5 (12)	39.5 (12)	68.1 (11)	68.3 (9)
15	β-Quartz	SiO_2		26.2 (100)	20.5 (20)	49.6 (10)	41.6 (4)	45.1 (4)	58.9 (4)		

[* Relative Intensities are in parenthesis]

coals. Smaller size coals (38-45 μm) had a higher con-
centration of dolomite than the larger size (75-90)μm.

One important observation which can be made from
all these X-ray diffraction patterns is the presence of
amorphous material in the sample, as evidenced by the
broad maxima in the background radiation of the diffrac-
tion patterns. In the case of a purely crystalline
sample the background should rise steadily as the dif-
fraction angle (2θ) is decreased. (Cullity, 1956)

The characterization of both composition and parti-
cle size was made possible by combined scanning electron
microscopy and energy despersive X-ray analysis. In a
few cases electron microprobing was also performed to
obtain a better quantification of the elemental concen-
trations. Crystal structure as viewed with the scanning
electron microscope were compared with the standard
mineral crystal structure to identify the mineral com-
position. Appendix B gives a list of common mineral
found in coals with their standard crystal forms. The
results are presented for three main type of minerals
identified kaolinite, sulfate and carbonates and pyrites.

5.4.1.1 Kaolinite.

As mentioned earlier kaolinite (a hydrous layer
lattice silicate $[Al_2Si_2O_5(OH)_4]$ is the major mineral
found in coals accounting for about half of the total
weight of minerals. Fig.5.6 shows a variety of Kaolin
type particles exibiting varying composition of Si and
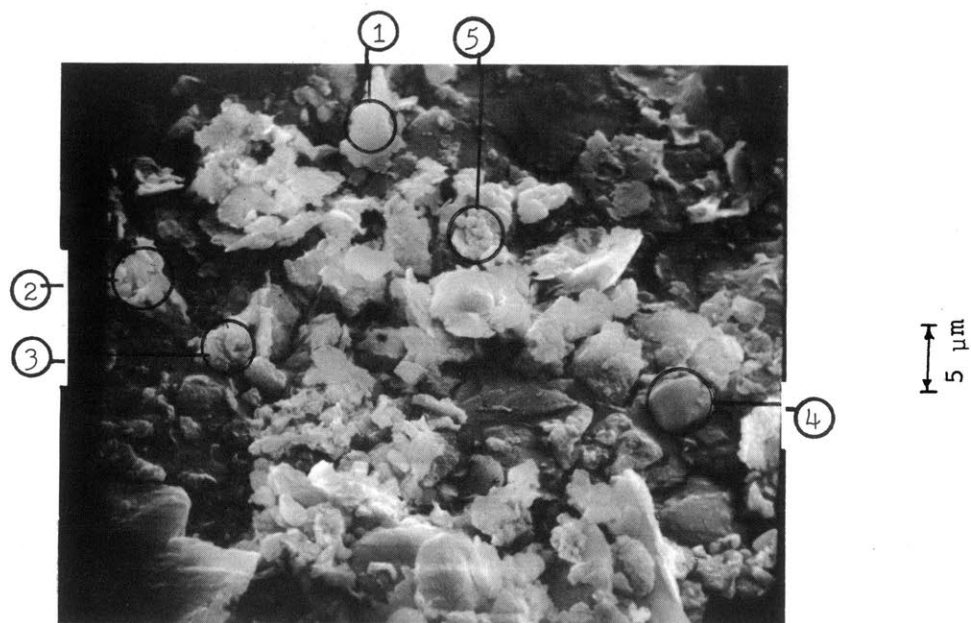
.A. Variety of Kaolin Type Mineral Particles Showing
Varying Composition of Si and Al
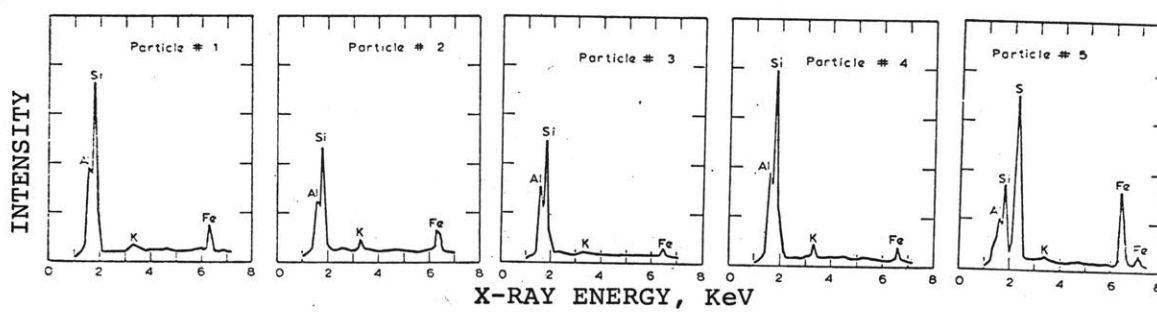
.B. EDXRA of Particles Encircled in Fig. A.

Typical Sample of LTA of Bituminous Coal

Figure 5.6

Al. The particles range from less than 1µm to about 5µm in size and possess minute and thin rhombic plate-like shapes. The abundance elemental analysis on 5 of the particles is shown on EDXRA curves (Fig. 5.6). Particles numbered from 1 to 4($\sim$5µm size) show Si/Al atomic ratio varying from 1.6 to 2.2. Since pure Kaolinite particle has a Si/Al ratio of unity, these results indicate that Illite [$K_{1-1.5}Al_{5-5.5}Si_{6.5-7}O_{20}(OH)_4$] and/or quarts [$SiO_2$] may also be present here. A small amount of K identified by EDXRA supports this picture. Particle number 5, which is different in appearance showing a group of small ($\sim$1µm) balls, shows mainly pyritic composition with Si, Al and K also present. This type of particle will be discussed under the heading of pyrites in section 5.4.1.3. Fig. 5.7 shows some more silicate particles with varying amounts of aluminum. Analysis of the encircled particle shows mainly Si with traces of K and Fe.

Fig. 5.8 shows Kaolinite-type particles again about 5µm in size, seen when a polished surface of a lignite coal particle (75-90µm size) was microprobed. Table 5.3 gives the main metal concentrations calculated as oxides on six different particles on the polished surface. Also shown is a particle exhibiting mainly iron. [White yellow shiny color under reflected light shows it is pyrite (FeS_2)]. This will be discussed under section 5.4.1.3.
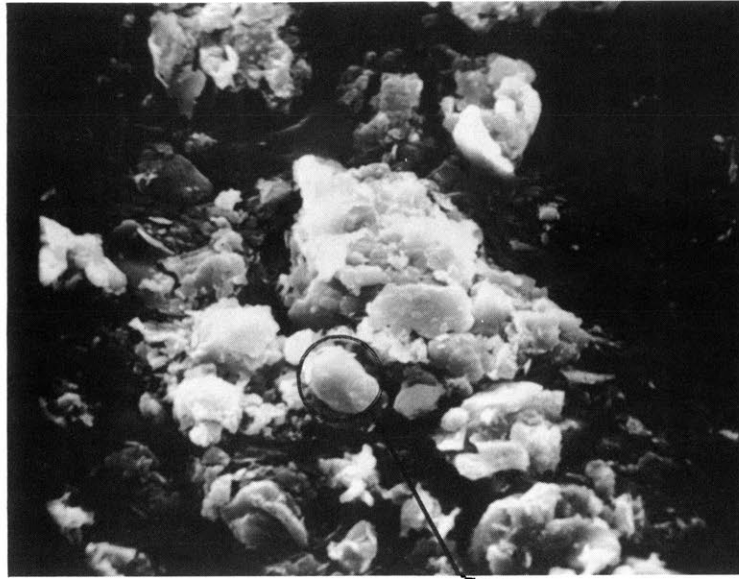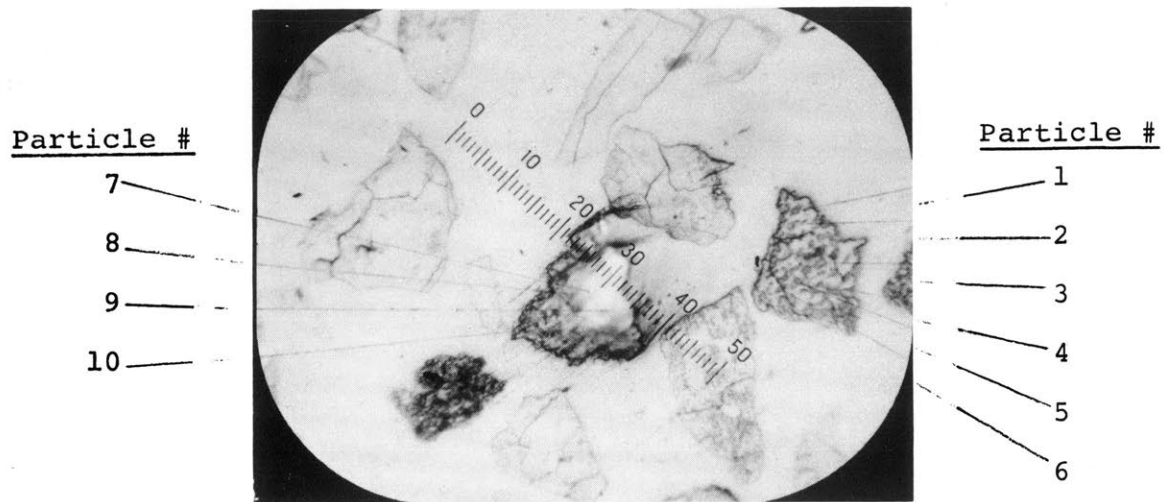
.A. Mainly Silicate Particles Composed of Varying
Amount of Al.
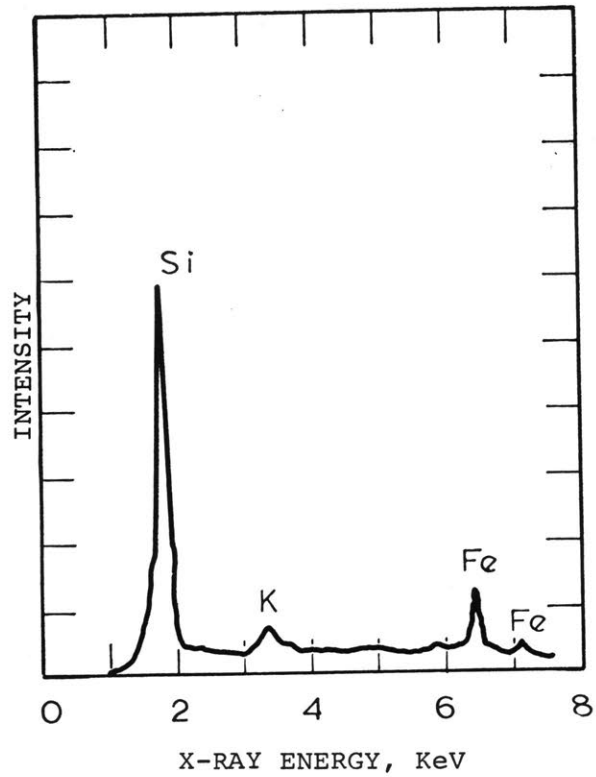
.B.   EDXRA Of Encircled Particle in Fig. A.

Quartz and Silicates in LTA of Bituminous Coal

Figure 5.7

100 μm

Distribution of Ash in (75-90 μm)
Bituminous Coal Particles. Center
particle shows basically FeS_2 (white
shiny); particle on the right hand
side shows islands of kaolinite type
structure.

Figure 5.8

Table 5.3 Concentration of Major Oxides Obtained by Electron

Microprobing, Particles on Figure 5.8

Particle #	SiO_2	Al_2O_3	FeO	CaO	MgO	K_2O	Total	SiO_2/Al_2O_3
1	42.88	36.16	0.45	0.11	0.10	0.01	79.71	1.19
2	41.37	34.59	0.51	0.07	0.10	0.00	76.64	1.20
3	51.55	26.23	0.61	0.13	0.70	1.83	81.05	1.95
4	57.74	11.79	0.92	2.31	0.97	14.34	88.07	4.90
5	34.92	27.82	2.54	8.34	2.65	0.21	76.48	1.26
6	2.51	96.17	0.0	1.39	0.0	0.0	100.07	0.03

SiO_2 and Al_2O_3 amounts to a total of from 76 to

100% weight of the particles. In a Kaolinite particle

$[Al_2Si_2O_5(OH)_4]$, Al_2O_3 and SiO_2 contribute about 86% of

the weight, and the weight ratio of SiO_2/Al_2O_3 is 1.18.

Particles 1,2 and 4 satisfy this requirements. Particle

No. 6 is probably pure corundum type structure.

5.4.1.2   Sulfates and Carbonates.

Ca and Mg compounds exist mainly as sulfates

(Gypsum $CaSO_4.2H_2O$, Bassanite $CaSO_4.\frac{1}{2}H_2O$, anhydrite,

$CaSO_4$) or carbonates [Calcite $CaCO_3$, Dolomite $CaMg(CO_3)_2$].

Fig. 5.9.A.1. shows an agglomerated bunch of crystalline

mineral particles of overall size of about 30 μm. At

higher magnification (Fig. 5.9.A.2) the individual

particles mainly in the shape of crystalline hexagonal
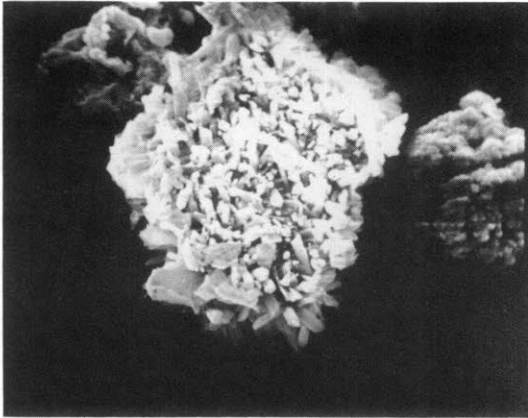
.A.1 Agglomerated Crystalline Mineral Particles.
Main Constituents are Ca and S.

.A.2 Surface of A.1 at Higher Magnification.
Crystals are Mixture of Calcium Sulfate and Calcium Carbonate.

FIG. . B EDXRA of Fig. A.2
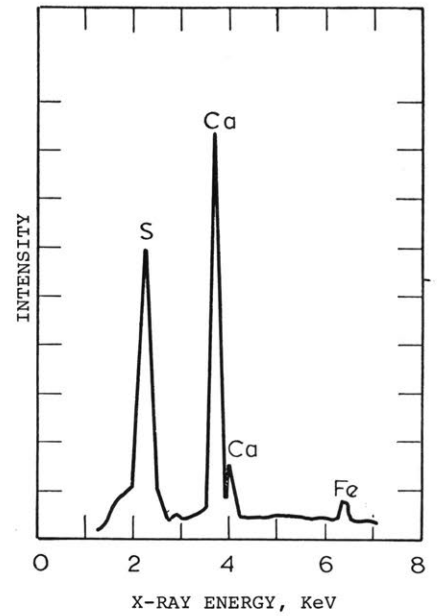
Sulfate and Carbonates in LTA of (38-45 μm) Bituminous Coal

Figure 5.9

bars of less than 1 μm in diameter and about 5 μm long, can be observed. The Ca/S ratio as seen by EDXRA [Fig.5.9.B] is about 1.6 giving an indication of the presence of mixture of Gypsum [$CaSO_4.2H_2O$] and calcite or Aragonite [$CaCO_3$] crystals. It is possible that Gypsum in the process of low temperature ashing was dehydrated to Bassanite [$CaSO_4.\frac{1}{2}H_2O$] or anhydrite [$CaSO_4$]. Similar behavior is exhibited in Fig.5.10. Long monoclinic prismatic particles (A) and short rhombohedral prismatic particles (B) are seen in Fig.5.10.A.2 which is the encircled group of particles in Fig.5.10.A.1 at higher magnification. EDXRA (Fig.5.10.B) of both particles A and B indicate that long monoclinic particles (A) are $CaSO_4$ and short rhombohedral particles (B) are $CaCO_3$. The small amount of sulfur in case of (B) could be a consequence of the penetration of X-rays below the surface to a sulfate particle.

Fig.5.11.A shows a radiating group of large to small crystals with hexagonal faces about 1 μm in size and again about 5 μm long. EDXRA (Fig. 5.11B) shows the presence of Ca, Si, Al, Fe and S. Presence of $CaSO_4$ and $CaCO_3$ is one possibility along with similar compounds of Si, Al and Fe.

5.4.1.3 Pyrites.

Iron exist in coals mainly as pyrites (FeS_2). Other forms of Fe, for example coquimbite [$Fe_2(SO_4)_3.9H_2O$]; siderite [$FeCO_3$], have been detected in minor
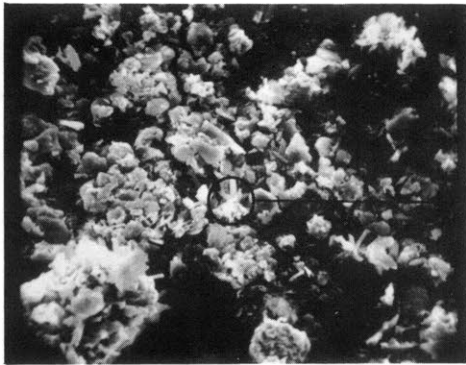
.A.1 A variety of Mineral Particles (5-7 μm) of
      Widely Varying Composition
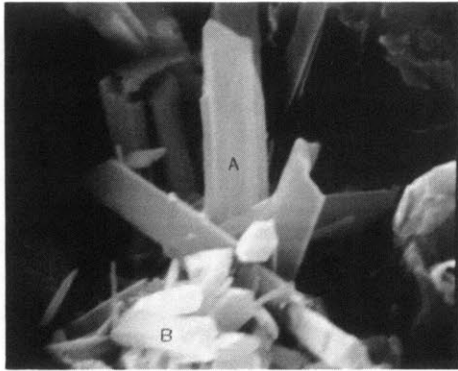
.A.2 The Circled Group of Particles in A at Higher
      Magnification
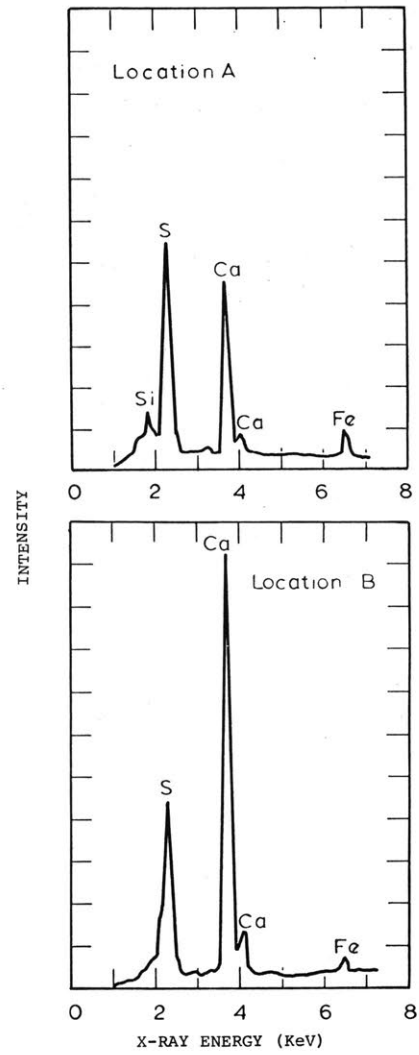
Fig. B. B. EDXRA of Fig. A.2 at Two
            Locations

Sulfate and Carbonates in LTA of Bituminous (38-45 μm) Coal

Figure 5.10

.A. A Radiating Group of Large to Small Calcium Carbonate
     Crystals. Some sulfur is also evident from EDXRA
     showing presence of some $CaSO_4$ type structure.
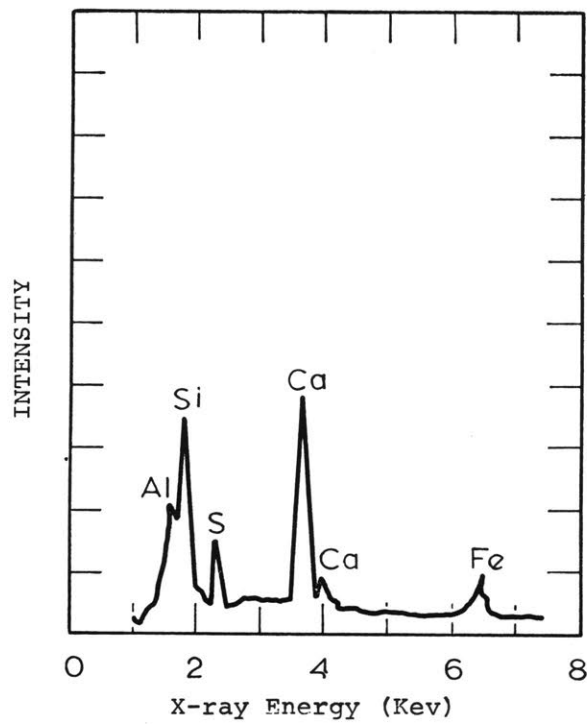
.B. EDXRA of Figure A.

Figure 5.11 . Mixed Sulfate and Carbonate in LTA

quantities. Fig. 5-12-A2, which is the group of particles in Fig. 5.12.A.1 encircled at higher magnification, shows a number of pyritic particles. The particles are crystalline, pyritohedron, octahedron and some resembling cubic structure. The particles are uniformly sized at about 1 m diameter. EDXRA (Fig. 5.12B) gives an atomic ratio of Fe to S of about a half confirming the presence of FeS_2 type structure.

Some other crystalline structures of pyrite are also identified. Fig. 5.13 shows the cubic and triangular crystals of about 0.5μm in size while Fig. 5.14 shows a big prismatic pyramidal crystal of pyrite about 15μm in size. These observations indicate that pyritic particles may have a bimodal distribution, with peaks at about 1μm and 15μm.

Electron microprobing of polished surfaces of both lignite and bituminous coal also showed pyritic particles. Particle numbers 7, 8, 9, 10 in Fig. 5.8 which appeared yellow while under reflected light had the composition expressed in Table 5.4 where the concentrations of the metallic elements are expressed as their oxides.
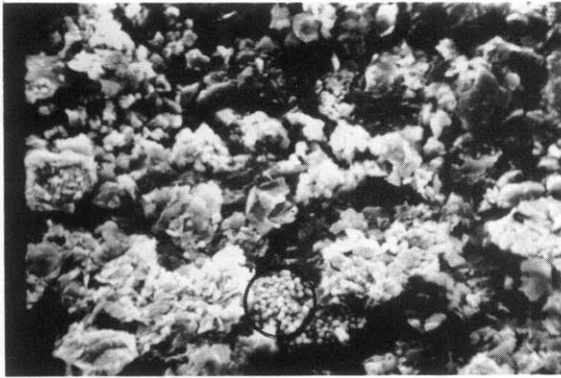
A. 1. Variety of Mineral Particles Showing Varying
        Composition.
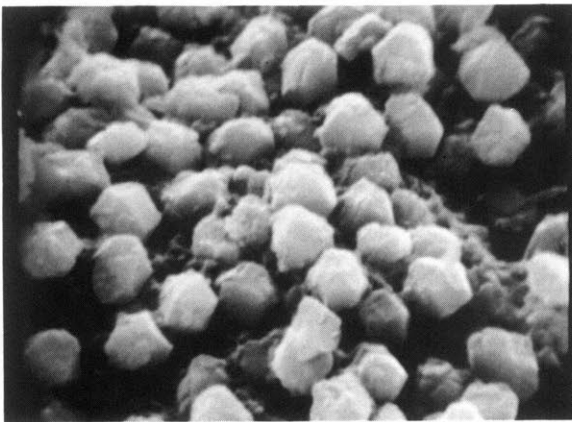
A.2. The Circled Group in A.1 at Higher Magnification.
      Crystals are pyritohedron, octahedron or combinations.
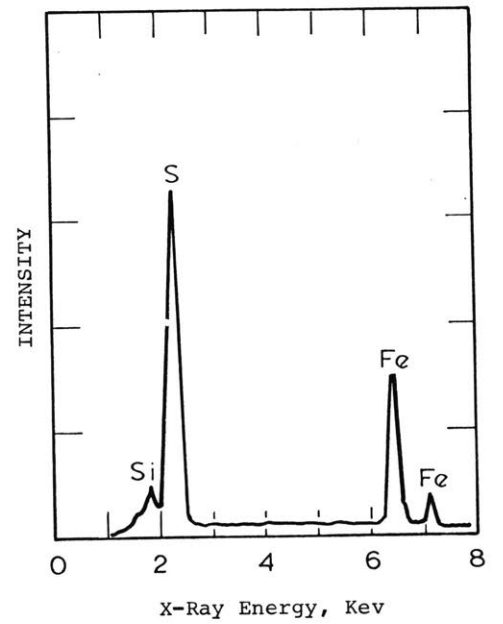
B. EDXRA of Fig. A.2.

Typical Pyrites in LTA of (75-90) μm Bituminous Coal

Figure 5.12
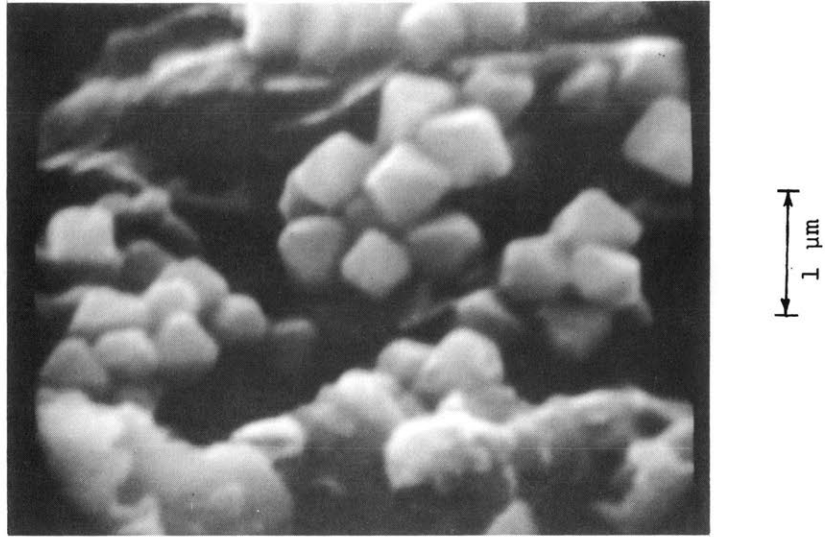
A. Cubic and Triangular Crystals of Pyrites (FeS$_2$)
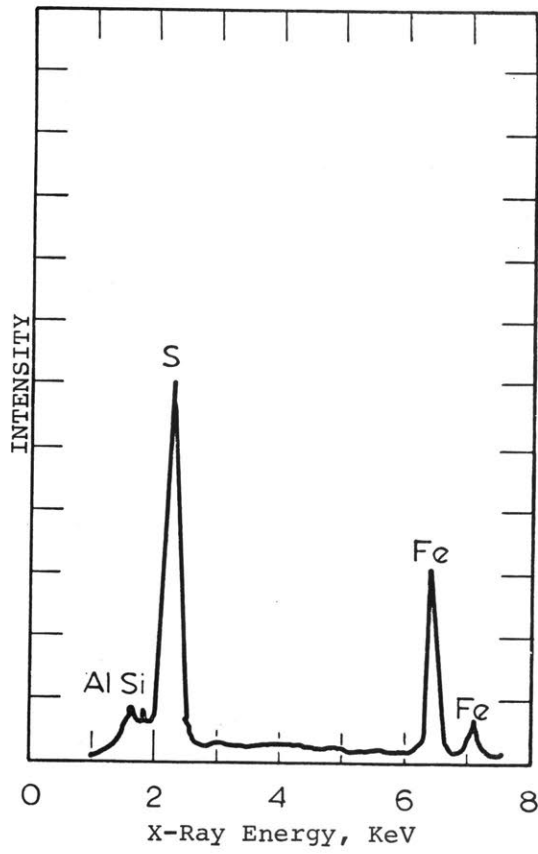
B. EDXRA of Fig. A.

Figure 5.13 Other Forms of Pyrites
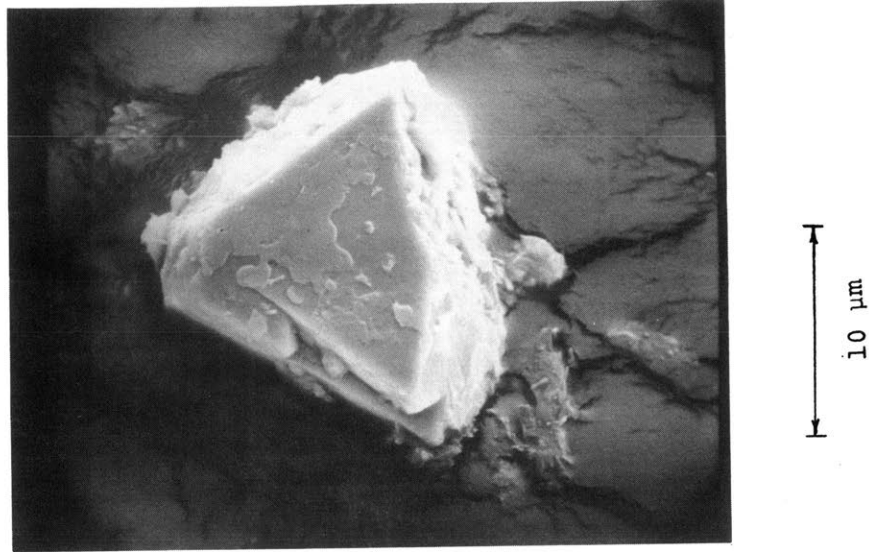
A. Prismatic Pyramidal Crystal of Pyrite (FeS_2)
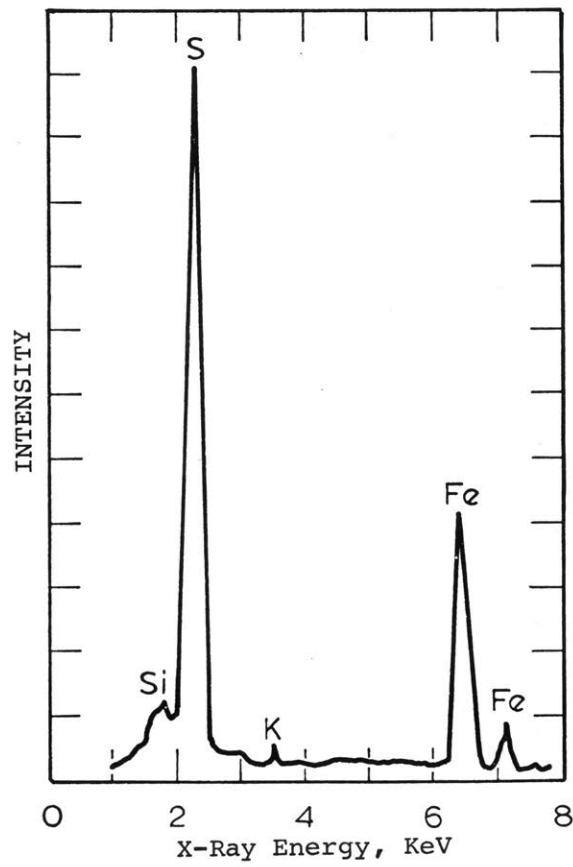
B. EDXRA of Fig. A.

Figure 5.14 Other Forms of Pyrites

Table 5.4   Microprobe Analysis of Metals in "Pyrite"

Particles seen in Figure 5.8

Particle #	SiO_2	Al_2O_3	FeO	CaO	MgO	K_2O	Total	Fe Calculated as FeS_2 (%)
7	0.07	0.00	55.57	0.05	0.04	0.00	55.73	92.88
8	0.27	0.18	57.75	0.24	0.11	0.11	58.66	96.52
9	0.33	0.29	56.07	0.24	0.14	0.13	57.20	93.71
10	0.97	3.31	54.20	0.29	0.23	0.20	59.20	90.59

Although sulfur was not probed, the total oxides concentration below 60 percent indicate that Fe should be in a different form than FeO. Calculations as FeS_2 shows that the particles were mainly pyritic. The particle sizes could not be determined using the relatively low resolution of the optical microscope attached to the electron microprobe.

5.4.1.4   Sulfur

Sulfur in coal can be present in organic, pyritic and sulfate forms. The amounts of the three different forms in the coals used in this study are given in Table 4.5. The last two forms of sulfur, pyritic (or sulfide) and sulfate are a part of the mineral matter of the coal. The amount of elemental sulfur found in coal is usually negligible.

Sulfide or pyritic sulfur is mainly present as FeS_2 as shown in Fig. 5.12, 5.13 and 5.14. Calcium seems to be the major element contributing for sulfate sulfur (Fig. 5.9, 5.10 and 5.11). Fe may also contribute to sulfate sulfur in the form of coquimbite $[Fe_2(SO_4)_3 \cdot 9H_2O]$ (Fig. 12). Other forms like barite $[BaSO_4]$, sphalertie $[ZnS]$ have been also reported in the literature [Gluskoter 1975].

5.4.2 Ash Particle Size Distribution

5.4.2.1 Effect of Coal Type

Due to hetrogeneity of the minerals present in the low temperature ash, particle size distribution was estimated for the three main groups kaolinite, carbonate and sulfates and pyrites.

Kaolinite particles had a maximum dimension ranging in size from 1 to 5μm; this corresponds to a mass mean diameter of 4μm assuming spherical particles. But since the particles observed are more plate-like, the average size is smaller and more like 2-3μm.

Sulfates and carbonates were mainly those of calcium with monoclinic bar-type shape. The average size was about 1μm on face and 5μm length giving an average spherical diameter of 2μm.

Pyrites were found mainly in uniformly sized ball-shaped particles of about 1μm diameter. The larger pyrite pyramidal particle of about 15μm was also identified. Although the finding of the larger particle may be coincidental, it does give possibility of a bimodal

distribution, as noted earlier.

The individual particle size distributions of pyrite, sulfate and carbonate and kaolinite are shown by Rosin-Rammler functions in Figure 5.15. The distributions were obtained by counting particles of the specific type in the representative photomicrographs obtained from a scanning electron microscope.

A composition of 50% kaolinite, 10% sulfate and carbonate and 40% pyrite for bituminous ash and 50% kaolinite, 40% sulfate and carbonate and 10% pyrite for lignite ash was assumed. Based on these compositions and taking into account the densities of the different species, overall particle size distributions were calculated and are shown by Rosin-Rammler functions in Figure 5.16. The mass median size of the mineral matter is about 2μm in both cases.

5.4.2.2 Effect of Coal Size on Ash Particle Size

Distribution

No effect of particle size of coal was observed on the ash particle size distribution of low temperature ash. The ash particles are not expected to be affected by coal particle size until the latter are ground to sizes comparable to the ash mean size, i.e., 2μm.
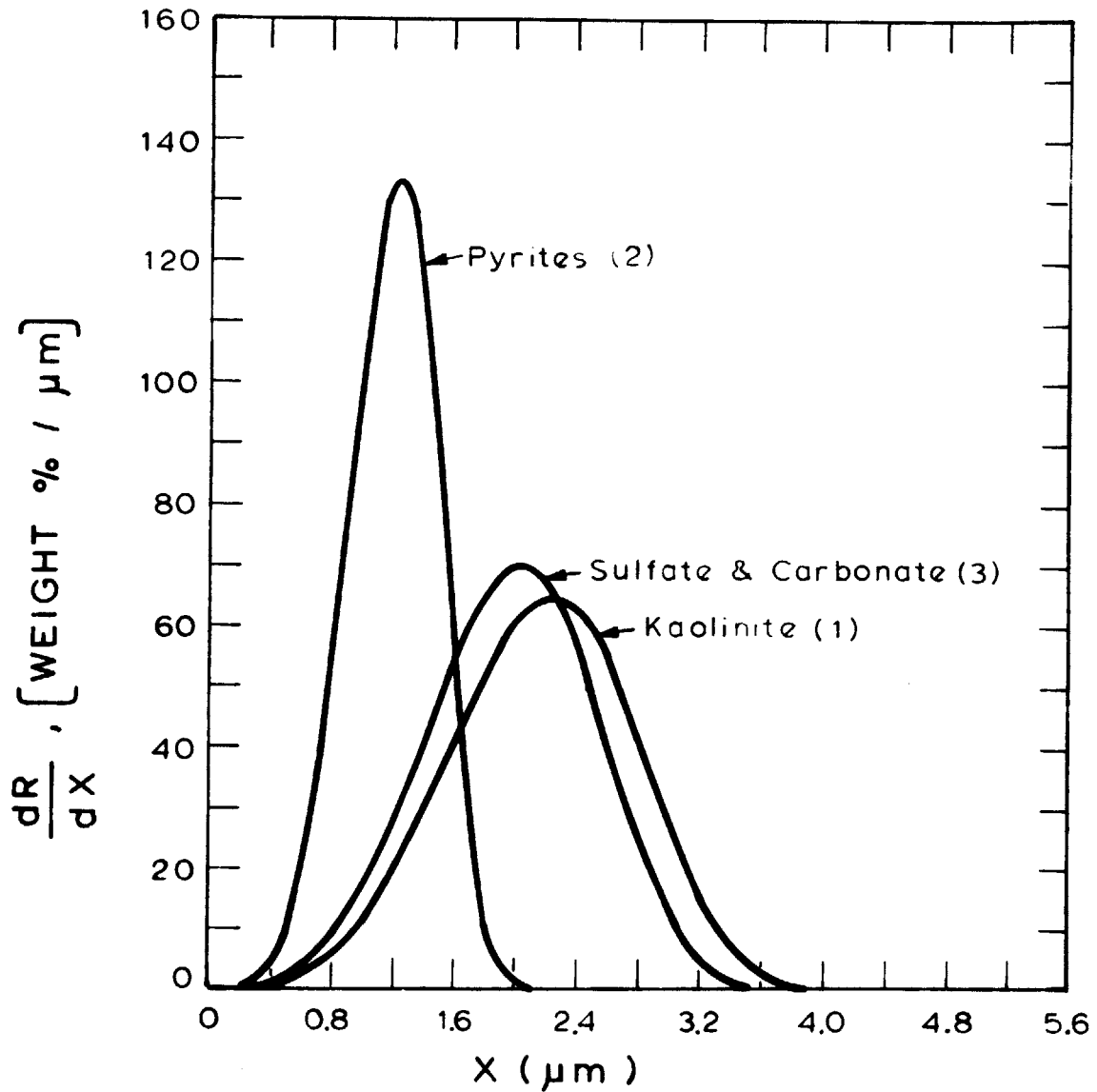
Frequency Distribution of Individual Species of Mineral Matter in Lignite

Species	Xmed (μm)	X'(μm)	s	b
1 Kaolinite	2.21	2.40	4.10	0.0276
2 Pyrites	1.224	1.31	4.64	0.2857
3 Sulfate Carbonate	1.98	2.18	4.00	0.0443

Figure 5.15

FREQUENCY DISTRIBUTION OF MINERAL MATTER IN COAL

	Bituminous	Lignite
$X'(\mu m)$	1.90	2.20
$X_{med}(\mu m)$	1.68	1.98
S	2.99	3.56

Rosin - Rammler Relation

$$\frac{dR}{dX} = 100\, bs\; X^{S-1} exp\,(-bx^{S})$$

$$b = (1/X')^{S}$$

Left plot: $\frac{dR}{dx} \cdot \left[\text{WEIGHT } \% / \mu m\right]$ vs $X(\mu m)$, with curves labeled Lignite and Bituminous.

Right plot: R vs $X(\mu m)$, with curves labeled Lignite and Bituminous.

dotted lines are Rosin - Rammler fit
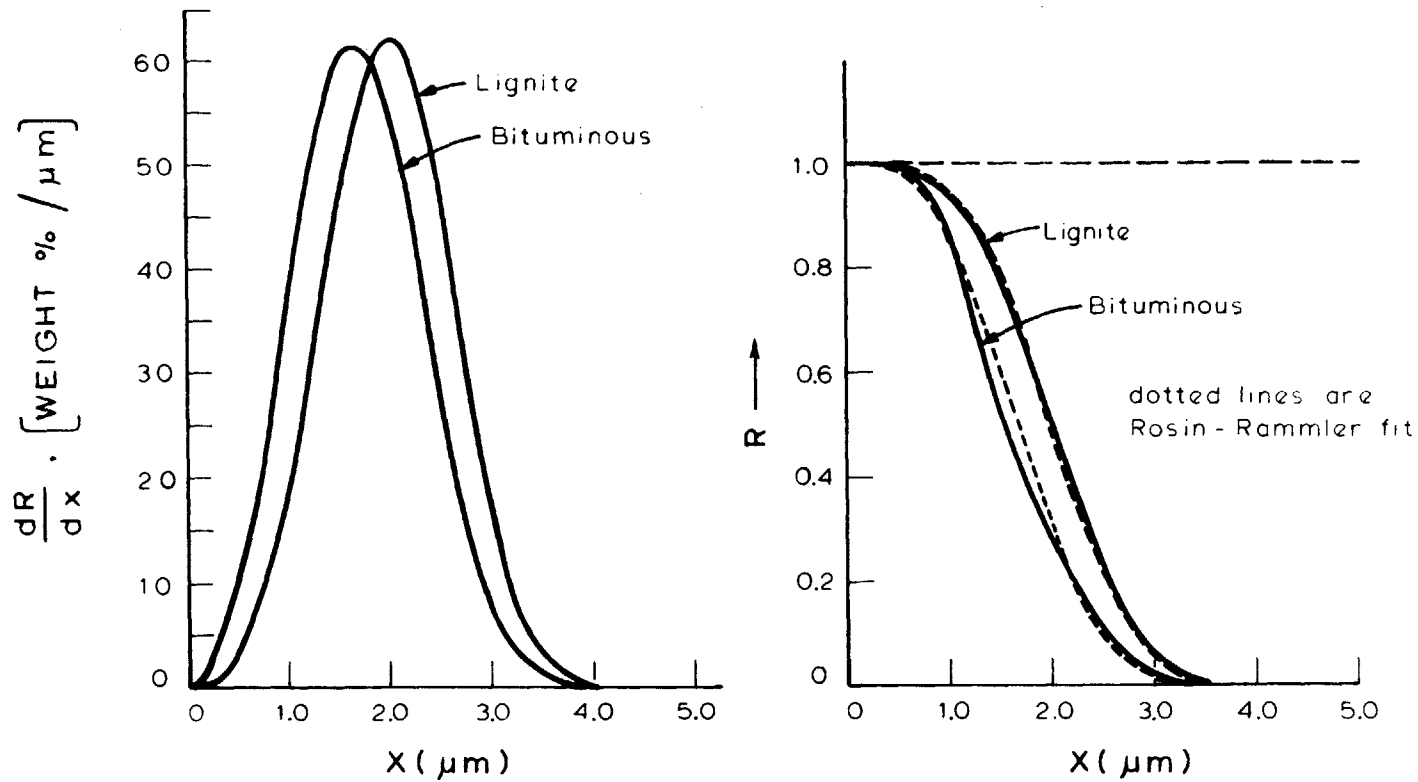
Figure 5.16

5.4.3 Relation Between Low Temperature Ash (LTA) and ASTM Ash.

Due to the requirement for expensive instrumentation for low temperature ashing mineral matter is calculated most of the time from the ASTM ash content of the coal. Usually ASTM ash is lower than the mineral matter content because of decomposition and volatilization losses during ashing procedure. The losses are attributable mainly to the partial or complete loss of water of constitution of the kaolinite and illite, conversion of pyrite (FeS_2) to ferric oxide, and dissociation of carbonate and sulfates to metal oxides with release of CO_2 or SO_2. In view of this it may be appropriate to derive a relation between the mineral matter of coal (as determined from the low temperature ash) and ASTM ash. Based on a proposed decomposition scheme (Table 5.5) and assuming the weight loss mainly contributed by kaolinite, pyrite, sulfate and carbonate reactions a formula is derived relating mineral matter in coal and ASTM ash.

$$M.M. = ASH + 0.625 \; S_{pyr \atop coal} + 0.833 \left[S_{sulf \atop coal} - S_{sulf \atop ASH} * \frac{ASH}{100} \right]$$

$$+ \frac{ASH}{100} \left[0.162 \; (SiO_2 + Al_2O_3)_{ASH} + 0.79 \; CaO_{ASH} \right.$$

$$\left. + 1.1 \; MgO_{ASH} \right] \tag{5.1}$$

It is also assumed that the contribution of $CaSO_4$ and $MgSO_4$ to CaO and MgO is negligible compare to

Table 5.5

Proposed Decomposition Scheme from Original Mineral Matter to ASTM Ash During Ashing Procedure

	Mineral Matter Species	REACTION	ASTM ASH SPECIES	Weight loss % of MM Specie	Weight loss % of ASTM Ash Specie
1.	Kaolinite $Al_2Si_2O_5(OH)_4$	$Al_2Si_2O_5(OH)_4 \longrightarrow Al_2O_3 \cdot 2SiO_2 + 2H_2O$ $Al_2O_3 + 2SiO_2 \quad (14\%)$ $Al_2O_3 + 2SiO_2 \quad (86\%)$	$Al_2O_3 + 2SiO_2$	14% of Kaolinite	16.2% of $(SiO_2 + Al_2O_3)$
2.	Pyrite FeS_2	$2FeS_2 + 3.5\ O_2 \longrightarrow Fe_2O_3 + 2SO_2$ (sulfur = 128) (oxygen = 48)	Fe_2O_3	33% of FeS_2 or 62.5% of Pyritic Sulfur in Coal	50% of Fe_2O_3
3.	Sulfates $CaSO_4$ $MgSO_4$ $Fe_2(SO_4)_3$	$CaSO_4 \longrightarrow CaO + SO_3$ $MgSO_4 \longrightarrow MgO + SO_3$ $Fe_2(SO_4)_3 \longrightarrow Fe_2O_3 + 3SO_3$ $SO_4 = 96, \quad SO_3 = 80$	CaO MgO Fe_2O_3	83.3% of Sulfate Sulfur in Coal	
4.	Carbonates $CaCO_3$ $MgCO_3$	$CaCO_3 \longrightarrow CaO + CO_2$ $MgCO_3 \longrightarrow MgO + CO_2$	CaO MgO	44% of $CaCO_3$ 52% of $MgCO_3$	79% of CaO 110% of MgO

contributions from $CaCO_3$ and $MgCO_3$. Table 5.6 shows the experimental and calculated values of MM from ash analysis, in the four coal samples.

The formula thus derived provides good agreement for high Ca and Mg coals (lignite coals).

Formula 5.1 needs detailed analyses of the ash samples which is not always available. Several empirical formulae are available in the literature of which Parr Formula 5.2 (ASTM standard specifications D 388-38) is most widely used.

Parr Formula:

$$Mineral\ Matter\ (MM) = 1.08 * ASH + 0.55 * Sulfur_{(Coal)} \quad (5.2)$$

Table 5.7 compares the values of mineral matter obtained experimentally and by using Parr Formula.

Table 5.6 Comparison of Calculated and Experimental MM in Coal.

coal →	LIG (75-90)	LIG (38-45)	BIT (75-90)	BIT (38-45)	
Ash	8.38	9.60	12.40	10.96	% of original dried coal
Spyr.	0.18	0.17	2.65	2.57	
Ssulfate	0.07	0.07	0.73	0.71	% of original dried coal
Sorganic	0.73	0.71	1.72	1.67	
Al_2O_3	16.33	16.41	19.12	19.15	
SiO_2	21.69	26.80	36.15	37.52	
$Al_2O_3 + SiO_2$	38.02	43.21	55.27	56.67	
CaO	31.95	28.44	5.36	4.65	% of Ash
MgO	9.68	9.02	.73	.73	
SO_3	13.48	13.45	3.72	3.72	
Ssulf	5.39	5.38	1.49	1.49	
$S_{sulf}^{coal} - S_{sulf.}^{ASH} \cdot \frac{ASH}{100}$	-0.38*	-0.45*	0.55	0.55	

Table 5.6 (Continued)

Coal→	LIG (75-90)	LIG (38-45)	BIT (75-90)	BIT (38-45)	
MM(Calculated)	11.70	13.11	16.25	14.52	% of original coal
LTA (MM)	11.51	13.31	18.14	15.61	% of original coal
$\dfrac{LTA}{(MM)_{CALC.}}$	0.98	1.02	1.12	1.07	

[For further detail analysis of Coals see Chapter 4]

*Transformation or organic and pyrite sulfur in original coal to sulfate sulfur in ash, during ashing procedure.

FORMULA:

$$M.M. = ASH + .625\ S_{pyr\ coal} + .833 \left[S_{SULF\ COAL} - S_{SULF\ ASH} * \frac{ASH}{100} \right] + \frac{ASH}{100} [.162(SiO_2 + Al_2O_3)_{ash} +$$

$$0.79\ CaO_{ash} + 1.1\ MgO_{ash}] \tag{5.17}$$

Table 5.7

Comparison of MM Calculated by Parr Formula and Experimental LTA

	Coal	ASTM ASH % of Dried Coal	Total Sulfur % of Dried Coal		MM (LTA)	MM PARR FORMULA	LTA (MM) ASH	LTA (MM) PARR (MM)	
1.	LIGNITE (75-90 μm)	8.36	0.98		11.51	9.59	1.37	1.20	
2.	LIGNITE (38-45 μm)	9.60	0.95		13.31	10.89	1.39	1.22	
3.	BITUMINOUS (75-90 μm)	12.40	5.09		18.41	16.19	1.46	1.12	
4.	BITUMINOUS (38-45 μm)	10.96	4.94		15.61	14.55	1.42	1.07	

The Parr Formula gives poor agreement for low sulfur, high calcium, magnesium (Lignite) coals because Parr formula does not account for the loss of carbon dioxide from carbonates in the mineral matter. Several modifications were made by different investigators in the Parr formula and some of the resulting formulae are listed below.

KMC (King, Maries and Crossley, 1936) Formula

$$MM = 1.09 \text{ Ash} + 0.5 \text{ Spyr} + 0.8 \text{ } CO_2 - 1.1 \text{ } SO_{3_{ASH}} + SO_{3_{Coal}}$$

$$+ 0.5 \text{ Cl} \tag{5.3}$$

BCF (Brown, Caldwell and Fereday, 1952) Formula

$$MM = 1.06 \text{ Ash} + 0.53 \text{ S} + 0.74 \text{ } CO_2 - 0.32 \tag{5.4}$$

FF (Fereday and Flint, 1953) Formula

$$MM = 1.06 \text{ Ash} + 0.67 \text{ S} + 0.66 \text{ } CO_2 + 0.30 \tag{5.5}$$

Millot (Millot, 1958) Formula

$$MM = 1.13 \text{ Ash} + 0.5 \text{ Spyr} + 0.8 \text{ } CO_2 - 1.1 \text{ } SO_{3_{ASH}} + SO_{3_{Coal}}$$

$$+ 0.5 \text{ Cl} \tag{5.6}$$

All these formulae suffer from the fact that they use an average factor for the water of hydration of the silicate minerals which could vary significantly from coal to coal as the total amount of kaolinite varies markedly from coal to coal.

5.5 Concluding Remarks

The mineral matter from four different coal samples was obtained by low temperature ashing (LTA) technique in its essentially unaltered state. Identification of the major minerals was performed by using x-ray diffraction patterns. X-ray diffraction showed that the major minerals in the coal were kaolinite, illite, lawsonite, quartz, pyrite, coquimbite, calcite, bassanite, dolomite and anhydrite. Characterization of composition and particle size was performed by the combination of scanning electron microscopy (SEM) and energy dispersive x-ray analysis (EDXRA). Electron microprobing was also performed for some polished samples of coals to identify ash crystallites by measuring elemental composition.

The minerals in coals mainly consisted of kaolinite ranging from 1 to 5μm platelets (2.5μm volume average mean size of equivalent sphere), carbonates and sulfates mainly of calcium of about 2μm average size and pyrites about 1μm average size. The overall mass median sizes of low temperature ashes from both coals were computed to be about 2μm. Original coal size had no effect on the particle size of mineral matter.

Finally, although a secondary objective, a relation was derived between the amount of low temperature ash and ASTM ash based on a proposed decomposition scheme. The derived formula gave good agreement for low sulfur, high Ca and Mg containing (Lignite) coals. A discussion of other empirical formulae is also presented.

CHAPTER 6

BEHAVIOR OF ASH AT HIGH TEMPERATURES

I. Effect of Combustion Temperatures, Size, and Type
    of Coal on Particle Size Distribution of Ash

6.1 Introduction

An important aspect of this thesis is to determine the
effect of combustion chamber parameters on particle size
distribution of ash produced during coal firing. In order
to optimally design any combustor, gasifier and ash separa-
tion equipment and to estimate ash vaporization rates,
knowledge of composition and size distribution of ash is
essential.

Although it is recognized that the type of firing
equipment, gas velocities, turbulence, collection equip-
ment, and size influence the particle size distribution of
fly-ash, there has been no systematic study of the effects
of combustion temperature, coal size and coal type on the
number and size of the ash particles produced.

This chapter is devoted to the study of the effect of
combustion temperature, coal types (two coals, a bituminous
and a lignite) and size of the coal particles (two sizes,
38-45μm and 75-90μm) on the resulting particle size distri-
bution of ash. Attempts were also made to characterize the
density of the ash particles produced.

6.2 Experimental

The free fall, hot wall furnace described previously was used. Experiments were performed in air with two coals,two particle sizes and at three furnace temperature settings. The particle temperature was measured in each case by using a Leeds & Northrup 8620-series disappearing filament-type optical pyrometer. The velocity of the particles was measured by using a Thermo-System Inc. Laser Doppler Anemometer in an independent experiment simulating the original flow conditions of free-falling particles. Table 6.1 lists the experimental conditions and ranges. Samples of ashes from each experiment were collected at the bottom of the furnace after a cooling section and were analyzed for particle size distribution.

Particle Size Analysis: Particle sizes of the ash produced were measured microscopically using a Zeiss TGZ3 particle size analyzer. A Cambridge steroscanning electron-microscope was used to examine the ash particles and to take representative photographs. The photographs were enlarged to facilitate the measurement of particle sizes by use of the Zeiss particle size analyzer. The Zeiss particle size analyzer operates semi-automatically, the individual particles being measured on the enlarged photomicrographs. A sharply defined circular spot of light is made equal in size to the particle in photograph and then, by depressing a foot switch, this measurement

TABLE 6.1

Experimental Conditions

Coals - Lignite and Bituminous

Sizes - (38-45)μm and (75-90)μm

Mode of Experiments - Free-Fall

Stoichiometry - $\phi \approx 0.5$

Main Gas Velocity - $V_{main} \approx 4$cm/sec at furnace temperature

Carrier Gas Velocity - $V_{carrier} \approx 30$ cm/sec, at furnace temp.

Coal Flow Rate - $\dot{m}_{coal} \equiv 0.1$ gm/minute

Furnace Temperature (K)	Particle* Temperature (K)	Average Velocity of Particles (cm/sec)**		Residence Time (sec) in 15 cm Hot Zone	
		(38-45)μm	(75-90)μm	(38-45)μm	(75-90)μm
1000	1360				
1250	1465				
1500	1640	18.9	21.6	0.79	0.6
1830	1910	20.8***		0.72	

* Particle temperature by L&N Optical Pyrometer, possible error $\pm$ 30°C

** Average velocity by TSI Laser Doppler Anemometer with Lignite particle in inert atmosphere

*** Determined at 1860°K Furnace Wall Temperature

is recorded automatically on 1 of 48 counters that are cor-
related to the spot size. At the same time, a punch marks
the particle image so that it will not be counted again.
From 200 to 2000 particles were counted on each sample to
obtain representative size distributions.

Once particle sizes were measured from a photograph
and grouped into different size fractions, the distribution
was presented in terms of the volume percent of particles
above size x as a function of size x. Rosin-Rammler and
Log-normal distribution functions were used to fit the
data and calculate volume mean diameters and the spreads
in size distributions. In most cases the Rosin-Rammler
function provided a better fit of the actual distribution
than the Log-normal. Therefore, all the results were
fitted by th Rosin-Rammler distribution.

In order to translate the volume mean diameter to
weight mean diameter, knowledge of density variation is
necessary. It was found that the density of the particles
was not constant but varied with particle size. The ash
particles were density fractionated into two fractions
($\rho<1$, $\rho>1$) using a sink and float method and the mean
volume size of each fraction was determined. The particles
in each of these fractions were assumed to be of uniform
density and a mass median diameter was calculated from the
volume mean diameter. Two samples were density fractionated
for four density fractions by using heavier liquids.

6.3   Theory

The particle size distribution of ash is influenced by the physio-chemical processes involved during the combustion of pulverized coal. At combustion temperatures, the mineral matter which is heterogeneously distributed in the coal goes through chemical decomposition and phase change. Samll droplets of liquid ash in turn, can coalesce and produce larger droplets. If the probability of particle-particle collision is very low, each coal particle can produce a minimum of one ash particle (complete agglomeration) or a maximum equal to the number of ash particles in the original coal (no agglomeration). In this section, various possible mechanisms of the formation of ash and their influence on the resulting particle size distribution will be discussed.

6.3.1   No Agglomeration

If it is assumed that the mineral matter does not agglomerate during combustion, the resulting particle size distribution of ash will be the same as their original distribution in the unreacted coal, as shown in Figure (6.1) with a mean ash particle size of about $2\mu m$. It was also observed before that the mineral matter distribution in the original coal is independent of the original coal size; therefore the ash particle size distribution from different sized coals should be the same.

FREQUENCY DISTRIBUTION OF MINERAL MATTER IN COAL

	Bituminous	Lignite
$X'(\mu m)$	1.90	2.20
$X_{med}(\mu m)$	1.68	1.98
S	2.99	3.56

Rosin - Rammler Relation

$$\frac{dR}{dX} = 100\, bs\ \ X^{S-1} exp\,(-bx^S)$$

$$b = (1/X')^S$$

Lignite

Bituminous

$\frac{dR}{dx} \cdot \left[WEIGHT\ \% / \mu m \right]$

X (μm)

Lignite

Bituminous

dotted lines are
Rosin - Rammler fit

R ⟶

X (μm)
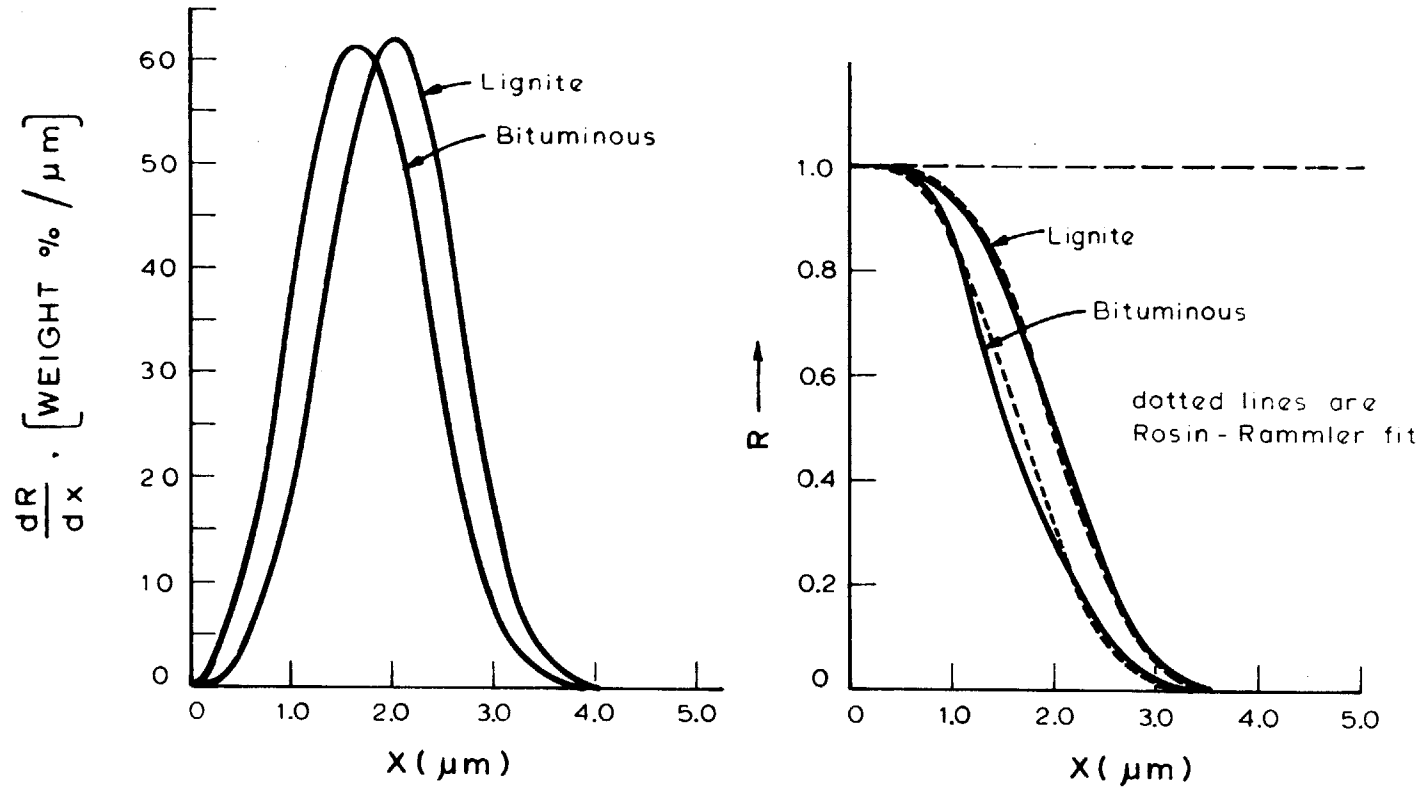
Figure 6.1

6.3.2 Complete Agglomeration

It has been observed by several investigators
(Paulson and Ramsden 1970, Ramsden 1969, Yerushalmi et al
1975,Lightman and Street 1968, Street et al 1969, Mitchell
and Lee 1962) and in the present study that finely distri-
buted particles of mineral matter in coal agglomerate at
combustion temperature. Although various theories of coal-
escence and agglomeration of ash are proposed, there is at
present no procedure for quantitatively estimating the
number of ash particles formed per coal particle.

One postulate is that all of molten ash particles in
a coal particle agglomerate. At combustion temperatures,
the randomly distributed particles of mineral matter go
through chemical reactions and phase transformation. The
molten droplets of mineral matter are retained in the
carbon matrix (Figure 6.2). As the coal particle burns the
combustion front approaches and passes the fused ash drop-
lets, the ash particle may separate or continue to attach
to the receding carbon front. The size of the ash droplet
which detaches from the surface of the char particle is
determined by the surface tension between char and ash. A
criterion of the detachment of ash from char surface can
be formed by equating the gravitational force and the
surface tension.

Figure 6.2   Ash Agglomeration Mechanism Assuming a Shrinking Core Model
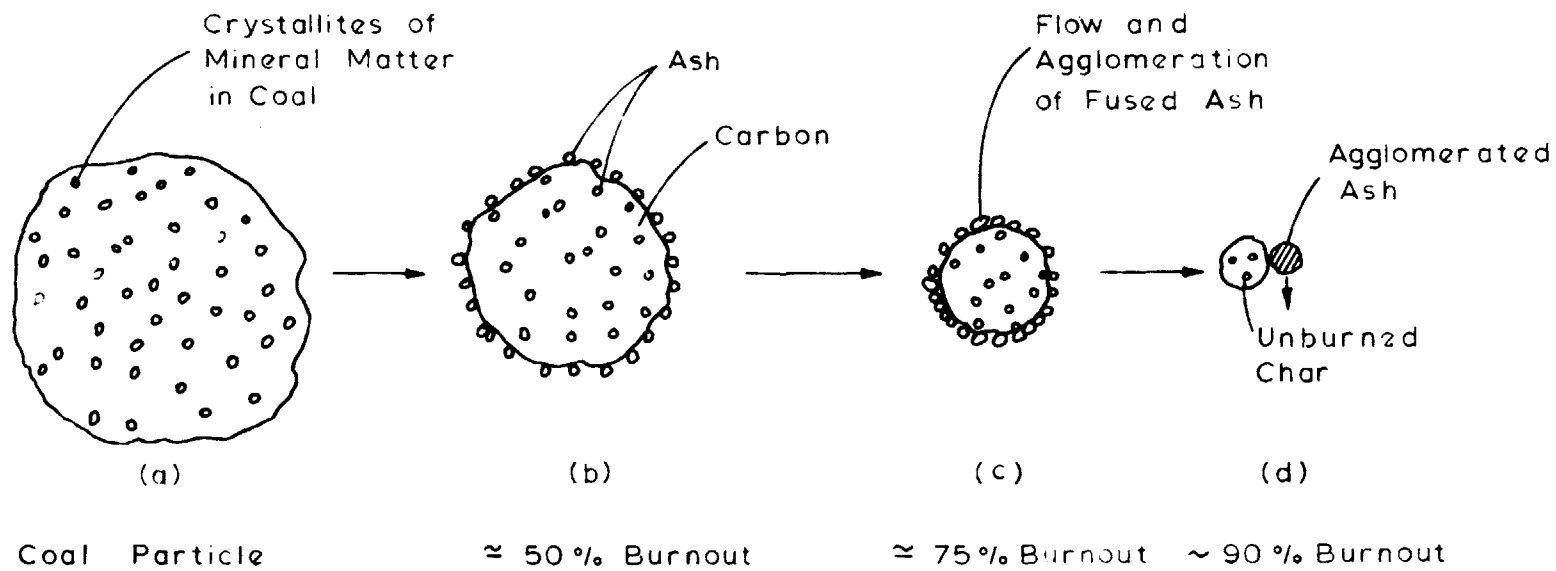
The gravitational force exerted on an ash particle of radius r_a and density $\rho_a = \frac{4}{3}\pi r_a^3 \rho_a g$ (6.1)

surface tension between ash and char particle =

$2\pi r_a(1+\cos\theta)\gamma$ (6.2)

where

θ = contact angle between ash and char

γ = coefficient of surface tension of molten ash

Equating the two forces yields the critical value of contact angle θ, i.e.,

$$\theta_c = \cos^{-1}(\frac{2r_a^2\rho_a g}{\gamma} - 1)$$ (6.3)

if $\theta > \theta_c$ the ash particle would detach from the char surface due to gravity.

Taking the coefficient of surface tension of fused ash to be 320 dynes/cm* (Raask, 1966), the contact angle required to detach an ash particle of 10 m (density = 3 gms/cc) from the char surface will be = 179.7 degrees. Raask (1966) has reported contact angles between synthesized coal ash and graphite surface to be of the order of 160° at about 1400°C. Although slag-coal interface properties would vary significantly due to variation in ash composition and temperature, the detachment of ash from char due to gravity would require almost complete non-

---

*This value of surface tension for carbon-ash interface was obtained experimentally between 1300-1400°C and when the composition of ash was SiO_2=42.0%, Al_2O_3=23.9%, Fe_2O_3= 17.8%, CaO=4.6%, K_2O=2.9%, Na_2O=2.7%, SO_3=1.9%.

wetting conditions ($\theta \approx 180°$). Under all practical conditions it can be assumed that surface tension forces would hold the ash particle to the surface of char particle.

Based on the above analysis, as the combustion front approaches and passes the molten ash droplets the droplets agglomerate and finally when the carbon is completely consumed all the droplets coalesce into a single droplet. The ash droplet thus formed together with others of like origin will be released into the gas stream and will eventually solidify. This mechanism would give rise to ONE ASH PER COAL PARTICLE.

The distribution of ash produced by complete agglomeration of mineral matter inside individual coal particle, as discussed above, would be the same as of the parent coal particles, assuming the distribution of mineral matter inside the coal particle to be independent of coal size (Chapter 5). The computed distribution of ash particles on /ash/coal basis for the four coal samples is shown in Figure 6.3

6.3.3 Partial Agglomeration and Fragmentation

In reality, fragmentation of a coal particle may take place during combustion resulting in more than one ash particle per coal particle. If all the ash particles in a coal agglomerate to form one ash particle the number of ash particles per coal particle will be determined by
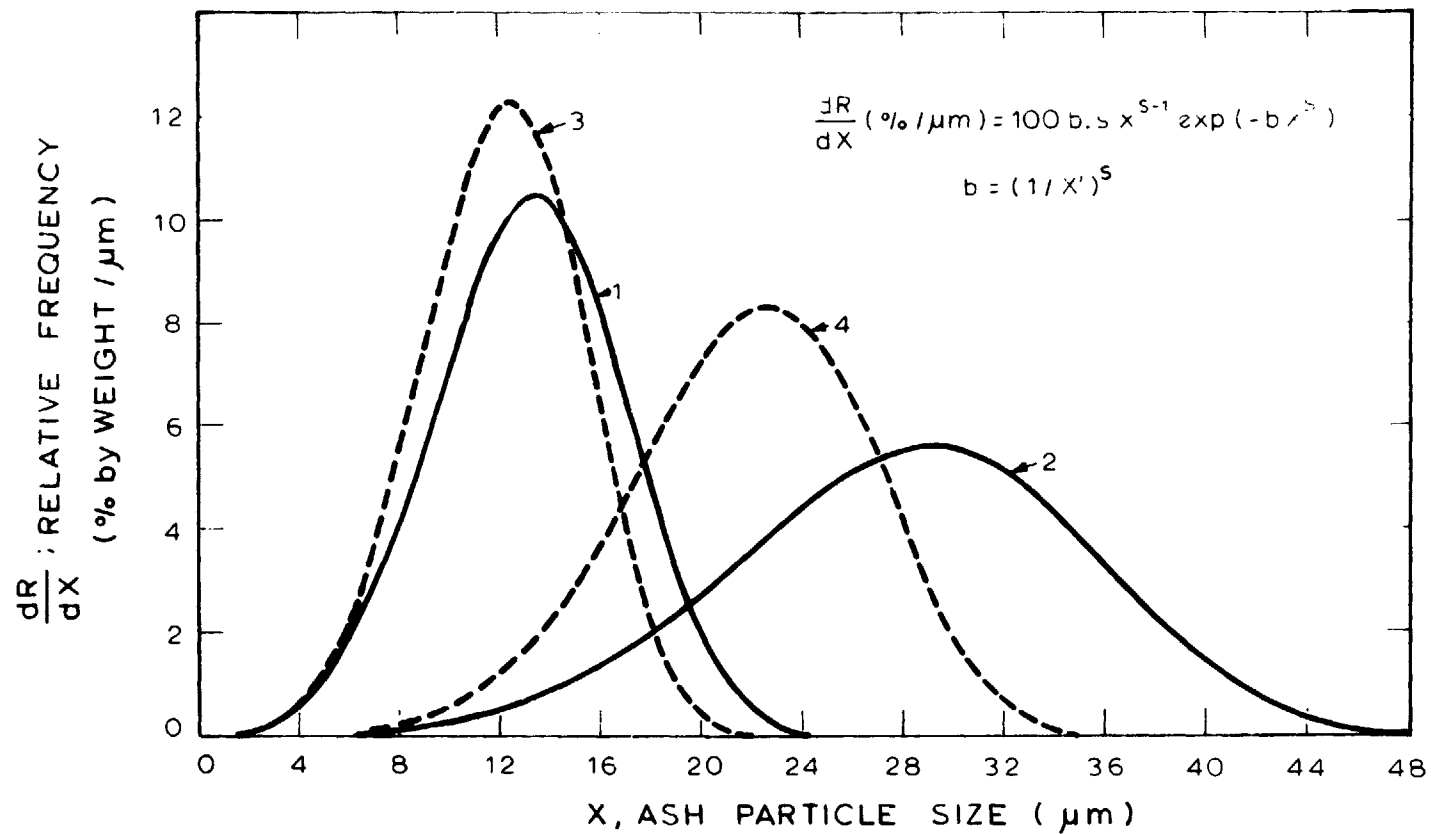
Computed Ash Particle Size Distribution Assuming One Ash Particle Per Coal Particle

		X medium	X	S
1	Bituminous (38-45)	13.5	14.6	4.00
2	" (75-90)	29.7	30.8	4.55
3	Lignite (38-45)	12.0	13.4	4.30
4	" (75-90)	21.7	23.7	5.22

Figure 6.3

the fragmentation of the coal particles. The extent of fragmentation and thus the number of ash particles produced per coal particle is a strong function of the burning behavior of the coal particles.

Combustion characteristics and kinetics of pulverized coal particles have been studied by several investigators (Thring and Essenhigh 1963, Field et al 1967, Essenhigh 1955, Mulcahy and Smith 1969, Essenhigh et al 1965, Howard and Essenhigh 1967 a,b), for a wide variety of coals and conditions. It has been observed that the rate of combustion is governed by a combination of the diffusion of oxygen to the surface of the char (diffusion control), a function of particle diameter, and the sequence of stages whereby oxygen combines with the carbon surface and the product of combustion diffuse away (chemical control). Evidence has been obtained supporting internal combustion (Gray et al 1967, Lightman and Street 1968, Ramsden and Smith 1968, Street et al 1969). Large holes in the external surfaces of the particles provide the path for the flow of oxidant. It has been also recognized that pulverized coal forms hollow spheres on rapid heating.

The present study has also focussed on the combustion characteristics of pulverized coal particles, in connection to their influence on the resulting particle size distribution of ash particles. It is observed that bituminous (typical swelling coal) and lignite (essentially non-

swelling) coals behave quite differently during combustion.
The combustion characteristics of both coals and their ef-
fect on resulting ash size distribution will be discussed
in the following paragraphs.

6.3.3.1 Lignite

The characteristics of lignite and bituminous
coal have been described previously. As the lignite par-
ticles are heated in an oxidizing environment, the finely
distributed ash particles experience the temperature-time
history of the parent coal particles and undergo phase
transformation. Since the original size of the mineral
matter in coal averages at about 2μm, the granular particles
change to spherical shape at significantly lower temperature
(<1000°C) compared to the fusion temperature of the overall
ash (Appendix C).

Although in unreacted lignite particles there are no
visible pores, fissures and crevices are developed during
combustion (Figure 6.4), showing evidence of burning in
depth and through pores. On further combustion the parti-
cle thus produced may form one ash particle by complete
internal agglomeration, finally resulting in two or more
ash particles per coal particle.

Stages in the combustion of lignite are shown in
Figures 6.5 and 6.6. Figure 6.5 shows the state of
incomplete combustion at 1000°K furnace temperature
(particle temperature 1360°K), containing both
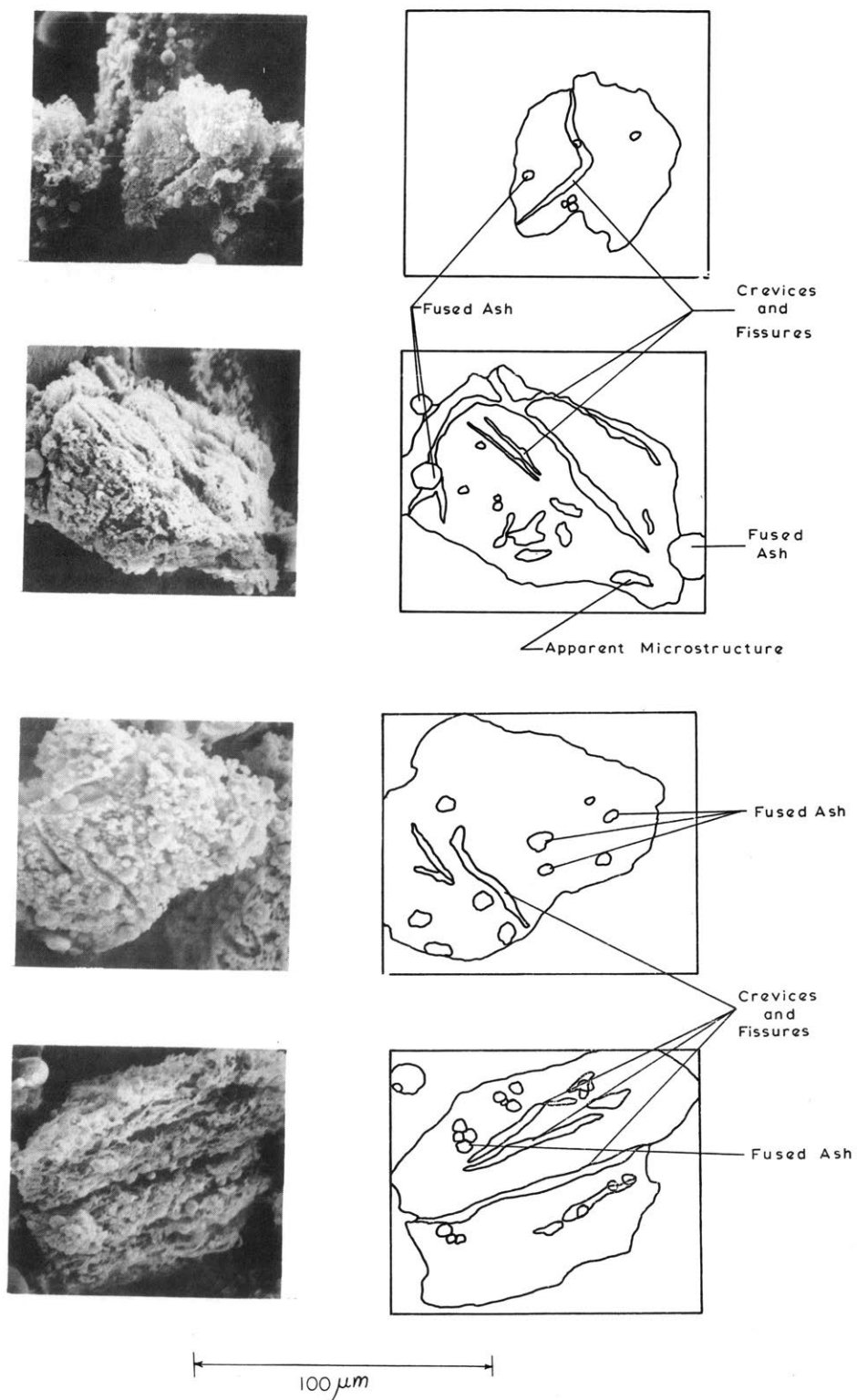
Char Particles From LIGNITE (75-90) at 1830K Furnace Temperature Showing the Process of Fragmentation
of Coal and Internal Agglomeration of Ash

Figure 6.4
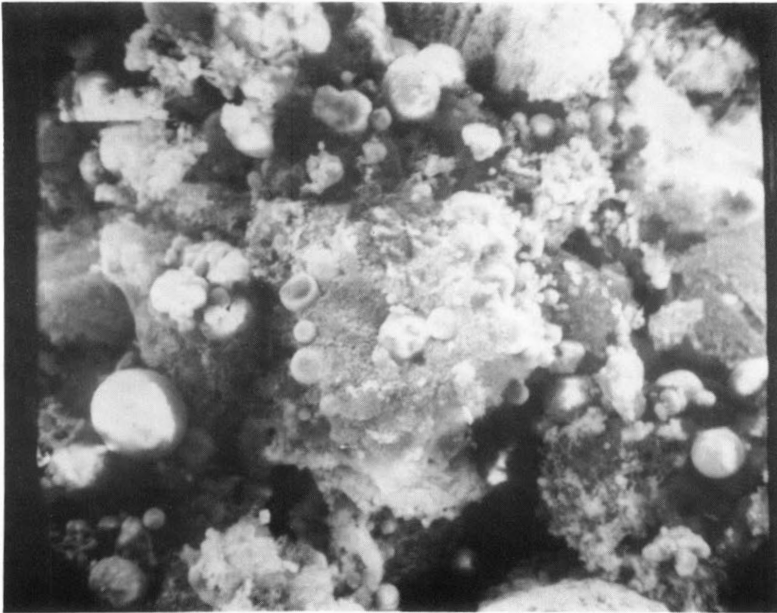
├──────────┤
40 μm

LIGNITE (75-90), Incomplete Combustion
                    Temperature = 1000 K

(A)

├──────┤
10 μm

Matrix of Highly Porous Structure of Residual
Carbon and ASH

(B)

Figure 6.5

20 μm X520
A

20 μm X500
B

Distribution of Ash Particles for 75-90 μm Lignite Coal
A. in a partially combusted state, 1250 K
B. after complete combustion. 1830 K

Figure 6.6

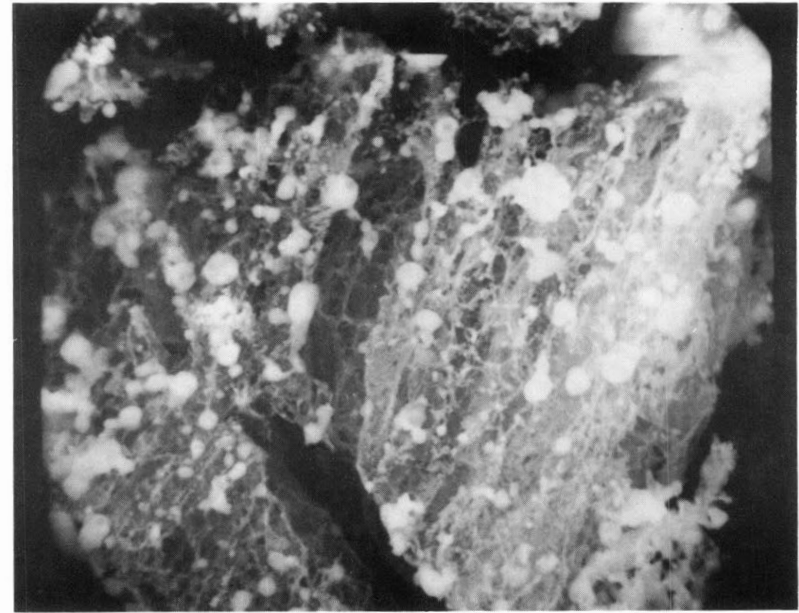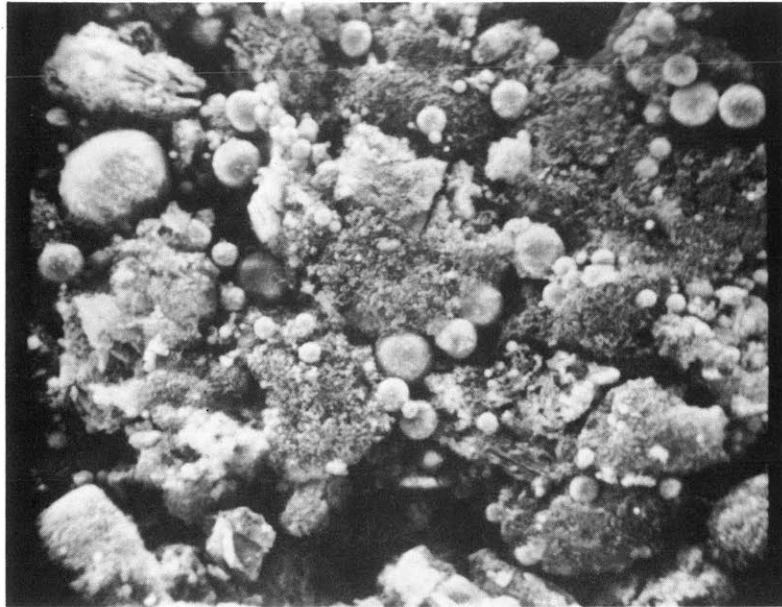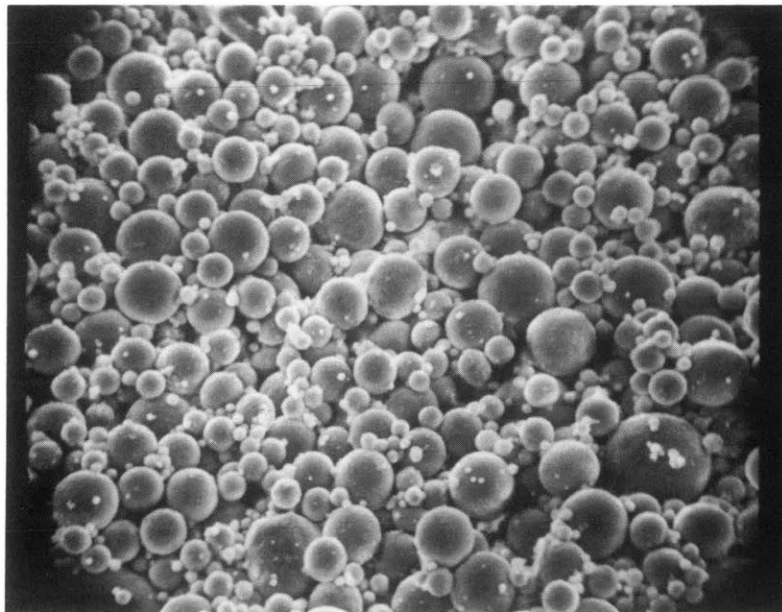agglomerated ash particles, up to 20μm in size (6.5.a)
and small (about 2 m) particles representing the origi-
nal mineral matter, fused and attached to the char matrix
(6.5b). A similar behavior at a furnace temperature of
1250°K (1465°K, particle temperature) buth with a higher
concentration of ash spheres is shown in Figure (6.6a).
Figure 6.6b shows a state of complete combustion at 1830°K
furnace temperature for (75-90μm) lignite particles, where
a large number of small particles about 2μm to small num-
ber of large particles about 30μm are observed.

6.3.3.2 Bituminous

The combustion characteristics of bituminous coal
are different from those of lignite. Bituminous coal con-
tains a fair quantity of tarry material with a wide boiling
range. This tar softens at a low temperature ($\sim$200°C) and
is exuded from the particle by the low boiling component
as they vaporize. As the temperature rises to 200-300°C
and the expanding gases "bubble", the tar on the surface
chars. If the particle cools at this stage a nearly hollow
sphere or "cenosphere" results. At higher temperatures
(about 600-700°C) all the volatiles are given up and a
coke particle is formed. Figure 6.7 shows such a particle
after subjecting it to 1000°K furnace temperature in an
oxidizing atmosphere. The increase in size from the origi-
nal size (75-90)μm to about 200μm is an indication of the
highly swelling characteristics of bituminous coals.

200 μm
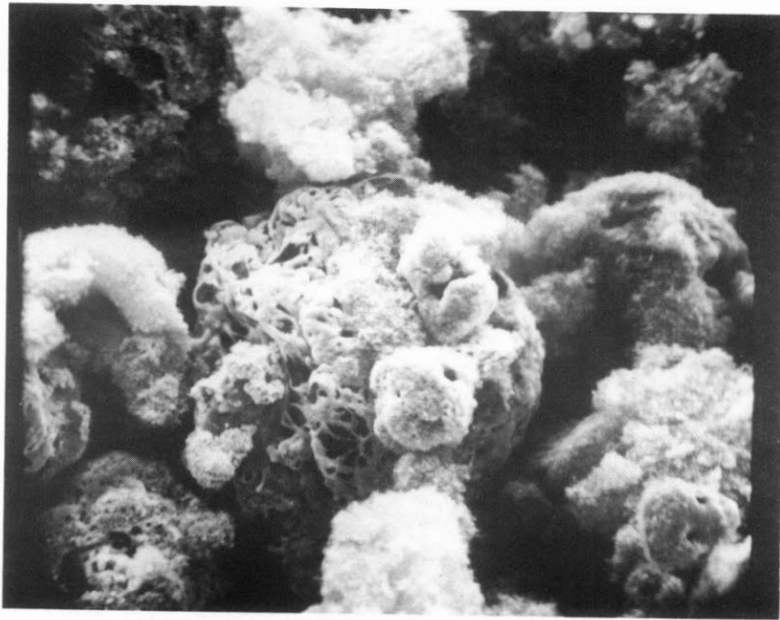
Char "Cenosphere" from Bituminous Coal
(75-90) size in Oxidizing Atmosphere
at 1000 K

A

200 μm
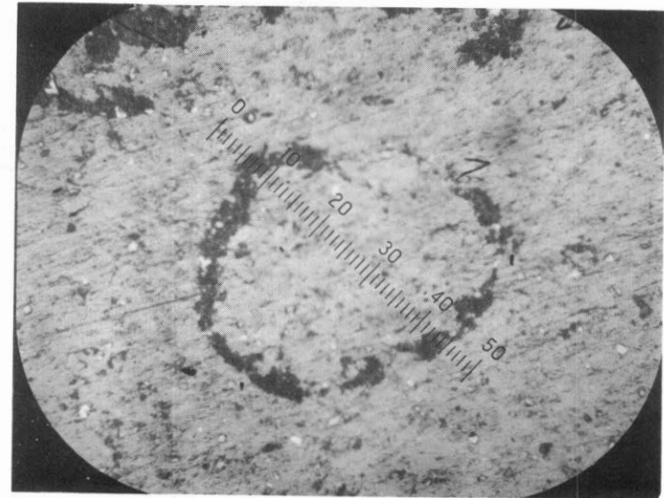
Optical Microscope Photograph of the
Char "Cenosphere"

B

Figure 6.7

Figure 6.7b is an optical micrograph of the cross sections

of a coke cenosphere showing distribution of ash particles

(white shiny islands on the periphery) embedded in the

cenosphere walls. EDXRA and EMA both show Si, Al, Fe

present in the ash particles. Figure 6.8A shows the coke

particles after devolatilization of 75-90μm bituminous

coal at 1000°K in an inert atmosphere. Three typical type

of cenospheres are observed, balloon (a), lacy and 'c'

type (b),and thick walled with many internal cross parti-

tions (c). Ash particles in each case were embedded in

the wall of the char cenosphere. Some broken particles

indicate that the volatile matter must have escaped due

to the increase in internal pressure.

Figure 6.8B shows the sketches of the three typical

cenospheres shown in Figure 6.8A. As the combustion pro-

ceeds the thinned out portions of the cenospheres may

break and lead to the formation of many particles. Each

individual char particle thus formed may produce one ash

particle on complete combustion due to total internal

agglomeration of ash. This eventually would lead to more

than one ash particle per coal particle.

Although the mechanism of formation of ash from coal

combustion is very different from swelling (bituminous)

to non-swelling (lignite) coals, both types should produce

more than one ash particle per coal particle, with the

number being significantly lower than the number of

a   ⊢————————⊣   b   c
200 μm
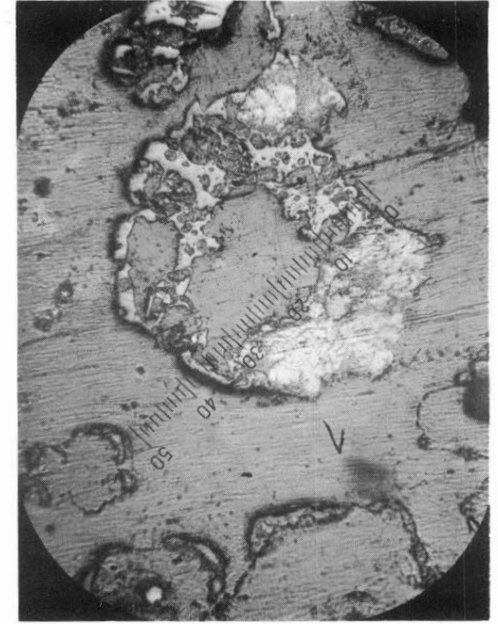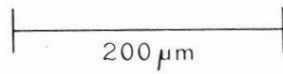
Bituminous Coal (75-90) devolatilized in inert atmosphere, T = 1000 K
(Various types of cenospheres seen under reflected light)

Figure 6.8(A)

Ash

Carbon

Ash

Carbon
Matrix

200 μ

Ash
(Unfused)

Space Inside
the Char Matrix

(a)   (b)   (c)
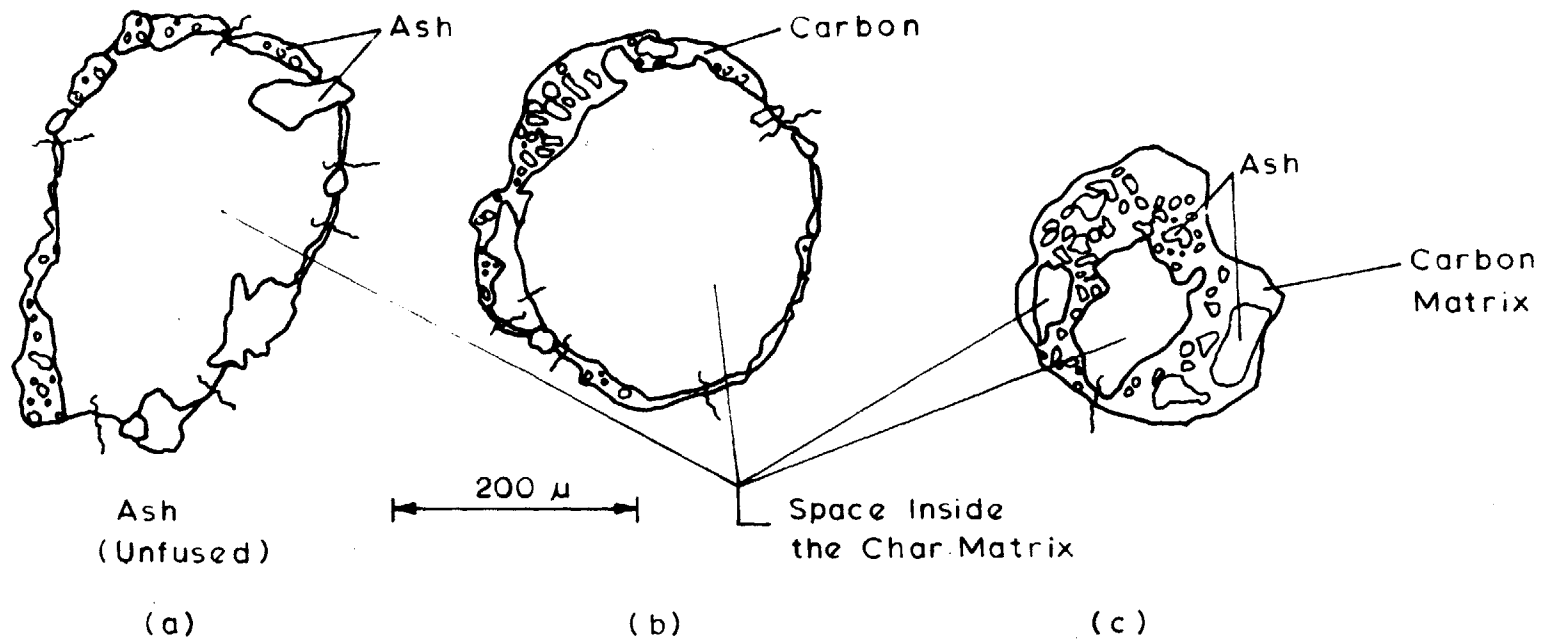
⌐ Represents the thinned out section of the char matrix which may break
   and produce additional particle on subsequent combustion

Sketches of Char Cenospheres from Bituminous Coal (1000 K)

Figure 6·8 (B)

original ash particle per coal particle. One ash per ash and one ash per coal particle assumptions should give the lower and the upper value of the number of ash particles produced per coal particle. The exact number has to be determined by experimental methods.

6.3.4 Formation of Ash Cenospheres

Mineral Matter during combustion not only undergoes physical change (fusion, agglomeration, vaporization) but also goes through thermal decomposition and chemical reaction with the carbon matrix. Some molten droplets of ash may expand due to internal evolution of gas. For example droplets derived from kaolinite may contain bubbles of water vapor, those derived from calcite may contain CO_2 or quartz may react with carbon matrix to form CO.

$$Al_2Si_2O_5(OH)_4 \rightarrow Al_2O_3 \cdot 2SiO_2 + 2H_2O \qquad (6.4)$$

(Kaolinite)

$$CaCO_3 \qquad \rightarrow CaO + CO_2 \qquad (6.5)$$

$$SiO_2 + C \qquad \rightarrow SiO + CO \qquad (6.6)$$

$$SiO_2 + 2C \qquad \rightarrow Si + 2CO \qquad (6.7)$$

$$SiO_2 + 3C \qquad \rightarrow SiC + 2CO \qquad (6.8)$$
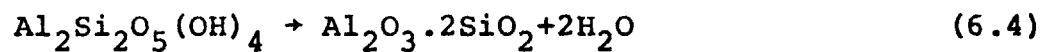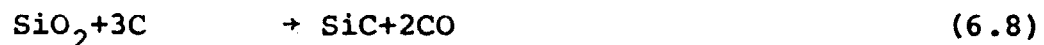
The pressure of these trapped gases within the molten droplets may cause the drop to expand into a hollow thin-walled sphere (cenospheres) before the droplets solidify. If it is assumed that chemical reactions are very rapid under

combustion conditions, the rate of growth of these ceno-
spheres is governed by the viscosity and the surface
tension of the fused ash. Experimentally, it was
observed that the cenospheres were about a factor of 2
to 3 bigger in size than the dense spheres of ash. The
time required for the formation of a cenosphere of about
20μm in size from 6 m original dense size is about 34
msecond. The rate of growth of cenospheres under viscous
relaxation is described in Appendix D.

The number and size of cenospheres formed obviously
influences the particle size distribution of ash. Small
amounts (less than 10% of the mass) do not affect the
mass median particle size seriously, but may result in a
significant increase in the volume mean size.

6.4 Experimental Results and Discussion of Results

The results of particle size distribution are repre-
sented in two categories:

a. Density distribution of ash and its effect on
overall particle size distribution.

b. Effect of temperature, coal size and coal type
on the particle size distribution of ash.

6.4.1 Density Distribution of the Ash

6.4.1.1 Density Fractionation of Ash

Due to the formation of cenospheres some ash
particles were found to be lighter than water and were

separated from the total ash collected by a sink and float
method. The particles lighter than water were termed
"cenospheres" although cenospheres could have densities
varying from less than 1 to about 3.5. Figure 6.9 shows
the amount of "cenospheres" as weight percent of total ash
as a function of furnace temperature. The amount of ceno-
spheres formed peaks at 1500°K (about 6 percent by weight).
The packed density of ash cenospheres was estimated to be
about 0.4 gms/cc which gives a real density of about 0.8
gms for cenospheres if a void fraction of 0.5 is assumed
for randomly packed spherical particles.

Figures 6.10(A) is a density plot of the ash which
sank in water, termed as "dense ash", for the same samples.
The mean density at 1500°K is lower than the densities at
1250 and 1830°K. Although due to very small sample sizes
(about 0.1 gm) of the ash samples produced from experi-
ments, complete density fractionation of all the samples
was not possible; two samples, one for lignite (38-45μm)
and another for bituminous coal (75-90μm) at 1500°K were
density fractionated for four fractions using mixtures of
carbon tetrachloride ($\rho\equiv1.6$ gm/cc) and bromoform ($\rho\equiv2.86$
gms/cc) by sink and float method. The density for these
two samples varied continuously from less than 1.0 to
more than 2.86 gms/cc, as shown in Figure 6.10(B). A
two parameter function like Rosin-Rammler describes the
variations in the density reasonably well. The density of
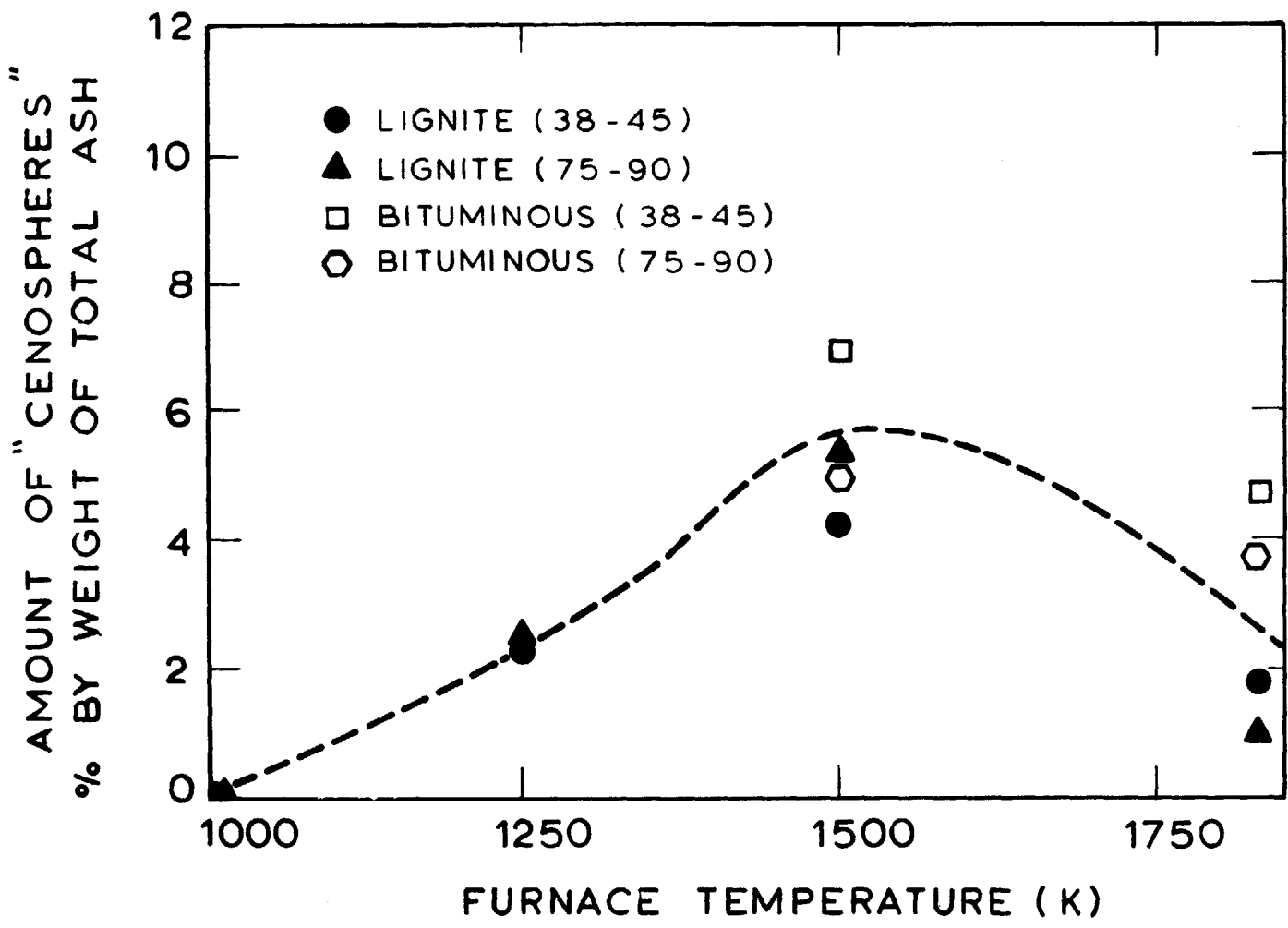
Effect of Combustion Temperature on Amount of Cenospheres Formed

Figure 6.9
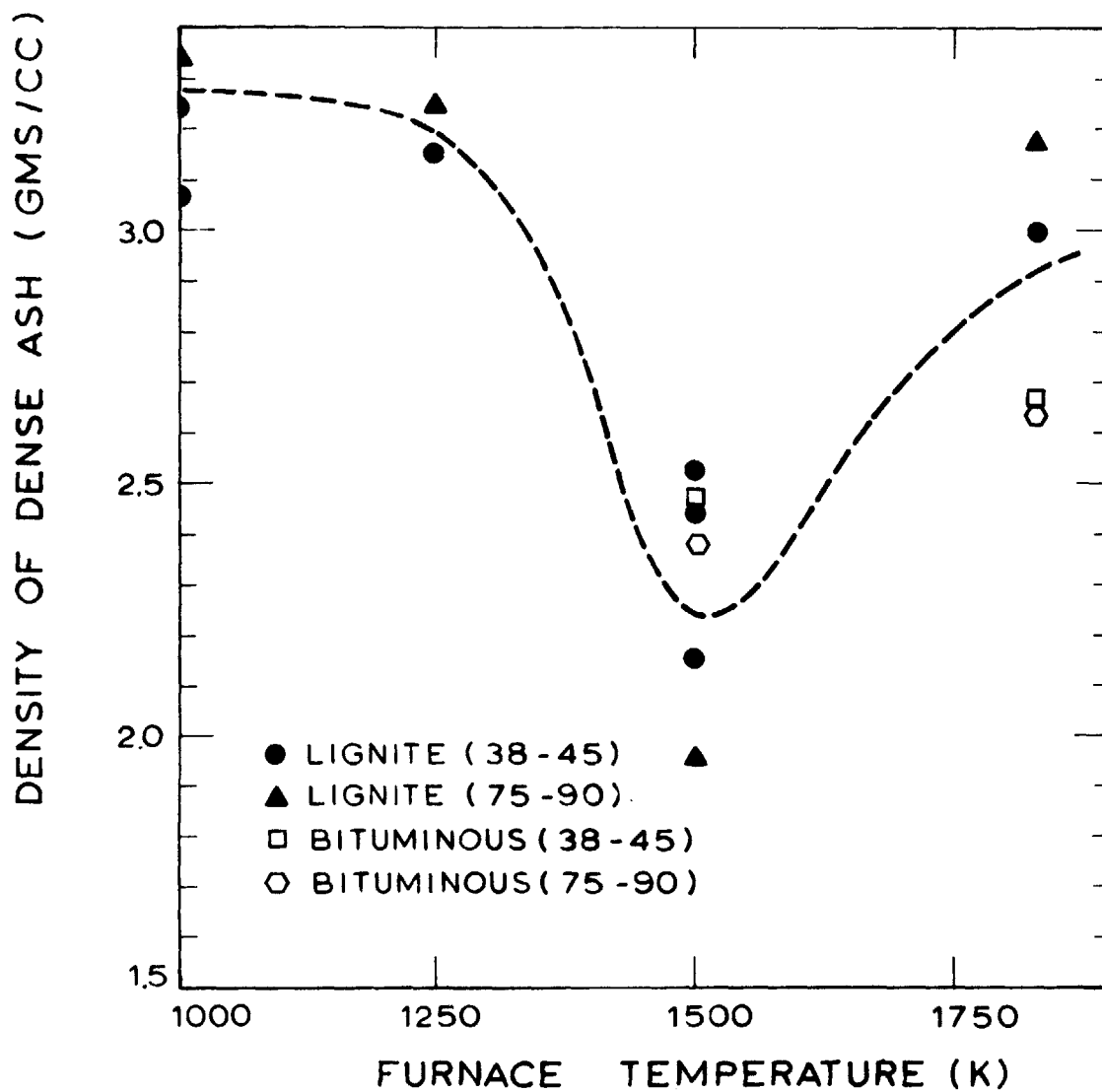
Effect of Combustion Temperature on Density of Ash

Figure 6.10(A)

FREQUENCY DISTRIBUTION

CUMULATIVE

● LIG (38-45) μm : 1500 k
▲ BIT (75-90) μm : 1500 k

$\frac{dR}{dS} = f(S) = $ WEIGHT %/(gms/cc)

$\dot{S} = 2.48$ gms/cc
$S = 3.37$

S (gms/cc)

R (%)

S (gms/cc)
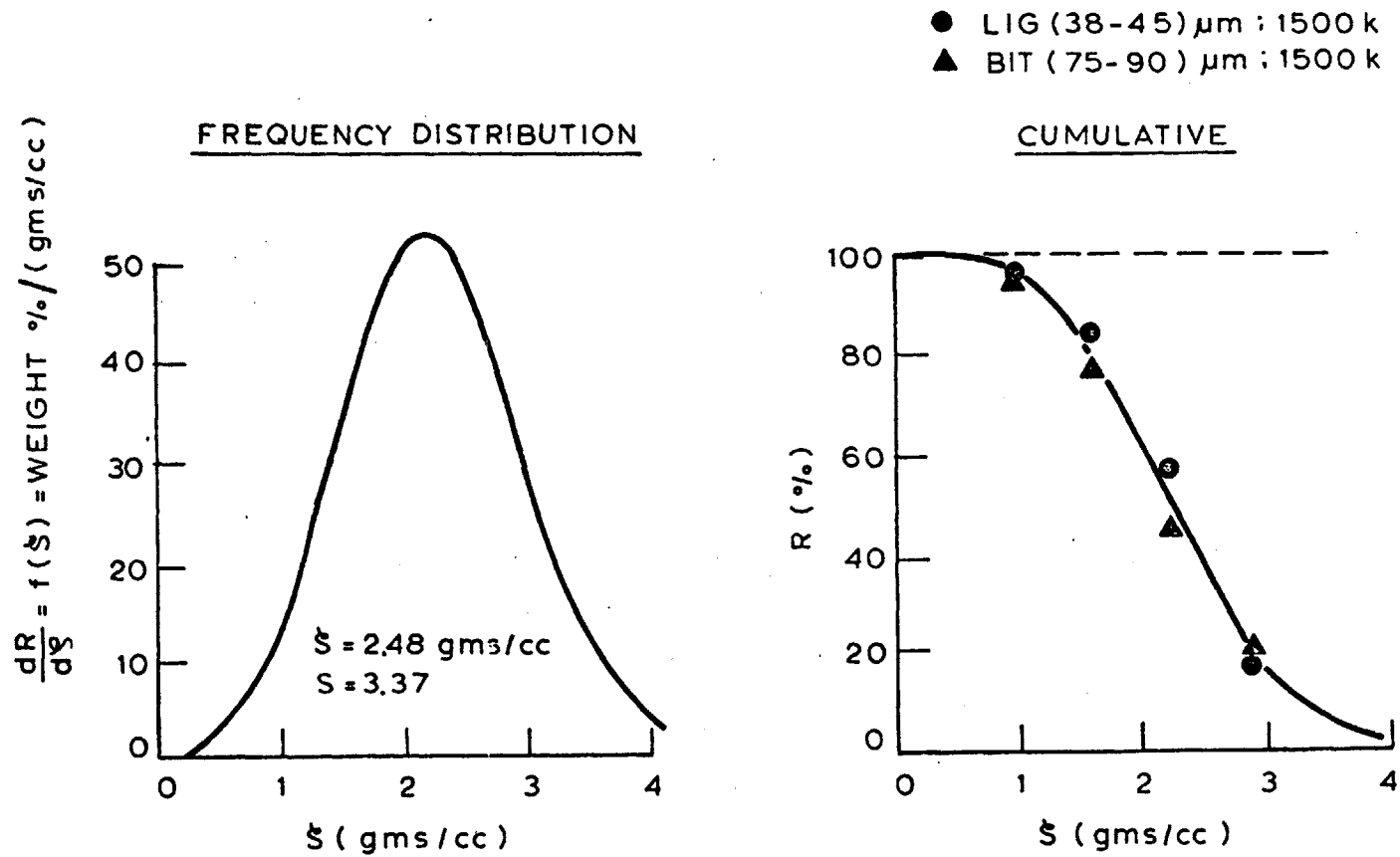
Fig 610 (B) Density Variations of Ash

other samples is also expected to vary continuously as shown for two samples and since the mean dense ash density and amount of cenospheres is determined experimentally, the density variation can be computed using a two-parameter fit, as shown in Figure 6.10(C).

The maximum production of cenospheres (and minimum ash density) is found at a furnace temperature of 1500°K. As explained in section 6.3.4, increases in temperature above 1500°K may lead to a lowering of the viscosity of the ash and an increased rate of gas production leading to bursting of the cenospheres. At lower temperatures (1250°K) due to very high viscosity, the growth of ceno-spheres is very slow (Appendix D).

6.4.1.2 Particle Size of Cenospheres

Particle size distribution of ash cenospheres was measured for all the samples. A typical distribution of cenospheres, dense ash and overall ash is shown in Figure 6.11 for ash from 38-45μm bituminous coal at 1830°K fur-nace temperature. Figure 6.12 is the frequency plot for the same distribution using estimated Rosin-Rammler param-eters from Figure 6.10, with 1 ash/coal curve also added for comparison. As can be seen the cenospheres are much larger than the dense ash. Volume median size for the dense ash is about 7μm while for the cenosphere it is about 19μm. Similar results are shown for a 1500°K furnace tem-perature (Figure 6.13).

1 Lig (38-45) and Bit (75-90) ; 1500 K
2 Bit (38-45) and Bit (75-90) ; 1830 K
3 Lig (38-45) and Lig (75-90) ; 1830 K
4 Lig (38-45) and Lig (75-90) ; 1250 K

$$R = 100 \ exp\left[-\left(\frac{\mathcal{S}}{\mathcal{S}'}\right)^{S}\right]$$

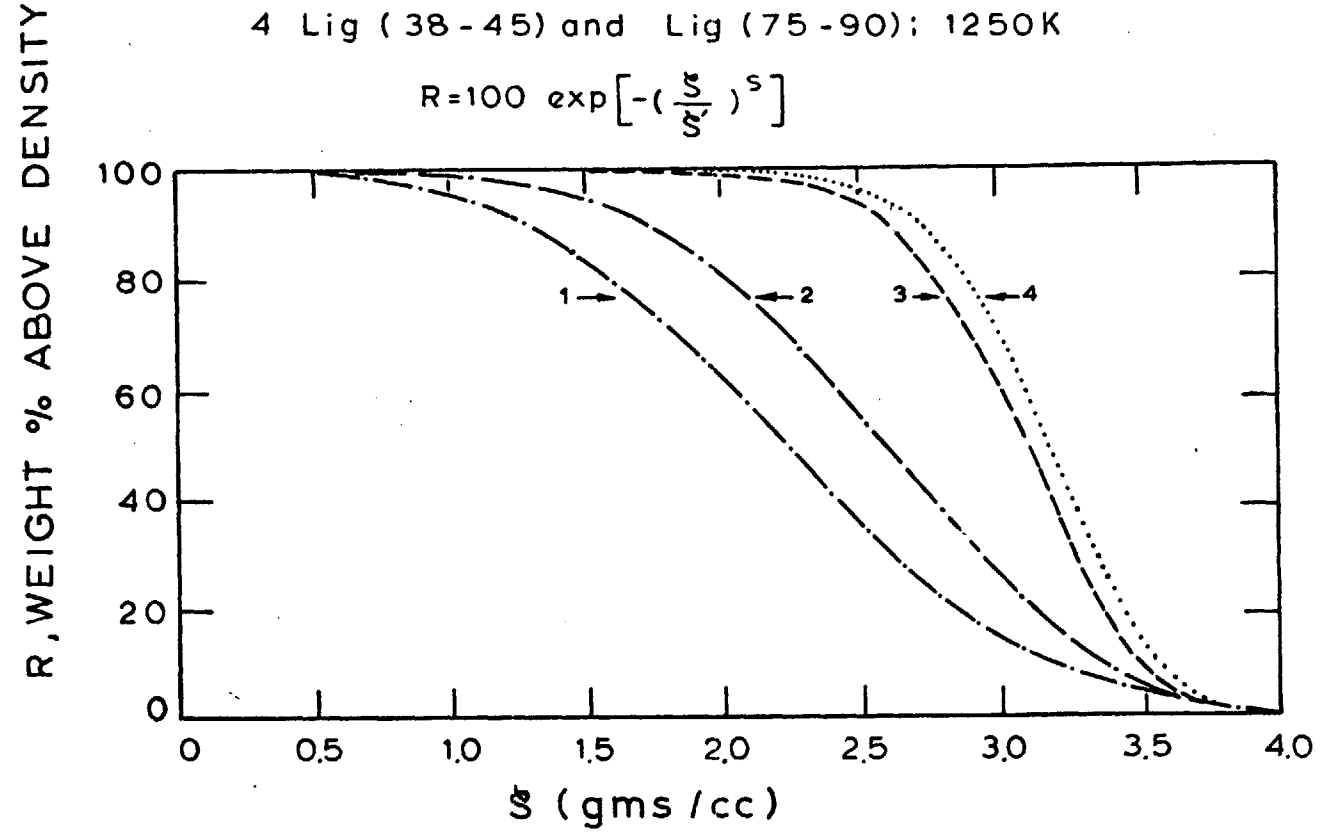Fig 6.10 (c) Density Variations of Ash Using Two Parameter
Fits
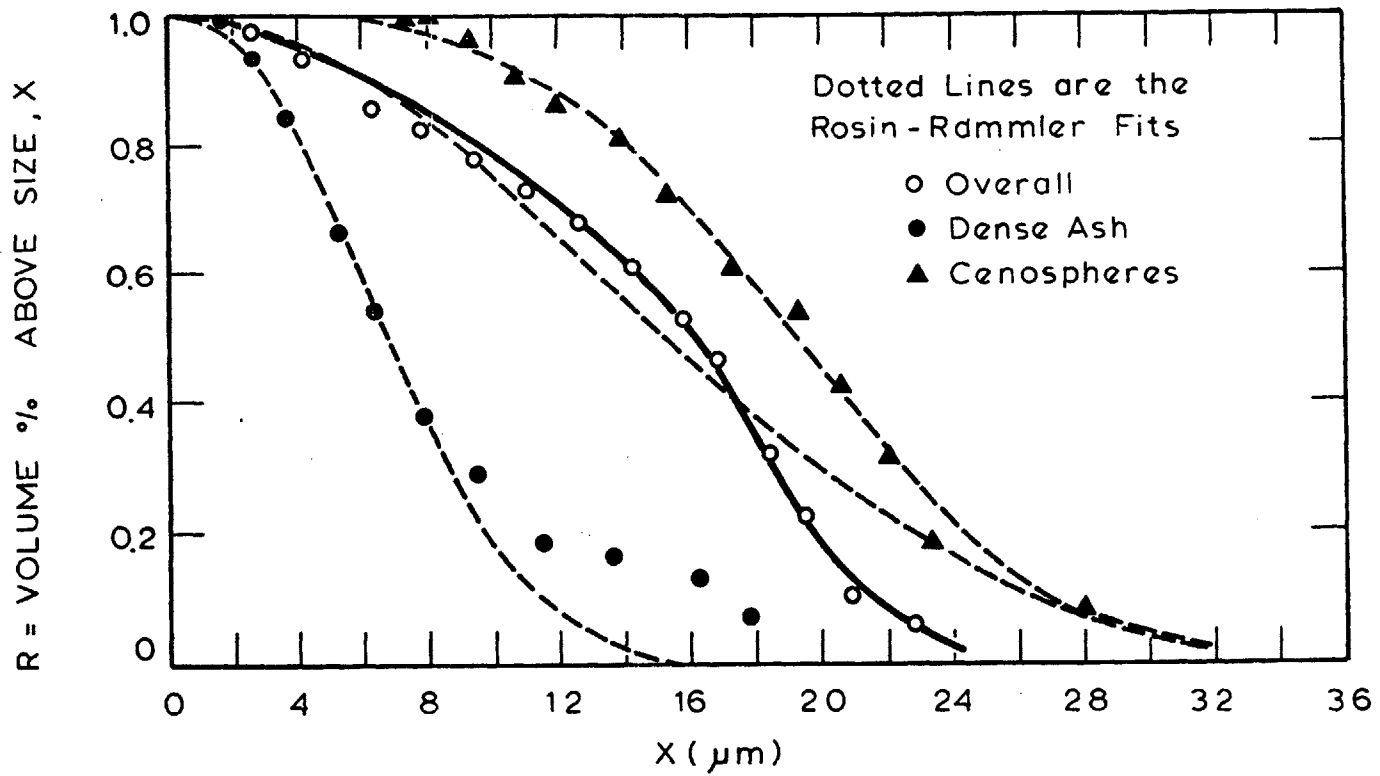
Size Distribution of Ash from Bituminous (38 - 45) Coal at 1830 K

Figure 6.11
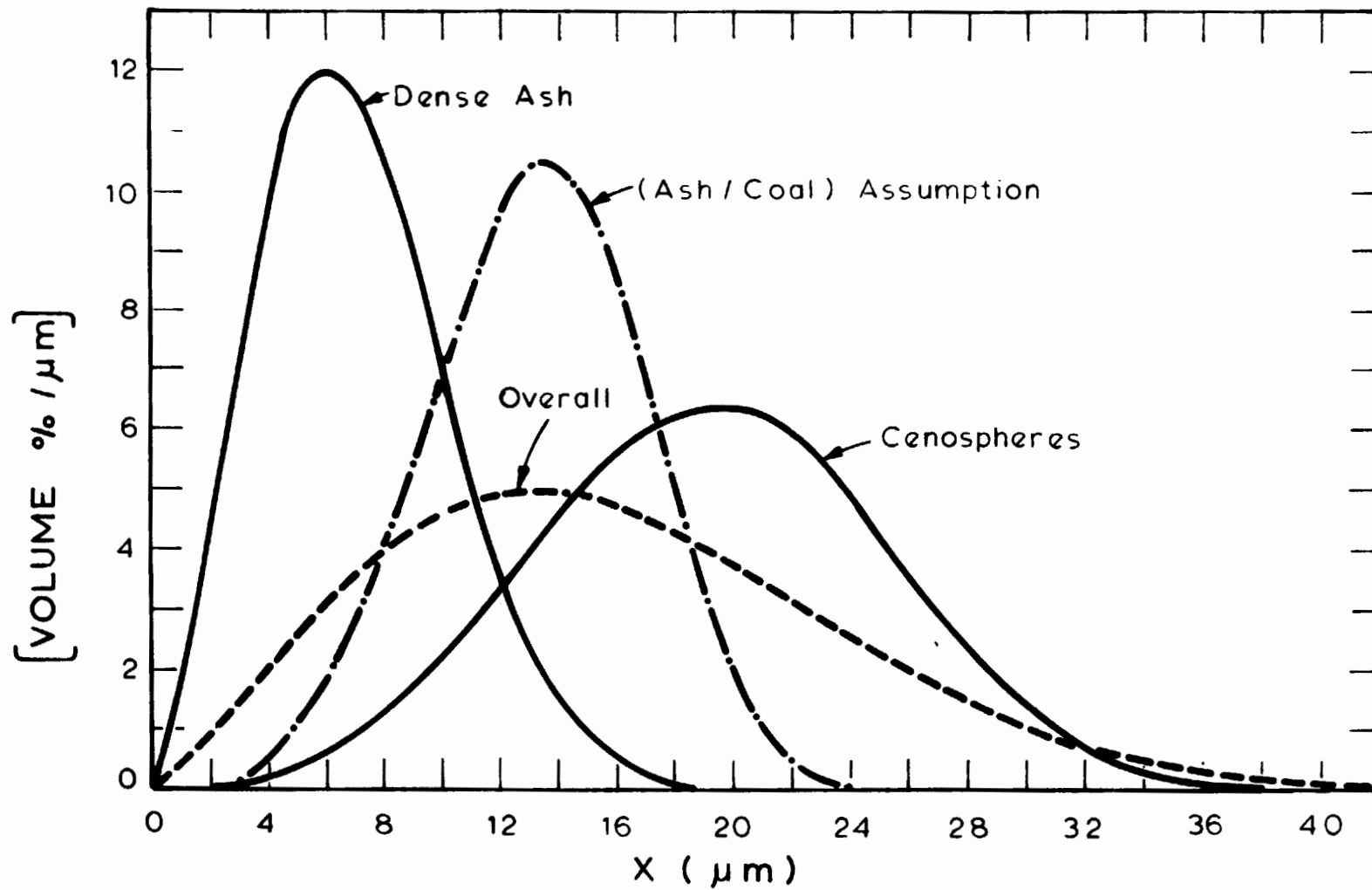
Volume Frequency Distribution for Ash from Bituminous (38-45) Coal at 1830 K (Rosin-Rammler Fit)

Figure 6.12
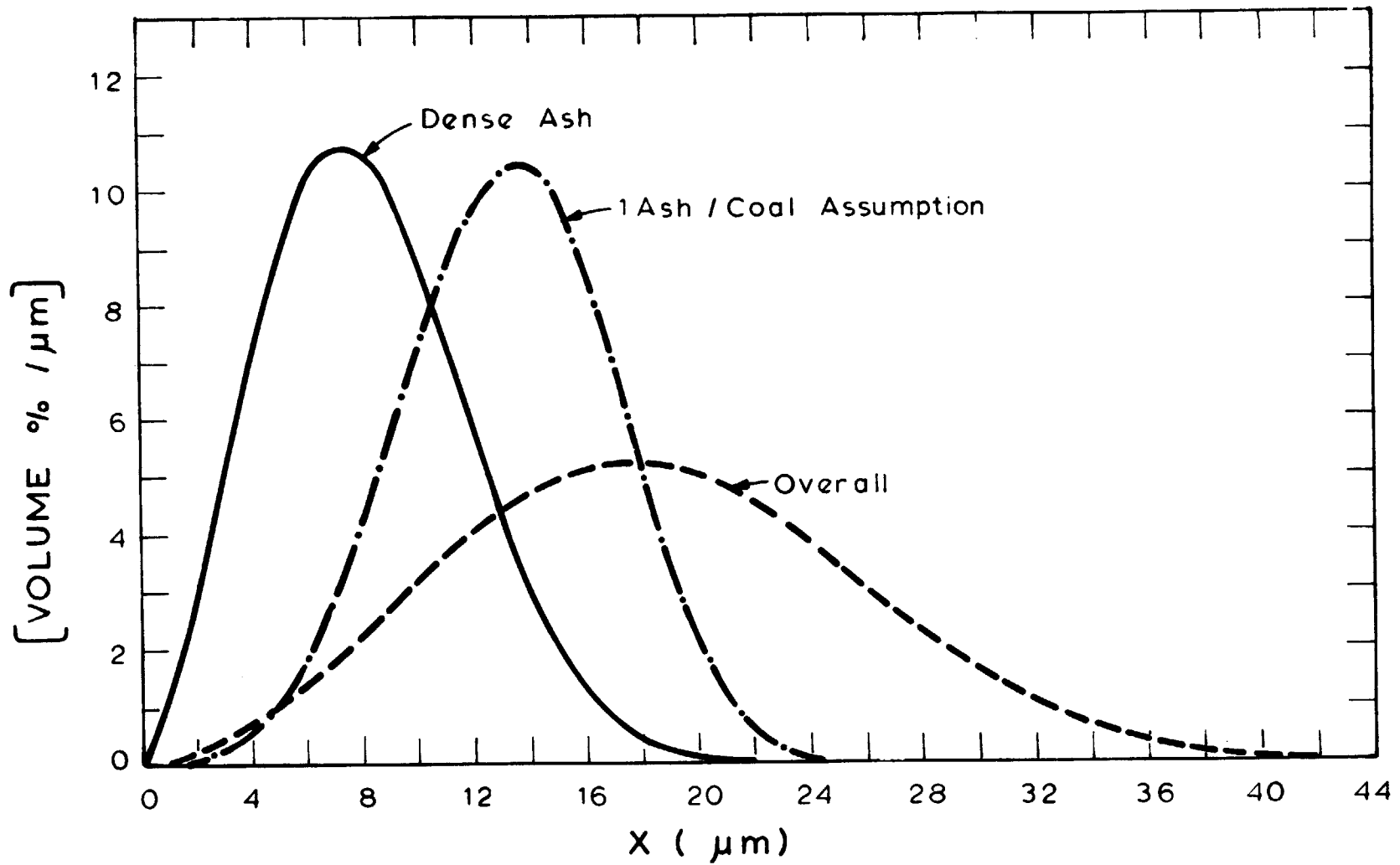
Volume Frequency Distribution for Ash from Bituminous (38-45) Coal at 1500 K (Rosin Rammler Fit)

Figure 6.13

Figure 6.14 and 6.15 show the particle size distri-
bution of ash obtained from Lignite (38-45) and (75-90)μm
sizes at three different temperatures. The volume mean
ash size at 1500°K is larger than the size at 1250 and
1830°K, mainly because of the larger amount of cenospheres
formed. Although the maximum amount of cenosphere formed
was about 6 percent by weight, due to their lower density
(ρcenosphere/ρ dense ash$\simeq$0.25) they may account for more
than 20 percent of the volume, and thus can affect the
volume mean size of ash significantly.

6.4.2 Effect of Temperature, Coal Size and Coal Type

The cenospheres were removed from the ash samples
and the effect of these parameters on particle size dis-
tribution of dense ash was investigated.

Effect of temperature on overall particle size dis-
tribution can be seen in Figure 6.14 and 6.15. Size
distribution of dense ash for lignite (38-45) and (75-90)
μm size is plotted for three temperatures in Figure 6.16
and 6.17. There is no obvious trend showing effect of
combustion temperature on ash. The deviations between
different runs are the statistical variations. (See
Appendix F) The overall mass median size for dense ash
produced from (38-45)μm lignite is 8.5μm (S D = 1.4μm
taking average of all seven runs. 1 ash/coal assumption
gives mass median size of 11.99μm which results in the
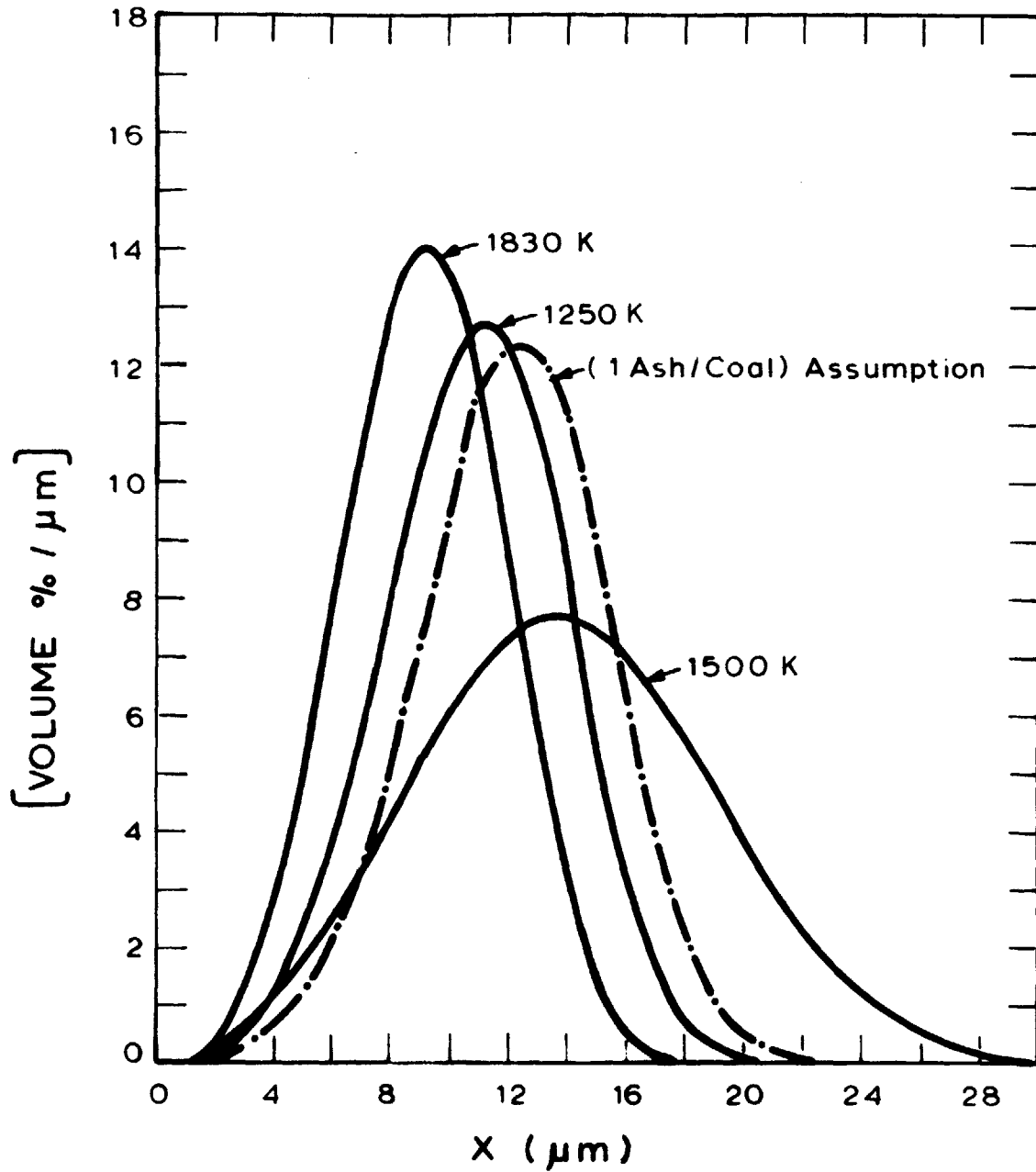
Effect of Combustion Temperature on Ash Particle
Size Distribution from Lignite (38-45)

Figure 6.14
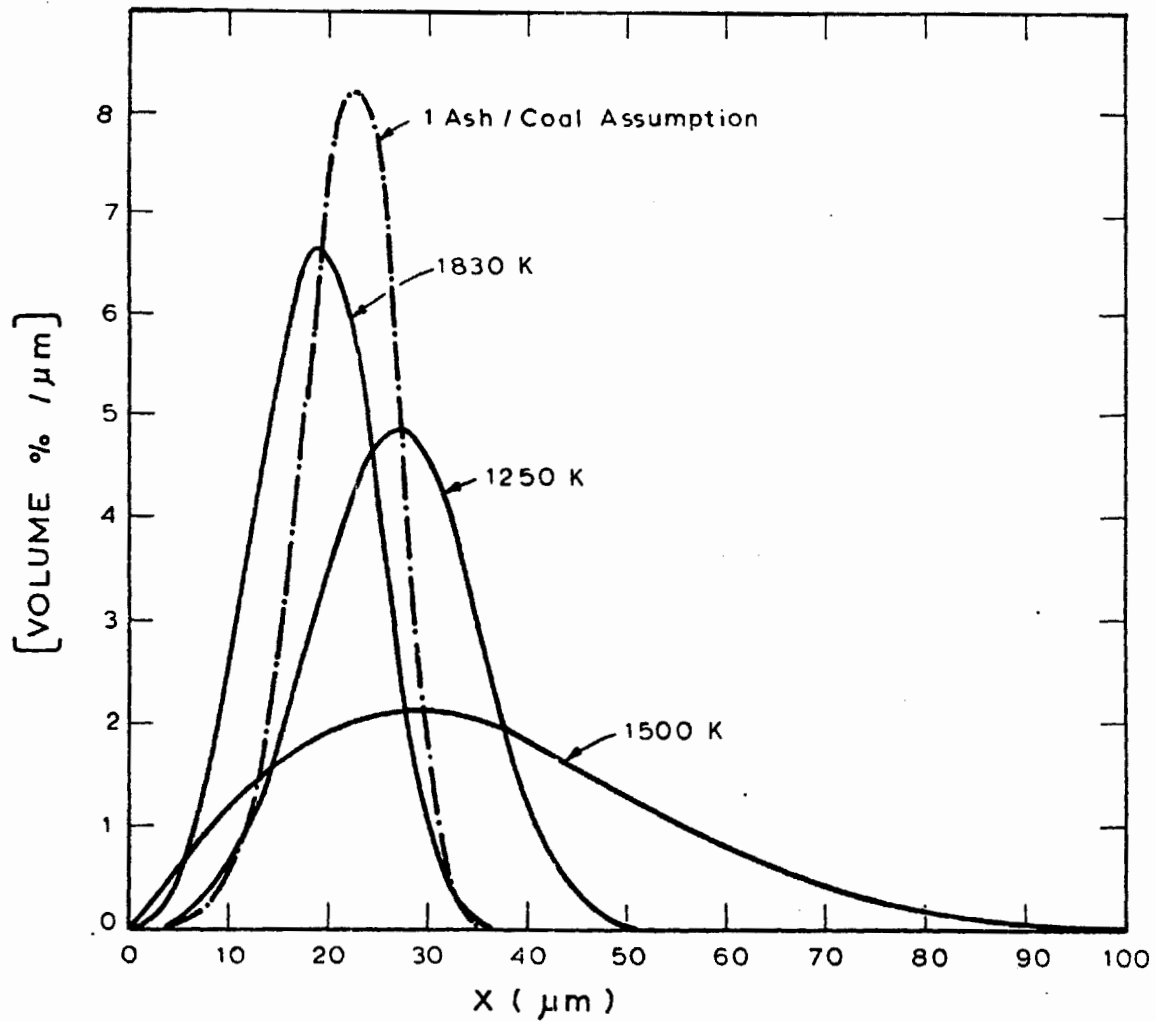
Effect of Combustion Temperature on Ash Particle Distribution from Lignite (75 - 90) μm
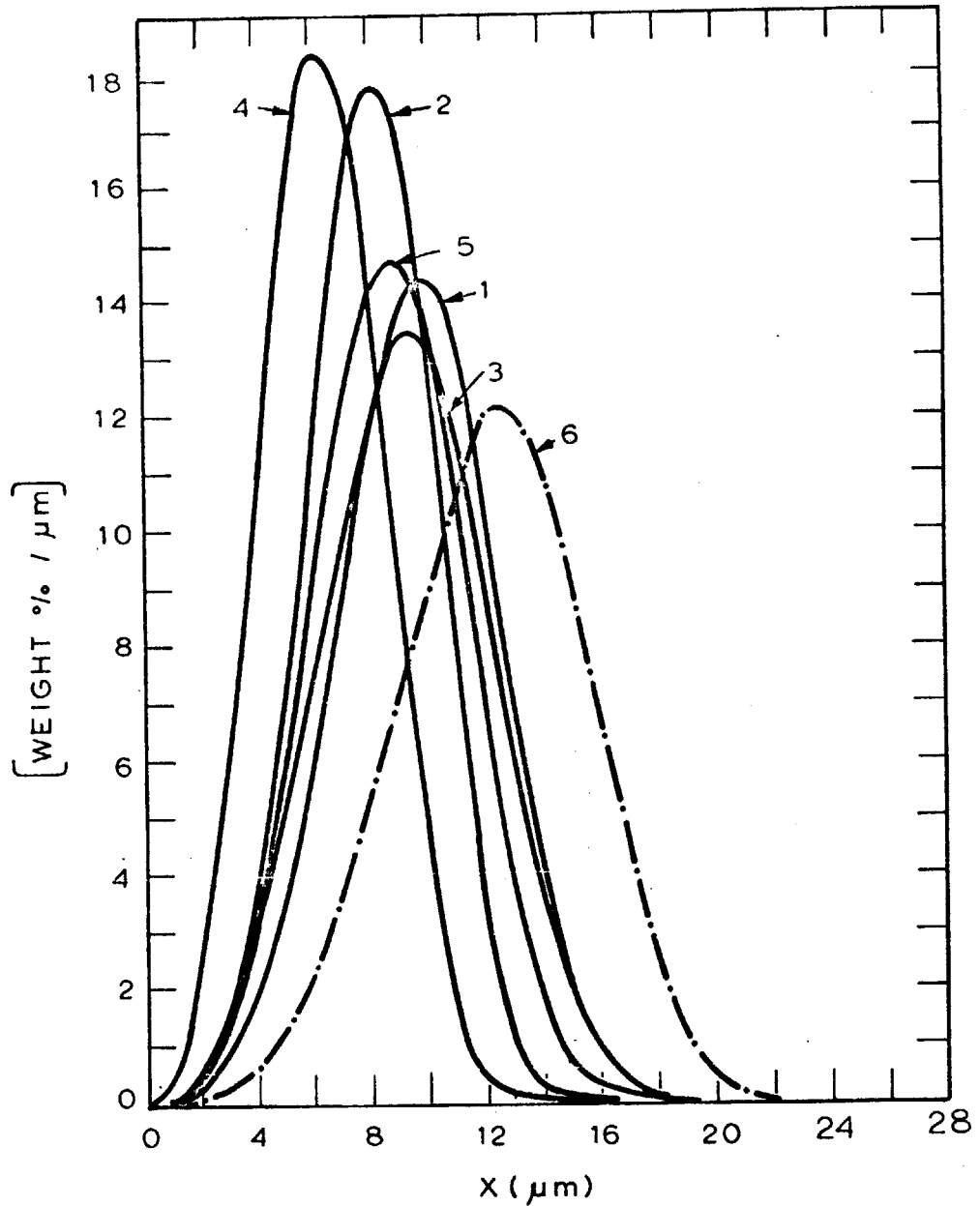
Figure 6.15

Particle Size Distribution of Dense Ash from (38-45) μm Lignite

	Temperature	Xm (μm)	X' (μm)	S
1	1250	9.79	10.62	4.0
2	1250	8.00	8.83	4.15
3	1500	9.26	10.26	3.57
4	1500	6.3	7.0	3.32
5	1830	9.2	10.1	3.68
6	1 Ash / Coal	11.99	13.37	4.30

Figure 6.16
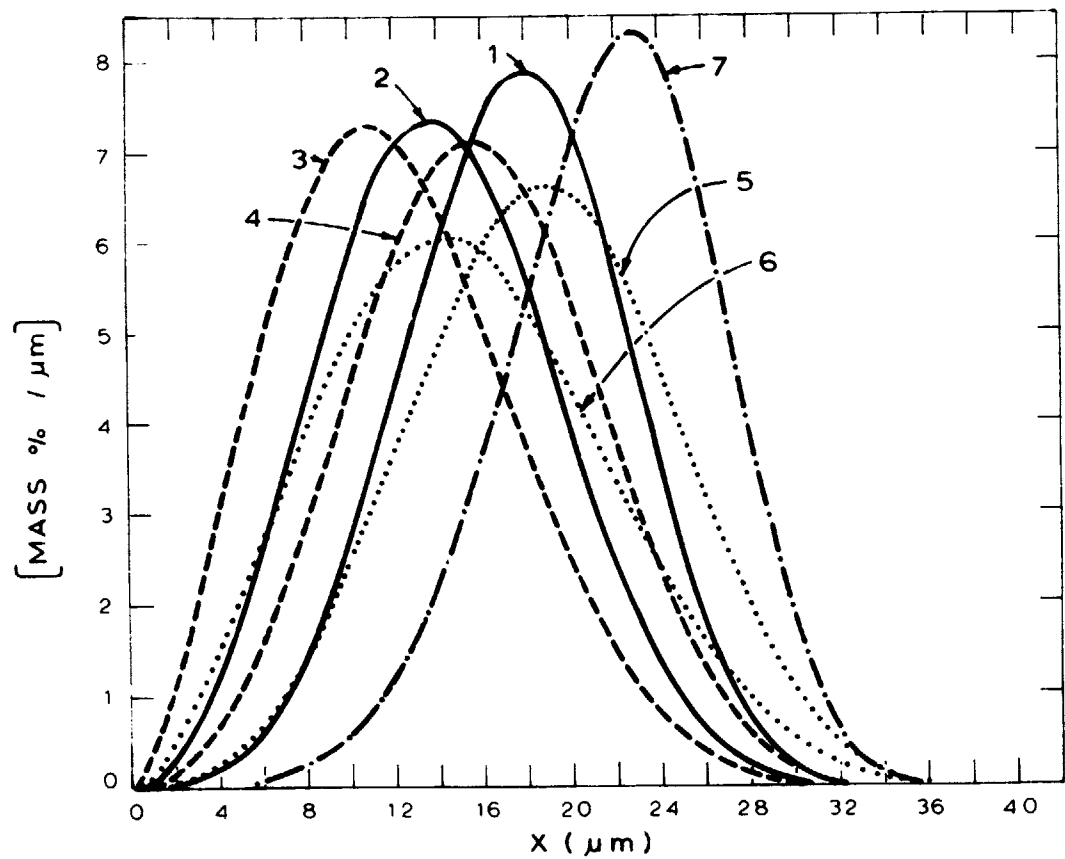
Size Distribribution of Dense Ash from Lignite (75-90)

	Temperature(K)	Xm (um)	X (um)	S
1	1250	17.8	19.3	4.0
2	1250	12.7	15.8	2.97
3	1500	11.7	13.6	2.42
4	1500	15.7	17.6	3.225
5	1830	18.7	20.8	3.59
6	1830	14.9	17.2	2.58
7	'Ash /Coal	21.71	23.67	5.22

Figure 6.17

formation of 2.8 ash particles per coal particle on an average. Similar analysis for 75-90μm lignite gives an overall average median size of 15.25μm (S.D.=2.75μm) and formation of 2.9 ash particles per coal particle. Distribution of dense ash from bituminous coal (38-45)μm is shown in Figure 6.18. Average ash size produced is 8.5μm (S.D. = 0.64)μm) resulting in the formation of about 5 ash particles per coal particle.

Coal size has almost no influence on the number of ash particles produced per coal particle. The mean size of ash particle size distribution is proportional to the parent coal size.

The type of coal has an influence on the number of ash particle produced per coal particle. Bituminous coal produced larger number of ash particles (5 compared to 3 from Lignite) than lignite. This is consistent with the theory of ash formation discussed in Section 6.3.3.

6.4.3 Particle Size Distribution of Ash as a Function of Carbon Burnout

It is already recognized (Section 6.3) that the number and size of the agglomerates of ash formed are influenced by the burning behavior of coal particles. Combustion through pores or on surface would produce different results. To obtain the size distribution of ash as a function of carbon burnout, low temperature ashing of partially burned char is required. This aspect
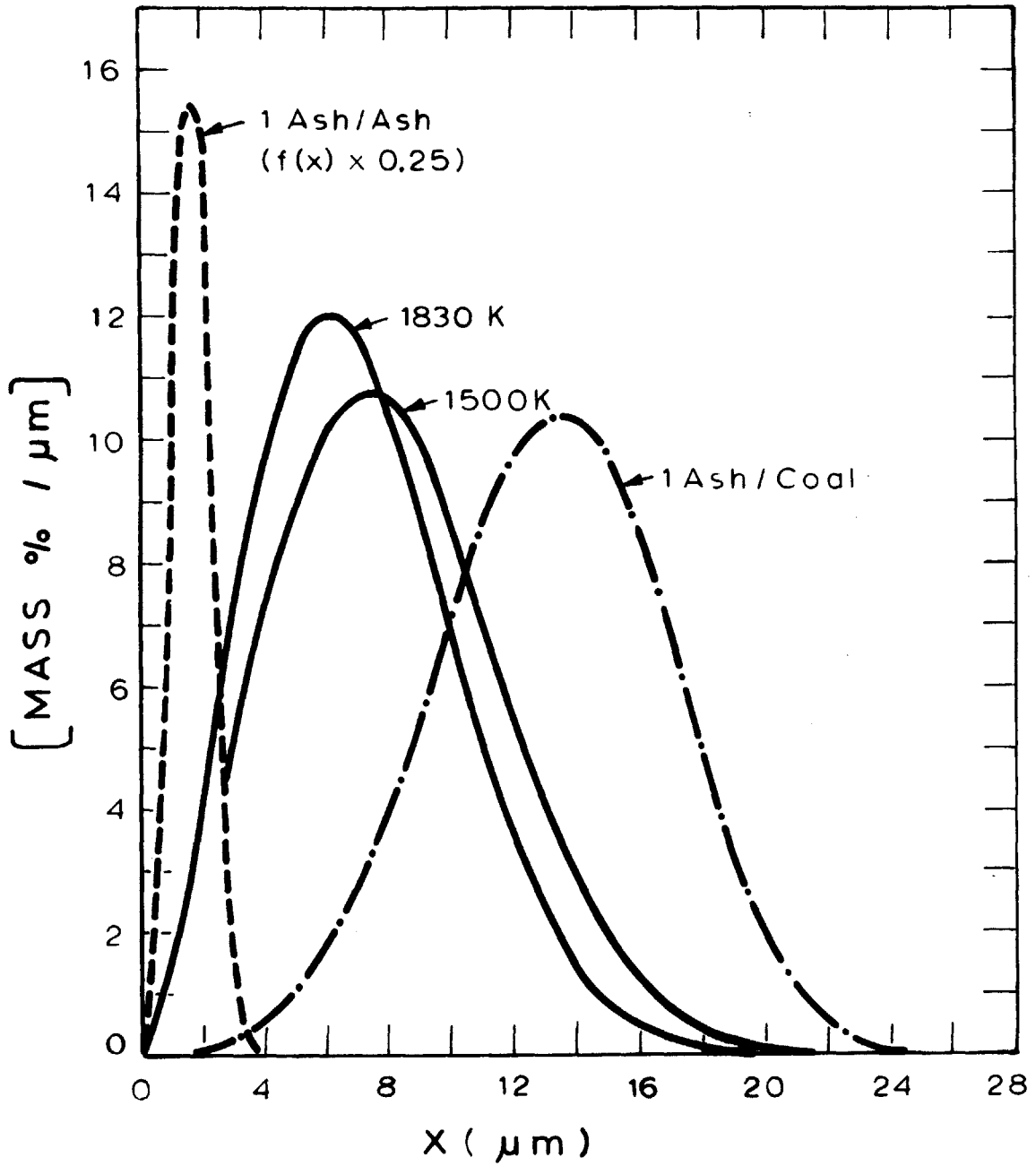
Dense Ash PSD from (38-45) um Bituminous Coal

Temperature (K)	X'(μm)	Xm(μm)	S
1500	9.17	7.9	2.42
1830	7.9	6.8	2.3
1 Ash / Coal	14.58	13.50	4.0
1 Ash / Ash	1.90	1.68	2.99

Figure 6.18

was not studied experimentally but computations were per-
formed on the basis of experimental information regarding
the distribution of mineral matter in original coal and
at complete combustion, and some simplistic models. The
computed ash particle size distributions on a shrinking
sphere model as a function of carbon burnout are shown in
Figure 6.19. The computations were performed graphically
for a 40μm mass median coal particles with 10% ash of 2μm
size, randomly distributed throughout the coal. As can be
seen the mean particle size of ash increases as the carbon
burnout increases due to increasing agglomeration. It
was also assumed that the ash particles continue to stick
to the char surface and separates only at complete 100%
burnout.

6.5 Conclusions

1. Part of the ash formed during coal combustion are in
the form of hollow spheres (cenospheres) whose density
vary continuously from less than 1 gm/cc to about 3.5 gms/
cc. The cenospheres have larger volume mean size than the
dense ash.

2. 1500°K furnace temperature (particle temperature
1640°D) is about the critical temperature of maximum
amount of cenosphere formation. At lower temperatures the
growth rate of cenospheres is very slow due to high vis-
cosity and recrystallization of fused ash and at higher

SHRINKING SPHERE MODEL

Basis : Coal Size, 40 μm Mass
Median
Rosin Rammler Distribution
s = 4.5
Ash = 10 % by Weight of Coal
Ash in Original Coal 2.0
μm Mass Median
Rosin Rammler , s = 3.0

	% Carbon Burnout	Ash Size (μm) Mass Median
1	0	2.0
2	25	2.1
3	50	2.6
4	75	3.8
5	100	13.4

WEIGHT % / μm

ASH PARTICLE SIZE (μm)
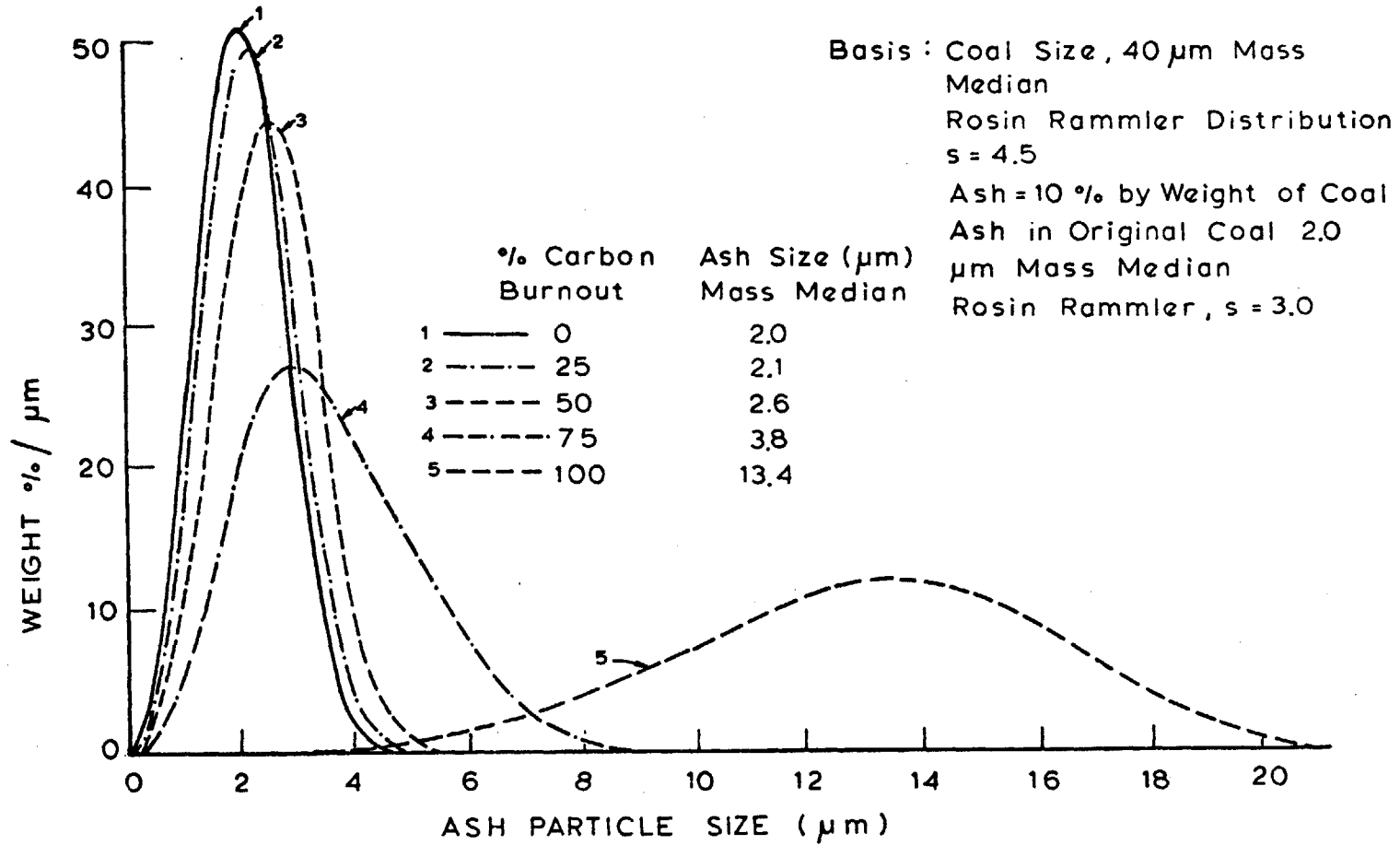
Fig 6 19 Effect of Carbon Burnout on PSD of Ash (Shrinking Sphere Model)

temperature due to lower viscosity and higher rate of gas production bursting of cenospheres may occur.

3. The dense particle size distribution does not show any trend as a function of combustion temperature.

4. Original coal size has no major effect on the number of ash particles produced per coal particle. The mass median size of ash particle produced is proportional to the mass median size of the parent coal particle.

5. Coal type influences the number of ash particles produced about 2.8 particles of ash per coal particle and bituminous coals produced about 5.

6. The number of ash particles produced per coal particle can be explained on the basis of a proposed "fragmentation and cenosphere formation of char" theory.

7. The proposed mechanistic theory is evidenced by the sequential char burnout photomicrographs and ash-coal surface properties calculations.

6.6 Implications

The knowledge of mean ash particle size and its distribution for given coal size, coal type and temperatures have practical implications. Some are listed below.

    a. A critical temperature for maximum stable ash cenosphere formation is found. Depending on type of fly-ash separation equipment to be

used, the ash particle size can be varied by vary-
ing combustion temperature. Larger particle
sizes may be desired if a bag filter is used but
lower density ash (cenospheres) should be avoided
in case cyclone separators or electrostatic
precipitators.

b. Vaporization: The amount of vaporization of ash
species can be calculated once the particle size
and composition is known. It can be shown that
the vaporization of ash scales as inversely pro-
portional to the square of the particle diameter
(Appendix E gives the equations for ash vapori-
zation characteristic times). Figure 6.20 gives
the characteristic times for vaporization as a
function of particle size and composition for
three different temperatures. For an MHD com-
bustor where residence times are small (~50 msecs)
and temperature about 2700°K, complete vaporiza-
tion of SiO_2 is possible and other species Al_2O_3,
MgO, CaO would vaporize partially. Since the
particle size of ash is dependent on the amount
and mode of carbon burnout, the amount of vapor-
ization and the composition of the vaporized
species in a given time and at a given tempera-
ture are significantly influenced. Table 6.2
gives typical characteristic times for the vapor-
ization of different species at three temperatures
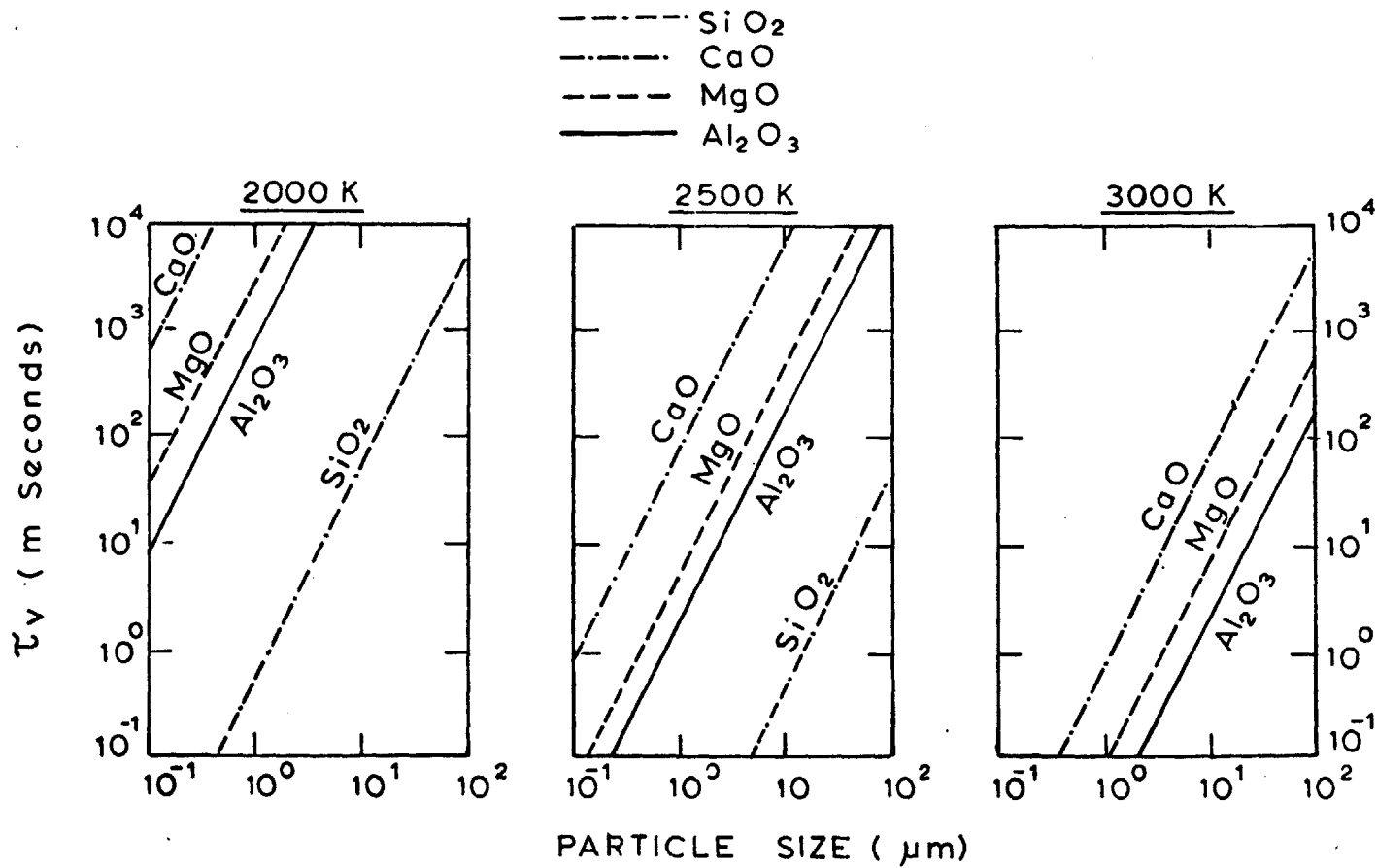
Fig 6.20 Characteristic Vaporization Times For Ash Species

TABLE 6.2

Characteristic Vaporization Times in msec

Species	Temperature (°K)	τ_v (mSeconds)		
		1 ash/ash	5 ash/coal	1 ash/coal
SiO_2	2000	5.4×10^{-1}	8.2	2.4×10^1
Al_2O_3	2000	8.0×10^2	1.2×10^4	3.6×10^4
CaO	2000	6.3×10^4	9.6×10^5	2.8×10^6
MgO	2000	3.0×10^3	4.6×10^4	1.4×10^5
SiO_2	2500	4.6×10^{-3}	7.0×10^{-2}	2.1×10^{-1}
Al_2O_3	2500	1.9	2.9×10^1	8.5×10^1
CaO	2500	8.0×10^1	1.2×10^3	3.6×10^3
MgO	2500	5.0×10^1	7.6×10^2	2.2×10^3
SiO_2	3000	–	–	–
Al_2O_3	3000	2.6×10^{-2}	4.0×10^{-1}	1.2
CaO	3000	9.0×10^{-1}	1.4×10^1	4.0×10^1
MgO	3000	7.3×10^{-2}	1.1	3.3

for the three cases for 10% ash and 40μm mass
median coal size. The three cases are:

a. 1 ash/ash , no agglomeration , $\bar{x}_{ash}$= 2μm

b. 5 ash/coal , partial agglomeration, $\bar{x}_{ash}$= 7.8μm

c. 1 ash/coal , complete agglomeration, $\bar{x}_{ash}$=13.4μm

c. Heat Transfer and Emissivities: The heat flux to
the walls of the combustor is dominated by the
continuum radiation from ash and partially burned
coal particles and by banded gas radiation con-
tributed primarily by CO_2 and H_2O. The particle
cloud emissivity is the contribution from ash and
char particle clouds which can be calculated
using the formula given below (Hottel and
Sarofim, 1967)

$$\varepsilon = 1-\exp(-caL/4) \qquad (6.9)$$

where

ε = emissivity of the cloud

c = particle concentration, number per unit
   volume

a = projected area of each particle

L = path length, characterizing dimension

The emissivities of the ash particle cloud for the same three cases as mentioned in Section 6.6.b and for three path lengths covering the dimensions of laboratory scale to prototype MHD combustors are listed in Table 6.3

TABLE 6.3

Emissivity of Ash Particle Cloud

	$\bar{x}$ (μm)	ϵ L=61cm	ϵ L=305cm	ϵ L=610cm
a. 1 ash/ash	2.0	0.220	0.710	0.920
b. 5 ash/coal	7.8	0.047	0.212	0.380
c. 1 ash/coal	13.4	0.028	0.130	0.244

The computations are based on 10% ash in coal and coal combustion at stoichiometric conditions at 2000°K.

As can be seen from the table, the ash cloud emissivity may change significantly i.e. 0.22 (1 ash/ash) to nearly transparent 0.028 (1 ash/coal) for L=61cm.

The overall particle cloud emissivity can be approximated by

$$\epsilon_p = 1-\exp[-1.5(\frac{\epsilon_c \cdot f_{v_1c}}{dc} + \frac{\epsilon_a \cdot f_{v_1a}}{da})L] \qquad (6.10)$$

where ϵ_c and ϵ_a are the emittances of the char and ash, f_{v_1c} and f_{v_1a} the fractional volume of space occupied by particle size distribution and L the mean beam length for the particle cloud.

The total contribution of particulate and banded emissivities can be approximated by

$$\varepsilon = \varepsilon_p + \varepsilon_{CO_2+H_2O} - \varepsilon_p \varepsilon_{CO_2+H_2O} \qquad (6.11)$$

6.7 Recommendations

1.   Experiments should be performed with more coals and more particle sizes and over a wider range of temperatures.

2.   Ash particle size distribution should be determined as a function of char burnout. Since it is very difficult to experimentally obtain the PSD of ash in unburned char, a combination of free fall experiments followed by low temperature ashing should give overall particle size distribution of ash in partially burned char.

CHAPTER 7

BEHAVIOR OF ASH AT HIGH TEMPERATURES

II.   Mineralogy of Ash under Simulated Combustor Conditions

7.1   Introduction

Chemical reactions which occur in the mineral phases during combustion and gasification of coal at high temperatures are not yet fully understood. When coal is heated in oxidizing or gasification conditions, the minerals associated with it undergo thermal decomposition, interaction with the coal substance, and interaction with each other. These chemical changes are accompanied by changes of form-ash formation, clinkering and fusion and partial volatilization of some components, depending on the temperatures reached in the combustion chamber. For the case of a conventional combustor, although significant losses of minor elements (Na, K, etc.) is possible, the vaporization of the major oxides (S_iO_2, Al_2O_3, Fe_2O_3, CaO, MgO) is most of the time negligible. In the case of a MHD combustor, however, due to high temperature of combustion ($\sim$2700°K) significant amount of vaporization of the major mineral oxides is possible.

The purpose of this chapter is to identify the thermal decomposition reactions causing the change in chemical form and weight of mineral matter up to conventional combustion temperatures (1900°K). The coal particles (two types: a bituminous and a lignite) are reacted in a free-fall furnace in a dispersed mode providing heating rates of the order of

10^5°C/sec and residence time of about one second, simulating actual combustor conditions.

7.2 Experimental

Three types of ash samples are produced to study mineralogy of ash:

a. Low temperature ash - to obtain the original state of mineral matter in coal;

b. ASTM ash - to obtain state of mineral matter after reacting coal in oxidizing atmosphere at 750°C (1023°K) in a crucible;

c. Free Fall Ash - to obtain state of mineral matter in simulated combustor conditions at different temperatures.

Experiments were performed for both coals; bituminous and lignite and both sizes (38-45μm and 75-90μm) at three different temperatures in the free fall mode. The condition of experiments, furnace temperature, particle temperature, and residence times are tabulated in Chapter 6 (Table 6.1).

The analysis of crystalline phases developed at each temperature was performed by using a General Electric X-ray diffractometer. Each sample was X-rayed by using monochromatic CuKα radiation (λ=1.54050A°) from 2 angle of 5° to 100° with a scanning speed of 2° per minute and chart speed of 0.5 inch per minute. Minerals were identified by locating the peaks of the diffracted beam intensity.

7.3 Results

The mineralogical changes occuring as a function of temperature will be discussed for the two types of coals separately since the minerals present in the coals differed considerably.

7.3.1 Lignite

The major minerals identified in the low temperature ash of lignite are bassanite [$CaSO_4 \cdot 1/2H_2O$], kaolinite [$Al_2Si_2O_5(OH)_4$], lawsonite [$CaAl_2SiO_4 \cdot 2H_2O$], quartz [SiO_2], dolomite [$CaCO_3 \cdot MgCO_3$], and rutile [TiO_2]. Details of low temperature ash characterization are presented in Chapter 5.

The results of the change in mineral phases occuring at three temperatures in free fall mode and in ASTM ash for both size coals are shown by diffraction patterns in Figure 7.1 and 7.2, and the different phases existing at each condition are listed in Table 7.1. The behavior for the two sized coals was almost similar. The Stable phases at 1830K furnace temperature were quartz [SiO_2], gehlenite [$2CaO \cdot SiO_2 \cdot Al_2O_3$], lime [CaO], and magnesia [MgO]. In the intermediate regime of temperatures other phases anhydrite [$CaSO_4$], anorthite [$CaO \cdot 2SiO_2 \cdot Al_2O_3$], and hematite [$Fe_2O_3$] also existed

7.3.2 Bituminous

The diffraction patterns of low temperature ash from bituminous coals showed the presence of kaolinite [$Al_2Si_2O_5(OH)_4$],
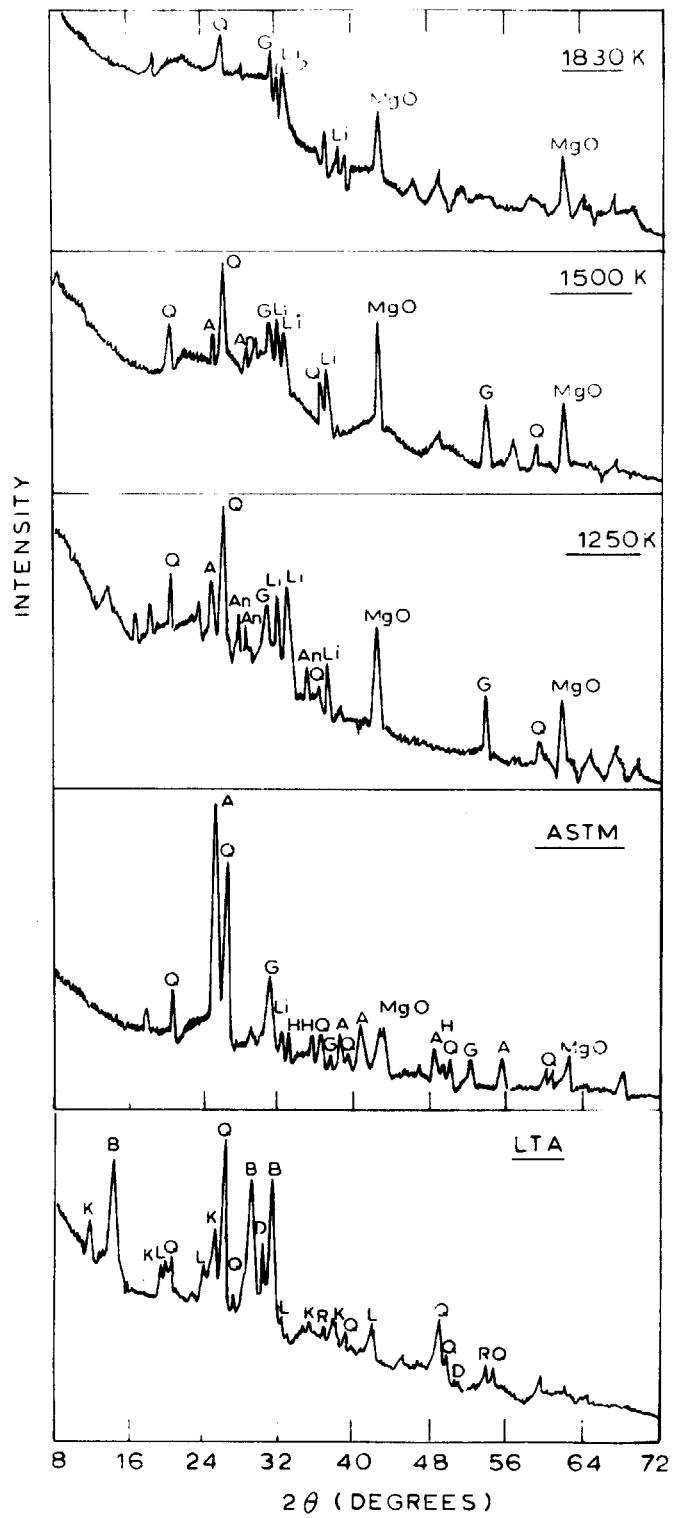
Figure 7.1

Diffraction Patterns Showing the Effect of
Temperature on Mineral Phases for Lignite
(38-45 µm)

Figure 7.2

Diffraction Patterns Showing the Effect
of Temperature on the Mineral Phases
for Lignite (75 - 90 μm)

Table 7.1

MINERAL PHASES PRESENT AT DIFFERENT TEMPERATURES
IN ASH PRODUCED FROM LIGNITE

LTA	ASTM	1250K	1500K	1830K
Kaolinite $[Al_2 Si_2O_5 (OH)_4]$	Gehlenite $[2CaO \cdot SiO_2 \cdot Al_2O_3]$	Gehlenite	Gehlenite	Gehlenite
		Anorthite $[CaO \cdot 2SiO_2 \cdot Al_2O_3]$	Anorthite	
Bassanite $[CaSO_4 \cdot 1/2H_2O]$	Anhydrite $[CaSO_4]$	Anhydrite	Anhydrite	
Dolomite $[Ca Mg (CO_3)_2]$	Lime [CaO] Magnesia [MgO]	Lime Magnesia	Lime Magnesia	Lime Magnesia
Lawsonite $[CaAl_2SiO_4 \cdot 2H_2O]$				
Rutile $[TiO_2]$				
Quartz $[SiO_2]$	Quartz	Quartz	Quartz	Quartz
	Hematite $[Fe_2O_3]$			

illite [$K_{1-1.5}Al_{5-5.5}Si_{6.5-7}O_{20}(OH)_4$], quartz [$SiO_2$],
pyrite [FeS_2], coquimbite [$Fe_2(SO_4)_3 \cdot 9H_2O$], calcite
[$CaCO_3$], and anhydrite [$CaSO_4$].

The transformation of mineral phases under oxidizing
conditions is again shown by diffraction patterns obtained
for different samples (Figure 7.3 and Figure 7.4) and the
phases existing at each temperature are listed in Table 7.2.
The stable phases at 1830K furnace temperatures were quartz
[SiO_2], hematite [Fe_2O_3], lime [CaO], corrundum [Al_2O_3], and
mullite [$3Al_2O_3 \cdot 2SiO_2$].

In both lignite and bituminous, the structure of diffrac-
tion pattern became diffused at high temperature and showed
one or two broad maxima. This behavior is characteristic
of the presence of glassy or amorphous phase (Cullity, 1956).

Table 7.3 gives minerals identified from the diffrac-
tion patterns and the expected 2θ in degrees for the first
eight intensities for the CuKα radiation.

7.4 Discussion of Results

Thermal decomposition, interaction of mineral phases
with coal and interaction of one phase with another, all
reactions are responsible to form a new phase. It is
impossible to fully explain all the reactions involved in
each case because of the complexity of the system. Some
possible reactions and mechanisms will be discussed, start-
ing from the original phase in the raw coal (low temperature
ash) to the formation of a new phase.

Figure 7.3

Diffraction Patterns Showing the Effect of Temperature on Mineral Phases for Bituminous (38 - 45 μm) Coal
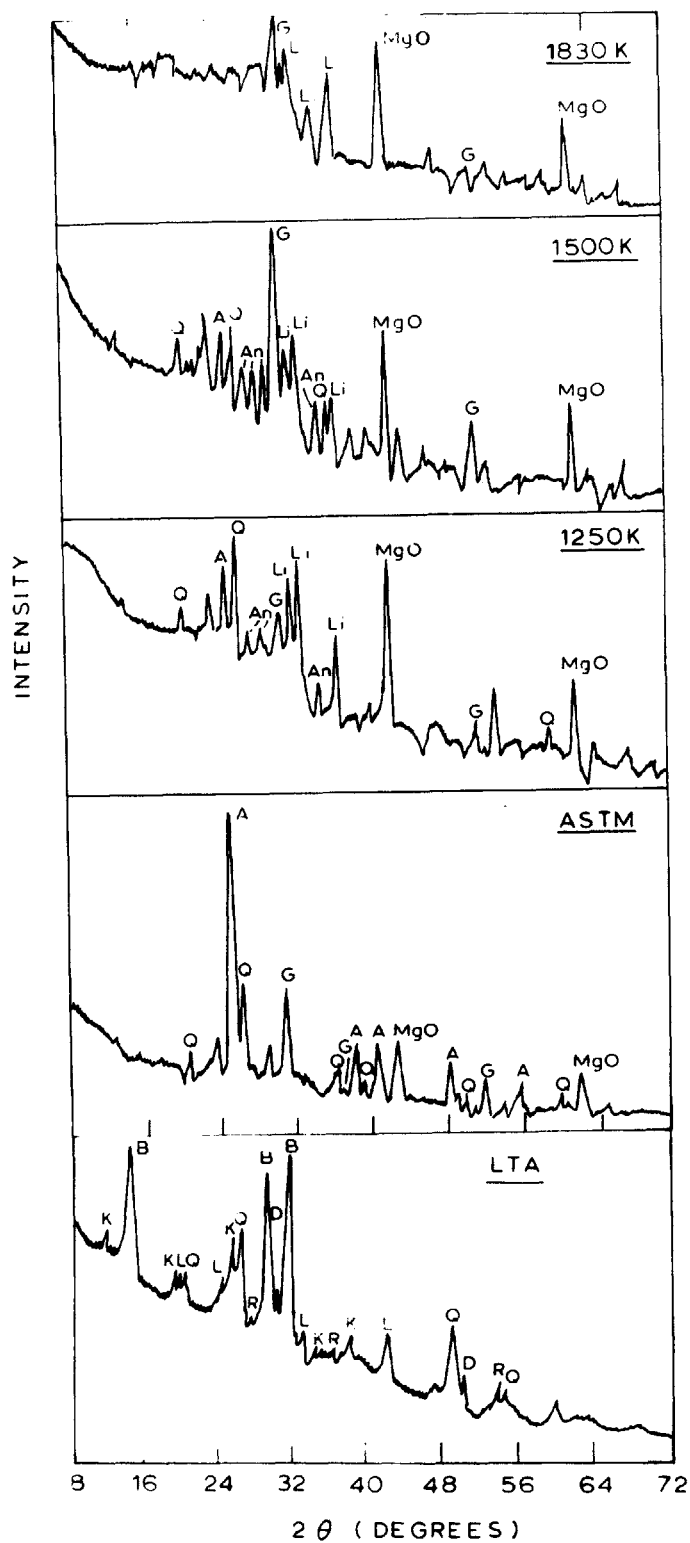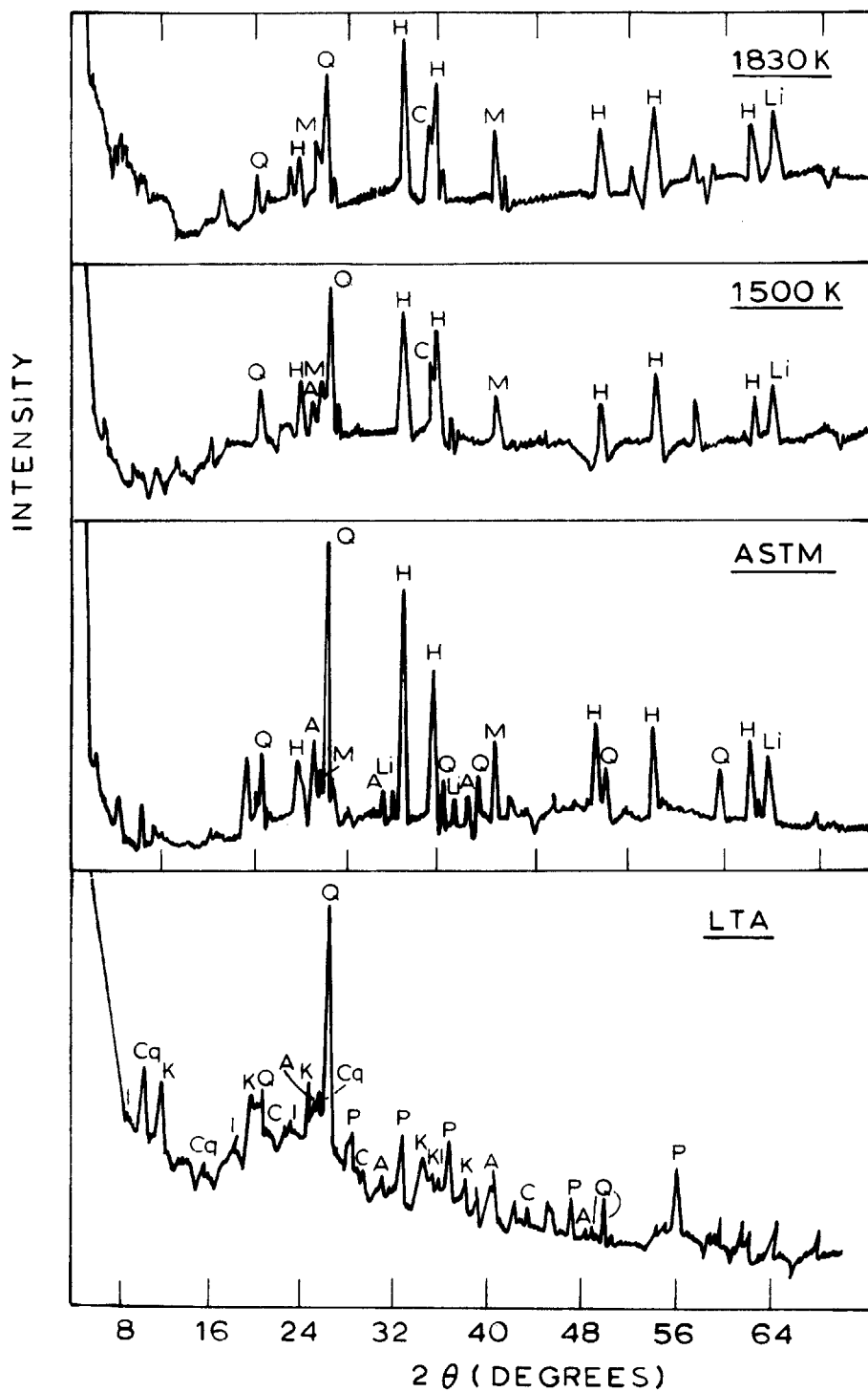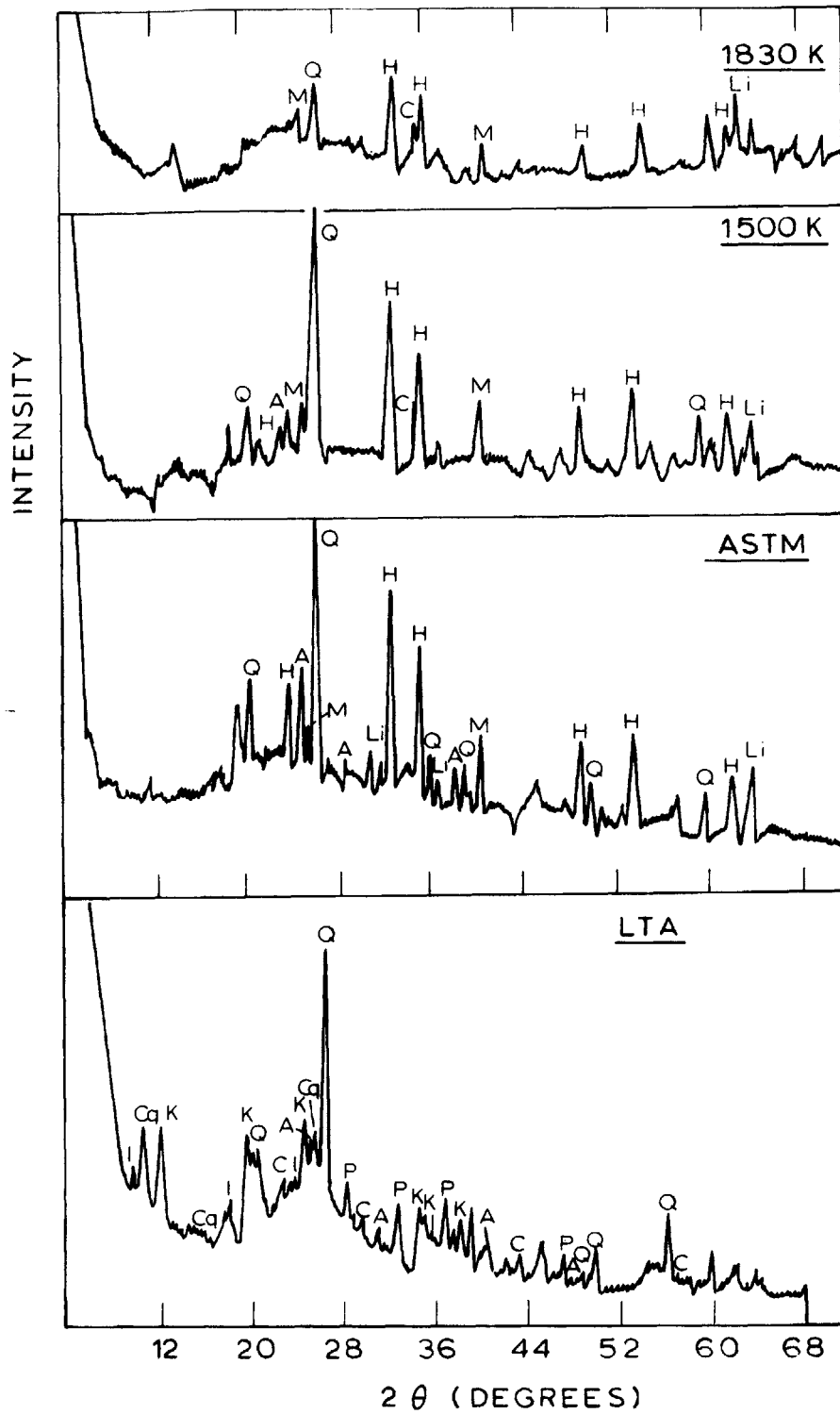
Figure 7.4

Diffraction Pattern Showing the Effect of Temperature on the Mineral Phases for Bituminous (75 - 90 μm) Coal

Table 7.2

MINERAL PHASES PRESENT AT DIFFERENT TEMPERATURES
IN ASH FORMED FROM BITUMINOUS COAL

LTA	ASTM	1500K	1830K
Kaolinite $[Al_2Si_2O_5(OH)_4]$ Illite $[K_{1-1.5}Al_{5-5.5}Si_{6.5-7}O_{20}(OH)_4]$	Mullite $[3Al_2O_3 \cdot 2SiO_2]$	Mullite Corundum $[Al_2O_3]$	Mullite Corundum
Quartz $[SiO_2]$	Quartz	Quartz	Quartz
Pyrites $[FeS_2]$ Coquimbite $[Fe_2(SO_4)_3 \cdot 9H_2O]$	Hematite $[Fe_2O_3]$	Hematite	Hematite
Calcite $[CaCO_3]$	Lime $[CaO]$	Lime	Lime
Anhydrite $[CaSO_4]$	Anhydrite	Anhydrite	

Table 7.3

PEAK POSITIONS AND INTENSITIES OF MINERALS
FOR CuKα RADIATION [λ=1.5405A°]

	MINERAL	SYMBOL	FORMULA		2θ (degrees) FOR EIGHT MOST INTENSE PEAK							
1	Anhydrite	A	$CaSO_4$		25.4 (100)*	31.4 (33)	38.6 (22)	40.8 (20)	48.7 (15)	55.7 (14)	52.3 (11)	52.3 (10)
2	Anorthite	An	$CaO \cdot 2SiO_2 \cdot Al_2O_3$		27.9 (100)	28.0 (75)	22.0 (60)	27.3 (55)	28.6 (45)	27.8 (35)	30.2 (25)	35.5 (25)
3	Bassanite	B	$CaSO_4 \cdot 1/2H_2O$		29.8 (100)	14.7 (95)	31.9 (50)					
4	Calcite	C	$CaCO_3$		29.4 (100)	39.4 (18)	43.1 (18)	47.5 (17)	48.5 (17)	36.0 (14)	23.0 (12)	57.4 (08)
5	Coquimbite	Cq	$Fe(SO_4)_3 \cdot 9H_2O$		10.7 (100)	32.2 (76)	16.3 (64)	26.5 (62)	19.3 (44)	24.4 (42)	9.4 (40)	25.4 (34)
6	Corundum	Cr	Al_2O_3		43.4 (100)	35.1 (90)	57.5 (80)	25.6 (75)	68.2 (50)	52.5 (45)	37.8 (40)	66.5 (30)
7	Dolomite	D	$CaMg(CO_3)_2$		31.0 (100)	51.1 (30)	51.25 (30)	41.1 (30)	50.6 (20)	67.4 (15)	45.0 (15)	37.4 (10)
8	Gehlenite	G	$2CaO \cdot SiO_2 \cdot Al_2O_3$		31.4 (100)	52.1 (35)	37.4 (25)	24.2 (20)	36.9 (20)	44.3 (16)	60.9 (16)	39.3 (14)
9	Hematite	H	Fe_2O_3		33.3 (100)	54.4 (60)	35.7 (50)	49.6 (40)	62.5 (35)	64.1 (35)	41.0 (30)	24.3 (25)

[*Relative intensities are in the parenthesis]

Table 7.3 (Cont.)

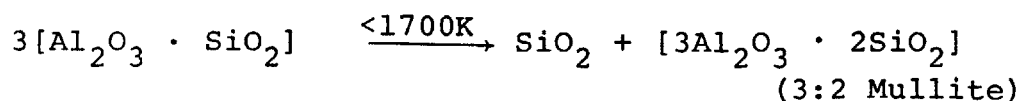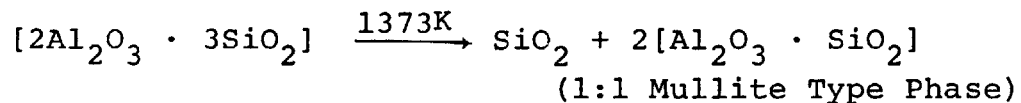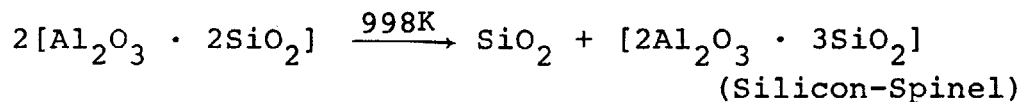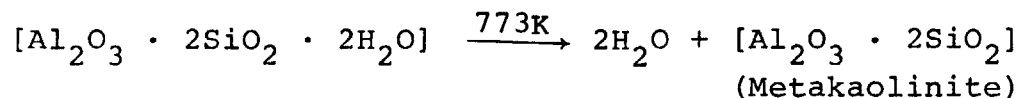|	MINERAL	SYMBOL	FORMULA	2θ (degrees) FOR EIGHT MOST INTENSE PEAK							
10	Illite	I	$K_{1-1.5}Al_{5-5.5}Si_{5.5-7}O_{20}(OH)_4$	19.9 (100)*	26.5 (100)	35.9 (100)	8.9 (80)	61.8 (80)	18.1 (60)	22.9 (60)	31.3 (60)
11	Kaolinite	K	$Al_2Si_2O_5(OH)_4$	24.9 (100)	12.3 (100)	62.4 (100)	38.4 (90)	19.8 (80)	35.0 (80)	35.9 (80)	37.7 (80)
12	Lawsonite	L	$CaAl_2SiO_4 \cdot 2H_2O$	32.9 (100)	34.2 (70)	42.5 (70)	24.4 (60)	21.3 (50)	34.1 (50)	18.2 (40)	33.6 (40)
13	Lime	Li	CaO	37.4 (100)	33.1 (45)	32.2 (34)	64.1 (10)	91.5 (09)	103.3 (09)	147.7 (06)	67.3 (05)
14	Magnesia	Mg	MgO	42.9 (100)	62.3 (52)	109.7 (17)	127.2 (15)	78.6 (12)	36.9 (10)	94.0 (05)	74.2 (04)
15	Mullite	M	$3Al_2O_3 \cdot 2SiO_2$	26.3 (100)	26.0 (95)	40.8 (60)					
16	Pyrite	P	FeS_2	56.3 (100)	33.0 (84)	37.1 (66)	40.8 (52)	47.4 (40)	28.5 (36)	95.2 (27)	64.4 (24)
17	Quartz	Q	SiO_2	26.0 (100)	49.2 (90)	58.8 (80)	65.7 (80)	67.1 (80)	40.6 (60)	44.1 (60)	73.2 (60)
18	α-Quartz	Q	SiO_2	26.7 (100)	20.8 (35)	50.2 (17)	60.0 (15)	36.5 (12)	39.5 (12)	68.1 (11)	68.3 (09)
19	β-Quartz	Q	SiO_2	26.2 (100)	20.5 (20)	49.6 (10)	41.6 (04)	45.1 (04)	58.9 (04)		
20	Rutile	R	TiO_2	27.4 (100)	54.2 (50)	36.0 (41)					

[*Relative intensities are in the parenthesis]

It should be emphasized here that the phases formed are not only the function of maximum temperature reached but can be the function of the rate of heating and/or cooling. If a slag is melted at high temperature and is then cooled slowly, a temperature will be reached at which crystals begin to separate from the melt. The liquid temperature of the system defines the maximum temperature at which the liquid and solid phases can coexist. If the slag is cooled further, more crystals will separate and will increase in amount on further cooling until the whole slag becomes solid at the solidus temperature. The formation of the complex phases will be dependent on the rate of cooling and separation may occur. For example, quartz may react with $CaSO_4$ and kaolinite to form Gehlenite or Anorthite type phases but on rapid cooling may separate out again. The best way to get the right phases at high temperatures in situ is to perform X-ray diffraction on particles at high temperatures. This is not possible in case of free fall experiments due to short residence times. The effect of cooling and heating rates can be determined by performing experiments at different cooling and heating rates. The results presented here do not take into account any of such effects and should be looked at with these qualifications.

7.4.1 <u>Kaolinite</u> $[Al_2Si_2O_5(OH)_4]$:

Kaolinite existed in both bituminous coal and lignite. In case of bituminous coal, kaolinite seems to be the major source of silica and alumina, but in lignite low temperature ash other silica, alumina containing phase Lawsonite $[CaAl_2SiO_4 2H_2]$ was also found. Thermal decomposition of kaolinite has been studied in great detail in past because of its importance in the ceramic industries, and there is a general agreement between authors on the experimental observations on the decomposition of kaolinite. The generally agreed decomposition scheme of kaolinite is its initial transformation to matakaolinite $[Al_2O_3 \cdot 2SiO_2]$, then to silicon spinel $[2Al_2O_3 \cdot 3SiO_2]$, and finally to mullite $[3Al_2O_3 \cdot 2SiO_2]$. The whole series of reactions is as follows:
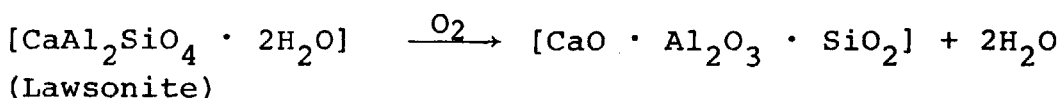
kaolinite

$$[Al_2O_3 \cdot 2SiO_2 \cdot 2H_2O] \xrightarrow{773K} 2H_2O + [Al_2O_3 \cdot 2SiO_2]$$
(Metakaolinite)

$$2[Al_2O_3 \cdot 2SiO_2] \xrightarrow{998K} SiO_2 + [2Al_2O_3 \cdot 3SiO_2]$$
(Silicon-Spinel)

$$[2Al_2O_3 \cdot 3SiO_2] \xrightarrow{1373K} SiO_2 + 2[Al_2O_3 \cdot SiO_2]$$
(1:1 Mullite Type Phase)

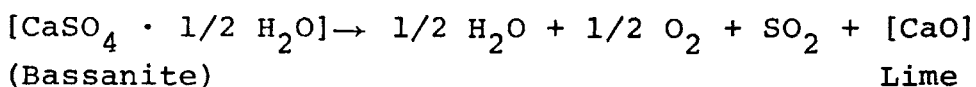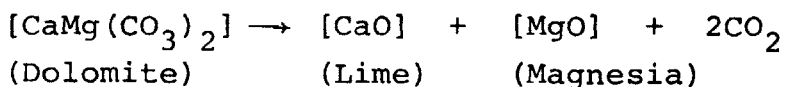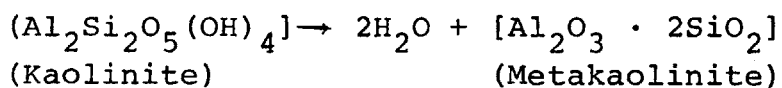$$3[Al_2O_3 \cdot SiO_2] \xrightarrow{<1700K} SiO_2 + [3Al_2O_3 \cdot 2SiO_2]$$
(3:2 Mullite)

Formation of curundum $[Al_2O_3]$ has also been reported from metakaolinite.

The x-ray diffraction results obtained for bituminous coal in this study are consistent with the previous findings. Stable 3:2 mullite phase persisted above ASTM (1023K) temperature. The coal particle temperature was about 1300K where the furnace temperature was (1000K) and so the temperature of minerals associated with it. Corundum $[Al_2O_3]$ also appeared above 1500K furnace temperatures. The transformation temperatures reported in literature are in general agreement.

In case of lignite, entirely different behavior was observed. Expected mullite or corundum phases were not observed, instead two mixed phases of silica-aluminates with calcium oxides, gehlenite $[2CaO \cdot SiO_2 \cdot Al_2O_3]$ and anorthite $[CaO \cdot 2SiO_2 \cdot Al_2O_3]$ were found. These phases were the results of interaction between more than one original phase present in lignite. The interacting phases could have been kaolinite, dolomite, lawsonite, and bassanite. The reaction scheme producing the high temperature phases gehlenite and anorthite can be represented as follows:

$$[Al_2Si_2O_5(OH)_4] \rightarrow 2H_2O + [Al_2O_3 \cdot 2SiO_2]$$
(Kaolinite)   (Metakaolinite)

$$[CaMg(CO_3)_2] \rightarrow [CaO] + [MgO] + 2CO_2$$
(Dolomite)   (Lime)   (Magnesia)

$$[CaSO_4 \cdot 1/2 \, H_2O] \rightarrow 1/2 \, H_2O + 1/2 \, O_2 + SO_2 + [CaO]$$
(Bassanite)   Lime

$$[CaAl_2SiO_4 \cdot 2H_2O] \xrightarrow{O_2} [CaO \cdot Al_2O_3 \cdot SiO_2] + 2H_2O$$
(Lawsonite)

$$[Al_2O_3 \cdot 2SiO_2] + 2[CaO] \longrightarrow \underset{\text{(Gehlenite)}}{[2CaO \cdot SiO_2 \cdot Al_2O_3]} + SiO_2$$

$$[Al_2O_3 \cdot 2SiO_2] + [CaO] \longrightarrow \underset{\text{(Anorthite)}}{[CaO \cdot 2SiO_2 \cdot Al_2O_3]}$$

$$[CaO \cdot Al_2O_3 \cdot SiO_2] + SiO_2 \longrightarrow \underset{\text{(Anorthite)}}{[CaO \cdot 2SiO_2 \cdot Al_2O_3]}$$

$$\underset{\text{(Anorthite)}}{[CaO \cdot 2SiO_2 \cdot Al_2O_3]} + [CaO] \longrightarrow \underset{\text{(Gehlenite)}}{[2CaO \cdot SiO_2 \cdot Al_2O_3]} + SiO_2$$

Gehlenite and anorthite both were found up to 1500K but at higher temperature (1830K furnace temperatures), anorthite reacts with lime to produce gehlenite and silica.

7.4.2 **Illite** $[K_{1-1.5} Al_{5-5.6} Si_{6.5-7} O_{20} (OH)_4]$

Illite, a major clay mineral found in most coals, was identified in bituminous coal but did not exist in lignite. Formation of mullite in case of bituminous coal ash can also be explained starting from illite. The sequence of reactions forming mullite proceeds as follows:

$$\text{Illite} \xrightarrow[600-900K]{} \underset{H_2O}{\text{Illite}+} \xrightarrow[1123-1173K]{} \text{Destruction of Illite Structure}$$

$$\underset{\text{Mullite}}{[3Al_2O_3 \cdot 2SiO_2]} \xleftarrow[<1400K]{} \underset{\text{Spinel Phase}}{[2Al_2O_3 \cdot 3SiO_2]} \xleftarrow[T<1173K]{}$$

A glass-phase may also result by interaction with small amounts of Ca and Mg. The presence of glass phase or amorphous phase was indicated by the diffused pattern and broad maxima in the x-ray diffraction patterns for temperatures above 1500K.

7.4.3 <u>Quartz</u> [SiO_2]:

Quartz was found in both bituminous coal and lignite. Although quartz was relatively stable up to 1830K temperatures, it diminished in quantity considerably above 1500K. This could be due to its consumption in the formation of other phases at high temperatures.

7.4.4 <u>Pyrites</u>:

Bituminous coal ash contained a fair amount of pyrites, about one third of the total ash. Pyrite is the main constituent in most of the coals contributing for the presence of Fe. Lignite ash although shows small amount of Fe on elemental analyses and did not show clear peaks of pyrites in its x-ray diffraction patterns.

The stable phase above 1000K originated from pyrite was hematite (Fe_2O_3) by the liberation of sulfur from the pyrite by heating it in air - the so-called roasting process.

$$FeS_2 + 11/4\ O_2 \longrightarrow 1/2\ Fe_2O_3 + 2SO_2 \qquad (1)$$
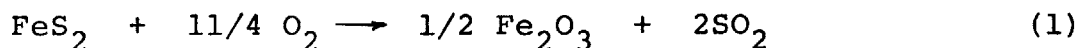
In excess air, the reaction can also proceed as follows (Schwab and Philinis, 1947):

$$FeS_2 + 7/2\ O_2 \longrightarrow 1/2\ Fe_2(SO_4)_3 + 1/2\ SO_2 \qquad (2)$$
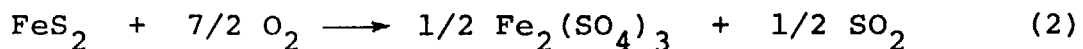
Schwab found that oxidation proceeded mainly by equation (1) and that products formed were largely Fe_2O_3 with small amount of $Fe_2(SO_4)_3$ -12% at 400°C - decreasing with increase in temperature. At temperatures above 1000K, the stable product is only Fe_2O_3.

In inert atmosphere, decomposition of pyrite at 325°C forming FeS_{1-x}, (x=0.1-0.3) and further decomposition at 700°C to FeS (pyrrhotite) has been also reported in literature (O'Corman and Walker, 1973). It has been found that pyrrhotite (FeS) in oxidizing atmosphere forms sulfate at temperatures in the range 230-550°C but above 550°C it reacts further to form oxide. In case of coal combustion, initially pyrite particles may undergo a reducing or inert atmosphere due to the diffusion of oxygen to the inner depth of coal but at complete combustion, the ultimate product is the iron oxides. It is possible to have FeO, Fe_3O_4, and Fe_2O_3 all present at higher temperatures according to the oxidizing potential of the atmosphere. The overall mechanism of the formation of hematite can be written as follows:

$$[FeS_2] \xrightarrow{\text{excess } O_2} Fe_2(SO_4)_3 \longrightarrow [Fe_2O_3]$$

$$[FeS_2] \text{(Pyrite)} \xrightarrow{\text{oxidizing}} [Fe_2O_3] \text{ Hematite}$$

$$[FeS_2] \xrightarrow{\text{reducing or inert}} [FeS] \text{(Pyrrhotite)} \longrightarrow [FeSO_4] \longrightarrow [Fe_2O_3]$$
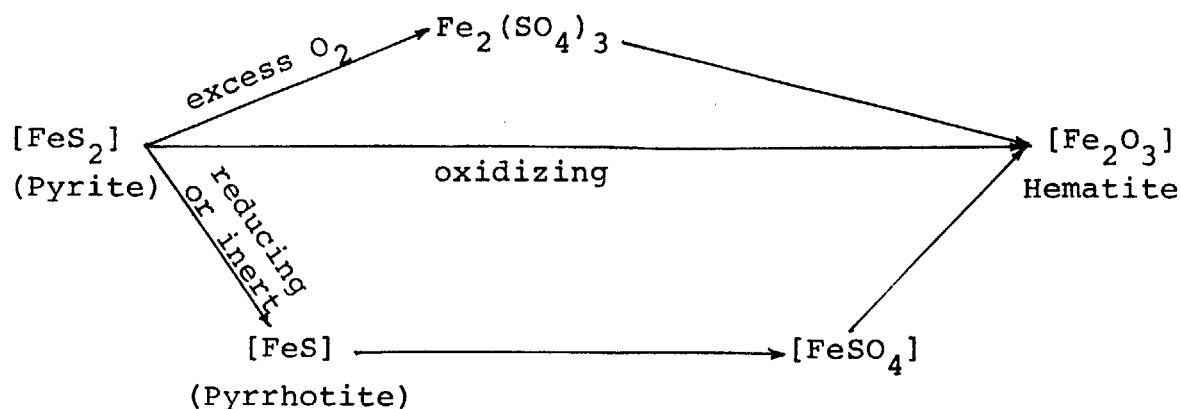
7.4.5 <u>Carbonates</u>:

The principle carbonates found in the low temperature ash were dolomite [$CaCO_3 \cdot Mg\ CO_3$] and calcite [$CaCO_3$]. Mg mainly existed as dolomite in lignite ash. The high temperature phases resulting from dolomite are oxides of calcium and magnesium and from calcite oxide of calcium.

The carbonates on heating decompose according to the equation:

$$RCO_3 \rightarrow RO + CO_2$$
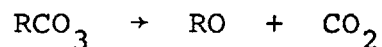
The oxides CaO and MgO produced by decomposition of $CaCO_3$ and $MgCO_3$ are stable and undergo no further change. Initial decomposition temperature of 810-920°C have been reported for calcite (Murray and Fischer, 1951).

Decomposition rates of $CaCO_3$ are investigated by several authors. According to Furnas (1931), the decomposition of limestone [$CaCO_3$] begins at the outer surface of the particle and then travels inwards at a constant rate given by the expression:

$$R = 18.9 \times 10^{-5}\ \exp\ [0.00724T]$$

where:

R = rate of advance of interface in μm/sec

T = temperature in °K

The time required to decompose a 2 μm diameter $CaCO_3$ particle at 1000°C will be about 0.5 second. At 1830K the decomposition time for the similar particle will be only 9 msec.

More recent data calcination of limestones are obtained
by Battelle (1970) and TVA Fundamental Research Branch
(reported in Kellogg's Report (1972)). Battelle data ob-
tained over the temperature range 1147°K to 1404°K for
particle sizes ranging from 105μm to 44μm, gave an activation
energy of about 24 Kcal/g mole for decomposition. TVA data
gave an activation energy of about 30 Kcal/gmole and on this
basis, the times required for 75% calcination for different
particle sizes and gas temperature are presented in Table 7.4.

The decomposition time for 75% calcination is of the
order of a few milliseconds for 57μm particle. For a
2μm $CaCO_3$ particle the time required would be much smaller
than this. But the overall time would be controlled by
heat transfer. A 100μm coal particle would require about
4 msec to heat up to 1800°K gas temperature (Appendix A)
and therefore this would be the minimum time required for
the decomposition of $CaCO_3$.

TABLE 7.4

Time Required for 75% Calcination (TVA, 1969)

Activation Energy = 30 Kcal/gmole

Temperature (°K)	Time (seconds)				
	1273	1373	1473	1573	1830
Particle Size (μm)					
161	0.41	0.17	0.081	0.042	0.011
99	0.24	0.10	0.049	0.025	0.006
57	0.14	0.061	0.029	0.015	0.004

In case of the free fall experiments, the residence time was of the order of 1 second and the mean size of carbonate particles is about 2 μm (Chapter 5). Therefore, complete decomposition of $CaCO_3$ is possible above 1250K in less than 1 second residence time. The observations were consistent with these calculations.

Decomposition of dolomite has also been studied extensively. The decomposition temperatures of $MgCO_3$ are lower than those of $CaCO_3$; therefore, decomposition of dolomite may proceed in two steps:

$$CaMg(CO_3)_2 \rightarrow MgO + CO_2 + CaCO_3 \rightarrow MgO + CaO + 2CO_2$$
$$600°C \qquad\qquad\qquad 850°C$$
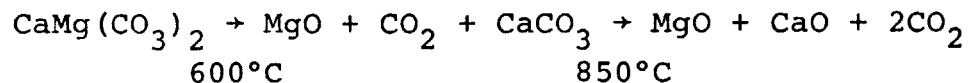
7.4.6 Sulfates:

Calcium sulfate is the main specie found in lignite ash responsible for the presence of large amount of calcium. Low temperature ash of lignite contained calcium sulfate in the form of bassanite [$CaSO_4 \cdot 1/2\ H_2O$] which may be derived from original gypsum [$CaSO_4 \cdot 2H_2O$] and bituminous low temperature ash contained small amount of anhydrite [$CaSO_4$]. Coquimbite [$Fe_2(SO_4)_3 \cdot 9H_2O$] was also found in bituminous ash which could have been derived by oxidation of pyrites (Section 7.4.4). The high temperatures stable phases were CaO and Fe_2O_3 resulting due to decomposition of sulfates. $CaSO_4$ continuously diminished above 1250K as can be seen by diffraction patterns of lignite ash.

CaSO$_4$ may decompose to form CaO or interact with some other component to form glassy phase:

$$CaSO_4 \rightarrow CaO + SO_3$$

$$CaSO_4 + SiO_2 \rightarrow CaSiO_3 + SO_3$$
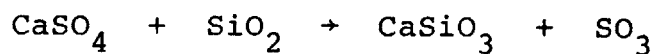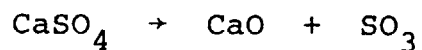
CaSO$_4$ may be responsible for the formation of gehlenite and amorthite phases, as were found in lignite ash at 1500K and above. The reactions can be written as follows:

$$[Al_2O_3 \cdot 2SiO_2] + 2[CaSO_4] \rightarrow [2CaO \cdot SiO_2 \cdot Al_2O_3] + SiO_2 + 2SO_3$$
$\quad$ Metakaolinite $\qquad$ Anhydrite $\qquad\qquad$ Gehlenite

$$[Al_2O_3 \cdot 2SiO_2] + [CaSO_4] \rightarrow [CaO \cdot 2SiO_2 \cdot Al_2O_3] + SO_3$$
$\qquad\qquad\qquad\qquad\qquad\qquad\qquad$ Anorthite
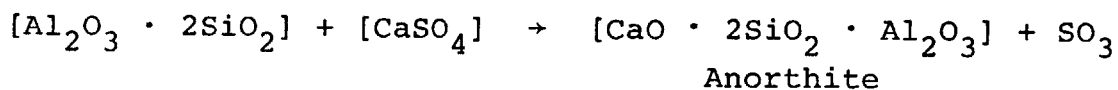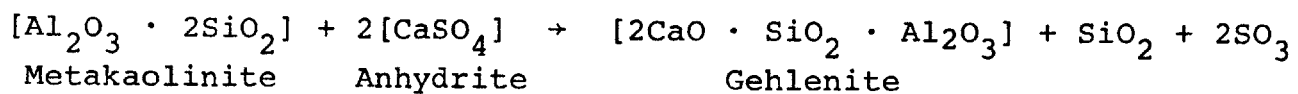
The decomposition of coquimbite [Fe$_2$(SO$_4$)$_3$ 9H$_2$O] may proceed in two steps as follows:

$$[Fe_2(SO_4)_3\ 9H_2O] \rightarrow Fe_2(SO_4)_3 + 9H_2O \rightarrow Fe_2O_3 + 3SO_3 + 9H_2O$$
$\quad$ Coquimbite
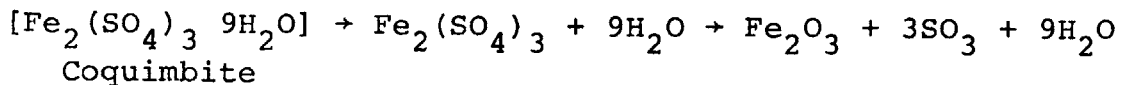
7.5 General Comments:

The mineral phases present during coal combustion at combustion temperatures can be explained starting from the original phases present in the coal. The phases undergo thermal decomposition, interaction with coal and interaction with each other during combustion. The interaction of phases together to form a new phase crystalline or amorphous is also evidenced by the ash particle size distribution study at high temperatures (Chapter 6). It was found that

the finely distributed minerals agglomerate internally during combustion and results in the formation of bigger agglomerates. The agglomerated phase may be crystalline or glassy, evidence of which is provided by the diffused structure of diffraction patterns and presence of broad maxima in diffraction patterns above 1830°K.

The minerals present in bituminous and lignite differ considerably and therefore the phases present at the complete combustion are also markedly different.

The phase present could also be influenced by the rate of heating and cooling of coal particles. The phases examined here may not present the true phases existing at high temperatures, as they may be the results of some recrystallization during rapid cooling.

CHAPTER 8

BEHAVIOR OF ASH AT HIGH TEMPERATURES

III. Weight Loss of Ash

8.1 Introduction

During the combustion of coal, the minerals associated
with it undergo thermal decomposition, interaction with organic
matter in coal and interaction with each other. The chemical
changes in the phases (Chapter 7) are also accompanied by
changes in the weight of the ash produced. The weight loss in
ash may also be contributed by partial or complete volatiliza-
tion of some components mainly the low vapor pressure alkali
compounds, sulfur released mainly in the form of its oxides
and silica. At MHD temperatures partial or complete vaporiza-
tion of low vapor pressure ash species like Al_2O_3, CaO, MgO etc
is also possible as is explained by the characteristic vaporiza-
tion time scale in Section 6.6.b.

Volatilization of alkali compounds has been studied in
great detail by several investigators because of its importance
in the formation of boiler deposits. No attempts were made in
the present study, towards the volatilization of alkali com-
pounds.

Ash losses of about 25% by weight of ASTM ash for lignite
and about 6% for bituminous were observed at 1830°K in oxidizing
atmosphere. Examination of X-ray diffraction patterns (Chapter 7)

showed the presence of a fair quantity of $CaSO_4$ in ASTM ash and continuous transformation of $CaSO_4$ to CaO at higher temperatures.

Another component of coal ash that can apparently volatilize under combustion conditions to an extent is silica, present in coal either as quartz or as silicates. The vapor pressure of SiO_2, itself, although appreciable, particularly at temperatures above 2000°C, is not large enough at the usual combustion temperatures. But silica may volatilize as the more volatile monoxide SiO formed by reduction of silica. The evidence for the existence of SiO at combustion temperatures has been shown by many investigators, [Zapffe (1944), Shick (1960), Kay and Taylor (1963), Raask and Wilkins (1965)].

The purpose of this chapter is first to evaluate the extent of $CaSO_4$ decomposition under simulated combustor conditions and second to show from thermodynamic data the extent and the mechanism of silica vaporization, and finally to examine the effect of combustion conditions on the weight loss of ash produced.

8.2 Experimental

Four types of experiments were performed.

a. Free Fall - The description of the experimental conditions for free fall runs in oxidizing atmosphere is given in Chapter 6 (Table 6.1). The total weight loss of ash was determined gravimetrically and the amounts of individual oxides

present in each sample were determined by atomic absorption spectrometry. The analysis was performed for five major oxides CaO, MgO, SiO_2, Al_2O_3 and Fe_2O_3. The amounts of sulfate and minor oxides were determined by assuming that CaO did not vaporize and could be used as tracer. Some samples were also sent to outside laboratories (M.I.T. Chemical Lab, Galbraith Labs., Tennessee) for the analysis of sulfates and other oxides to provide double checks on the analysis.

b. Crucible - For the same temperature conditions as for free fall, samples of coals and ASTM ash in alumina crucibles were heated in the furnace for 1 hour. Chemical analyses similar to those in the free fall experiments were performed.

c. Silica Vaporization Runs - In order to investigate the possible reactions between silica and carbon, a series of experiments were carried out in which mixtures of finely ground silica and excess carbon contained in a graphite crucible, were heated in argon atmosphere. The highest temperature attainable in the furnace was 2250°K. The samples were removed after known residence times and weighed. The samples along with graphite crucibles were also ashed in the conventional ashing furnace (750°C) to determine the weight loss of silica during experimentation. Samples before and after ashing were also analysed by x-ray diffraction in order to examine any changes in the form of silica.

d. Crucible Experiments up to 2250°K - Ash loss experiments were performed up to 2250°K in argon atmosphere starting from ASTM ash in graphite crucibles. Ash losses were also estimated during crucible devolatilization runs up to 2250°K in inert atmosphere followed by ASTM ashing of the devolatilized samples (Kobayashi, 1976).

8.3 Weight Loss of Ash in Oxidizing Atmosphere: up to 1830°K

8.3.1 Results

Figures 8.1 and 8.2 show the loss of ASTM ash as a function of temperature for crucible and free-fall runs. Lignite ash lost as much as 25% and bituminous about 6% at 1830"K temperature. The weight losses approached an asymptotic value at about 1500°K. Figures 8.3 and 8.4 show the weight losses of SiO_2, total major oxides, and SO_3+minor oxides as determined by atomic absorption analysis of the samples. The total weight loss measured and computed from individual oxides analysis are also plotted. The shaded area is the discrepancy in the data and can be attributed to errors in oxide analysis and possible variations in the ash content of different samples. These results are presented only for lignite ash. High temperature bituminous ash could not be completely dissolved and so atomic absorption was not accurate enough to draw firm conclusions.

Crucible Experiments (τ = 1 hour)
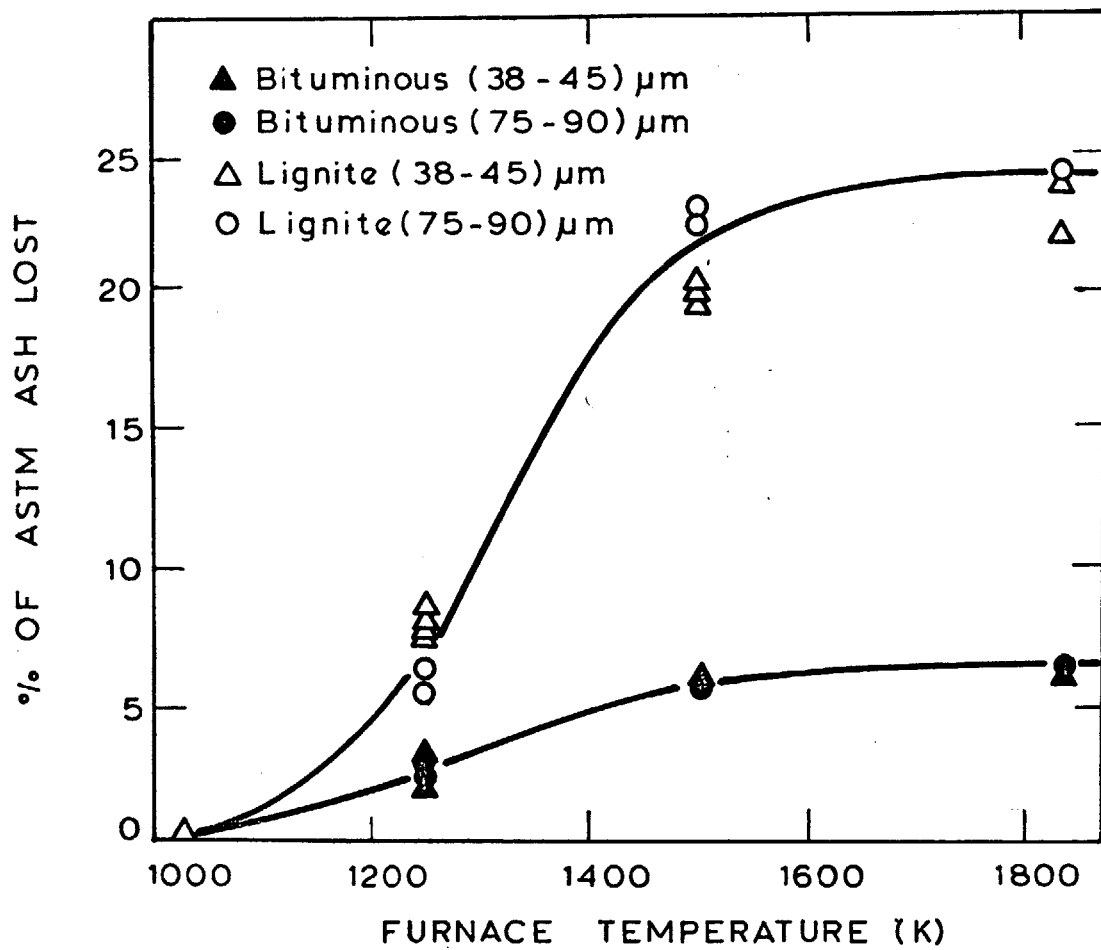
Fig 8.1 Weight Loss of ASTM Ash in Crucible
Experiments
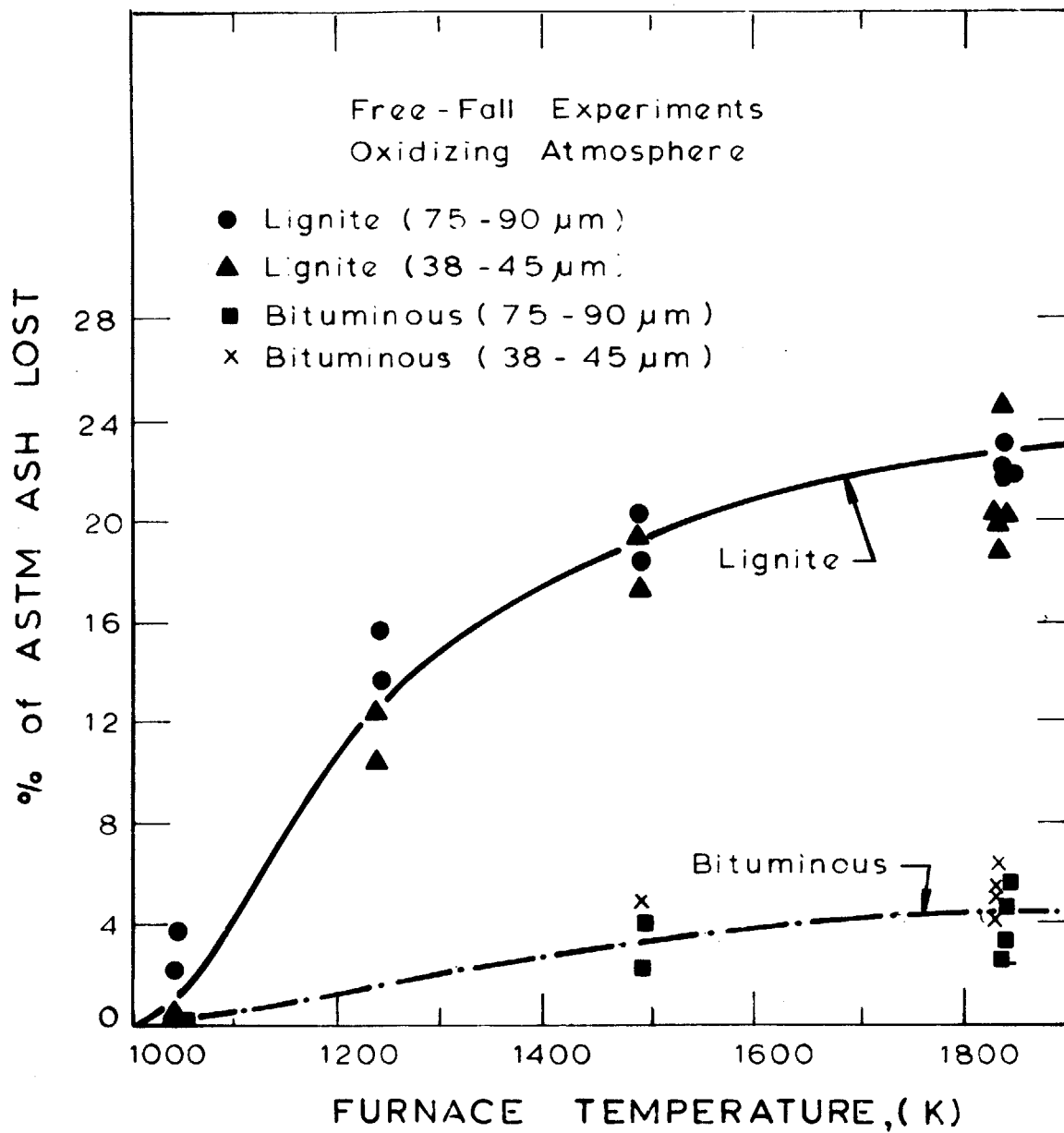
Effect of Furnace Temperature on Ash
Loss in Free-Fall Mode

Figure 8.2
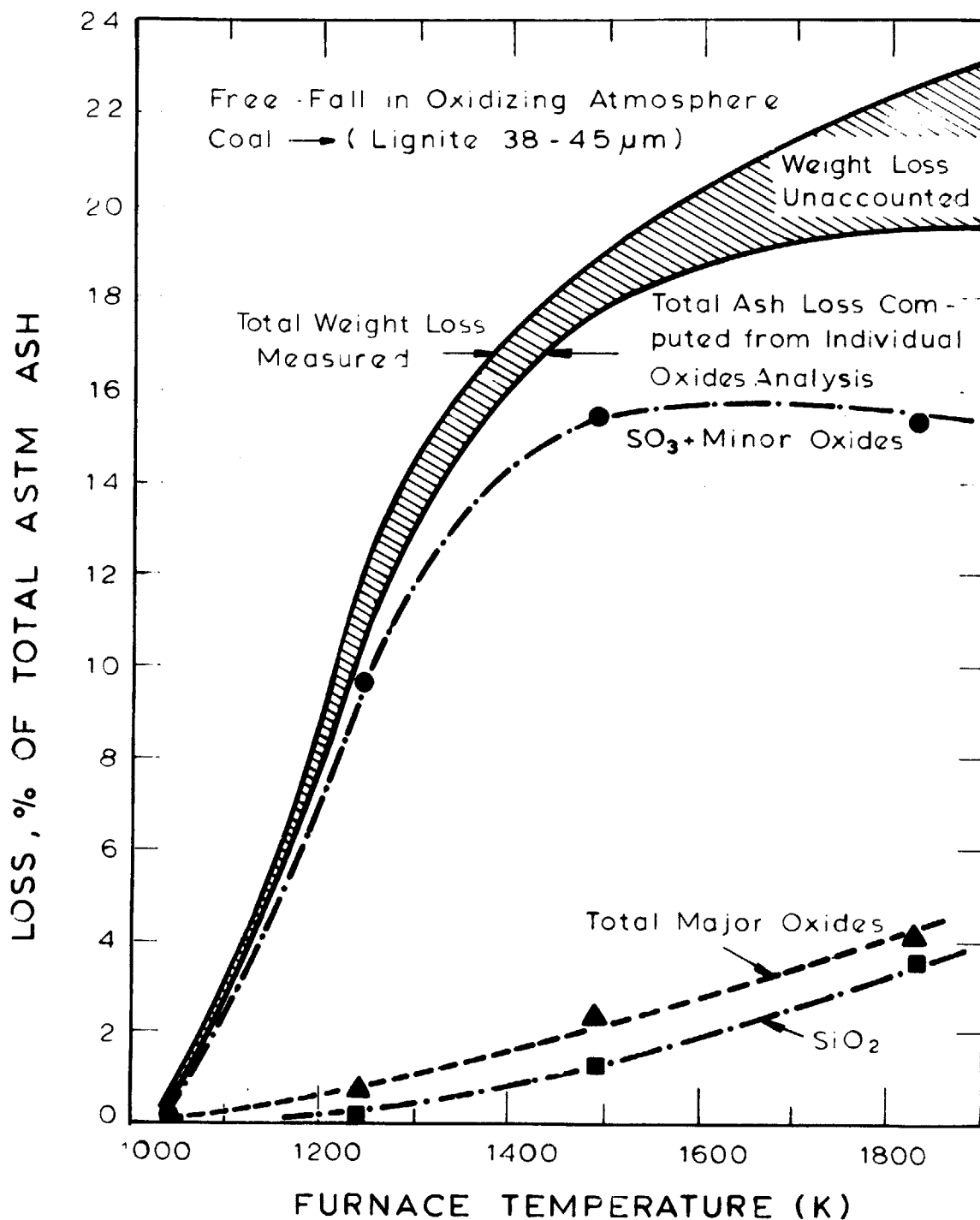
Figure 8.3 Loss of Individual ash species upto 1830 K
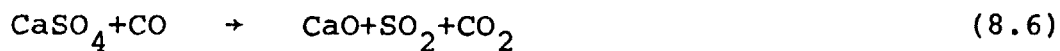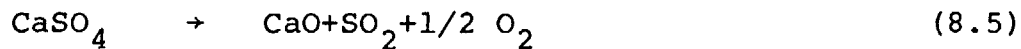in Oxidizing Atmosphere for (38-45) micron
Lignite
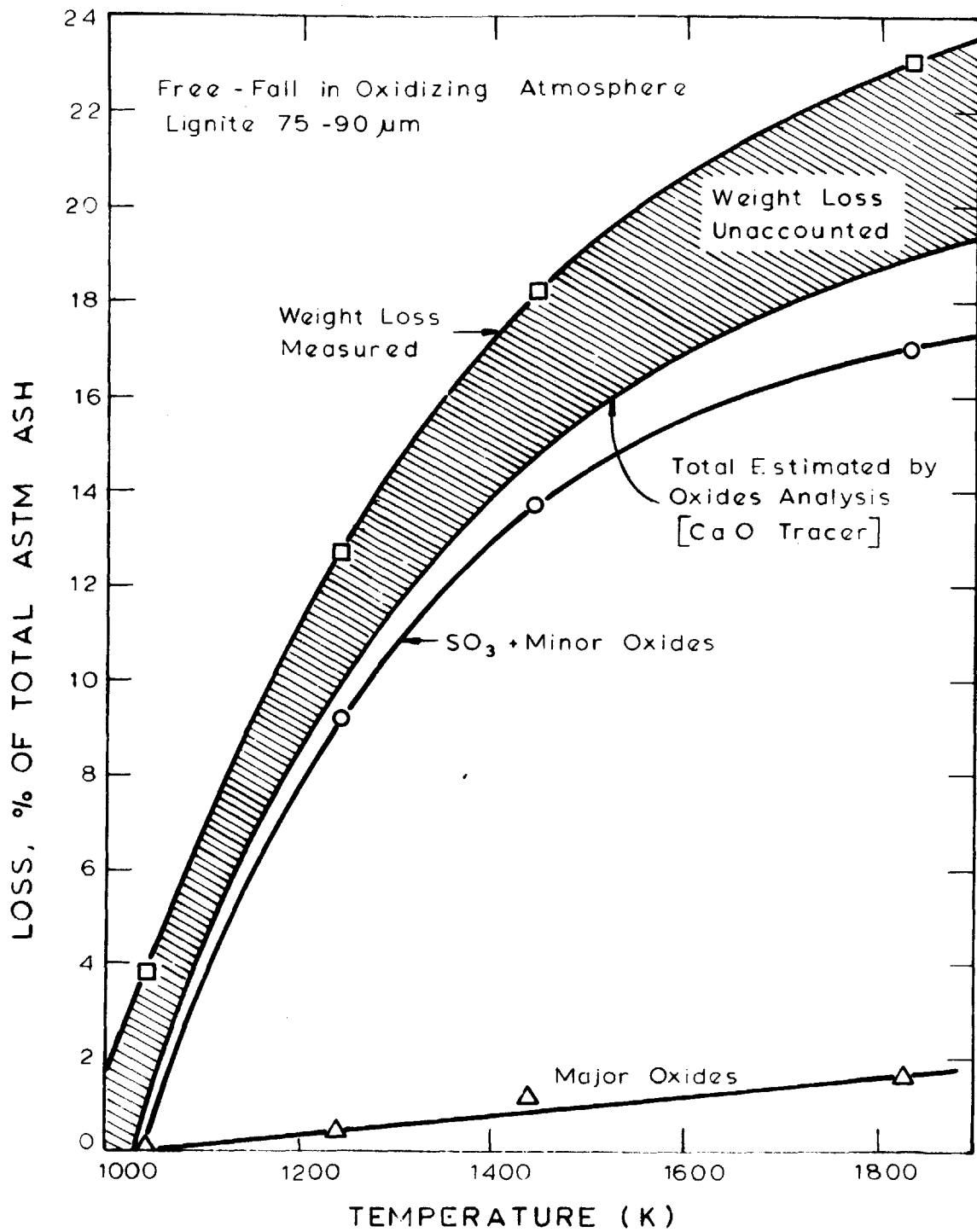
Figure 8.4 Loss of Individual ash species upto 1830 K in Oxidizing Atmosphere for Lignite.
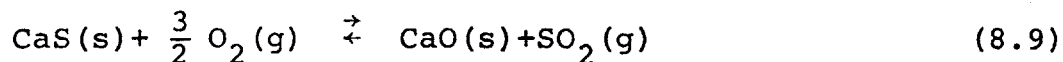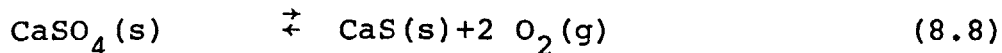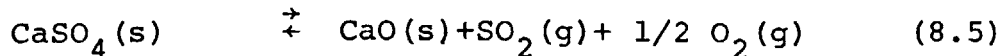
8.3.2 Discussion of Results

The main weight loss is due to the thermal decomposition of $CaSO_4$ initially present in coal as bassanite [$CaSO_4 \cdot 1/2\ H_2O$] or formed during ashing procedure from dolomite or $CaCO_3$. Some governing reactions can be written as follows:

$$CaCO_3 \rightarrow CaO+CO_2 \tag{8.1}$$

$$CaMg(CO_3)_2 \rightarrow MgO+CaO+2CO_2 \tag{8.2}$$

$$2FeS_2 + \frac{11}{2}\ O_2 \rightarrow Fe_2O_3+4SO_2 \tag{8.3}$$

$$CaO+SO_2+ \frac{1}{2}O_2 \rightarrow CaSO_4 \tag{8.4}$$
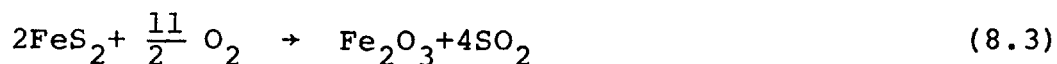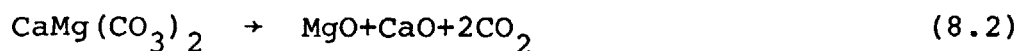
At higher temperature $CaSO_4$ decomposes probably due to following reactions:

$$CaSO_4 \rightarrow CaO+SO_2+1/2\ O_2 \tag{8.5}$$

$$CaSO_4+CO \rightarrow CaO+SO_2+CO_2 \tag{8.6}$$

$$CaSO_4+4CO \rightarrow CaS+4CO_2 \tag{8.7}$$

Three phases of calcium $CaSO_4$, CaS and CaO can be present at equilibrium depending on the partial pressure of O_2, SO_2 or CO_2 and CO. An equilibrium phase diagram with $CaSO_4$, CaO and CaS as the solid phases and O_2 and SO_2 as the gaseous species can be constructed by considering the following reactions:

$$CaSO_4(s) \quad \overset{\rightarrow}{\leftarrow} \quad CaO(s) + SO_2(g) + 1/2 \ O_2(g) \qquad (8.5)$$

$$CaSO_4(s) \quad \overset{\rightarrow}{\leftarrow} \quad CaS(s) + 2 \ O_2(g) \qquad (8.8)$$

$$CaS(s) + \frac{3}{2} \ O_2(g) \quad \overset{\rightarrow}{\leftarrow} \quad CaO(s) + SO_2(g) \qquad (8.9)$$

Only two of these three equilibrium reactions are independent, but all three are presented here in order to define the phase boundaries of the existence of any two solid phases. The free energy of formation for these reactions is obtained from various sources and the values along with the references are listed in Table 8.1. The phase diagram as constructed from these values at 1000, 1250, 1500, 1750 and 2000°K temperatures is shown in Figure 8.5. Also shown are locations for bituminous and lignite ash, assuming all sulfur from coal converts to SO_2 and partial pressure of O_2 to be 0.11 atmosphere (corresponding to $\phi=0.5$). It is apparent from the phase diagram, that due to the low partial pressure of SO_2, formation of CaS is not probable unless combustion is carried out in inert or reducing atmosphere. 1500°K seems to be about the temperature, above which CaO and below which $CaSO_4$ is favored thermodynamically.

The results of figure 8.1, 8.3 and 8.4 are plotted in figure 8.6 as % $CaSO_4$ decomposed as a function of temperature for lignite ashes. Free fall results are replotted on the basis of measured particle temperatures. The equilibrium values corresponding to $\phi = 0.5$ and $CaSO_4 = 3.1\%$ by weight of coal (Lignite) provide reasonable agreement with the

TABLE 8.1

FREE ENERGY OF FORMATION FOR $CaSO_4$ DECOMPOSITION REACTIONS

Number	Reaction	$\Delta G°$ (Kcal/gmole)	References
8.5	$CaSO_4(s) \rightleftharpoons CaO(s)+SO_2(g)+1/2\ O_2(g)$	110,320-56.80T	1, 2
8.8	$CaSO_4(s) \rightleftharpoons CaS(s) + 2O_2(g)$	218,510-74.88T	3, 4, 5
8.9	$CaS(s)+ \frac{3}{2}O_2(g) \rightleftharpoons CaO(s)+SO_2(g)$	-108,190+18.08T	

T = Temperature in °K

1. Zawadzki (1932)

2. Dewing and Richardson (1959)

3. Kelley (1937)

4. JANAF Tables (1965)

5. Wriedt and Darken (1972)
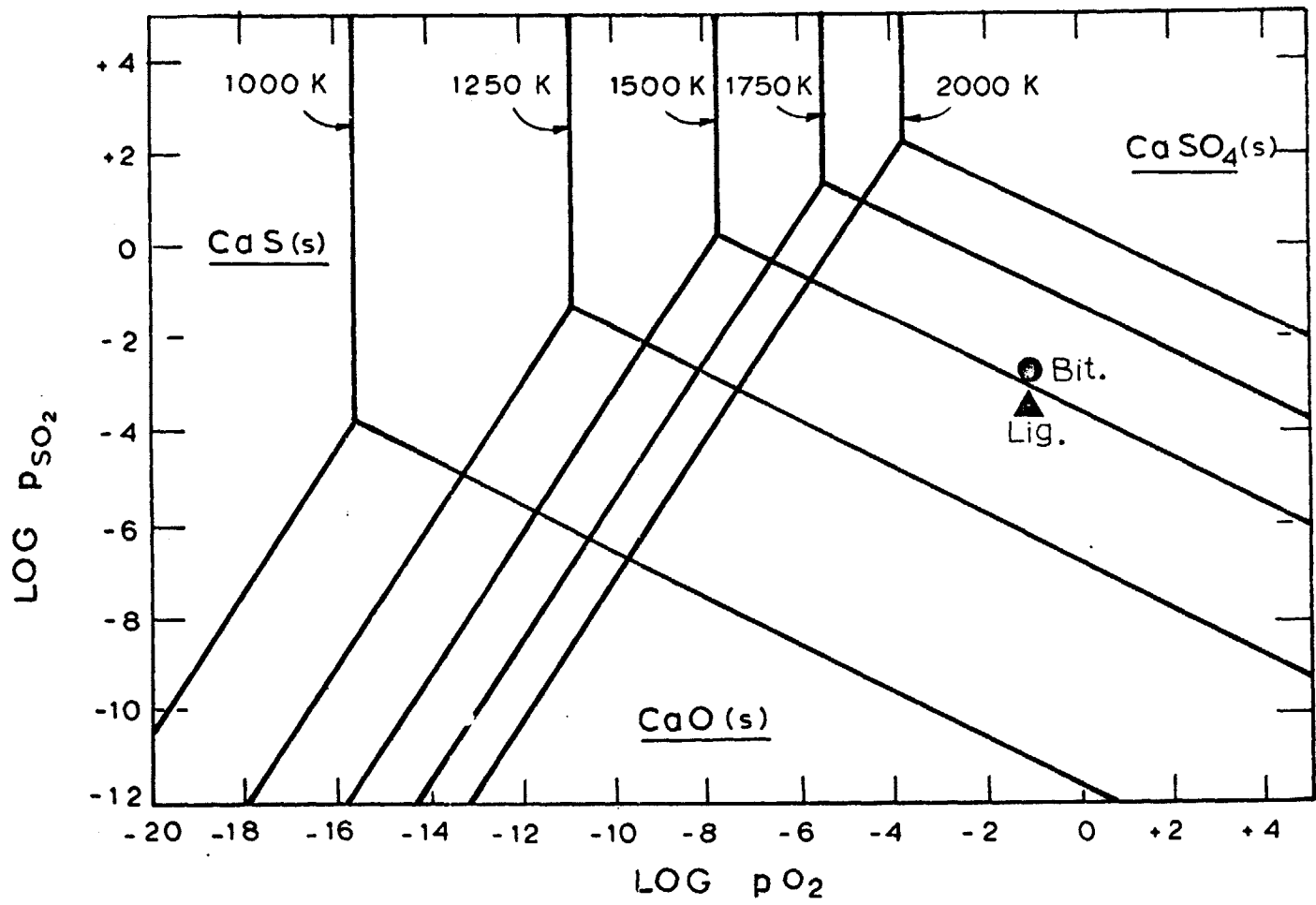
Fig. 8.5 Phase Diagram of $CaSO_4$, CaS and CaO at 1 Atm Total Pressure
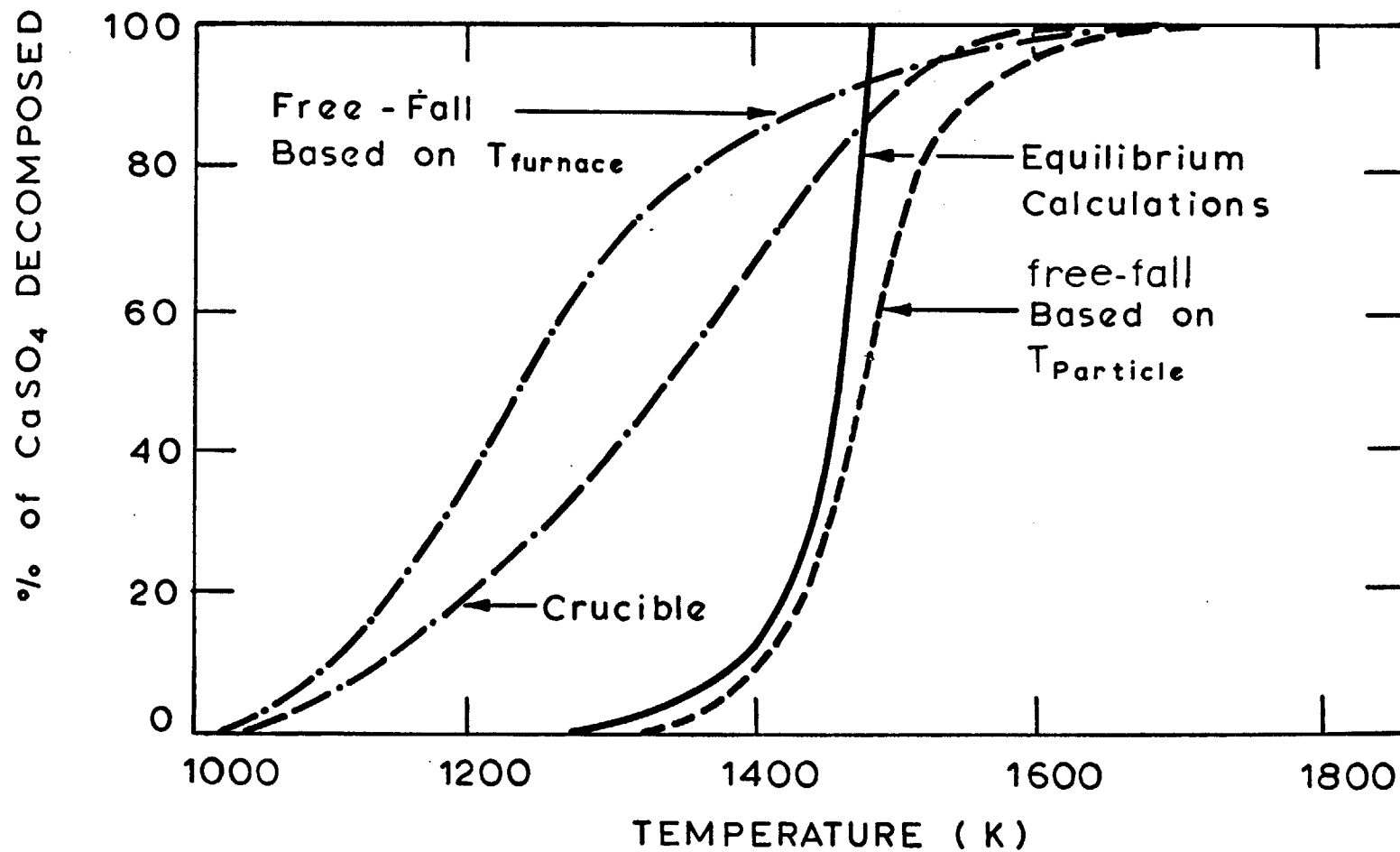
CaSO₄ Decomposition as a Function of Temperature for Lignite

Figure 8.6

measured value in free-fall experiments. Crucible experiments gave higher values of $CaSO_4$ decomposition. It is difficult to define the crucible experiments because SO_2 formed during decomposition will diffuse away from the reaction front resulting in additional decomposition; the equilibrium decomposition will depend on the local SO_2 concentration which is unknown. Also it is difficult to define the stoichiometry as the partial pressure of O_2 may be very different on the surface of the crucible than in the depth of the bed. In the case of free-fall, due to a continuous flow of coal and combustion air, a plug-flow assumption and therefore reasonably uniform stoichiometry, is justified.

No kinetic data on the decomposition of $CaSO_4$ at these temperatures are available from literature, but from the close correspondance of the free-fall results with the experimental results kinetics do not seem to be controlling for both free-fall and crucible experiments. Above 1600° K, more than 90% $CaSO_4$ decomposition is observed. These results are also supported by x-ray diffraction studies.

It is apparent from equilibrium relations that the decomposition of sulfates is pressure dependent. Therefore in actual combustor, operating at higher pressures (5-8 atmosphere), the amount of $CaSO_4$ decomposed would be less at the same temperatures. The computed effect of pressure on $CaSO_4$ decomposition is shown in figure 8.7
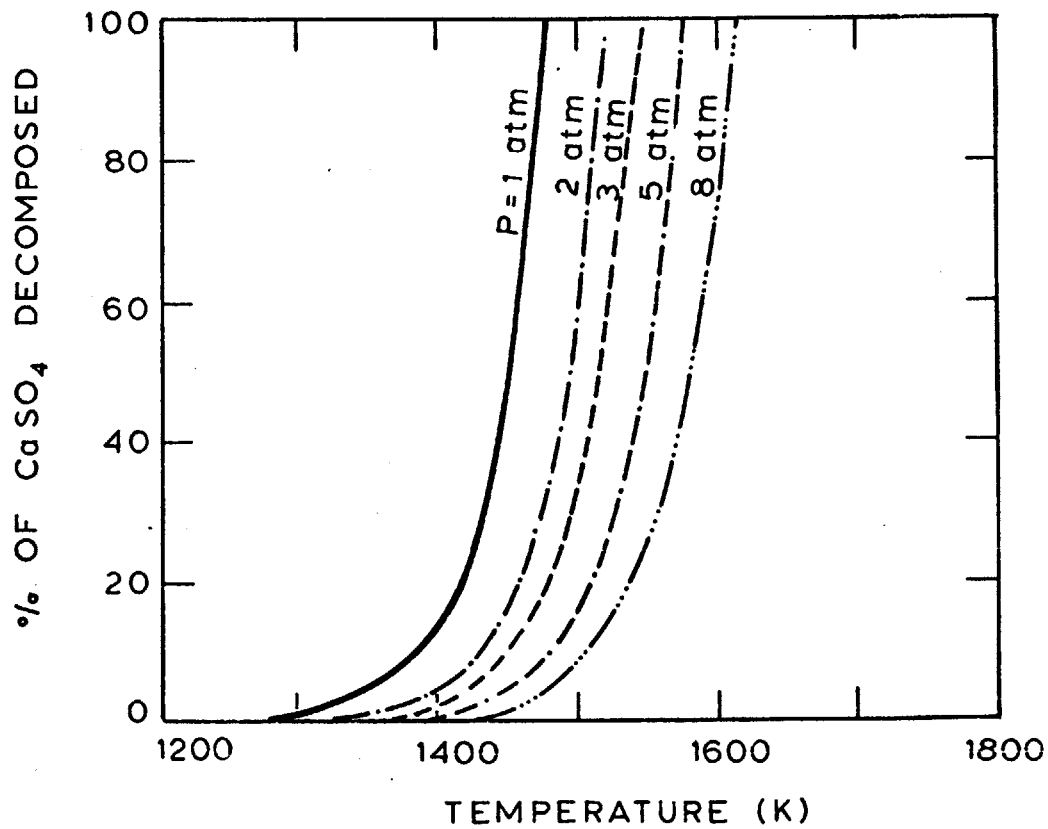
Fig. 8.7 Effect of Pressure on CaSO Decom-
position

8.4 Weight Loss of Silica

8.4.1 Results

Table 8.2 shows the experimental results of silica-graphite heating. The variables under study were temperature, time and carbon to silica ratio. The weight loss of silica was determined for each run by ashing the samples of residual carbon and solid products of silica-carbon reaction. The weight loss of silica can be attributed partly due to vaporization as more volalite SiO and partly due to the transformation to SiC. The fraction of original silica going to SiO and SiC was calculated based on a derived formula (see Appendix G for the derivation of formula) assuming reactions (8.12) and (8.14).

It can be seen from the table that at 2117 and 2250° K about 25% of the original SiO_2 was lost due to formation of gaseous SiO and the rest converted to SiC. At 1967 K 24-30% silica was lost as SiO, a small amount was converted to SiC and the rest of the silica was present as SiO_2. X-ray diffraction of the samples supported these findings. The solid phase after ashing showed the presence of only SiC at 2117 and 2250°K and only SiO_2 at 1967°K. The effect of silica/carbon ratio and time was secondary in nature.

In an oxidizing atmosphere, the loss of silica up to 1830° K, for lignite was below 4 percent (figure 8.3 and 8.4).

TABLE 8.2

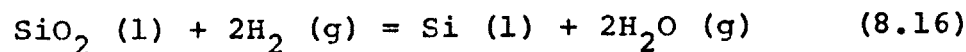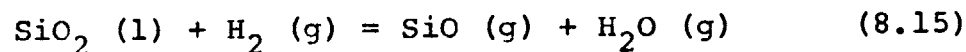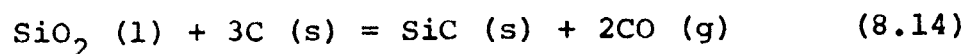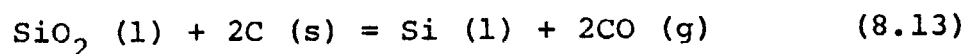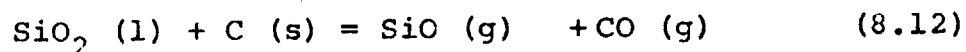## RESULTS OF SILICA-GRAPHITE

HEATING EXPERIMENTS

Run No.	Tempera-ture (°K)	Time (min)	C/SiO_2 (Weight Ratio)	Absolute Loss of Silica Weight (%)	Fraction of Original Silica Converted to:	
					SiO	SiC
S1	2117	45	1.75	50.9	0.27	0.72
S2	2117	45	3.66	53.4	0.31	0.68
S3	2117	10	3.94	47.8	0.22	0.78
S4	2117	10	4.13	45.1	0.18	0.80
S5	2117	20	1.77	47.3	0.22	0.75
S6	2117	20	6.15	47.0	0.21	0.77
S11	2117	20	5.01	44.0	0.17	0.82
S12	2117	120	1.79	52.6	0.30	0.69
S13	2117	120	2.84	53.0	0.30	0.69
S14	2117	120	2.92	49.5	0.24	0.76
S15	2117	120	6.70	45.3	0.16	0.89
S16	2250	30	3.65	47.6	0.22	0.77
S17	2250	30	4.10	49.8	0.25	0.75
S18	1967	30	3.77	25.5	0.24	0.03
S19	1967	30	4.20	32.2	0.30	0.08

8.4.2 Discussion of the Results

In oxidizing of neutral atmosphere, reaction 8.11 instead of reaction 8.10 has been considered by many

$$SiO_2 \ (1) \ \rightarrow \ SiO_2 \ (g) \tag{8.10}$$

$$SiO_2 \ (1) \ \rightarrow \ SiO \ (g) + \tfrac{1}{2}O_2 \ (g) \tag{8.11}$$
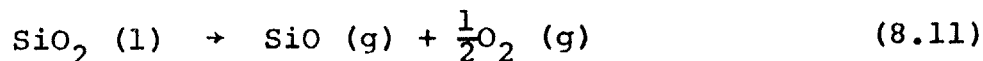
authors [Shick (1960), Zapffe (1944), Raask and Wilkins (1965)] to be the most important reaction responsible for silica decomposition and volatilization. Other reactions (8.12) to (8.16) are also possible in reducing conditions

$$SiO_2 \ (1) + C \ (s) = SiO \ (g) \quad + CO \ (g) \tag{8.12}$$

$$SiO_2 \ (1) + 2C \ (s) = Si \ (1) + 2CO \ (g) \tag{8.13}$$

$$SiO_2 \ (1) + 3C \ (s) = SiC \ (s) + 2CO \ (g) \tag{8.14}$$

$$SiO_2 \ (1) + H_2 \ (g) = SiO \ (g) + H_2O \ (g) \tag{8.15}$$

$$SiO_2 \ (1) + 2H_2 \ (g) = Si \ (1) + 2H_2O \ (g) \tag{8.16}$$

$$SiO_2 \ (1) + CO \ (g) = SiO \ (g) + CO_2 \ (g) \tag{8.17}$$
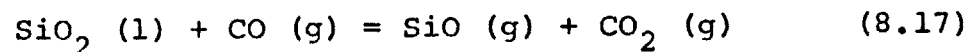
The free energy of formation of these reactions as obtained from JANAF tables (1965) is given in Table 8.3 and Figure 8.8.

It can be seen from the free energies, that the SiC producing reaction of carbon and silica (8.14) is most

Table 8.3

Free Energy of Formation for Silica Reactions

	Reactions	ΔG° (k cal/g mole)
8.10	$SiO_2(l) \rightleftharpoons SiO_2(g)$	$136.38 - 0.038\ T$
8.11	$SiO_2(l) \rightleftharpoons SiO(g) + \frac{1}{2} O_2(g)$	$184.0\ - 0.0566\ T$
8.12	$SiO_2(l) + C(s) \rightleftharpoons SiO(g) + CO(g)$	$155.15 - 0.07656\ T$
8.13	$SiO_2(l) + 2C(s) \rightleftharpoons Si(l) + 2CO(g)$	$165.01 - 0.085\ T$
8.14	$SiO_2(l) + 3C(s) \rightleftharpoons SiC(s) + 2CO(g)$	$137.39 - 0.0767\ T$
8.15	$SiO_2(l) + H_2(g) \rightleftharpoons SiO(g) + 2H_2O(g)$	$123.50 - 0.04276\ T$
8.16	$SiO_2(l) + 2H_2(g) \rightleftharpoons Si(l) + 2H_2O(g)$	$101.62 - 0.01735\ T$
8.17	$SiO_2(l) + CO(g) \rightleftharpoons SiO(g) + CO_2(g)$	$117.98 - 0.037\ T$

T is temperature in °K
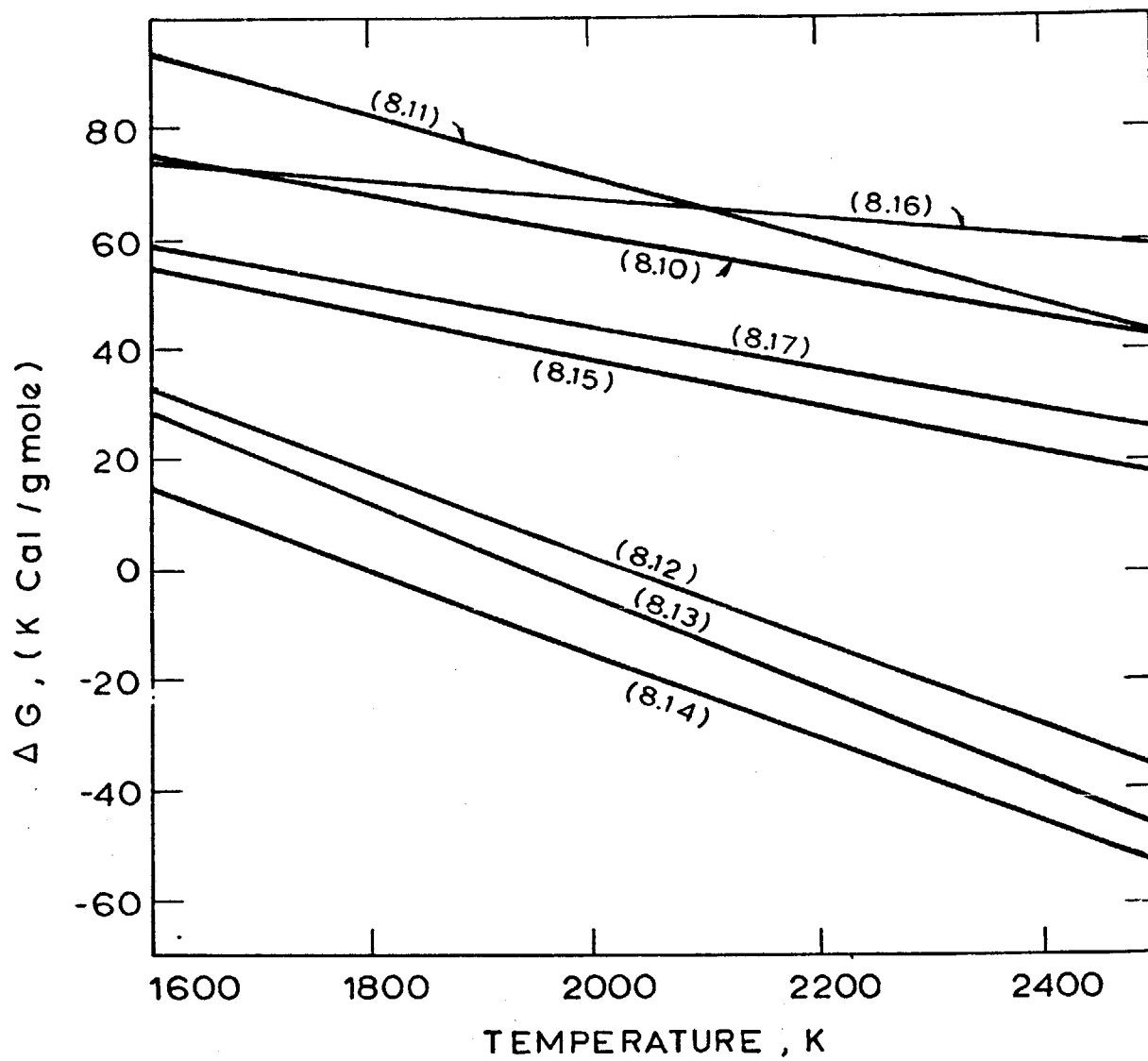
Free Energy of Formation for Silica
Reactions (JANAF TABLES, 1965)

Figure 8.8

favorable thermodynamically. It has been shown by Beecher
and Rosenweig (1961) that this reaction is also most favor-
able kinetically among all possible C-SiO$_2$ reactions in
chars. Rosenweig and Beecher (1963) conclude that at lower
temperatures below (1700 K) reaction 8.12 potentially can
control, but at higher surface temperatures,reaction (8.14)
is dominant.

The results of crucible experiments at 2117 and 2250°
K show a conversion of about 25% of original silica to SiO
and the rest to SiC. At lower temperature 1967 K, about
24-30% conversion to SiO and very little to SiC. It is
believed from these results that at about 1967 K formation
of SiO, reaction (8.12) is favored and above 2117K reaction
(8.14) is favored. The question is why at 1967 K the loss
of silica was only 24-30% and not 100%.and why above 2117 K
conversion to SiC was not 100%. Since at 1967K time effect
was not investigated, it is possible that weight loss would
reach 100% if enough time is provided. This hypothesis
needs to be tested in future experiments varying the resi-
dence time at 1967K. In all the experiments, the final
temperature was reached by slow heating within about 30
minutes. While proceeding to 2117 or 2250° K, the sample
experienced some time at lower temperatures which may be
responsible for the loss as SiO. Once the higher tempera-
ture is reached the remaining SiO$_2$ was converted to SiC.
The fact that the conversion to SiO was about the same
at 2117 and 2250° K is consistent with this theory since

all the samples experienced about the same residence time at intermediate temperatures. Although, these results are not complete, they do suggest a sharp transition for the formation of SiC. Further investigations can be made by rapid heating to temperatures above 2100° K looking for 100% transformation of SiO_2 to SiC.

SiO formed according to reaction (8.12) or (8.17) is an unstable specie and it either oxidizes to SiO_2 or disproportionates into stable species when cooled. At the conclusion of the run at 1967° K, some condensation products were observed on the cooler parte of the furnace (supporting graphite rod). These products under scanning electron microscope showed two distinct type of particles, spherical and rod-like about 0.3 to 1 μm in size, (figure 8. 9). These products are believed to be due to disproportionation of unstable SiO according to reaction 8.18

$$SiO = Si + SiO_2 \qquad\qquad (8.18)$$

Similar observations were made by Raask and Wilkins (1968).

In an oxidizing atmosphere, the loss of silica may occur either by reaction 8.11, or due to local reducing conditions inside the coal particle, by reactions such as 8.12. Figure 8.3 and 8.4 show a small loss of silica (less than 4 percent at 1830° K) in oxidizing conditions for lignite. The partial pressure of SiO according to reaction (8.11) at 1830° K (po_2 = 0.1 atm, P_{total} = 1 atm) is about 8×10^{-10} atm. The partial pressure of SiO if SiO_2 vaporizes

5 μm
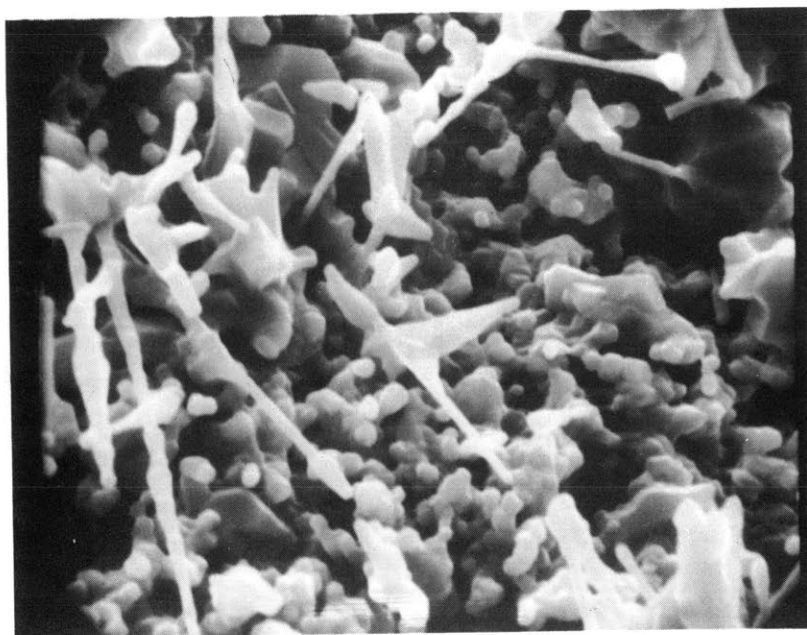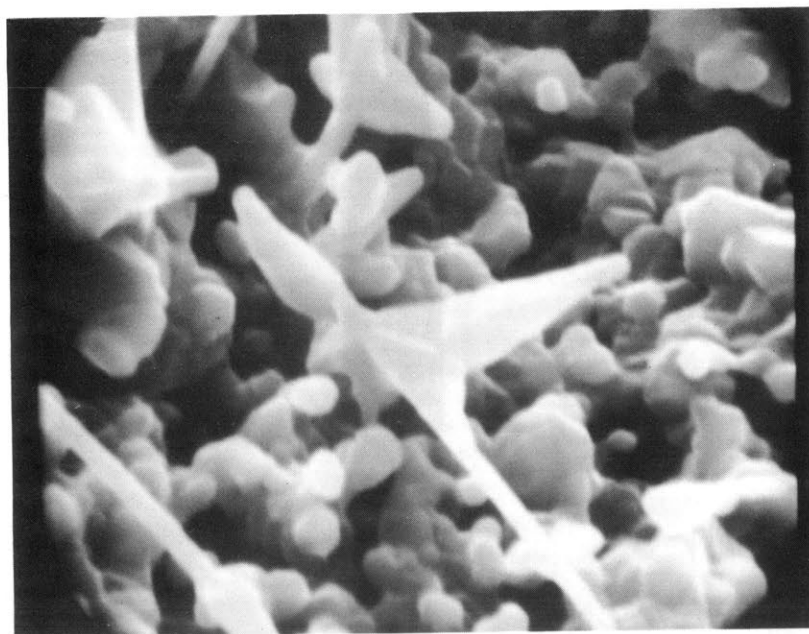
5 μm

Scanning Electron Micrograph of Condensation Products
of SiO

Figure 8.9

completely by reaction (8.11) for a $\phi = 0.5$ and 3 percent

SiO_2 by weight of coal, is about 6×10^{-4} atmosphere. There-

fore reaction (8.11) is expected to contribute to the vapor-

ization of a maximum of a part per million of the silica.

It is therefore concluded that the reducing reactions

such as 8.12 dominate.

8.5 Weight Loss of Ash in Inert Atmosphere

Figures 8.10 and 8.11 show the measured weight loss

of ash for four cases.

(1) ASTM ash in graphite crucibles heated in inert

atmospheres to 1967, 2117 and 2250° K.

(2) ASTM ash in alumina crucibles heated in oxidizing

atmospheres to 1830 ° K.

(3) Coal in alumina crucibles heated in oxidizing

atmospheres to 1830° K.

(4) Coal heated in inert atmospheres to 2250° K and

subsequently ashed at ASTM conditions [data generated

in a parallel study by Kobayashi (1976)].

It should be noted that the mineral matter heated to

a given peak temperature experiences different oxidation

histories in the above experiments. Points to note include:

(1) The weight losses from experiments 1 and 4 are in

good agreement ($\pm$ 5%) at high temperatures (above 1830° K)

and are attributable to the vaporization of the ash con-

stituents which have appreciable vapor pressure at these

temperatures (at 2250° K, P_{FeO} = 1 mm Hg, $P_{Al_2O_3}$ = 0.2 mm
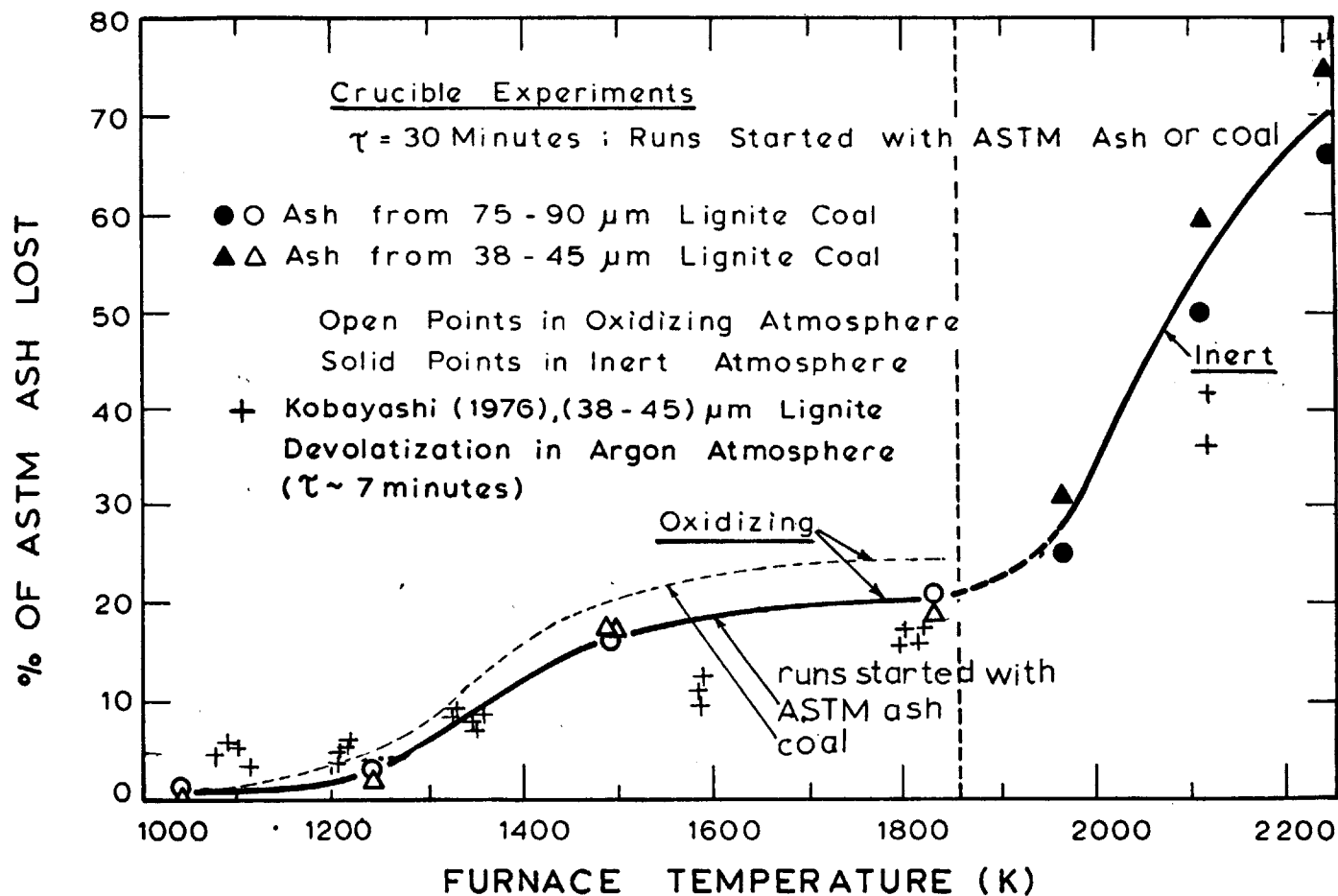
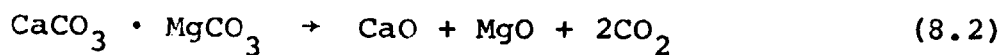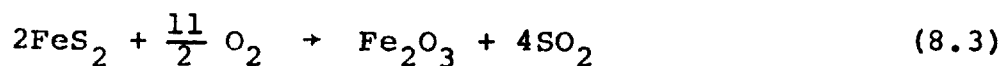Effect of Temperature on Weight Loss of Lignite Ash up to 2250 K

Figure 8.10
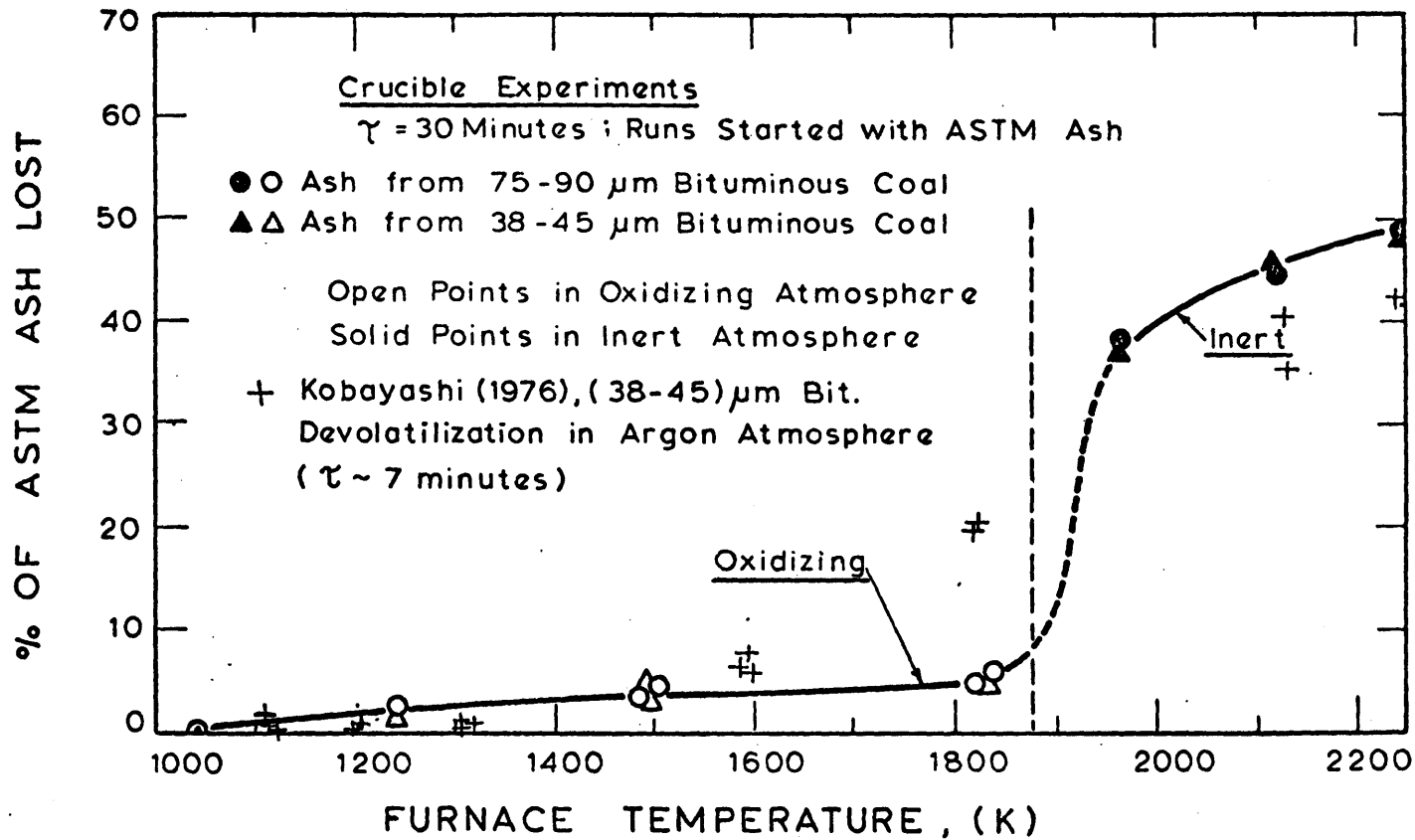
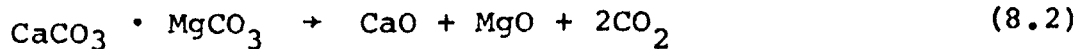Effect of Temperature on Weight Loss of Bituminous Ash Up to 2250 K

Figure 8.11

Hg, $P_{MgO} = 0.1$ mm Hg). The amount of vaporization will be influenced both by the production of suboxides through reactions with carbon (e.g. Al_2O_3 may form Al_2O which has a vapor pressure of 0.3 mm Hg at 2000°C) which augment vaporization and by formation of composite oxides which decrease vaporization.

(2)   Below 1830° K, the weight loss is a function of the history of heating in addition to peak temperature. Differences between cases (3) and (4) of about 4% for lignite can be attributed to the increased silica vaporization in coal due to SiO_2-C reactions.

(3)   In case (4) the weight loss at about ASTM ashing conditions is 5 percent higher than the other cases for lignite. This difference in weight loss between oxidizing and inert conditions can be explained by the differences in the $CaSO_4$ formation in the initial phases of the experiment. Analysis of coal and ASTM ash (chapter 4) shows that lignite ASTM ash contained more sulfate sulfur (about 0.38 percent by weight of coal) than the coal from which it was derived. This is probably due to transfer of some pyritic and organic sulfur to sulfate sulfur during ASTM ashing procedure by the following sequence of reactions:

$$2FeS_2 + \frac{11}{2} O_2 \rightarrow Fe_2O_3 + 4SO_2 \tag{8.3}$$

$$CaCO_3 \cdot MgCO_3 \rightarrow CaO + MgO + 2CO_2 \tag{8.2}$$

$$CaCO_3 \rightarrow CaO + CO_2 \tag{8.1}$$

$$CaCO_3 \cdot MgCO_3 \rightarrow CaO + MgO + 2CO_2 \qquad (8.2)$$

$$CaCO_3 \rightarrow CaO + CO_2 \qquad (8.1)$$

$$CaO + SO_2 + \frac{1}{2}O_2 \rightarrow CaSO_4 \qquad (8.4)$$

$$MgO + SO_2 + \frac{1}{2}O_2 \rightarrow MgSO_4 \qquad (8.20)$$

SO_2 liberated due to oxidation of pyrites is picked up by CaO or MgO produced from decomposition of dolomite or calcite. Reactions (8.3) and (8.20) are favorable thermodynamically at ashing temperatures, ($\Delta G° = -141.9$ kcal/gmole, $\Delta G° = -30.31$ kcal/gmole). 0.38 percent of the weight of coal is equivalent to 4.75% by weight of ash (ASTM ash $\approx$ 8%). In inert atmosphere FeS_2 decomposes first to FeS and then to Fe and sulfur is lost by sublimation. CaO produced by decomposition can not form $CaSO_4$ due to absence of O_2. Therefore the ash produced should weigh about 4.75 percent less than that produced by ASTM method in oxidizing atmosphere. The weight loss of ash up to 1830°K in an oxidizing atmosphere was explained earlier on the basis of $CaSO_4$ decomposition.

(4) In case of bituminous coal ash, the amount of Ca and Mg are very low in mineral matter, therfore weight losses in inert and oxidizing atmospheres up to 1400 K are about the same. But at 1830 K the weight loss of bituminous ash during devolatilization in argon is about 12% more than in oxidizing atmosphere. In the absence of air decomposition reaction of FeS_2 to first FeS and then

to Fe at about 1700 K are well documented (Wunderlich, 1952), which could account for the additional loss, but Kobayashi determined the ash content after ashing the devolatilized coal samples by ASTM procedure, which sould reoxidize Fe to Fe_2O_3, providing the same final species as the experiments in oxidizing atmospheres. There is a possibility that Fe formed by decomposition of FeS_2, forms some composite phase with other species present in ash and does not oxidize during subsequent ashing. Such hypothesis will need to be tested by performing x-ray diffraction of devolatilized coal samples.

8.6 Concluding Remarks:

It is shown that combustion conditions have a significant influence on the weight loss of ash which can be expected under combustion or gasification conditions. Up to 1830° K, the losses are mainly accounted by decomposition of $CaSO_4$ initially present in coal or formed during combustion. At high temperatures, 2250° K, weight losses up to 70% are observed, silica, being the most volatile among the major oxides present in ash, plays an important role in the volatilization of ash at high temperatures. Above 2100° K, silica forms SiC by reactions with carbon and inhibits further vaporization. The formation of silica is shown by independent experiments in which silica and excess graphite were heated in inert atmosphere up to 2250° K. At about 1950° K, silica volatilizes in the form of morevolatile SiO which being

an unstable specie, on cooling, disproportionates to give

Si and SiO_2 in inert atmosphere.   In the presence of oxygen

SiO may oxidize back to SiO_2.

Although several interesting features relative to the

volatilization of ash are uncovered, the data are pre-

liminary in nature. Further work is required to completely

understand the vaporization characteristics of ash.   X-ray

diffraction for devolatilized samples can reveal the dif-

ferences observed between oxidizing and inert conditions

for bituminous ash. More controlled experiments in the

transition range (between 1950 - 2100° K), rapid heating

runs above 2100° K and long time runs below 1950° K are

needed to ascertain the conclusions drawn here. Kinetic

information is needed to quantify the extent of completing

Si-C reactions.

CHAPTER 9

CONCLUSIONS

1.   a.   Mineral matter is distributed in coal in the

            form of small inclusions of varying compositions.

      b.   The mineral matter mainly consists of kaolinite

            ranging from 1 to 5 μm platelets,carbonates

and sulfates of calcium about 2 μm average size and

pyrites about 1 μm average size. Other minerals found

in minor quantities are illite,quartz,lawsonite,coquimbite

and rutile.

      c.   The overall mean particle size of mineral matter

            in pulverized coals,on the basis of kaolinite,

pyrite and sulfate and carbonates is estimated to be

about 2 μm.

      d.   Original coal size did not have any effect on

            the particle size distribution of mineral

matter in coal.

2.   A relation is derived between the amount of mineral

matter (low temperature ash) and ASTM Ash on a proposed

decomposition scheme. The derived formula gives good

agreement for low sulfur, high Ca and Mg containing coals

(lignite).

3.   When coal particles are heated, associated mineral

matter undergoes profound chemical and physical trans-

formations. The combustion conditions have significant

impact on the behavior of ash at high temperatures.

4. The mineral matter undergoes thermal decomposition, interaction with coal and interaction with each other during combustion. These reactions result in the formation of new phases which are crystalline or amorphous (glassy). Differences are observed between lignite and bituminous ashes as the original mineral matter present in the two types of coals also differ.

5. The chemical decomposition of mineral matter constituents is controlled more by thermodynamic than by kinetic constraints. Allowances must be made, however, for the temperature differential between the particle and gas and for the reactions between mineral matter and carbon.

6. Thermal decomposition and interaction of mineral phases are associated with the weight changes of ash.

a. From ASTM ashing temperature (1023°K) to 1830°K, lignite ash lost about 25% of its weight and bituminous about 6% of its weight. The weight loss is accounted mainly due to decomposition of $CaSO_4$. Part of $CaSO_4$ in lignite is formed by interaction of dolomite of calcite with pyrites during ashing procedure in the presence of oxygen.

b. During devolatilization of lignite in inert atmosphere, an ash loss of about 5% is observed even below ASTM ashing temperature. Pyrites in inert atmosphere decomposes to pyrrhotite (FeS) and then to

Fe and the liberated sulfur sublimes. No additional $CaSO_4$ formation takes place which explains the 5% loss of ASTM ash under inert conditions.

    c.   Minor amounts of SiO_2 loss are observed up to 1830°K in oxidizing atmosphere which are probably due to formation of more SiO by reduction from carbon.

    d.   At higher temperatures, above 2000°K, formation of SiC is dominant due to reactions of SiO_2 with carbon.

7.   Significant augmentation of the vaporization of mineral constituents occurs above 2000°K due to formation of lower oxides by reduction with carbon. Lignite ash lost about 70% and bituminous about 50% of its weight at 2250°K.

8.   Along with chemical transformations, simultaneous physical changes in ash take place causing fusion, agglomeration and finally vaporization.

    a.   Small particles ($\sim$2 μm) of mineral matter in the original coal fuses at about 1000-1200°K and agglomerate to form bigger particles as the char surface recedes. The fused ash particles retain on the surface of char particle due to surface tension forces.

    b.   The main agglomeration of fused ash particles occur only during the final stages of burnout when the ash particles are drawn together on the receding reacting carbonaceous surface.

    c.   Part of the ash formed is in the form of hollow spheres (cenospheres) which is responsible for a distribution of densities in the ash produced. The

density of ash varies from less than 1 to about 3.5 gms/cc.

d. The formation of cenospheres is governed by the viscous relaxation of the fused ash and the kinetics of gas evolution. The temperature range in which cenospheres are formed (about 1200°K - 1500°K) is explained by the use of a simple theoretical model.

e. The particle size distribution of dense ash does not show any trend as a function of combustion temperatures up to 1830°K.

f. The number of ash particles produced per coal particle are about 3 for lignite and about 5 for bituminous. The formation of more than one ash particle per coal particle is explained on the basis of "fragmentation and cenosphere formation of char" theory.

g. Original coal size has no major effece on the number of ash particles produced per coal particle. The mass median size of ash particles produced is proportional to the mass median size of the parent coal particles.

CHAPTER 10

RECOMMENDATIONS

1. Determine the minerals present in coals quantitatively. During this thesis only their presence was identified, no effort was devoted towards obtaining quantitative information regarding their concentration.

2. Experiments should be performed with more coals and more particle sizes and over a wider range of temperatures.

3. Ash particle size distribution should be determined as a function of char burnout. Since it is very difficult to experimentally obtain the particle size distribution in the unburned char, a combination of free-fall experiments followed by low-temperature ashing should give overall particle size distribution of ash in partially burned char.

4. Numerical models should be constructed based on agglomeration mechanisms. Various models of coal burning e.g. shrinking sphere, pore diffusion, can be accounted in the model and the effect on resulting PSD of ash can be studied.

5. Importance of silica-carbon reactions are identified. More work is required at wide range of temperatures to identify the regimes in which SiO, SiC, Si formations

take place.

6. Vaporization of other species of ash should be
studied at high temperatures.

7. Kinetic information regarding ash vaporization are
important for MHD applications. This information can
be obtained by performing short residence time experi-
ments in a laminar flow furnace capable of providing
short residence times.

APPENDICES

APPENDIX A.   Heating Rates and Residence Time in a Free Fall Furnace

A.1   Estimation of Maximum Heating Rates

Maximum heating rate can be calculated by assuming the coal particles into a preheated gas stream without any carrier gas. Let a pulverized coal particle at temperature T_p be dropped into the furnace at temperature T_f.

If the particle is assumed to be isothermal (A.1.2) i.e. $\frac{dT_p}{dr} = 0$, and spherical, the heat balance on the particle gives

$$- \frac{4}{3}\pi r^3 (\rho C_p)_p \frac{dT_p}{dt} = 4\pi r^2 \frac{k_{amb}}{r}(T_p - T_f) \qquad (A.1)$$

If heating is only by conduction,

$$\frac{dT_p}{dt} = \frac{3k_{amb}}{\rho C_p r^2} (T_f - T_p) \qquad (A.2)$$

If heating is by radiation,

$$\frac{dT_p}{dt} = \frac{3\sigma (T_f{}^4 - T_p{}^4)}{(\rho C_p)_p \cdot r} \qquad (A.3)$$

Example: 100 μm diameter coal particle dropped into a

furnace filled with air at 1500°C

average temperature ≃ 750°C

thermal properties of coal at 750°C (Badzioch,

ρ = 1.2 gm/cm^3 et al 1964)

C_p = 0.1 cal/gm·°C

k_{air} = 0.26×10^{-3} cal/cm·sec·°C
1500°C

$\frac{dT}{dt}$ (by conduction) = 3.84×10^5 °C/sec

$\frac{dT}{dt}$ (by radiation) = 6.7 ×10^4 °C/sec

Since the heating rate due to conduction is inversely

proportional to the square of the diameter, for a 40 μm

particle the heating rates would be about 2.4×10^6 °C/sec.

In the actual experimental system the heating rate would

be less than these values because the gas stream carry-

ing the coal particles has to be heated up also.

A.2 Isothermality of the Coal Particles

The transient equation for heat transfer in a sphere

is

$$\frac{dT}{dt} = \alpha \left(\frac{2}{r} \frac{dT}{dr} + \frac{d^2T}{dr^2} \right)$$

and

$$\text{Biot number} \quad \text{Bi} = \frac{\text{Internal Resistance}}{\text{External Resistance}}$$

$$= \frac{h \cdot r}{k_p} = \frac{k_{air}}{k_p} \qquad \text{(A.4)}$$

at 750°C $\quad k_{air} = 0.16 \times 10^{-3}$ cal/cm·sec°C

$\quad\quad\quad\quad\quad k_p = 0.5 \times 10^{-3}$ cal/cm·sec°C

$\quad\quad\quad\quad\quad$ Bi $= 0.32$

k_p increases faster than k_{air} as the temperature is increased and at higher temperatures, $k_{air} \ll k_p$. Therefore internal resistance can be neglected and the assumption of isothermality of pulverized coal particles is justified.

A.3   Terminal Velocity and the Residence Time of Particles in the Free-Fall Furnace

For a spherical particle, in the laminar flow $(N_{Re_p} < 0.1)$, the terminal velocity is given by

$$v_t = \frac{(\rho_p - \rho_{amb}) g d_p^2}{18 \mu_{amb}} \qquad \text{(A.5)}$$
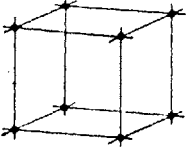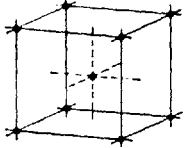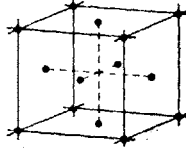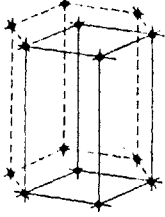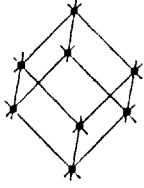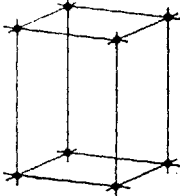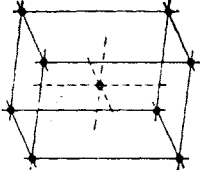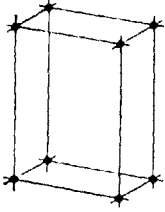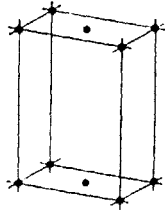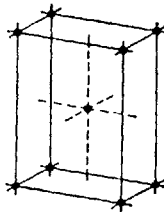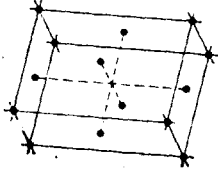
The calculated terminal velocities and the residence time in the 15 cm hot zone of the furnace at four furnace temperatures and two coal sizes (42 and 85 μm) used in this study are shown in Table A.1.

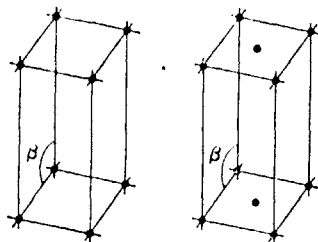Table A.1   Terminal Velocity and Residence Time of Coal Particles

Temp. (K)	ν_T (cm/sec)		τ (sec), in 15cm hot zone		$N_{Re_p} = \dfrac{\rho dp V_t}{\mu}$	
	42 μm	85 μm	42 μm	85 μm	42 μm	85 μm
1050	2.47	10.1	6.07	1.48	0.0080	0.067
1250	2.21	9.0	6.79	1.66	0.0055	0.045
1500	1.96	8.0	7.65	1.87	0.0036	0.030
1830	1.71	7.0	8.77	2.14	0.0023	0.019

Appendix B

1. Crystallography Nomenclature:

Latticle structure exist in 14 different forms as listed below.

(1) P   (2) I   (3) F
Isometric

(4) C or P   (5) R   (6) P
Hexagonal   Rhombohedral   Tetragonal

(7) I
Tetragonal

(8) P   (9) C   (10) I

(11) I
Orthorhombic

Symmetry
Angles
Edges

Isometric

$\alpha = \beta = \lambda = 90°$

$(a = b = c)$

$a_1 = a_2 = a_3$

Hexagonal

$\alpha = \beta = 90°$

$\lambda = 120°$

$(a = b \neq c)$

$a_1 = a_2 = a_3 \neq c$

Rhombohedral

$\alpha = \beta = \lambda \neq 90°$

$a = b = c$

Tetragonal

$\alpha = \beta = \lambda = 90°$

$(a = b \neq c)$

$a_1 = a_2 \neq c$

Orthorhombic

$\alpha = \beta = \lambda = 90°$

$a \neq b \neq c$

(12)P   (13)C
Monoclinic

(14)P
Triclinic

Symmetry
Angles
Edges

Monoclinic
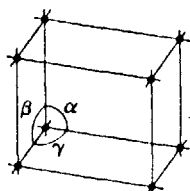
$\alpha = \lambda = 90° \neq \beta$

$a \neq b \neq c$

Triclinic

$\alpha \neq \beta \neq \lambda$

$a \neq b \neq c$

Each of the crystal system listed above could have crystal classes as mentioned below.

Crystal System	Crystal Class
Isometric	Hexoctahedral Gyroidal Hextetrahedral Diploidal Tetartoidal
Hexagonal Hexagonal division	Dihexagonal-dipyramidal Hexagonal-trapezohedral Dihexagonal-pyramidal Ditrigonal-dipyramidal Hexagonal-dipyramidal Hexagonal-pyramidal Trigonal-dipyramidal
Hexagonal Rhombohedral division	Hexagonal-scalenohedral Trigonal-trapezohedral Ditrigonal-pyramidal Rhombohedral Trigonal-pyramidal
Tetragonal	Ditetragonal-dipyramidal Tetragonal-trapezohedral Ditetragonal-pyramidal Tetragonal-scalenohedral Tetragonal-dipyrramidal Tetragonal-pyramidal Tetragonal-disphenoidal
Orthorhombic	Rhombic-dipyramidal Rhombic-disphenoidal Rhombic-pyramidal
Monoclinic	Prismatic Sphenoidal Domatic
Triclinic	Pincaoidal Pedial

2. <u>Crystallography of Standard Minerals Found in Coal</u>

   [Dana's Book of Mineralogy]

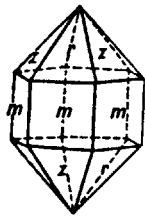1. <u>Kaolinite [Al$_2$ Si$_2$ O$_5$ (OH)$_4$]</u>

   Monoclinic; prismatic • In very minute, thin, rhombic

   or hexagonal-shaped plates • Usually in claylike

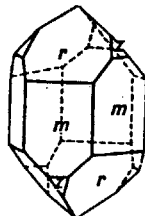   masses, either compact or friable.

2. <u>Quartz [SiO$_2$]</u>

   α-Quartz-hexagonal-R; trigonal, trapezohedral
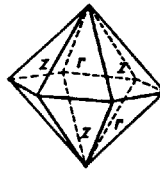
   β- Quartz-hexagonal-trapezohedral
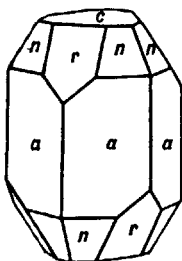
   Crystals-prismatic; hexagonal dipyramid (a)

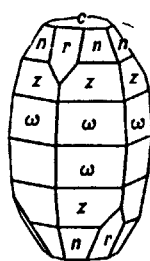   rhombohedron (b)

   doubly terminated

   hexagonal dipyramid (c)

   (quartzoid)

   (a)   (b)   (c)

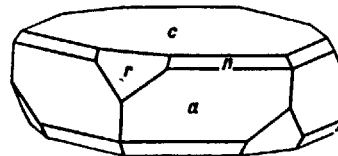3. <u>Corundum [Al$_2$O$_3$]</u>

   Hexagonal-R; scalenohedral • Crystals usually prisma-

   tic or tapering hexagonal pyramids (a, b) • often
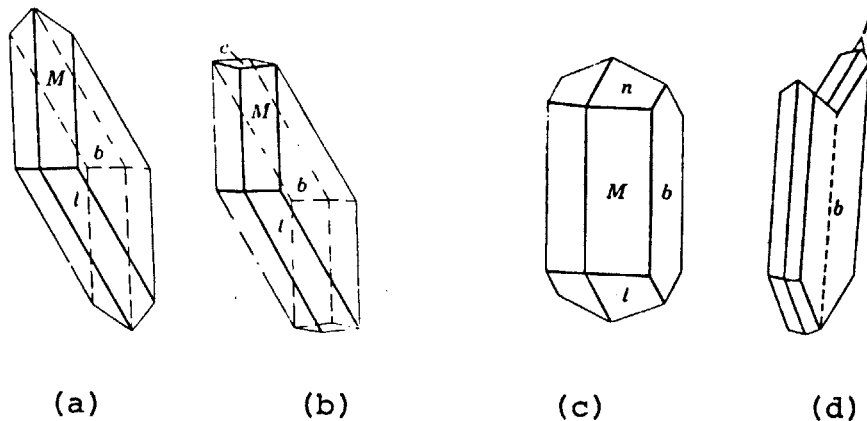
   rounded into barrel shapes. Frequently with deep

   horizontal

   striations.

   Many show

   rhombohedral

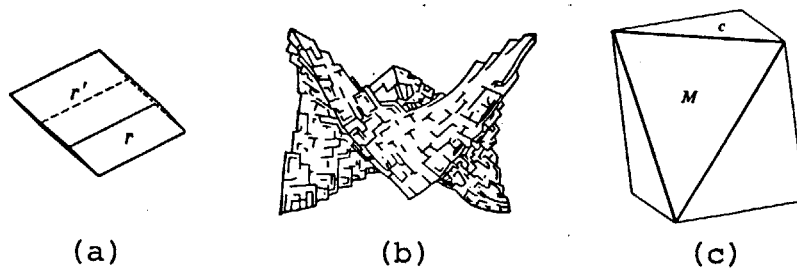   faces (c).

   (a)   (b)   (c) Usually

   ruddy crystallized or massive with parting planes

   nearly in angle; course or fine granular.

4. <u>Gypsum</u> [CaSO$_4$ · 2H$_2$O]

Monoclinic; prismatic (a, b, c) · Twins common (d)

(a) (b) (c) (d)

5. <u>Dolomite [CaMg(CO$_3$)$_2$]</u>

Hexagonal-R; rhombohedral · Crystals usually unit rhombohedron (a), more rarely a steep rhombohedron and base (c) or "saddle shaped" crystals (b).
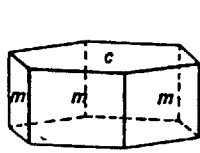

(a) (b) (c)

6. <u>Calcite [CaCO$_3$]</u>

Hexagonal-R, hexagonal-scalenohedral • Crystals are

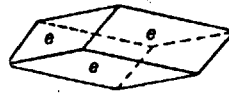extremely varied in habit; often highly complex.

Three important habits:

(1) prismatic, in long or short prisms with rhombohe-

dral terminations (a, b)

(2) rhombohedral, both low and steep rhombohedrons

(c, d, e)

(3) scalenohedral, often with prism faces and rhombohe-

dral truncations (f, g, h, i)
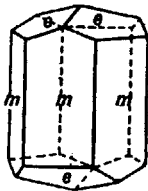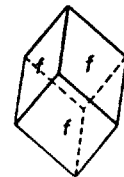
(a)   (b)   (c)   (d)
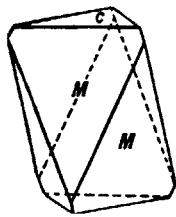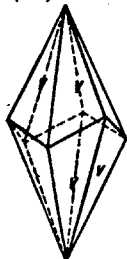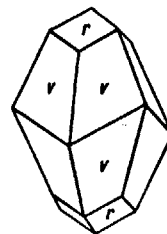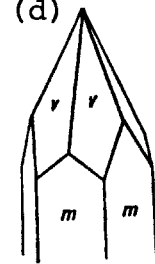
(e)   (f)   (g)   (h)
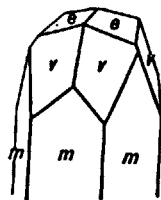
(i)

7. Aragonite [CaCO$_3$]

Orthorhombic; dipyramidal • Steep dipyramid and first order prism (a). Tabular (b), twinned (c), pseudo-hexagonal twins (d).
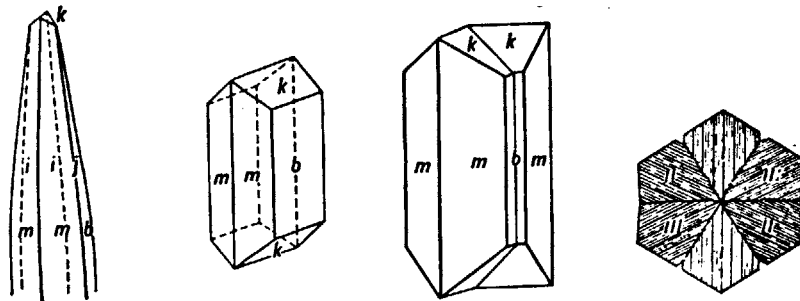
(a)   (b)   (c)   (d)

8. Pyrite [FeS$_2$]

Isomeric; diploidal • Frequently in crystals common forms are cubic (a); pyritohedron (b), octahedron (c) and characteristic combinations of these three (d, e, f).
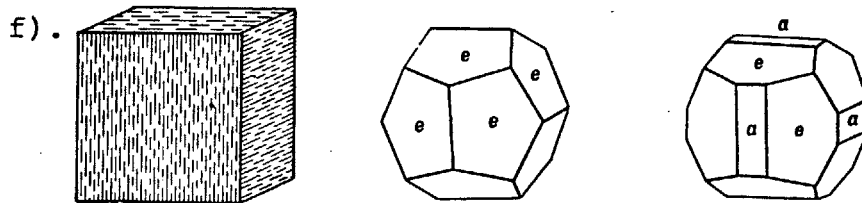
(a)   (b)   (c)
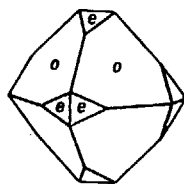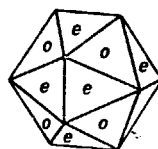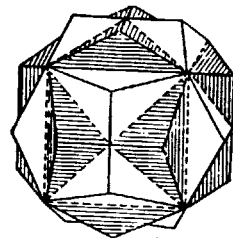
(d)   (e)   (f)

9. **Marcasite [FeS$_2$]**

Orthorhombic; dipyramidal. Crystals commonly tabular

parallel to basal plane showing short vertical prisms

(a)   (b)   (c)
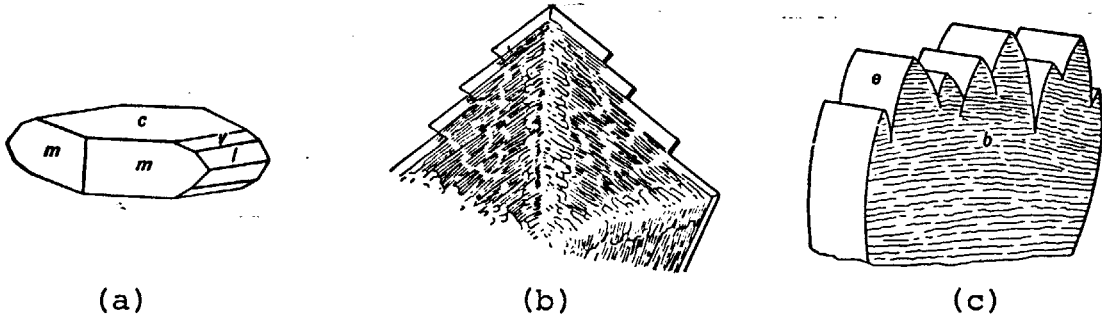
and low first-order prisms (a). Often tweinned giving

cockscomb (b) and spear-shaped groups (c).

10. **Hematite [Fe$_2$O$_3$]**

Hexagonal-R; hexagonal-scalenohedral. Crystals often

show triangular markings (a, b). Edges of plates may

be beveled with rhombohedral forms (c). Thin plates

may be grouped in rosette forms (iron roses) (d).

(a)   (b)   (c)   (d)
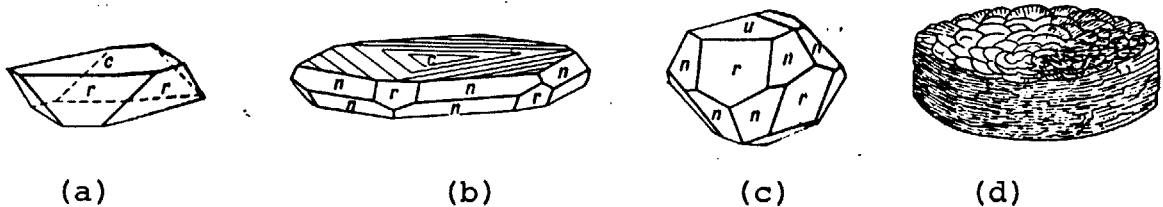
11. **Magnetite [Fe$_3$O$_4$]**

Isomeric; hexaoctahedral. Frequently in crystals of

octahedral habit (a), occasionally twinned. More

(a)   (b)   (c)
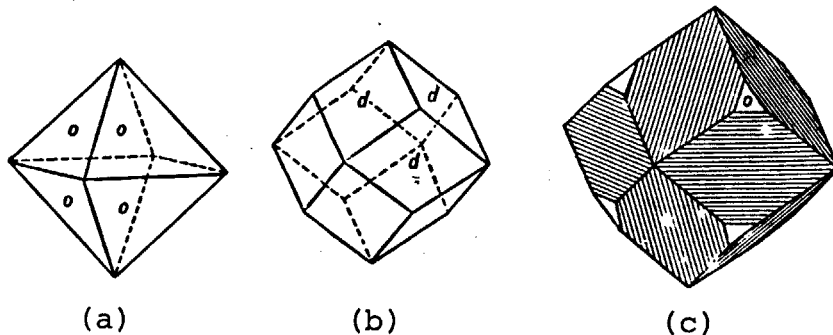
rarely in dodecahedrons (b). Dodecahedrons may be striated parallel to the intersection with octahe-drons (c).

Fusion of Ash Particles During Coal Combustion.

It was shown by J. Frenkel (1945) that under the influence of surface tension, crystalline bodies can display a viscous flow. Finely divided particles (1 - 10μm) can fuse at viscosities which are order of magnitude higher than required for viscous flow in bulk.

The change in shape of a crystalline body on heating is the result of the action of surface tension on the sharp edges of small irregular shapes which forces the particles to assume a spherical form. Frenkel (1945) has shown that in cases where the initial shape of particle deviates from that of a perfect sphere, the relaxation time (t) is given by

$$r = r_o \exp (-t/\tau) \qquad (C.1)$$

and

$$\tau = 4 \pi \eta r/\gamma \qquad (C.2)$$

where r = distance from the center of a sphere of equivalent volume having radius r_o

η = coefficient of viscosity

γ = coefficient of surface tension

if the value of surface tension and time of exposure at high temperature is known, the viscosity at which the irregular shape particle transforms to sphere can be calculated.

For example

$$r = 320 \text{ dynes/cm}$$

[for coal-slag interface between 1300-1400°C

slag composition, SiO_2=42.0%, Al_2O_3=23.9%, Fe_2O_3=17.8%,

CaO=4.6%, MgO=2.2%, K_2O=2.9%, Na_2O=2.7%, SO_3=1.9%,

Raask (1966)]

$$t = 1 \text{ second (free-fall furnace)}$$

Let the thickness of moving surface be one-half of the radius, i.e., $r_o/r = 2$

$$\eta = [\frac{t\nu}{4\pi r}] \frac{1}{\ln \frac{r_o}{r}}$$

The viscosity of a coal ash, fully melted and free from crystals can be calculated by using Watt's empirical formula. (Watt and Fereday, 1969)

$$\log_{10}\eta = \frac{10^7 m}{(T-423)^2} + c \qquad\qquad (C.4)$$

where

η = viscosity in poise

T = temperature in degree, Kelvin

$m = 0.00835 \ SiO_2 + 0.00601 \ Al_2O_3 - 0.109$

$c = 0.0415 \ SiO_2 + 0.0192 \ Al_2O_3 + 0.0276 \ Fe_2O_3$
$+ 0.016 \ CaO - 3.92$

SiO_2, Al_2O_3, Fe_2O_3, CaO are percent by weight of total ash.

Range of application of the formula is

Temperature = 1000-1800°C

SiO_2 = 40-80%

Al_2O_3 = 17-57%

Fe_2O_3 = 3-30%

CaO = 2-30%

MgO = 1-10%

The basis of the concentration of oxides is

$SiO_2 + Al_2O_3 + Fe_2O_3 + CaO + MgO = 100$

The confidence limits of estimating viscosity from this formula is estimated to be $\pm$ 0.05 by the authors.

Based on this formula the temperature at which lignite or bituminous ash fuses can be calculated. Table C.1 gives the temperature of fusion for bituminous and lignite ash for different particle sizes, assuming the particles have the average composition of ash. In fact, initially before agglomeration, the composition of individual ash particles is quite different than the mean composition which may influence the fusion temperature.

It is clear from Table C.1 that irregular shaped particles should transform to spheres at a viscosity of the material several orders higher than required for the bulk flow (about 1000 poise) or at much lower temperature. Temperatures ranging from (1000-1200°K) are sufficient to fuse the particles.

TABLE C.1

Particle Radius (μm)	Viscosity (poise)	Temperature of Fusion (K)*	
		Bituminous Ash	Lignite Ash
0.1	3.7×10^6	1120	1003
1.0	3.7×10^5	1172	1043
2.0	1.85×10^5	1191	1057
5.0	7.35×10^4	1217	1076
10.0	3.7×10^4	1238	1091
100.0	3.7×10^3	1325	1153

* The composition of ash is assumed to be as shown in Table 4.4.

Appendix D

Growth of Ash Cenosphere

The formation and size of cenospheres are controlled by the viscosity and surface tension of the fused ash, the rate of gas evolution and the rate of diffusion of gas through the melt. If the chemical reaction giving rise to gas evolution is very rapid, the growth of cenosphere is controlled by the viscous relaxation of the fused ash.

Let us assume a molten ash particle of outer radius r, and inside cavity of radius r_i containing gas. Let the pressure of gas inside the particle be p_i and outside p_o. The particle would expand if inside pressure $p < p_{eq}$ and expansion would cease when $p \rightarrow p_{eq}$ where equilibrium pressure p_{eq} for curved surface is given by
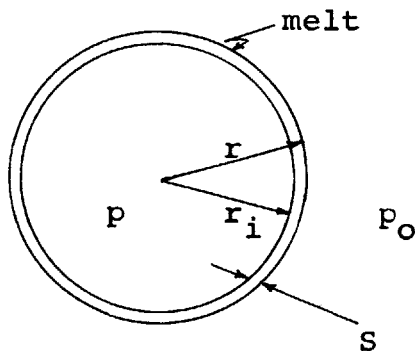
$$p_{eq} = p_o + 2\sigma [\frac{1}{r_i} + \frac{1}{r}] \qquad (D.1)$$

The pressure difference acting to increase the bubble size is

$$\Delta p = p - p_{eq} = p - p_o - 2\sigma [\frac{1}{r_i} + \frac{1}{r}] \qquad (D.2)$$

The rate of change of the radius of hollow sphere is given by

$$\frac{dr}{dt} = \frac{r^2 \Delta p}{4\eta S} \qquad (D.3)$$

where

η = viscosity of the fused ash

S = shell thickness = $r - r_i$

At a constant temperature, the gas inside cenosphere will follow Boyle's law

$$pv = k \quad \text{or} \quad p = \frac{k}{v} = \frac{k'}{r_i^3} \qquad (D.4)$$

Substituting (D.2) and (D.4) in Eqn. (D.3), we get

$$\frac{dr}{dt} = \frac{r^2}{4\eta(r-r_i)}[\frac{k'}{r_i^3} - p_o - 2\sigma(\frac{1}{r_i} + \frac{1}{r})] \qquad (D.5)$$

where r and r_i are related by

$$\frac{4\pi}{3}(r^3 - r_i^3) = \text{volume of shell} = \text{constant}. \qquad (D.6)$$

Example

If we start with a 12μm dense ash particle and say that a 40μm cenosphere results

$k' = pr_i^3$

p = equilibrium pressure when expansion of ceno-
   sphere has ceased i.e. $\Delta p = 0$

$p = p_o + 2\sigma(\frac{1}{r} + \frac{1}{r_i}) = 1 + 2 \times \frac{3.2 \times 10^{-4}}{10^{-4}} (\frac{1}{6} + \frac{1}{20})$

   $= 2.39$ atmosphere

$k' = 1.91 \times 10^{-8}$ atm. cc

time required for the expansion of this cenosphere to
from 12μm to 40μm diameter can be calculated by inte-
grating the inverse of dr/dt

$$t = \int 1/\frac{dr}{dt} \; dr = \int \frac{1}{f(r)} \; dt$$

where

$$f(r) = \frac{r^2}{4\eta(r-r_i)} \left[\frac{k'}{r_i^3} - P_o - 2\sigma(\frac{1}{r_i} + \frac{1}{r}) \right]$$

The integration from r=6μm to r=20μm gives the time
required for a 6μm radius sphere to form a 20μm radius
cenosphere. For η=1000 poise, which is the viscosity of
bituminous ash at about 1400°K by the Watt formula,
σ=320 dynes/cm, the value of the integration is = 34
mseconds. At other temperatures, the viscosity would be
different and the times required for the formation of
some cenospheres are given in Table D.1. Surface tension
of coal-slag interface is assumed to be independent of
temperature. Although no data are available showing the
effect of temperature on coal-ash interfacial tension,
measurement of surface tension of various glasses at dif-
ferent temperatures (Mitchell et al, 1952) show about a
2% increase in surface tension from 1000°C to 1300°C.

TABLE D.1

Effect of Temperature on the Time Required (t) to

Form an Ash Cenosphere of 20μm Radius Starting

from 6μm Radius Dense Ash

Temperature (K)	μ*(poise)	t(sec)
1000	9.25×10^9	3.15×10^5
1200	1.3×10^5	4.42
1400	8.4×10^2	0.029
1600	56.4	0.002
1800	11.3	0.0004
2000	4	0.00014

*Viscosity of bituminous ash from Watt formula

(Watt, 1969)

Although the viscosity and surface tension both may change significantly as a function of composition, and the absolute values of the time thus calculated may not be applicable but the above table compares the relative time scale of cenosphere formation from one temperature to another. If in our case we get stable cenospheres at 1500°K temperature with about 1 second of residence time, the formation of same size cenosphere at 1300°K would take more than 100 seconds and at 1800°K would require less

than 1 msecond.

These calculations are based on the assumption that the growth rate ceases when the pressure inside the bubble reaches the equilibrium pressure. It is possible that the pressure inside the bubble may be very high due to production of gas; for example if a 12μm $CaCO_3$ (density =2.7 gm/cc) decomposes completely, CO_2 released will be = 3.35×10^{-12} moles. Pressure inside a 40μm bubble formed at 1500°K would be 12.3 atmosphere which is much higher than the equilibrium pressure 2.39 atmosphere. In this case the cenosphere would continue to grow until it breaks.

The rate of gas production may also control the growth of cenospheres. In that case, k' in Eqn. (D.5) will be a function of the kinetics of reactions producing gas. It is not certain which decomposition reactions are responsible for the evolution of gas forming cenospheres and since there are numerous reactions possible an accurate estimate of expansion rates and times is not possible. The results of Table D.1 should therefore be used only as a means of comparison.

The narrow range of temperature for the formation of cenospheres can be evidenced from Table D.1. Below 1000°K cenospheres would not form because residence times are too small. Above 1600°K, the cenospheres have ample time to form and collapse. Peak cenosphere formation is as expected, at an intermediate temperature. Exact tempera-

ture estimation would require allowance for effect of composition on viscosity and surface tension and the kinetics of gas production.

APPENDIX E

Vaporization of Ash

Predictions of the amounts and composition of ash vaporized ash is of vital importance in the design of an MHD combustor. The particle size distribution and composition of ash constituents would be required to estimate the ash vaporization.

As the coal is heated in an oxidizing environment, the finely distributed ash particles experience the temperature time history of the parent coal particles and undergo phase transformations. At about 1000°C a significant fraction of the ash fuses to form glassy spheres. As the temperature rises further to about 1000 to 1200°C some of the small glassy spheres agglomerate and some of the ash beads separate from the residual char. Ash heating, melting and vaporization proceed simultaneously with char combustion. The vaporization of particles can be expressed in terms of the characteristic time scale of the process. If heat transfer is the dominating factor, a ratio of heat of vaporization to the heat flux would give the characteristic time scale. And for low vapor pressure materials, species diffusion would be the rate controlling step.

The resulting equations are:

Diffusion limited vaporization rate

$$\overset{\circ}{N}_A = \left(\frac{DP}{RT_\infty r} \right) \ln \left[\frac{P-p_{A\infty}}{P-P_{vp}} \right] \frac{gmole}{cm^2 sec} \qquad (E.1)$$

Heat transfer limited vaporization rate

$$\overset{\circ}{N}_A = \frac{h}{M_A C_{pA}} \ln \left[1 + \frac{M_A C_{pA}}{\lambda A} (T_\infty - T_s) \right] \qquad (E.2)$$

Combined heat and mass transfer would result

$$\left[\frac{P-p_{A\infty}}{P-P_{vp}} \right]^{\frac{sh}{N_u} \circ \frac{D}{\alpha}} = \frac{M_A C_{pA}}{\lambda A} \left(T_\infty - T_s \right) + 1 \qquad (E.3)$$

assuming

$$Le = \frac{sh}{N_u} = 1$$

and using the heat and mass transfer analogy, i.e.:

$$D \simeq \alpha = \frac{k}{\rho C_P}$$

after simplification

$$\left[\frac{P_{vp}}{P-P_{vp}} \right] = \frac{M_A C_{pA}}{\lambda A} \left(T_\infty - T_s \right) \qquad (E.4)$$

where:

$\overset{\circ}{N}_A$ = vaporization rate of ash specie = $\dfrac{g\ mole}{cm^2 \cdot sec}$

D = diffusivity of ash specie into surrounding media

P = total pressure

R = gas constant

T_∞ = temperature of the gas outside the film surrounding the vaporizing particle

r = radius of the particle

$P_{A\infty}$ = partial pressure of ash specie outside the film

P_{vp} = vapor pressure of ash specie at the particle surface temperature T_s

M_A = molecular weight of evaporating specie

C_{pA} = specific heat of evaporating specie

λA = latent heat of vaporization of evaporating specie

Sh = Sherwood number

Nu = Nusselt number

Le $\quad$ = Lewis number = sh/Nu

α $\quad$ = thermal diffusivity

Equation (E.4) can be solved for T_s and P_{vp} by trial and error for any specie and at a given gas temperature T_∞, as P_{vp} is a function of T_s.

Characteristic time constant is then given by:

$$\tau_v = \frac{\text{mass of the particle}}{\text{mass flux of vapor}} \qquad (E.5)$$

$$= \frac{4/3 \ \pi \ r^3 \ \rho_A}{\overset{\circ}{N}_A \cdot M_A \cdot 4\pi \ r^2}$$

$$\tau_v = \frac{\rho_A \cdot r}{3 \ \overset{\circ}{N}_A \ M_A} \quad \text{(sec)} \qquad (E.6)$$

Solid particles will be heated up both by conduction and radiation. Appropriate energy balance equations are obtained and finally depending upon the type and size of particle considered, a temperature-time history plot considering solid heating, melting and vaporization, can be constructed. Since the particle time-temperature history is now known, the amount of ash vaporized can be calculated at a given combustor temperature and residence time.

Appendix F

Statistical Analysis of the Particle Size Distribution
Results

To be able to claim that the differences between the
two experiments are genuine and significant, statis-
tical tests were performed (Wilson, C. 1972, Dixon and
Massey 1969). The t-test involves a determination of the
degrees of freedom of the problem, and the values for
varying degrees or freedom for significance levels of
90, 95, 99, 99.5 and 99.9% can be found from the t-
distribution tables.

Example   Figure 6.16   (Lignite 38-45μm)

Mean of 1 to 5 distributions at different tempera-
tures

$\bar{\mu}_1$ = 8.51μm

Standard deviation σ= 1.40μm

For 99% confidence limit and for (N-1)=5-1=4 degrees of
freedom, value of t=3.747.

The range of mean sizes are then

μ_2 = μ_1 ± St

where S = standard error = $\dfrac{\sigma}{(N-1)^{1/2}}$ = $\dfrac{1.4}{(5-1)^{1/2}}$ = 0.7

μ_2= 8.51±0.7×3.747

    = 5.89 to 11.13

i.e. The probability that the distributions having mean between 5.89μm and 11.13μm would belong to the same population as in question is 99 percent.

The mean for all runs 1 to 5 are within this range but 1 ash/coal assumption gives mean value of 11.99μm which is out of this limit i.e., the probability that the 1 ash/coal mean <u>does</u> <u>not</u> belong to the population defined by the mean sizes of ash at different temperatures is 99 percent.

Similarly, for Figure 6.17:

$N=6$, $\bar{\mu}_1 = 15.25\mu m$, $\sigma=2.75\mu m$

$$S = \frac{2.75}{(6-1)^{1/2}} = 1.23$$

t (99%, $N-1=5$) $= 3.365$

$\mu_2 = \mu_1 \pm St = 15.25\pm1.23*3.365$

$\quad = 11.11$ to $19.39\mu m$

Similar conclusions that the probability that the distribution 1 to 6 belong to the same population and 1 ash/coal assumption <u>does not</u> is 99 percent.

APPENDIX G

Derivation of Formula Relating Fraction of SiO_2 Converted to

SiO and SiC

Let the overall reaction be

$$SiO_2, \quad C \quad \rightarrow \quad SiO_2, \quad SiC, \quad C, \quad CO, \quad SiO$$
$$(a) \quad (b) \qquad (c) \quad (d) \quad (e) \quad (f) \quad (g)$$
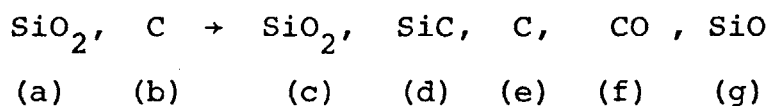
where a, b, c, d, e, f, g are the amount in grams of the
respective species.

Measured Quantities are

W_1 = a + b (starting weight of mixture)

W_2 = c+d+e (weight after heating)

W_3 = c + d (weight after ashing)

Let the reactions be

$$SiO_2(s) + 3C(s) \rightarrow SiC(s)+2CO(g)$$
$$SiO_2(s) + \quad C(s) \rightarrow SiO(g)+ CO(g)$$
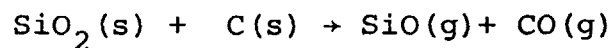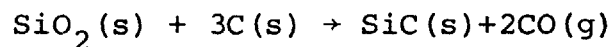
Let $\quad \alpha$ = weight of SiO_2 going to SiO

$\quad \beta$ = weight of SiO_2 going to SiC

$$\alpha = g \cdot \frac{60}{44} \qquad or \quad g = \frac{11}{15} \alpha$$

$$f = \frac{28}{60} \alpha + \frac{56}{60} \beta$$

$$W_1 - W_2 = f+g = \frac{18}{15}\alpha + \frac{14}{15}\beta \qquad\qquad (G.1)$$

$$W_3 = (a-\alpha-\beta) + \beta\frac{40}{60} = a-\alpha-\frac{1}{3}\beta \qquad\qquad (G.2)$$

Solving (G.1) and (G.2) for $\frac{\alpha}{a}$ and $\frac{\beta}{a}$ in terms of

W_1, W_2, W_3 and a we get

$$\frac{\alpha}{a} = \frac{7}{4}\left(1 - \frac{W_3}{a}\right) - \frac{5}{8}\left(\frac{W_1 - W_2}{a}\right) \qquad\qquad (G.3)$$

$$\frac{\beta}{a} = \frac{9}{4}\left(\frac{W_3}{a} - 1\right) + \frac{15}{8}\left(\frac{W_1 - W_2}{a}\right) \qquad\qquad (G.4)$$

where α/a and β/a are fractions of original SiO_2

converted to SiO and SiC, respectively.

LITERATURE CITATIONS

Ackerman, R. J. and R. J. Thorn, "Vaporization of Oxides",
Progr. Ceram. Sci, I, 39 (1961).

Anthony, D. B., "Rapid Devolatilization and Hydrogasifi-
cation of Pulverized Coal", Sc. D. Thesis, M.I.T.,
Chemical Engineering Dept. (January 1974).

ASTM Data File, Joint Committee on Powder Diffraction
Standards, 16 Park Lane, Swarthmore, Pennsylvania
19081 (1966).

ASTM Standard Specifications for Ash Fusion Test,
D-271-48 (1948).

ASTM Standard Specifications for Classification of Coals
by Rank, D 388-38 .

ASTM Standard Specification for Ash Determination,
D-371-72 (1972).

ASTRO Furnace Operation Manual, "Instruction and Opera-
tion Manual for ASTRO Ultra High Temperature Furnace,
Model 1000A-3560, Serial #F7305045", ASTRO Industries,
Santa Barbara, California 93102 (1973).

AVCO Report "Collaborative Program for MHD Power Generation",
Annual Report, Avco Corpn.,Everett, Mass. (Feb. 1974).

Babcock and Wilcox Co., "Steam", 37th Edition, McKibbin,
New York (1955).

Badzioch, S., D. R. Gregory and M. A. Field, "Investigation
of the Temperature Variation of the Thermal Conductivity
and Thermal Diffusivity of Coal", FUEL, (London) 43, 267
(1964).

Badzioch, S. and P. G. N. Hawksley, "Kinetics of Thermal
Decomposition of Pulverized Coal Particles", Ind. Eng.
Chem. Process Des. Develop., 9, 521 (1970).

Battelle Report, "Investigation of the Reactivity of
Limestone and Dolomite for Capturing SO_2 from Flue Gases",
Battelle Memorial Institute Final Report, (Nov. 20, 1970).

Baum, M. M. and P. J. Street, "Predicting the Combustion
Behavior of Coal Particles", Comb. Sci. and Techn., 3,
231 (1971).

Beecher, N. and R. E. Rosensweig, "Ablation Mechanisms in
Plastics with Inorganic Reinforcement", ARS J., 31, 532
(1961).

Brown, H. R. and D. J. Swaine, "Inorganic Constituents of Australian Coals, Part I, Nature and Mode of Occurrence", J. Inst. Fuel, 422 (Oct 1964).

Brown, R. N., "The Relation Between Calorific Value and Ash Content for British Industrial Grade Coals", J. Inst. Fuel, 461 (Nov. 1970).

Brown, R. L., R. L. Caldwell and F. Fereday, "Mineral Constituents of Coal", FUEL (London), 31, 261 (1952).

Combustion Engineering Co., "Combustion Engineering, a reference book on Fuel Burning and Steam Generation", edited by G. R. Fryling, Riverside Press, Cambridge, Massachusetts (1966).

Cullity, B. D., "Elements of X-Ray Diffraction", Addison-Wesley Publishing Co., Inc., Cambridge, Mass. p 101 (1956).

Dana's Manual of Mineralogy, 17th Edition, John Wiley and Sons, Inc. (1966).

Davison, R. L., D. F. S. Natusch and J. R. Wallace, "Trace Elements in Fly Ash, Dependence of Concentration on Particle Size", Environ. Sci. and Tech., 8, 1107 (Dec. 1974)

Dewing, E. W., and F. D. Richardson, "Decomposition Equilibria for Calcium and Magnesium Sulphates", Trans. Farad. Soc., 55, 611 (1959).

EPA, "Compilation of Air Emission Factors", U. S. EPA, (Feb. 1972).

Essenhigh, R. H., "The Mechanism of the Combustion of Carbon. A Theoretical Study", University of Sheffield Fuel Society Journal, 6, 15 (1955).

Essenhigh, R. H., R. Froberg and J. B. Howard, "Combustion Behavior of Small Particles", Ind. Eng. Chem., 57, No. 9, 32 (1965).

Estep, P. A., J. J. Kovach and C. Karr, Jr., "Quantitative Infrared Multicomponent Determination of Minerals Occurring in Coal", J. Anal.Chem., 40, 358 (1968).

Fereday, F. and D. Flint, "Use of Mineral Matter Formulae in the Classification of Coal", Fuel (London), 32, 115 (1953).

Field, M. A., "Rate of Combustion of Size Graded Fractions of Char from a Low Rank Coal Between 1200°K and 2000°K", Comb. and Flame, 13, 237 (1969).

Field, M. A., "Measurements of the Effect of Rank on Combustion Rates of Pulverized Coal", Comb. and Flame, 14, 237 (1970).

Field, M. A., D. W. Gill, B. B. Morgan and P. G. W. Hawksley, "Combustion of Pulverized Coal", BCURA, Leatherhead, England (1967).

Field, M. A. and R. A. Roberts, "Measurement of the Rate of Reaction of Carbon Particles with Oxygen in the Pulverized-Coal Size Range for Gas Temperatures Between 1400°K and 1800°K", BCURA Members Information Circular No. 325, (Aug. 1967).

Frenkel, T., "Viscous Flow of Crystalline Bodies Under the Action of Surface Tension", J. of Phys., Moscow, 9, 385 (1945).

Furnas, C. C., "Rate of Calcination of Lime Stones", Ind. Eng. Chem., 23, 534 (1931).

Gluskoter, H. J., "Electronic Low Temperature Ashing of Bituminous Coals", FUEL (London), 44, 285 (1965).

Gluskoter, H. J., "Clay Minerals in Illinois Coals", Jour. Sed. Petrology, 37, 205 (1967).

Gluskoter, H. J., "Inorganic Sulfur in Coal", ACS (Division of Fuel Chemistry), 169th National Meeting, 20, No. 2, 94-98, April 6-11 (1975).

Gray, M. D., G. M. Kimber and D. E. Granger, "Internal Burning in Pulverized Coal", FUEL (London) 46, 399 (1967).

Hamor, R. J. and I. W. Smith, "Fluidizing Feeders for Providing Fire Particles at Low, Stable Flows", FUEL (London) 50, 394 (1971)

Heywood, J. B., and G. J. Womack, "Open Cycle MHD Power Generation", Pergamon Press, Oxford (1969).

Hottel, H. C. and A. F. Sarofim, "Radiative Transfer", McGraw-Hill, New York (1967).

Howard, J. B. and R. H. Essenhigh, "Pyrolysis of Coal Particles in Pulverized Fuel Flames", Ind. Eng. Chem. Process Des. Devel., 6, 74 (1967).

Huff, W. R., J. H. Holden, L. F. Willmott and G. R. Strimbeck, "A Pilot-Scale Fluidized-Coal Feeder Utilizing Zone Fluidization", Bureau of Mines, Report of Investigations , No. 6488 (1964).

Hultgren, R., R. L. Orr, P. D. Anderson and K. K. Kelly, "Selected Values of Thermodynamic Properties of Metals and Alloys", John Wiley and Sons, New York (1963).

JANAF Tables of Thermochemical Data, D. R. Stull (Editor) Dow Chemical Co., Midland, Mich. (1965).

Juntgen, H. and K. H. VanHeek, "Gas Release from Coal as a Function of the Rate of Heating", FUEL (London) 47 103 (1968).

Kaiser, E. R., "Dust Emission from Coal-Fired Boiler Furnaces", Combustion, 22, 53 (1951).

Kay, D.A.R. and J. Taylor, "The Silica Reduction Reaction in the Blast Furnace", J. Iron and Steel Inst., 201, 67 (1963).

Kellogg Report, "Review of the Dry Limestone Injection Process", The M. W. Kellogg Company, Research and Engineering Development, Task #3, Final Report for Phase 1. Submitted to EPA, Office of Air Programs (May 1972).

Kelly, K. K., "Contribution to the Data on Theoretical Metallurgy: VII. The Thermodynamic Properties of Sulfur and Its Inorganic Compounds", Bull. U. S. Bureau of Mines, 406 (1937).

Kemezys, M. and G. H. Taylor, "Occurrence and Distribution of Minerals in Some American Coals", J. Inst. Fuel, 369, (Sept. 1964).

Kimber, G. M. and M. D. Gray, "Measurement of Thermal Decomposition of Low and High Rank Non-Swelling Coals at MHD Temperatures", MHD Program Report, Document No. MHD 32, BCURA (Jan. 1967).

Kimber, G. M. and M. D. Gray, "Rapid Devolatilization of Small Coal Particles", Comb. and Flame, 11, 360 (Aug.1967).

King, J. G., M. B. Maries and H. E. Crossley, "Formulae for the Calculation of Coal Analyses to a Basis of Coal Substance Free from Mineral Matter", Jour. Soc. Chem. Ind., 55, 277T (1936).

Kobayashi, H. "Kinetics of Rapid Devolatilization of Pulverized Coal", Sc. D. Thesis, Mechanical Eng., M.I.T. (Jan.1976).

Ladacki, M., "Silicone Carbide in Ablative Chars", AIAA J., 4, 1445 (1966).

Lightman, P. and P. J. Street, "Microscopic Examination of Heat Treated Pulverized Coal Particles," FUEL (London), 47 7 (1968).

Littlejohn, R. F., "Mineral Matter and Ash Distribution in 'As-Fired' Samples of Pulverized Fuels", J. Inst. Fuel,, 59 (Feb. 1966).

Loison, R. and F. Chauvin, "Pyrolysis Rapide Du Carbon", Chem. Ind. (Paris), 91, 269 (1964).

Lowry, H. H. (Editor), "Chemistry of Coal Utilization, Supplementary Volume", John Wiley and Sons, New York (1963).

Millot, J. O., "The Mineral Matter in Coal. I-The Water of Constitution of Silicate Constituents", FUEL (London) 37, 71 (1958).

Mitchell, D. W., S. P. Mitoff, V. F. Zackay and J. A. Pask, "Measurement of Surface Tension of Glasses", Glass Ind., 33, 515 (1952).

Mitchell, E. F. and G. K. Lee, "Agglomeration of Superfine Fly-Ash in High-Velocity Gas Streams", Forum on Dust Collection, Trans. Con. Inst. Min. Met., 65, 380 (1962).

Mitchell, R. S. and H. J. Gluskoter, "Mineralogy of Ash of Some American Coals: Variations with Temperature and Source". Submitted to FUEL (London) (1975).

Mulcahy, M. F. R. and I. W. Smith, "Kinetics of Combustion of Pulverized Fuel: A Review of Theory and Experiment," Rev. Pure and Appl. Chem., 19, 81 (1969).

Murray, J. A. and H. C. Fisher, "D.T.A. of White Coat Plastor", Proc. Amer. Soc. Test. Mat., 51, 1197 (1951).

O'Gorman, J. V. and P. L. Walker, Jr., "Mineral Matter Characteristics of Some American Coals", FUEL (London) 50 (1971).

O'Gorman, J. V. and P. L. Walker, Jr., "Thermal Behavior of Mineral Fractions Separated from Selected American Coals", FUEL (London) 52,71 (1973).

Parr, S. W., "The Classification of Coal", Illinois Eng. Exp. Sta. Bull., 180 (1928).

Paulson, C.A.J. and A. R. Ramsden, "Some Microscopic Features of Fly-Ash Particles and Their Significance in Relation to Electrostatic Precipitation," Atmospheric Environment, 4, 175 (1970).

Raask, E., "Slag-Coal Interface Phenomena", J. Engng. Power, 88, 40 (1966).

Raask, E. J. Inst. Fuel, 339 (Sept. 1968a).

Raask, E., "Fusion of Silicate Particles in Coal Flames" FUEL (London) 366 (1968b).

Raask, E. and D. M. Wilkins, "Volatilization of Silica in Gasification and Combustion Processes", J. Inst. Fuel, 38, 255 (June 1965).

Ramsden, A. R., "Application of Electron Microscopy to the Study of Pulverized Coal Combustion and Fly-Ash Formation", J. Inst. Fuel, 451 (Dec. 1968).

Ramsden, A. R., "A Microscopic Investigation into the Formation of Fly-Ash During the Combustion of a Pulverized Bituminous Coal", FUEL (London) 48, 121 (1969).

Ramsden, A. R. and I. W. Smith, "Further Evidence of Internal Burning in Particles of Pulverized Coal", FUEL (London) 47, 253 (1968).

Rosensweig, R. E. and N. Beecher, "Theory for the Ablation of Fiberglass-Reinforced Phenolic Resin", AIAA J., 1, 1802 (1963).

Rosin, P. and E. Rammler, "The Laws Governing the Fineness of Pulverized Coal", J. Inst. Fuel, 7, 29 (1933).

Rost, F. and P. Ney, "Zur Kenntnis der Kesselschlacken", Bnennstaff-Chemie, 37,201 (1956).

Sarofim, A. F., J. B. Howard, A. Padia and H. Kobayashi, "Heat Transfer and Kinetic Limitations in the Design of Single-Stage Coal Fired Combustors for Open-Cycle MHD Generators", 6th International Conference on MHD Electrical Power Generation, Vol. II. Open Cycle Components and Materials, Washington, D. C., p 305 (9th-13th June 1975).

Schick, H. L., "A Thermodynamic Analysis of the High Temperatures Vaporization Properties of Silica", Chem. Rev., 60 331 (1960).

Schwab, G. M. and J. Phillinis, "Reaction of Iron Pyrites: Thermal Decomposition, Reduction by Hydrogen and Aerial Oxidation", J. Am. Chem. Soc., 69, 2588 (1947).

Selvig, W. A. and F. H. Gibson, "Analysis of Ash from United States Coals", Bulletin U. S. Bureau of Mines, No. 567 (1956).

Shapatina, E. A., V. V. Kalyuzhnyi, and J. F. Chukhanov, "Technological Utilization of Fuel for Energy, 1-Thermal Treatment of Fuels, (1960) (Reviewed by Badzioch, S., BCURA Monthly Bulletin, 25, 285 (1961)).

Sinaiskii, N. A., A. G. Merkulov and M. S. Sharlovskaya, "Results of X-Ray Spectroscopic Analysis of Ash from Fossil Fuels", Teploenergetika, No. 12, 65 (1964).

Street, P. J., R. P. Weight and P. Lightman, "Further Investigation of Structural Changes Occurring in Pulverized Coal Particles During Rapid Heating", FUEL (London) 48, 343 (1969).

Tager, S. A., E. V. Samuilov, I. B. Rozhdestvenskii, R. V. Talumaa and F. M. Iakhilevich, "Development and Investigation of High-Temperature Combustor to be used for a Solid Fuel MHD Generator", Fifth Int. Conf. MHD Elec. Power Generation, Munich (1971).

Thring, M. W., R. H. Essenhigh, "Chemistry of Coal Utilization, Supplementary Volume", p 754, John Wiley and Sons, New York (1963).

TVA Report, "Removal of Sulfur Dioxide from Stack Gases", TVA Fundamental Research Branch, Monthly Project Report to EPA, Office of Air Programs, (Oct 1969).

Watt, J. D. and F. Fereday, "The Flow Properties of Slags Formed from the Ashes of British Coals, Part I, Viscosity of Homogeneous Liquid Slags in Relation to Slag Composition", J. Inst. Fuel, 99 (March 1969).

Wriedt, H. A. and L. S. Darken, "Equilibrium of Sulfur-Bearing Gases and Solids Relevant to the Burning of Limestones", Paper presented for publication in Trans. SME AIME (Feb. 1972).

Wunderlich, G., "Thermodynamics of Decomposition of Pyrites", Z. Elekt. 56, 218 (1952).

Yerushalmi, J., M. Klodney, R. A. Graff and A. M. Squires, "Agglomeration of Ash in Fluidized Beds Gasifying Coal: The Godel Phenomenon", Science, 187, 646 (1975).

Zapffe, C. A., "Conversion of Refractory Oxides to Suboxides at High Temperature", J. Am. Ceram. Soc., 27, 293 (1944).

Zawadzki, J., "Zur Kenntnis des System Calcium-Schwefel-Sauerstoff", Z.Anorg. allgem. Chemie, 205, 180 (1932).

BIOGRAPHICAL NOTE

The author, Ashok S. Padia, was born on July 16, 1948 in Bombay, India. He attended Shri Dayamand Vidyalaya, Bombay from which he received his secondary school certificate in 1964. He joined Birla Institute of Technology and Science, Pilani, India in 1965, after spending one year at Elphinston College, Bombay. He was awarded the Bachelor of Engineering degree in Chemical Engineering with a gold medal from BITS in 1970. In May 1970 he married the former Usha Modi.

He entered M.I.T. in September 1970 and was awarded the degree Master of Science in Chemical Engineering Practice in 1971 and Chemical Engineer in 1973. During his stay at M.I.T. he worked on several research projects. Other professional experience includes summer jobs at Scientific Energy Systems Incorporation, Watertown, Mass.

The author is a member of American Institute of Chemical Engineers, American Chemical Society, Combustion Institute and Society of Sigma Xi. He is the author of three technical publications.

At the present time, he has accepted an appointment as Research and Development Engineer in Halcon International, Inc., New York to begin in February 1976.